

Alma Mater Studiorum - Università di Bologna

**DOTTORATO DI RICERCA IN**  
**SCIENZE BIOTECNOLOGICHE, BIOCOMPUTAZIONALI,**  
**FARMACEUTICHE E FARMACOLOGICHE**

Ciclo 34°

**Settore Concorsuale:** 03/D1 - CHIMICA E TECNOLOGIE FARMACEUTICHE,  
TOSSICOLOGICHE E NUTRACEUTICO - ALIMENTARI

**Settore Scientifico Disciplinare:** CHIM/08 - CHIMICA FARMACEUTICA

**DEVELOPMENT OF NEW CHEMICAL ENTITIES TO**  
**TARGET NEUROINFLAMMATORY PATHWAYS**

**Presentata da:** Claudia Albertini

**Coordinatore Dottorato**

Prof.ssa Maria Laura Bolognesi

**Supervisore**

Prof.ssa Maria Laura Bolognesi

**Esame finale anno 2022**



## Abstract

Neuroinflammatory pathways are main culprits of neurodegenerative diseases' onset and progression, including Alzheimer's disease (AD). On this basis, several anti-inflammatory drugs were repurposed in clinical trials. However, they have failed, probably because neuroinflammation is a complex network, still not fully understood.

From these evidences, this thesis focused on the design and synthesis of new chemical entities as potential neuroinflammatory drugs or chemical probes. Projects 1 and 2 aimed to multi-target-directed ligand (MTDL) development to target neuroinflammation in AD. Polypharmacology by MTDLs is considered one of the most promising strategies to face the multifactorial nature of neurodegenerative diseases. Particularly, Project 1 took inspiration from a cromolyn-ibuprofen drug combination polypharmacological approach, which was recently investigated in AD clinical trials. Based on that, two cromolyn-(*S*)-ibuprofen codrug series were designed and synthesized. Parent drugs were combined via linking or fusing strategies in 1:2 or 1:1 ratio, by means of hydrolyzable bonds.

Project 2 started from a still ongoing AD clinical trial on investigational drug neflamapimod. It is a selective inhibitor of p38 $\alpha$ -MAPK, a kinase strictly involved in neuroinflammatory pathways. On the other side, rasagiline, an anti-Parkinson drug, was also repurposed as AD treatment. Indeed, rasagiline's propargylamine fragment demonstrated to be responsible not only for the MAO-B selective inhibition, but also for the neuroprotective activity. Thus, to synergistically combine these two effects into single-molecules, a small set of neflamapimod-rasagiline hybrids was developed. In the end BMX, a poorly investigated kinase, which seems to be involved in pro-inflammatory mediator production, was explored for the development of new chemical probes. High-quality chemical probes are a powerful tool in target validation and starting points for the development of new drug candidates. Thus, Project 3 focused on the design and synthesis of two series of optimized BMX covalent inhibitors as selective chemical probes.



## Table of contents

<b>Chapter 1</b> .....	<b>7</b>
1. Neuroinflammation .....	9
1.1 The central role of the microglia .....	12
1.2 Microglia in neurodegenerative diseases .....	13
<b>Chapter 2</b> .....	<b>19</b>
2. Objectives.....	21
<b>Chapter 3</b> .....	<b>27</b>
3. Alzheimer’s disease .....	29
3.1 Neuroinflammation in Alzheimer’s Disease .....	30
3.2 Drugs on the market to treat Alzheimer’s disease.....	35
3.3 Polypharmacology in Alzheimer’s disease .....	37
3.3.1 Strategies to design multi-target-directed ligands .....	41
3.4 Project 1: cromolyn-ibuprofen conjugates as potential “codrugs” for Alzheimer's disease treatment .....	43
3.4.1 The amyloidogenic pathway .....	43
3.4.1.1 A $\beta$ pathophysiology and neuroinflammation .....	44
3.4.2 Cromolyn and its potential application for AD treatment .....	46
3.4.3 Ibuprofen .....	48
3.4.4 Cromolyn-ibuprofen codrugs rationale of the project.....	50
3.4.4.1 Cromolyn-ibuprofen codrugs: design of a small set of 1:2 cromolyn-ibuprofen conjugates .....	52
3.4.4.2 Chemistry .....	53
3.4.4.3 Results and discussion.....	58
3.4.4.4 Cromolyn-ibuprofen codrugs: design of a small set of 1:1 cromolyn-ibuprofen conjugates .....	67
3.4.4.5 Chemistry .....	68
3.4.4.6 Results and discussion.....	69
3.5 Project 2: neflamapimod-rasagiline hybrids to target neuroinflammation in Alzheimer’s disease.....	72
3.5.1 Protein kinases as a druggable target for Alzheimer’s disease.....	72
3.5.1.1 p38 $\alpha$ -MAPK: a member of MAPK family .....	74
3.5.1.2 p38 $\alpha$ -MAPK involvement in Alzheimer's disease development .....	77
3.5.2 Protein kinase inhibitors as a valuable strategy against Alzheimer’s disease .....	78

3.5.2.1	Protein kinase inhibitors investigated in clinical trials for Alzheimer's disease	82
3.5.2.2	p38-MAPK inhibitors	85
3.5.2.3	Neflamapimod	88
3.5.3	MAO-B and its implication as a therapeutic target in Alzheimer's disease	90
3.5.3.1	Rasagiline	91
3.5.4	Neflamapimod-rasagiline hybrids: rationale of the project	94
3.5.4.1	Design of neflamapimod-rasagiline hybrids	95
3.5.4.2	Chemistry	99
3.5.4.3	Results and discussion	106
<b>Chapter 4</b>		<b>113</b>
4.	BMX: a member of TEC protein kinase family	115
4.1	BMX as a potential target to modulate neuroinflammation	118
4.2	Project 3: optimization of covalent BMX inhibitors	119
4.2.1	Design of covalent inhibitors targeting non-conserved cysteine residues	119
4.2.2	TEC kinase FDA approved inhibitors	122
4.2.2.1	BMX inhibitors	124
4.2.3	The importance of the chemical probes in chemical biology and drug discovery	125
4.2.4	The discovery of a new series of covalent BMX inhibitors: rationale of the project	126
4.2.4	Hit to lead optimization: design of new series of BMX inhibitors	128
4.2.5	Chemistry	131
4.2.6	Results and discussion	136
<b>Chapter 5</b>		<b>143</b>
5.	Conclusions and Perspectives	145
<b>Chapter 6</b>		<b>149</b>
6.	Experimental part	151
6.1	Synthesis of cromolyn-ibuprofen codrugs (1:2)	153
6.2	Synthesis of cromolyn-ibuprofen codrugs (1:1)	159
6.3	Synthesis of p38 MAPK/MAO-B potential dual inhibitors	161
6.4	Synthesis of BMX covalent inhibitors	167
<b>Bibliography</b>		<b>199</b>

# Chapter 1

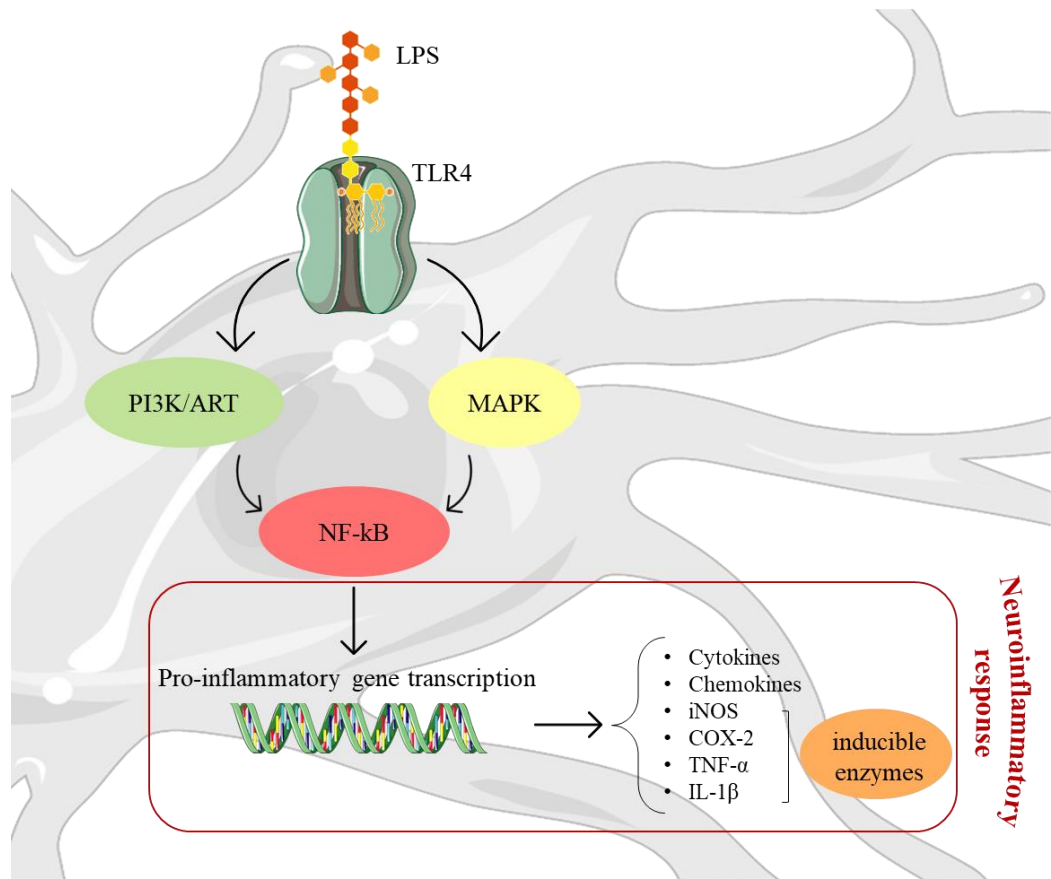




# 1. Neuroinflammation

Inflammation is a general physiological response activated by injury, infection, and trauma suffered by cells or tissues. Particularly, the inflammatory process involves various mechanisms finalized to eliminate extraneous pathogens, initiate tissue repair and angiogenesis, restoring the normal homeostasis.<sup>1</sup> Relatively to the central nervous system (CNS), all the inflammatory responses of the brain or of the spinal cord fall under the umbrella of “neuroinflammation”. Neuroinflammatory pathways involve the totality of CNS cells, including neurons and central glial cells.<sup>2</sup> The total glial cell population of CNS can be subdivided into four major groups: (1) microglia, which constitutes the immunocompetent and phagocytic cells of the CNS, (2) astrocytes, that maintain the homeostasis of the CNS including the blood-brain-barrier (BBB), (3) oligodendrocytes, that are the myelin-producing cells and (4) their progenitors NG2-glia.<sup>3</sup> Despite the complexity of immune response processes that occur in neuroinflammation, all of them are physiological and essential for the neuronal microenvironment. They can result in positive or negative effects on the CNS.<sup>1</sup> In physiological conditions, CNS homeostasis is maintained by elaborated crosstalk between glia and neurons. When a CNS infection or injury occurs, it provokes glial cell reaction, which activates and contributes to the inflammatory processes.<sup>4</sup> Particularly, microglia, astrocytes, endothelial cells, and peripherally derived immune cells play a central role in producing inflammatory mediators. Thus, cytokines, chemokines, reactive oxygen species (ROS), and secondary messengers contribute to biochemical, immune and physiological pathways activation.<sup>2</sup> Depending on the nature, the intensity, and the duration of the insult, neuroinflammatory processes could lead to beneficial or injurious consequences. For instance, acute or chronic inflammatory events demonstrated a correlation in many neurodegenerative diseases such as multiple sclerosis, Alzheimer’s disease (AD), Parkinson’s disease (PD), narcolepsy, and autism.<sup>5</sup> A common example of inflammatory stimulus is the lipopolysaccharide (LPS). It is the principal component of the external membrane of the Gram-negative bacteria that demonstrated to permeate the brain parenchyma by diffusion. In CNS, LPS can bind to Toll-like-receptor 4 (TLR-4) on the microglia surface activating several signal transduction pathways, including phosphatidylinositol-3-kinase/protein-kinase-B (PI3K/AKT) and mitogen-activated protein kinase (MAPK). These pathways lead to nuclear factor kappa B (NF-κB) activation and adaptive immunity activation that cooperate to eliminate the infecting microorganisms.<sup>1</sup> In turn, NF-κB

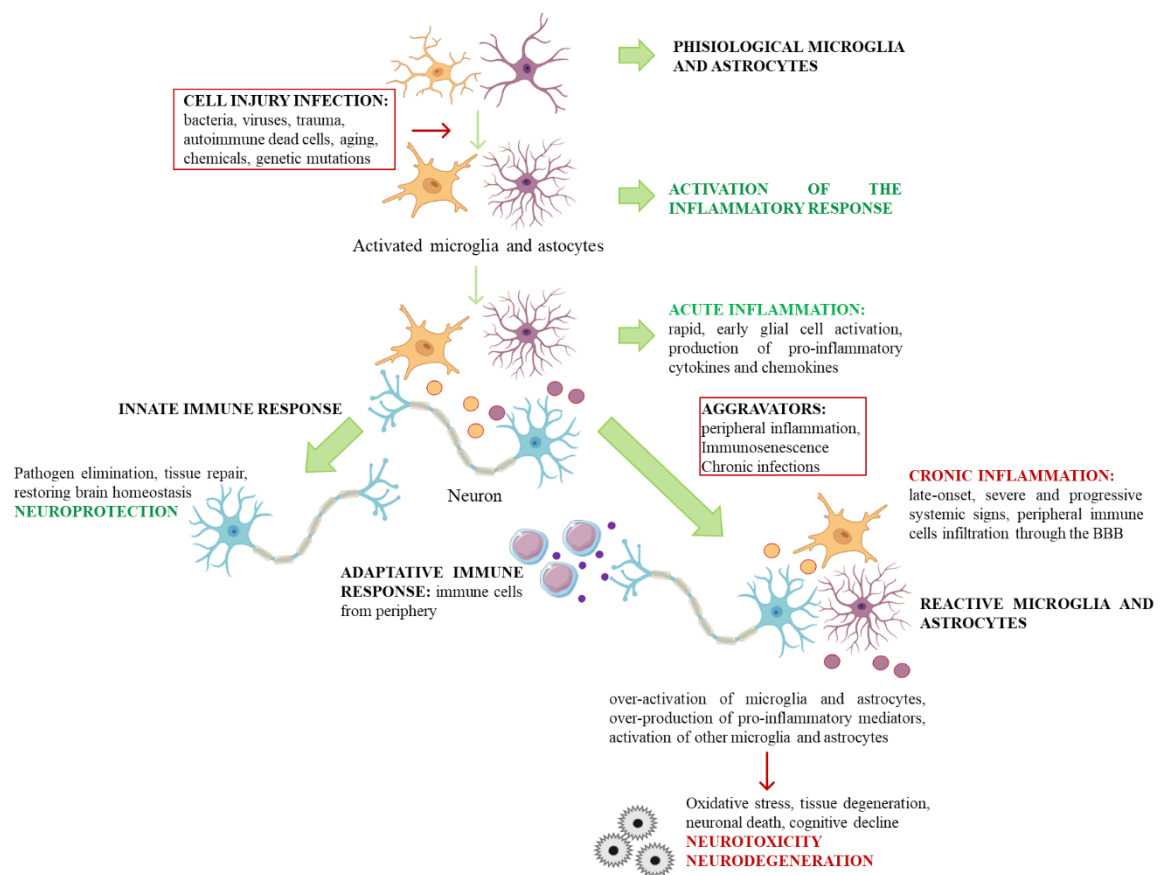
activation induces the expression of various pro-inflammatory genes that mediate the production of pro-inflammatory cytokines, chemokines, and inducible enzymes, such as inducible nitric oxide synthase (iNOS), cyclooxygenase-2 (COX-2), tumor necrosis factor- $\alpha$  (TNF- $\alpha$ ), interleukin-1 $\beta$  (IL-1 $\beta$ ), which result in a neuroinflammatory response (Figure 1).<sup>6</sup>



**Figure 1.** LPS stimulation in microglia cells and consequent neuroinflammatory response. (Figure adapted from doi: 10.1038/sigtrans.2017.23)<sup>6</sup>

The intensity of the activation of the neuroinflammatory pathway is influenced by the context, the duration, and the course of the primary stimulus or insult.<sup>2</sup> As said neuroinflammation is a physiological response; however, strong activation of glial cells can exponentially increase cytokine production leading to their overexpression/dysregulation.<sup>2</sup> Neurodegenerative diseases are characterized by an exaggerated and pathological neuroinflammatory activation.<sup>5</sup> From primary acute damage (an infection, an injury, or a mechanical insult) CNS glial cells are activated sustaining cytokine and chemokine production, infiltration of peripheral immune cells, edema, increased BBB permeability, and breakdown.<sup>5</sup> If the harmful insult persists, it can

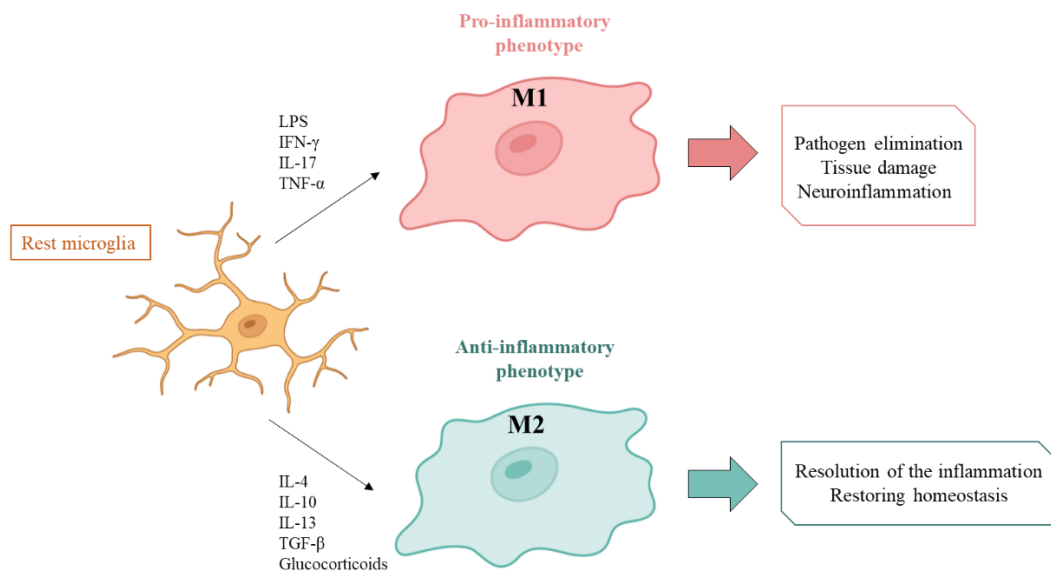
lead from acute inflammation to chronic inflammation, resulting in brain dysfunction mechanisms of misfolded or damaged proteins, that play a crucial role in neurodegeneration and cognitive decline.<sup>2</sup> On the other side, brief and mild activation of microglia and astrocytes usually produce a controlled inflammatory response with beneficial neuroprotective effects.<sup>7</sup> Transient neuroinflammation stimulates activation of CNS glia cells and the production of cytokines and chemokines but, in this case, it leads to physiological responses beneficial for the organism.<sup>2</sup> It takes place in the absence of tissue pathology and it is not associated with significant central infiltration of immune cells, BBB breakdown, or cell death.<sup>2</sup> To note, transient activation of the immune cells before injury or infection reduces the inflammatory process and increases neuroprotection (Figure 2).<sup>7</sup>



**Figure 2.** The innate and the adaptive immune responses are involved in the neuroinflammatory response. They can drive beneficial or injurious reactions depending on the duration and strengths of glia activation. (Figure adapted from doi: 10.1007/s12035-016-0297-1)<sup>7</sup>

## 1.1 The central role of the microglia

Microglia constitutes 12% of the cells in the brain, they are the macrophages of the CNS and the first-line brain defense. Microglia activation can be stimulated by several insults such as pathogens, tissue damage, abnormal stimulation, neurotoxins, infection, or injury and it is the first signal that a neuroinflammatory process is occurring.<sup>7</sup> From the morphological point of view, the resting ramified microglia state develops in an amoeboid morphology when microglia activates, characterized by cell body enlargement, shorter cell processes, and the presence of numerous cytoplasmic vacuoles, related to phagocytosis and pro-inflammatory functions (Figure 3).<sup>8</sup> This morphological change is also followed by an expression and upregulation of different surface markers such as TLR, NOOD-like-receptors, nucleotide-binding oligomerization domain, and scavenger receptors.<sup>8</sup>



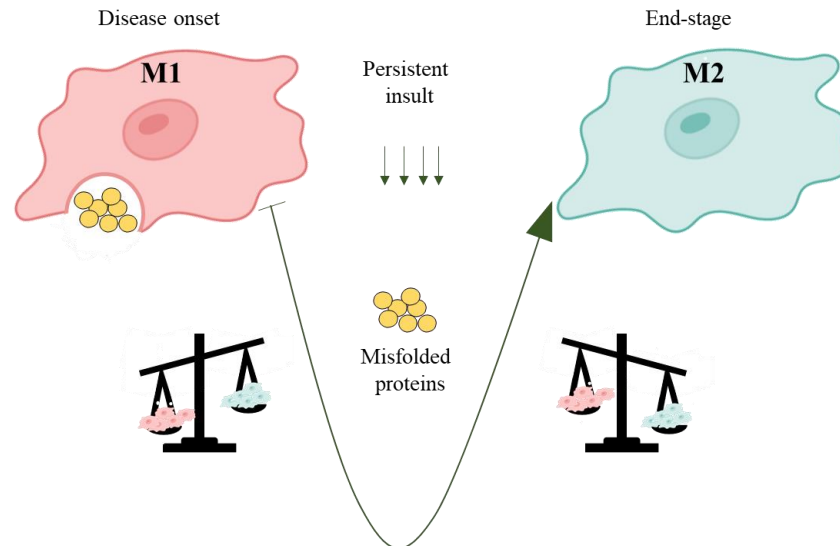
**Figure 3.** Description of microglia in resting state in physiological conditions when it regulates CNS homeostasis, and during neuroinflammation, when it acquires classical M1 or alternative M2 phenotypes, according to the nature of the local environment. (Figure adapted from doi: 10.3389/fnagi.2017.00148)<sup>8</sup>

However, many evidences highlighted a double nature of microglia activation, from its beneficial role in stimulating neuron survival to its neurotoxic nature.<sup>9</sup> The microglia heterogeneous dynamic activation, called “M1/M2 paradigm”, ranges from the pro-inflammatory phenotype (M1) by classical activation, to the anti-inflammatory phenotype (M2) by alternative activation.<sup>9</sup> Depending on the external stimuli, M1 or M2 activation occurs. Microglia pro-inflammatory phenotype activation results in neuronal death while

the anti-inflammatory phenotype activation outcomes in destroying pathogens (Figure 3).<sup>10</sup> Particularly, the M2 alternative microglia activation is involved (i) in regulating brain development by promoting neural cells and toxic aggregated elimination, (ii) in increasing neuronal survival thanks to trophic and anti-inflammatory factors release, (iii) in guiding the migration of stem cells to the site of inflammation and injury, and (iv) it might be involved in neurogenesis.<sup>8</sup> Thus, M2 microglia phenotype by stimulating immunosuppression and neuroprotection regulates anti-inflammatory factors and antagonizes the chronic inflammation and neurodegeneration of the M1 pro-inflammatory phenotype.<sup>10</sup> Indeed, M2 polarization guarantees CNS homeostasis and neurodegeneration prevention by an efficient phagocytosis process and promotes immunosuppression and neuron protection.<sup>7</sup> Considering all these reasons, M1 and M2 phenotypes and M1/M2 changes result be critically associated with neurodegenerative diseases, and their modulation could offer appropriate time windows and better therapeutic effects.<sup>10</sup>

## **1.2 Microglia in neurodegenerative diseases**

Neurodegenerative diseases are complex and multifactorial diseases and include all those conditions which affect structural or survival neuronal functions. Unfortunately, CNS cells, do not regenerate after damage by disease, ischemia, or physical trauma. For this reason, neurodegeneration results in progressive aggravation of the conditions and is challenging to treat.<sup>5</sup> As previously mentioned, there is a correlation between neuroinflammation, microglial activation, and neurodegenerative disorders such as AD, PD, amyotrophic lateral sclerosis (ALS) and Huntington's disease (HD).<sup>10</sup> It has been demonstrated that the major neurodegenerative diseases share a common M1 microglia activation phenotype with the consequent production of immune-inflammatory mediators (IL-1 $\beta$ , TNF $\alpha$ , and NO), inflammatory cytokines, and ROS, combined with impaired ability to regulate increased oxidative stress in the aging brain.<sup>11</sup> While at the basal level, the immune mediators act as scavengers to favor the normal turnover of neurons and fragment clearance of necrotic neurons,<sup>11</sup> in chronic conditions an unbalance of M1/M2 phenotypes occurs. Thus, the prolonged activation of microglia by toxic stimuli such as misfolded protein, and the further induction of degenerative dysfunction are promoted, compromising CNS physiological functions (Figure 4).<sup>12</sup>



**Figure 4.** The balance between microglia phenotypes M1 and M2 in neurodegenerative diseases. (Figure adapted from doi: 10.1007/s12035-014-9070-5)<sup>10</sup>

The cytotoxic activation of microglia favors the increased production of inflammatory cytokines and ROS causing serious damage to the brain since the CNS's ability to regulate oxidative stress is reduced. All these alterations contribute to brain dyshomeostasis, loss of neurons in the brain and spinal cord, and a vicious aggravation of CNS diseases.<sup>12</sup> Moreover, compromised brain homeostasis and changes in glial cell reactivity are influenced by aging. Indeed, the typical dysregulations observed in neurodegeneration are the same noted in aging CNS.<sup>13</sup>

#### Neuroinflammation in Parkinson's disease

PD is a neurodegenerative disease characterized by the progressive loss of dopaminergic neurons in the substantia nigra and the pathological accumulation of protein aggregates, Lewy bodies, and Lewy neurites. Its progression results in typical motor and non-motor symptoms such as resting tremors, bradykinesia, postural instability, cognitive impairment, and autonomic dysfunction due to nerve damage.<sup>14</sup> Their principal component is misfolded  $\alpha$ -synuclein, a protein that physiologically regulates the reserve pool of synaptic vesicles for neurotransmitters.  $\alpha$ -synuclein gene is one of the prevalent pathological genetic alterations observed in familial PD.<sup>15</sup> Physiologically  $\alpha$ -synuclein is localized intracellularly at the presynaptic terminals, while its mutated forms are released and are prone to aggregate. The imbalance between its synthesis and clearance takes part in PD pathogenesis and leads to the loss of neurons' normal functions.<sup>15</sup> However, the

release of  $\alpha$ -synuclein extracellularly by dying or dead dopaminergic neurons can induce microglia M1 phenotype, with the consequent increase of ROS production and pro-inflammatory cytokines. Overexpression of mutant  $\alpha$ -synuclein usually results in a more reactive M1 phenotype characterized by high levels of nitric oxide (NO) and pro-inflammatory cytokines such as TNF- $\alpha$ .<sup>10</sup> Microglia M1 phenotype activation sustains neuroinflammatory pathways that cover a substantial role in PD pathogenesis. Indeed, neuroinflammation seems to be inversely correlated with the survival of dopaminergic neurons in patients.<sup>16</sup> Indeed *in vitro* studies showed that iNOS inhibition in dopaminergic neurons by glucocorticoids, bromovalerylurea, and NOS inhibitors prevented neuronal death.<sup>17</sup> Considering the M2 microglia phenotype, specifically in PD it is not well understood. As previously said, M2 phenotype activation is related to anti-inflammatory cytokine secretion, microglia phagocytic function, and accelerated repair promoting dopaminergic neuron survival. However, the results from studies focused on the form of  $\alpha$ -synuclein that activates microglia were contradictory. In some studies, the pathogenic form of  $\alpha$ -synuclein promoted pro-inflammatory microglial response reducing phagocytosis<sup>18</sup> while in others, it is implicated in inhibiting inflammatory pathways and promoting phagocytosis.<sup>19</sup> Triggering receptors expressed on myeloid cells 2 (TREM2) and TLRs are the principal receptors involved with synuclein interaction as well as with the consequent stimulation of its clearance and extracellular level.<sup>14</sup> However, the monomeric state of the protein seems to be responsible for phagocytosis promotion while the aggregated state promotes pro-inflammatory cytokines release and inhibits phagocytosis. Thus, the main microglia phagocytosis regulator seems to be the  $\alpha$ -synuclein conformation.<sup>20</sup>

### Neuroinflammation in amyotrophic lateral sclerosis

ALS, also known as Lou Gehrig's disease, is a neurodegenerative disease that selectively affects motoneurons both peripherally and in the brain. It is an adult-onset disease that develops in familial or sporadic cases.<sup>21</sup> The ALS characteristic hallmark is a strong M1 neuroinflammatory response that involved the activation of microglia and astrocytes. These events mediate demyelination, and neuronal death also due to an autoimmune component by peripheral T cell infiltration.<sup>22</sup> As for other neurodegenerative diseases, also in this case misfolded protein accumulation contributes to M1 phenotype activation. Mutated Cu, Zn-superoxide dismutase 1 (SOD-1) are frequent in familial ALS while

mutated transactive response (TAR) DNA-binding protein 43 (TDP-43) is found especially in sporadic ALS.<sup>22</sup> TDP-43 is usually located in the nucleus where it is mainly involved in RNA processing. In ALS pathogenesis, TDP-43 mutations induce its mislocalization in the cytoplasm and it forms insoluble aggregates in the nucleus and cytoplasm. TDP-43, highly expressed in microglia, stimulates via NF- $\kappa$ B M1 phenotype increasing the neurotoxic inflammatory pathways.<sup>23</sup> In turn, SOD1 is principally studied concerning ALS immunopathogenesis. Accumulation of abnormal SOD 1 results in increased ROS production enhancing pro-inflammatory signaling in microglia. Indeed, in a mouse model was demonstrated that SOD-1 mutation increases typical M1 phenotype biomarkers such as iNOS, pro-inflammatory cytokines, including TNF- $\alpha$ , IL-1 $\beta$ , IL-6 and upregulates NF- $\kappa$ B signaling.<sup>24</sup> On the other side, M2 phenotype stimulation by IL-4 was found to improve motoneuron survival. In detail, microglia have both neuroprotective and cytotoxic functions in ALS.<sup>10</sup> As first response, M2 microglia phenotype activation occurs and may increase the neuroprotective effect. Subsequently, the prolonged neuronal stress and signaling lead to uncontrolled inflammatory responses and the microglia phenotype shift from M2 to M1.<sup>25</sup> Moreover, during the disease progression, M1 microglia phenotype is predominant, and contributes to the promotion and amplification of SOD 1 mutations, and aggravating motoneuron injury.<sup>10</sup>

### Neuroinflammation in Huntington's disease

HD is an autosomal dominant genetic disease that affects CNS. It originates from a mutation on the short arm of chromosome 4 which presents a repetition of the cysteine-alanine-glycine trinucleotide in the huntingtin gene. The translation of this repetition is an expanded polyglutamine tract in huntingtin (HTT) protein that is prone to misfolding.<sup>26</sup> HTT is expressed in different types of neural cells but it preferentially aggregates along the neuronal processes and axonal terminals. Its accumulation density is correlated with the level of neuron loss, which leads to preferential degeneration of medium spiny neurons in the striatum, the main HD hallmarks.<sup>27</sup> The most common motor behavior symptom of HD is chorea, which causes unwanted rapid, short-lasting involuntary movements in all muscles of the body, face, and extremities. Moreover, mild or more severe PD symptoms can be observed together with cognitive disorders and mental disturbs.<sup>28</sup> Despite also HD showing a neuroinflammatory pathological component, it is demonstrated to not be related to peripheral immune cells (lymphocytes and neutrophils)



influx. In this case, neuroinflammatory pathways involve inflammatory mediator release by microglia activation. Particularly, microglia response is locally stimulated by HTT neuronal expression. However, this proliferative microglia didn't directly contribute to neuronal loss.<sup>29</sup> It is inclined to localize along irregular neurites, and by its over-activation manifests the neurotoxic phenotype by toxin and inflammatory cytokines production. Moreover, reactive microglia is considered a proportional biomarker of HD progression. Particularly, NF- $\kappa$ B signaling has been described as one of the principal pathways through which HTT induces microglia activation. This results in an increment of NF- $\kappa$ B-mediated transcription of pro-inflammatory cytokines production *e.g.* IL-1 $\beta$ , IL-6, IL-8, and TNF- $\alpha$ .<sup>27</sup> In patients, microglia activation correlates with the disease progression, as demonstrated by the accumulation of reactive microglia and astrocyte found in HD brains.<sup>30</sup> However, microglia activation is evident since the presymptomatic HD phase and can be revealed up to 15 years before the projected age of onset.<sup>31</sup> In contrast to M1 microglia activation, the alternative M2 microglia phenotype allows phagocytosis, tissue repairment and neural regeneration. Although neuroinflammation remains relatively underexplored in HD, fewer M2 biomarkers than M1 were found but the entity of M1/M2 microglia shift is not well studied yet. However, in analogy with other neurodegenerative diseases, microglial activation may play a dual role also in HD pathogenesis. Thus, the targeting of specific M2 biomarkers pathways could offer potential therapeutic effects.<sup>26</sup>

### Neuroinflammation in Alzheimer's disease

As will be deeper explained in chapter 3, AD is the most common form of dementia worldwide. The areas of the brain that are more struck by AD pathological pathways are the frontal and temporal cortex, the amygdala, and the hippocampus. These areas suffer from macroscopic modifications such as enlargement and atrophy, which lead to cognitive and motor symptoms including memory problems, cognitive impairment, difficulty organizing thoughts and speaking as well as loss of movement coordination and difficulty in swallowing.<sup>32</sup> Typical AD biomarkers are  $\beta$ -amyloid (A $\beta$ ) plaques and neurofibrillary tangles (NFTs). Particularly, due to altered amyloid precursor protein (APP) proteolytic cleavage in neurons, A $\beta$  peptides prone to misfolding are produced. These can accumulate extracellularly and aggregate. Concerning NFTs, they form by hyperphosphorylated tau protein which is susceptible to misfolding.<sup>33</sup> Both, A $\beta$  plaques and NFTs, demonstrated the ability to attract and activate M1 microglia phenotype.

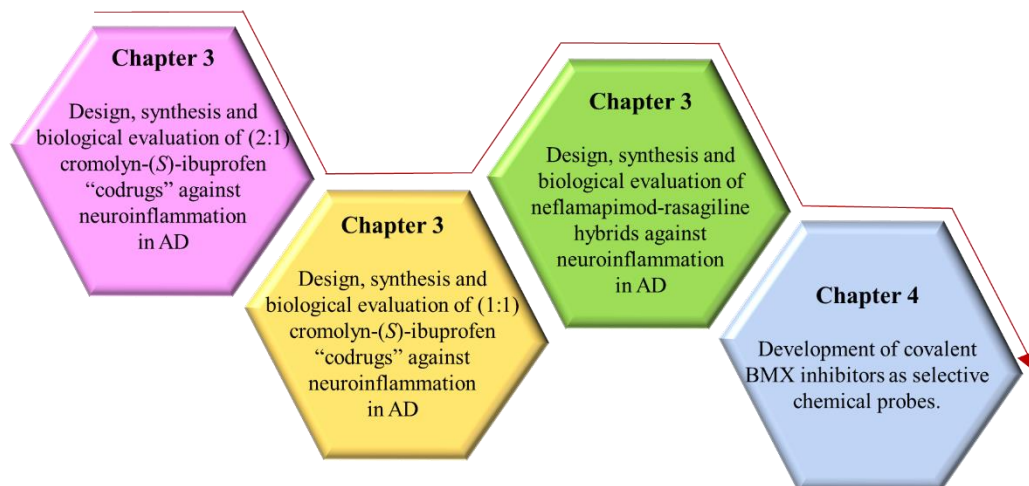
Activated microglia showed increased proliferation and increased expression of inflammatory markers such as CD36, CD14, CD11c, MHC-II, and iNOS stimulating NO production and pro-inflammatory cytokines. However, A $\beta$  accumulation can induce microglia alternative M2 activation, which is neuroprotective, and phagocytes A $\beta$  plaques.<sup>34</sup> Moreover, microglia are involved in NFTs phagocytosis is also possible since they are released from dead neurons.<sup>35</sup> As mentioned the phenotype expressed by microglia activation is influenced by the nature of inflammatory stimulation which occurs. AD pathogenesis involves acute M1 microglia activation by pro-inflammatory cytokines (IFN- $\gamma$ , IL-1 $\beta$ , and TNF- $\alpha$ ) production.<sup>34</sup> These induce microglia to shift into the pro-inflammatory M1 state. On the other side, cytokines induce M2 microglia activation that antagonizes the pro-inflammatory phenotype by enhancing A $\beta$  uptake and clearance.<sup>34</sup> Nevertheless, in relation to age, the number and size of A $\beta$  plaques might increase, reducing microglia phagocytic capability. Moreover, long-period microglia activation drives chronic inflammation which diverts its physiological and beneficial functions causing neurotoxicity and neurodegeneration.<sup>36</sup>

# **Chapter 2**



## 2. Objectives

Considering the crucial implication of neuroinflammatory pathological processes in neurodegeneration, this PhD thesis focused on the modulation of several neuroinflammatory pathways by small molecules. With this goal, a polypharmacological drug discovery approach and a chemical biology strategy were applied.

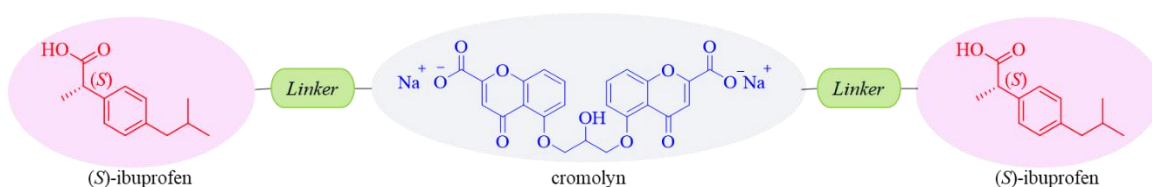


**Figure 5.** Graphical representation of the PhD thesis objectives to investigate neuroinflammatory pathways.

Starting from this rationale, the following specific objectives were pursued (Figure 5):

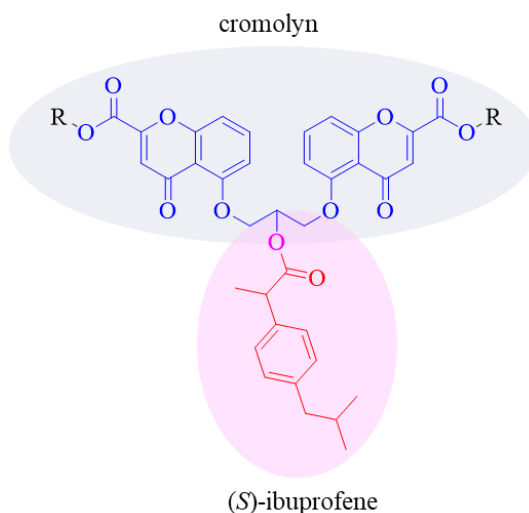
1. The first objective focused on the design and the synthesis of potential “codrugs” between cromolyn and (S)-ibuprofen to target neuroinflammation in AD. Cromolyn and ibuprofen are two anti-inflammatory drugs currently on the market. Cromolyn is mainly used for the treatment of asthma, while ibuprofen is a common non-steroidal anti-inflammatory drug (NSAID). The potential use of NSAIDs such as ibuprofen to interfere with neuroinflammatory processes and cytokine-induced A $\beta$  production in AD development, as well as the anti-aggregating activity of cromolyn, were largely studied in literature.<sup>37,38</sup> Starting from this evidence, Zhang *et al.* *in vivo* investigated a polypharmacological approach based on cromolyn-ibuprofen combination aiming to modulate different neuroinflammatory pathways in AD.<sup>39</sup> The results obtained revealed so promising that cromolyn-ibuprofen combination led up to the stage of phase III clinical trial.<sup>40-42</sup> Inspired by this strong evidence, aiming to overcome the limitations of the drug combination polypharmacological approach (*e.g.* complex administration regimen, risk of drug-drug interaction and side effects), and to

ameliorate the physical-chemical properties of the parent drugs, we design and synthesized a small set of cromolyn-(*S*)-ibuprofen multi-target “codrugs”.<sup>43</sup> Codrugs are single chemical entities conjugates potentially able to release the parent drugs by *in vivo* metabolism. With this in mind, cromolyn and the biologically active enantiomer *S* of ibuprofen were covalently joined in 1:2 ratio by selected linkers (ethanolamine, ethylene glycol, ethylenediamine) forming hydrolyzable bonds.<sup>43</sup> In this way, the codrugs, presenting parent drugs’ carboxylic acids masked by esters or amides, should be favored in bowel adsorption.<sup>44</sup> Moreover, if they are stable enough to reach unmodified the CNS, they should have easier BBB permeability in comparison with the parent drugs.<sup>44,45</sup> Thus, parent drugs could be released simultaneously, by codrug hydrolysis directly at central level, modulating different neuroinflammatory AD pathways and resulting in a synergistic effect (Figure 6).



**Figure 6.** Design of cromolyn-(*S*)-ibuprofen (1:2) codrugs by linking approach.

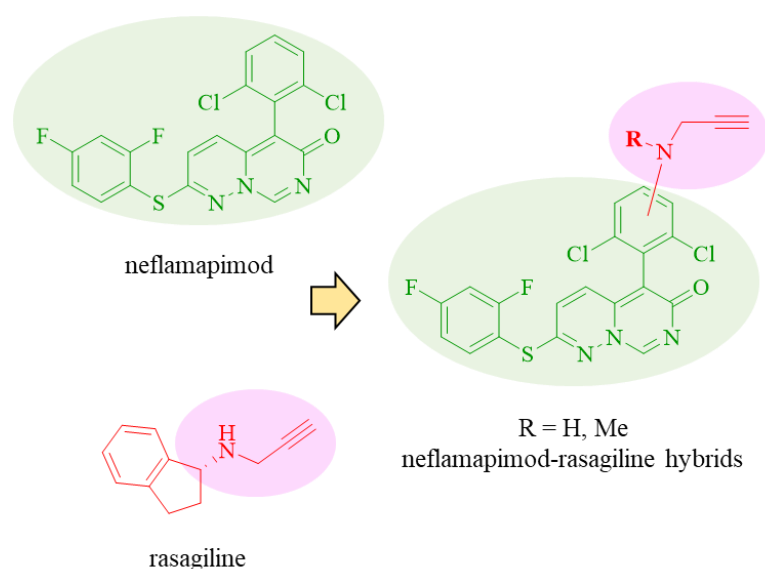
- Starting from the promising results obtained from the *in vitro* and *in vivo* investigation of the 1:2 cromolyn-(*S*)-ibuprofen codrugs,<sup>43</sup> the second objective of this thesis aimed to develop another small set of molecules that could produce an alternative *in vivo* ratio of cromolyn and (*S*)-ibuprofen. They were combined by a fusing approach to obtain codrugs with 1:1 ratio between the parent drugs. At first cromolyn’s carboxylic acid functions were masked by methyl or ethyl esters to benefit membrane permeation (bowel and BBB). Then, (*S*)-ibuprofen’s carboxylic acid was covalently bonded to the free hydroxyl function of cromolyn by a cleavable ester. In this way, we assume to overcome some limitations of the first codrug set. The lower molecular weight (MW) of the 1:1 cromolyn-(*S*)-ibuprofen codrugs could produce an enhanced BBB permeability.<sup>46</sup> (Figure 7).<sup>45</sup>



**Figure 7.** Design of cromolyn-(S)-ibuprofen (1:1) codrugs by fusing approach.

3. The third objective of this thesis took inspiration from neflamapimod (VX-745), a selective inhibitor of p38-MAPK alpha isoform (p38 $\alpha$ -MAPK) discovered by Vertex Pharmaceuticals. It was initially investigated for its application as anti-inflammatory in rheumatoid arthritis (RA) since p38 $\alpha$ -MAPK is a key kinase involved in inflammatory processes.<sup>47</sup> However, neflamapimod failed for RA therapeutic application because it demonstrated to significantly permeate the BBB. It was preferentially concentrated at the brain level detriment peripherally, causing considerable side effects on CNS.<sup>48</sup> Thus, aiming to exploit its good BBB permeability, in 2015 it was repurposed to target neuroinflammation in AD, and it is still under investigation in phase II clinical trial.<sup>49</sup> p38 $\alpha$ -MAPK is a key kinase involved in inflammatory processes, expressed both peripherally and at central level. For this reason, its inhibition could drive a beneficial anti-neuroinflammatory effect in AD. In addition to the main role in inflammatory pathways, p38 $\alpha$ -MAPK is also implicated in promoting apoptosis by p53 activation, synaptic dysfunction and, in response to oxidative stress, in favoring tau phosphorylation.<sup>50</sup> On the other side we were attracted from rasagiline, a selective monoamine oxidase B inhibitor (MAO-B) currently on the market for PD treatment. However, rasagiline demonstrated neuroprotective/neurorestorative activities in several *in vitro* and *in vivo* neurodegenerative models.<sup>51</sup> Thus, it was largely repurposed as a potential treatment in other neurodegenerative diseases, including a very recent clinical investigation in AD patients.<sup>52,53</sup> Such multiple effects of rasagiline seem to be attributed to its propargylamine fragment since propargylamine alone is also reported to be implicated

in neuroprotective, anti-apoptotic and anti-oxidative properties.<sup>54</sup> Thus, to combine synergically in single-molecules the anti-neuroinflammatory activity of neflamapimod and the neuroprotective/antiapoptotic effect of rasagiline a fragment integration approach was exploited. We designed and synthesized a small set of potential multi-target-directed ligands (MTDLs) introducing the propargylamine moiety on neflamapimod's scaffold. Aiming to maintain p38 $\alpha$ -MAPK inhibition we based on neflamapimod structure-activity relationship. Duffy *et al.* showed that every change on neflamapimod's scaffold leads to a significant reduction in its activity.<sup>55</sup> Moreover, considering neflamapimod-p38 $\alpha$ -MAPK crystal structure, there is only a solvent-exposed position.<sup>55</sup> Rasagiline's propargylamine fragment was introduced in that position, which is already reported in literature to well tolerate substituent introduction.<sup>56</sup> Thus, neflamapimod was de novo synthesized with an aniline function introduced on the scaffold. That aniline was exploited for introducing by nucleophilic substitution a propargylamine or a N-methylpropargylamine moiety. (Figure 8).



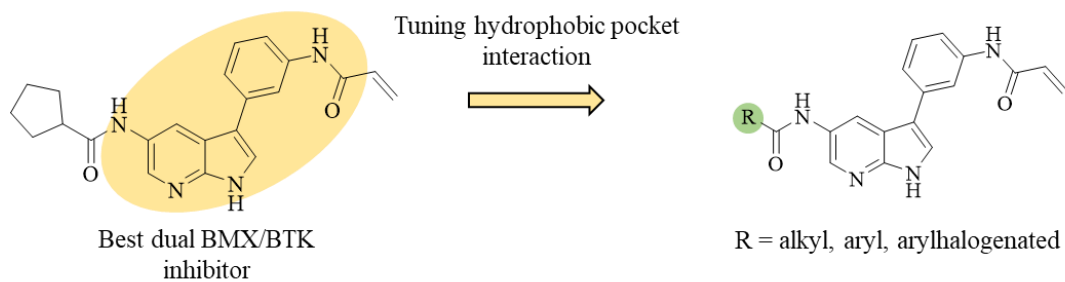
**Figure 8.** Design of neflamapimod-rasagiline hybrids by fragment integration strategy.

- The last objective of this PhD thesis was carried out at Tübingen University in Prof. Laufer and Prof. Gehring groups. The project focused on the optimization of covalent inhibitors for marrow tyrosine kinase on chromosome X (BMX). It is a non-receptor-type protein-tyrosine kinase and it is the last member discovered of the tyrosine kinase expressed in hepatocellular carcinoma (TEC) family.<sup>57</sup> Among the



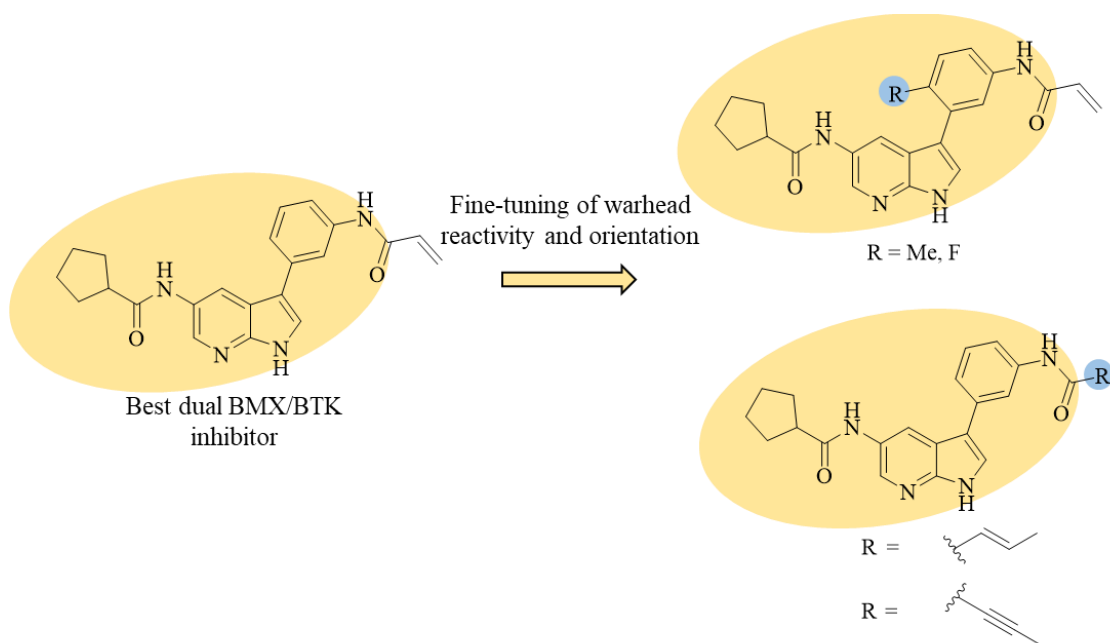
still not fully elucidated several pathways in which BMX could be involved, some evidence displayed its potential implication in CNS chronic inflammation, mediated by cytokine production.<sup>57</sup> Particularly, BMX was found upregulated *in vivo* rat model neuroinflammatory processes caused by traumatic brain injury.<sup>58, 59</sup> However, because of the reduced availability of selective BMX chemical probes, its role in health and disease is still not completely understood. Selective covalent inhibitors are taking hold not only in the drug discovery field but also as useful chemical probes.<sup>60</sup> Thus, the groups of Prof. Laufer and Prof. Gehring developed a new class of covalent BMX inhibitors derived from irreversible Janus kinase 3 (JAK 3) inhibitors.<sup>61</sup> These compounds were designed to target a non-conserved cysteine located in the solvent-exposed front region of the ATP binding pocket in  $\alpha$ D-1 position. Indeed, the 7-azaindole core series of the JAK3 inhibitors discovered targeted that cysteine and displayed also an inhibitory activity on BMX, which conserves the same  $\alpha$ D-1 residue.<sup>61</sup> Subsequently, by several modifications, some potent BMX covalent inhibitors were discovered (IC<sub>50</sub> in the nanomolar range), despite they showed a balanced activity on BTK, the closest TEC relative to BMX.<sup>61</sup> Starting from these promising results, the project focused on optimizing BMX covalent inhibitors by developing two different series of compounds.

- The first series of compounds was developed keeping unmodified the 7-azaindole core and the acrylamide warhead linked to the phenyl ring, in agreement with the most active covalent BMX/BTK inhibitors found.<sup>61</sup> Thus, to avoid the dual inhibitory profile on BMX and BTK, the 7-azaindole core series was expanded introducing different alkyl, aryl and aryl-halogenated substituents in position 5 where they could establish additional interactions with the hydrophobic pocket behind the threonine gatekeeper residue. Particularly, this pocket is slightly different from BTK because BMX presents Phe475 while BTK the Leu460. Thus, we aimed to exploit the N-acyl substituents to address the difference in the size of the pocket and to establish potential  $\pi$ -interactions to fine-tune BMX selectivity (Figure 9).



**Figure 9.** Design of a series of compounds by different N-acyl substituents in position 5 of the azaindole core to tune the interaction with BMX's hydrophobic pocket.

- The second series of compounds focused on fine-tuning the warhead reactivity and on optimizing the orientation of the aniline-warhead moiety positioned to the front pocket of the ATP binding site. Taking inspiration from the most potent aforementioned dual BMX/BTK inhibitors discovered by Forster *et al.*,<sup>61</sup> the acrylamide fragment was replaced with two different electrophilic warheads: the 2-butenamide and the 2-butyneamide. Moreover, to investigate how the phenyl ring orientation affects the warhead-  $\alpha$ D-1cystein interaction, a methyl or fluoro substituent was introduced in *ortho*-position of the phenyl ring with respect to the 7-azaindole introduction (Figure 9B).



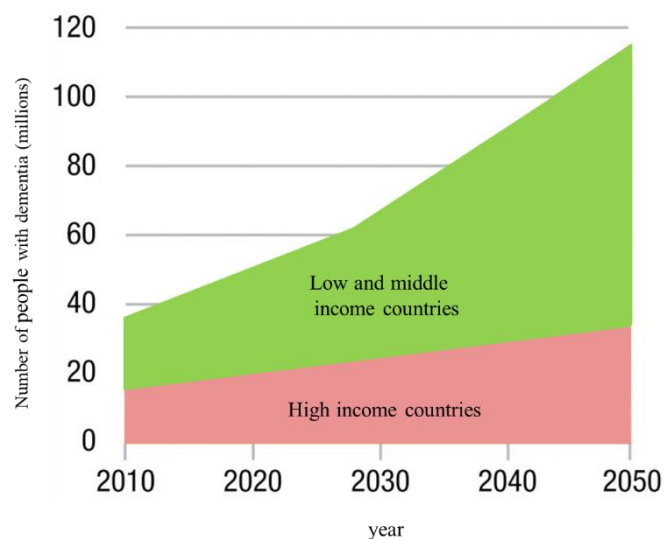
**Figure 10.** Design of a series of compounds tuning the electrophilic warheads' reactivity and orientation.

# Chapter 3



### 3. Alzheimer's disease

Alzheimer's disease (AD) is a chronic neurodegenerative disease that is the first cause of disability and dependency among older people globally. It is the most common form of dementia worldwide, contributing to 60-70% of cases, and it takes the seventh place among the causes of death.<sup>62</sup> Nowadays, more than 55 million people are affected by dementia, and about 10 million cases are registered every year with an expected incidence of 125% by 2050.<sup>62</sup> The most AD exposed fraction of the population are people older than 65. Thus, the increasing aging world population influences directly the increment of AD incidence. The main increment in AD diffusion is expected to hit low-income and middle-income countries, where the conditions of life are improving and dementia will affect up to 70% of people by 2050 (Figure 11).<sup>63</sup>



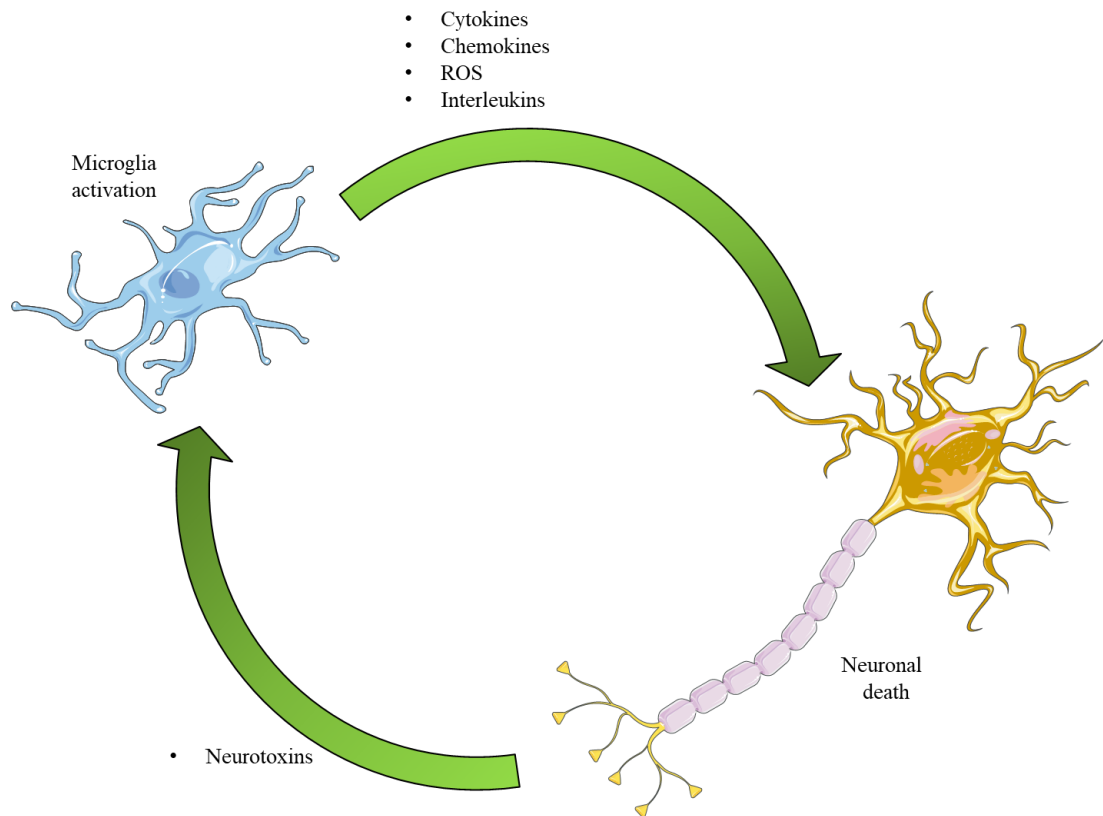
**Figure 11.** Alzheimer's disease global incidence expected by 2050. (adapted from <http://www.alz.co.uk/research/files/WorldAlzheimerReport.pdf>)<sup>64</sup>

The main areas of the brain suffering from AD are (i) the hippocampus, which plays a critical role in learning and memory processes, (ii) the amygdala, which regulates emotions, and (iii) the frontal cortex, involved in planning, executive function, expressive language, semantic and working memory.<sup>32</sup> Thus, among the various symptoms that characterize AD the main are cognitive function deterioration, progressive memory loss, difficulty with communication, loss of balance and coordination, weak muscles, including difficulty in speaking and swallowing.<sup>65</sup>

Like other neurodegenerative diseases, AD is characterized by a complex and multifactorial nature. The multiple pathological pathways that simultaneously occur in AD cooperate to drive the disease progression causing neuron, microglia, and astroglia alterations before that cognitive impairment is observed.<sup>66</sup> Focusing on AD pathogenesis, the cause longest considered responsible for the AD onset is the amyloid hypothesis, a neuron-centric, linear and quantitative model focused on a series of pathological consequences (*e.g.* tau hyperphosphorylation, synaptic dysfunction, inflammation, neuronal loss and, in the end, dementia) initiated by A $\beta$  plaques deposition.<sup>66</sup> Nowadays it is known that in parallel to the extracellular A $\beta$  accumulation, neuroinflammation,<sup>67</sup> alterations in the cerebral vessels,<sup>68</sup> aging, dysfunction of tau phosphorylation, and dysfunction in acetylcholine<sup>69</sup> balance contribute to the cognitive decline and the disease progression.<sup>70</sup> Moreover, many AD risk genes influence the microglial response pathways, the majors are apolipoprotein E (*APOE*) and *TREM2* gene. ApoE is the major component of lipoprotein, and its present both peripherally and in CNS. In CNS ApoE is present in A $\beta$  plaques contributing to the deposition of the A $\beta$  peptide. TREM2 is a protein expressed by microglia involved in A $\beta$  phagocytosis. TREM2 modifications may influence the binding of this protein to ApoE, negatively influencing the A $\beta$  clearance. In addition, several other proteins linked to the genetic risk of AD, act probably by ApoE and TREM2 signal modulation downstream, endocytosis, motility, and phagocytosis in microglia.<sup>70</sup>

### **3.1 Neuroinflammation in Alzheimer's Disease**

The high levels of inflammatory biomarkers shown by AD patients, and the identification of AD risk genes associated with the immune response evidenced the important role of neuroinflammation in AD pathogenesis. As previously mentioned (§ 1) neuroinflammation is a key process to protect the host from infections and injury in a relatively non-specific manner. At the same time, an increased systemic inflammation seems to increase the risk of developing AD.<sup>71</sup> Particularly, despite the relation between acute and chronic brain inflammation is still not clear, acute systemic inflammatory events that produce cytokines and TNF- $\alpha$  seem to predispose to long-term cognitive decline.<sup>71</sup> Moreover, when dysregulation and chronic activation of the inflammatory response take place, they drive negative effects on the host by extending the focal damage.<sup>71</sup>



**Figure.12** The correlation between microglial activation and neuronal death is characterized by microglia's release of neurotoxic or neuroprotective molecules. Neurotoxic molecules favor neuroinflammation and neuronal death, bringing to neurodegeneration. (Figure adapted from doi: 10.3892/mmr.2016.4948 ).<sup>72</sup>

Microglia activation is anyway essential for an appropriate phagocytosis function, brain homeostasis, neurogenesis, and neuronal survival. Both, acute and chronic microglia activation, can modulate neurogenesis. This suggests that the various molecules secreted from M1 or M2 microglia activation states, depending on the context, can promote or inhibit neurogenesis.<sup>73</sup> Moreover, the M2 anti-inflammatory neuroprotective state is characterized by the removal of apoptotic cellular fragments that seems to be a prerequisite for the repair functions, essential in conditions like neurodegenerative diseases.<sup>74</sup> On the other side, the damaging inflammatory consequences observed in AD, as in many other neurodegenerative diseases, are caused by the M1 microglia phenotype activation.<sup>74</sup> The M1 microglia inflammatory phenotype is sustained by A $\beta$  aggregates and tau NFTs that favor the M1 phenotype microglia activation and the consequent pro-inflammatory cytokines and chemokines production (Figure 12). Notably, it has been proposed that inflammation and microglia activation contribute as much or more to AD pathogenesis as do the plaques and tangles themselves.<sup>75</sup> Thus, APP, A $\beta$  deposition, and A $\beta$  clearance are closely influenced by the microglial balance between anti-inflammatory

and pro-inflammatory phenotype activation.<sup>74</sup> In particular, thanks to A $\beta$  similarity to some microorganisms' structures, microglia surface exposes receptors able to bind A $\beta$  and initiate the phagocytosis of A $\beta$  aggregates. As a response to receptor binding, by M2 phenotype activation, microglia starts to phagocyte A $\beta$  fibrils.<sup>75</sup> Consequently, these fibrils enter the endosomal/lysosomal pathway to be degraded by enzymes. In contrast, soluble A $\beta$  can be degraded by a variety of extracellular proteases. Especially in sporadic cases of AD, inefficient A $\beta$  clearance by microglia is identified as a major pathogenic pathway. Additionally, in a condition of AD chronic inflammation, while genes for pro-inflammatory factors result up-regulated, the expression of A $\beta$ -binding receptors is reduced.<sup>75</sup> Increased cytokine levels reduce A $\beta$  phagocytosis receptors, influencing negatively microglial phagocytic capacity, and TREM2 extracellular immunoglobulin domain mutations, compromising the phagocytic clearance of neuronal debris.<sup>75</sup> In healthy conditions, TREM2 promotes phagocytosis, proliferation, and survival. However, TREM2 variants, that are related to AD risk, impair the proper function of microglia in terms of activation, phagocytosis, inflammatory response, energy metabolism, and plaque deposition, influencing AD progression.<sup>73</sup> Particularly, AD pathogenetic pathways and the related markers on neuronal injuries, such as A $\beta$  plaques and NFTs, increase TREM2 expression.<sup>76</sup> Microglia response is ApoE-TREM2-dependent. Thus, ApoE acts as a chaperone for pathological species as it binds to A $\beta$ , in senile plaques, and NFTs, enhancing their degradation through microglial endocytosis and enzymatic activity.<sup>73</sup> TREM2 binding ApoE allows a more efficient microglia phagocytosis of A $\beta$ -ApoE complexes with respect to A $\beta$  alone. In this way, TREM2 influences the transition from homeostatic to neurodegenerative microglia phenotype, since in health conditions low APOE expression signaling is observed.<sup>73</sup>

Among the relevant classified targets for AD drug development, the Common Alzheimer's Disease Research Ontology (CADRO) underlines the central role of the neuroinflammatory hypothesis.<sup>77</sup> This awareness, together with the evidence that inflammation can be found in mild cognitive impairment subjects, even when A $\beta$  deposits are still not detectable, motivated many studies and AD clinical trials focused on anti-inflammatory drugs.<sup>78</sup> So far, aiming to investigate the modulation of the inflammatory process in AD patients, more than 30 drugs were studied (Table 1). Several anti-inflammatory drugs already on the market were repurposed to investigate their applicability in neuroinflammation modulation (Figure 13 and Table 1). NSAIDs were investigated aiming to interact with the arachidonic acid cascade. Moreover, NSAIDs are

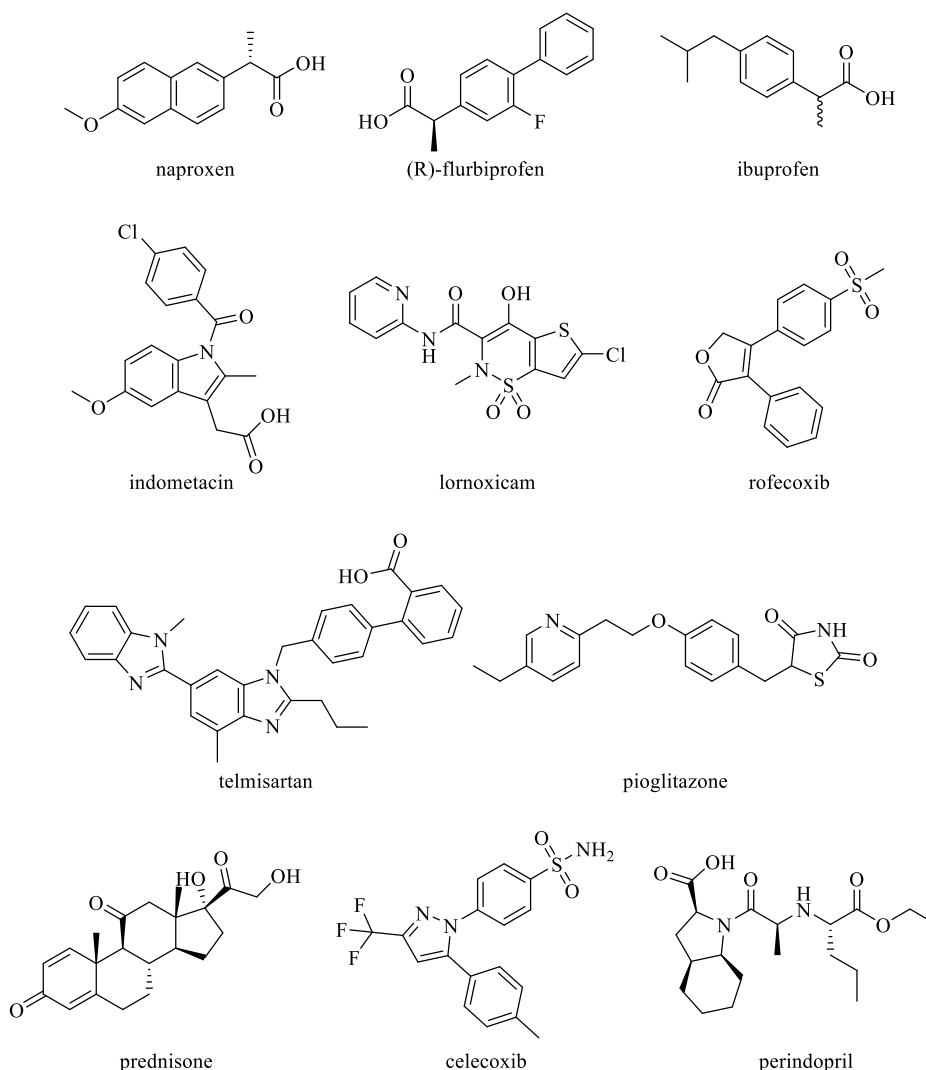


also involved in APP processing modulation, by stimulating the non-amyloidogenic  $\alpha$ -secretase.<sup>79</sup> Thus, the non-selective cyclooxygenase (COX) inhibitors naproxen,<sup>80-82</sup> (*R*)-flurbiprofen,<sup>83</sup> ibuprofen,<sup>84, 85</sup> indomethacin,<sup>86</sup> lornoxicam<sup>87</sup>, and the COX-2 selective inhibitors celecoxib<sup>82</sup> and rofecoxib<sup>81</sup> were investigated (Table 1).<sup>78</sup> Alternatively, the steroidal anti-inflammatory drug prednisone<sup>88</sup> was considered in an AD clinical trial. Prednisone demonstrates to suppress peripheral inflammatory markers without adverse effects in subjects with AD. Thus, the trial is based on exploiting synergically the potential anti-inflammatory and immunosuppressive effects that can be achieved by steroidal anti-inflammatory drugs.<sup>89</sup> Sargramostim,<sup>90</sup> is a human recombinant granulocyte-macrophage colony-stimulating factor that inhibits TNF-signaling, currently in use for leukemia treatment and repurposed against AD.<sup>91</sup> In addition, the fusion protein etanercept<sup>92</sup> which acts as TNF- $\alpha$  inhibitor, is in clinical use for rheumatoid arthritis (RA) but was also considered as AD-anti-inflammatory candidate in clinical trials.<sup>93</sup> Peroxisome proliferator-activated receptor- $\gamma$  (PPAR $\gamma$ ) agonists were studied since their stimulation displayed inflammatory response suppression. Thus, the angiotensin II receptors antagonist telmisartan,<sup>94</sup> on the market for hypertension treatment, was repurposed in AD since it demonstrate also to be a PPAR $\gamma$  agonist,<sup>95</sup> as well as pioglitazone,<sup>96</sup> an oral PPAR $\gamma$  agonist used as an anti-diabetic agent.<sup>97</sup> In the end, angiotensin-converting enzyme (ACE) inhibitor perindopril is currently repositioned in an AD clinical trial. An elevated level of ACE was observed in AD patients and perindopril<sup>98</sup> was displayed to reduce inflammatory mediators stimulation preventing cognitive impairment in AD mouse model.<sup>98</sup> Some beneficial effects were observed, as in the case of NSAIDs that showed a trend in reducing AD risk development,<sup>79</sup> and etanercept demonstrated a positive trend in patients treated by it.<sup>93</sup> However, there were no statistically significant changes in cognition, behavior, or global function. Thus, most of these trials failed, since they showed to be ineffective in delaying or ameliorating the pathological symptoms in patients affected by mild cognitive impairment or AD.<sup>78</sup>

However, the rising understanding of microglia's role in neuroinflammation along AD progression suggests a possible intervention by microglia-modulation: (i) by suppressing microglia pro-inflammatory properties to limit the deleterious effect of microglial activation; (ii) by modulating microglial phenotypic changes to promote microglia anti-inflammatory properties; (iii) by influencing microglial priming early in the disease process.<sup>99</sup>

**Table 1.** Drug candidates studied in clinical trials aiming to modulate neuroinflammation.<sup>100</sup>

Drug candidate	NCT number	Phase	Status
naproxen	NCT02702817	Phase II	Completed
	NCT00004845	Phase II + III	Completed
	NCT00007189	Phase III	Completed
(R)-flurbiprofen	NCT00322036	Phase III	Completed
	NCT00105547	Phase III	Completed
ibuprofen	NCT00239746	Phase I	Completed
	NCT01436188	Phase I	Completed
indometacin	NCT00432081	Phase III	Completed
lornoxicam	NCT01117948	Phase II	Completed
rofecoxib	NCT00004845	Phase II	Completed
celecoxib	NCT00007189	Phase III	Completed
prednisone	NCT00000178	Phase III	Completed
sargramostim	NCT01409915	Phase II	Completed
	NCT04902703	Phase II	Ongoing
etanercept	NCT00203320	Phase I	Completed
	NCT00203359	Phase I	Completed
	NCT01716637	Phase I	Completed
	NCT01068353	Phase II	Completed
pioglitazone	NCT00982202	Phase II	Completed
	NCT01931566	Phase III	Completed
	NCT02284906	Phase III	Completed
telmisartan	NCT02471833	Phase I	Ongoing
	NCT02085265	Phase II	Ongoing
perindopril	NCT02085265	Phase II	Ongoing

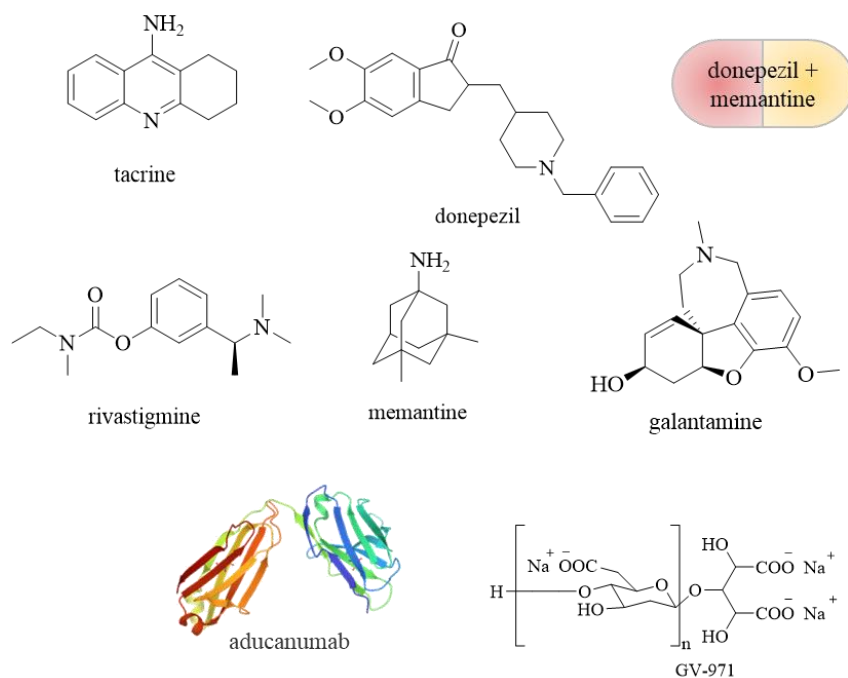


**Figure 13.** Structure of some drugs repurposed for AD treatment aiming to modulate neuroinflammation.

### 3.2 Drugs on the market to treat Alzheimer's disease

More than a hundred years ago the clinical psychiatrist and neuroanatomist, Alois Alzheimer, described for the first time “A peculiar severe disease process of the cerebral cortex”. However, for the first treatment that demonstrated efficacy against AD, we had to wait for 1993, when tacrine, was approved by Food and Drug Administration (FDA). Tacrine is a reversible acetylcholinesterase inhibitor (AChEi) that demonstrates cognitive improvement in AD patients.<sup>101</sup> However, it was withdrawn from the market in 2013 due to its correlation to liver toxicity.<sup>102</sup> Nevertheless, it paved the way for research into new therapies that aim to stop or slow the disease progression. After tacrine other 6 drugs were approved by FDA, donepezil, rivastigmine, and galantamine, that act by reversible inhibition of acetylcholinesterase (AChE);<sup>103</sup> memantine, a non-competitive antagonist of the N-metil-D-aspartato (NMDA) receptors;<sup>104</sup> the fixed-dose combination donepezil

+ memantine, and the last approved sodium oligomannate (GV-971) and aducanumab. Sodium oligomannate was approved in China in 2019, but FDA gave it the Investigational New Drug (IND) Approval only in 2020, after a successful Phase III clinical study in the US.<sup>105</sup> It is a mixture of linear acidic oligosaccharides from dimers to decamers that originate from the brown *algae*. GV-971 acts by reconstituting the gut microbiota, reducing bacterial metabolite-driven peripheral infiltration of immune cells into the brain, inhibiting A $\beta$  aggregation, and inhibiting neuroinflammation in the brain (Figure 14).<sup>106</sup> The newest drug controversially approved by FDA is aducanumab. It is an anti-amyloid antibody discovered by Biogen. It selectively binds to amyloid  $\beta$  fibrils and soluble oligomers and showed a reduction of A $\beta$  plaques in AD patients' brains.<sup>107</sup> Nevertheless, the evidence of cognitive benefit is not clear. For this reason, European Medicines Agency (EMA) refused aducanumab approval considering the data produced by the clinical studies insufficient. Indeed, the link between the A $\beta$  plaques reduction and the clinical improvement has not been well established. Moreover, the safety of the drug was controversial since abnormalities were observed in brain scan images of some patients and some of them suffered from swelling or bleeding.<sup>108</sup>

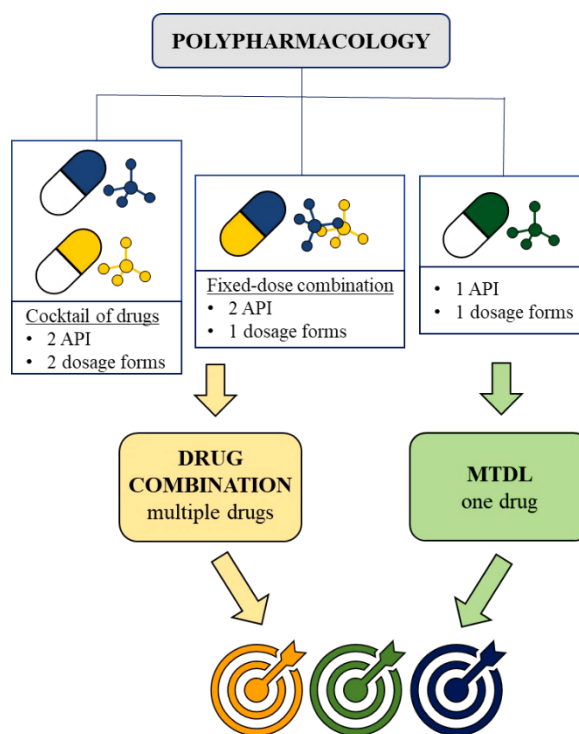


**Figure 14.** Drugs discovered for AD treatment. Notably, tacrine was withdrawn difrom the market because of its hepatotoxicity. Aducanumab was controversially approved by FDA but not by EMA which refused it.

Unfortunately, all the mentioned drugs have only a symptomatic effect. Thus, as previously highlighted (see § 3), the burdensome global impact of AD makes the need for new effective therapy developments increasingly urgent. Despite the strong motivation, so far across all types of AD therapies, the failure rate is more than 99%, and for disease-modifying therapies, the failure rate is 100%.<sup>109</sup> Among the reasons that may be considered responsible for the failures of so many AD clinical trials there are the too late disease stage in which the therapy is started, the incorrect drug dosage, the wrong treatment target, and the inadequate understanding of the complex AD pathology.<sup>110</sup>

### 3.3 Polypharmacology in Alzheimer's disease

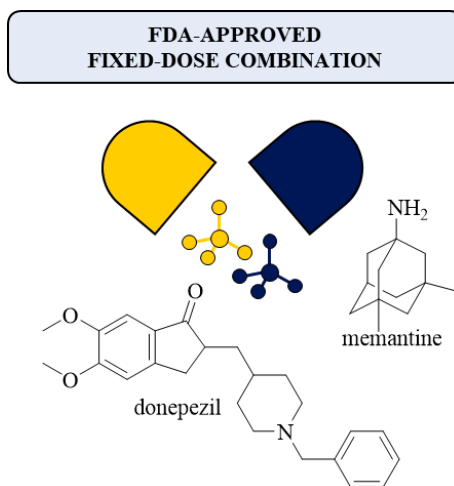
The concept of “magic bullets”—drugs, firstly introduced by Paul Erlich referred to drugs that hit specifically their proposed targets. This approach inspired many drug discovery studies resulting in the successful treatment of many human diseases.<sup>111</sup> However it doesn't seem similarly winning for the treatment of complex neurodegenerative diseases. Biological systems understanding pointed out the presence of a robust network of redundant pathways and alternative compensatory signaling routes that cooperate in physiological and pathological neurological processes.<sup>112</sup> This aspect assumes a crucial value, especially in complex and multifactorial disease such as AD, where the design of a potential drug candidate aiming to hit only one specific target assume a reductive meaning. Neurodegeneration is the result of the systemic collapse of brain physiological networks. Thus, it is improbable that the classical paradigm “one drug-one target-one disease” can restore the physiological situation.<sup>113</sup> Contrariwise, “polypharmacology”, focuses on simultaneous modulation of more targets involved in different pathological pathways aiming to obtain a synergistic effect, seems the most promising strategy.<sup>113</sup> The means to achieve polypharmacology are mainly two: multiple drugs binding to multiple targets (*i.e.*, drug combinations) and one drug binding to multiple targets (*i.e.*, multi-target-directed ligands (MTDLs)) (Figure 15).<sup>114,115</sup> Although the known multifactorial nature of AD, the drugs available on the market (see § 3.2) are small molecules that act on a single target (*e.g.* AChE, NMDA receptors) able only to mitigate AD symptoms.



**Figure 15.** Therapeutic possibilities to apply a polypharmacological approach. (Figure adapted from doi: 10.1002/med.21699)<sup>115</sup>

In a multifactorial pathologic condition, such as AD, the inhibition of one pathway is normally compensated by the higher activation of other pathways. This may produce resistance and result in the necessity of a higher dose, increasing the risk of side effects, as a consequence of off-target modulation.<sup>116</sup> Thus, the simultaneous modulation of multiple targets by one or more chemical entities is also positively correlated to the concept of lower dose usage.<sup>117</sup>

Polypharmacology based on multiple (combinations) or single (MTDLs) active pharmaceutical ingredients (APIs), may consider various options.<sup>115</sup> Polypharmacology by drug combinations is widely used in clinical practice. It is obtained by two or more APIs combined in a therapeutic regimen to give a drug cocktail or a fixed-dose combination. A drug cocktail is a combination of different dosage forms, each one containing a different API, while a fixed-dose combination refers to a single-dosage form containing multiple APIs (Figure 16).<sup>118</sup> Particularly, the only fixed-dose combination approved by the FDA for the symptomatic treatment of AD goes back to 2014, and it combines, in one capsule, the AChE inhibitor (AChEI) donepezil, and the NMDA receptor blocker memantine (Figure 16).<sup>119</sup>

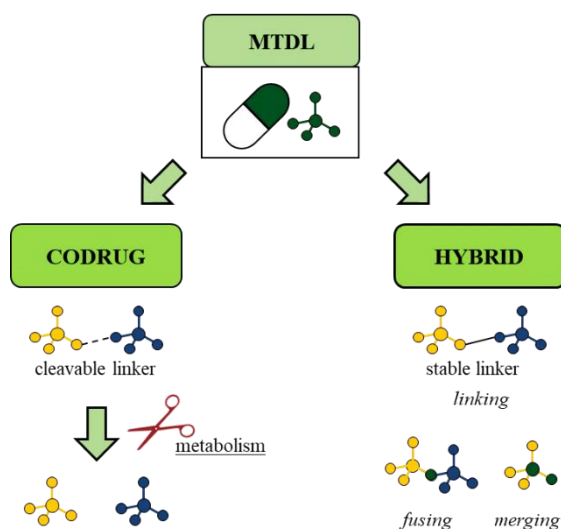


**Figure 16.** The only fixed-dose combination approved by FDA to treat AD. (Figure adapted from doi: 10.1002/med.21699)<sup>115</sup>

The use of a cocktail of drugs usually requires a quite complex therapeutic regimen in terms of the number of administrations daily. Concerning the use of a single API, it could expose polypathological patients to a higher risk of side effects by drug-drug interaction or displacement from plasma protein binding.<sup>120</sup> However, a personalized posology is permitted and the translation from the pre-clinical to the clinical phase is usually faster than for a completely new chemical entity.<sup>120</sup> Indeed, only experimental evidence of the additive or synergic effects of two known existing drugs by appropriate *in vitro* and *in vivo* models are required.<sup>121</sup>

On the other hand, a fixed-dose combination strategy, while maintaining the risk of pharmacokinetic interactions, could provide some advantages that could positively influence the compliance of patients, especially in the case of AD.<sup>120</sup> Despite the improved treatment adherence is still controversial, the simplified treatment regimen of a once-daily capsule and the possibility to sprinkle the capsule onto soft foods may favor the compliance of AD patients. With respect to the cocktail of drugs, it is particularly true in the case they manifest dysphagia or limited caregiver interaction.<sup>122</sup> The balance of the pro and cons in the combination therapies, led to consider it a successful clinical strategy to treat AD, as demonstrated by various symptomatic and disease-modifying applications of combination therapies under investigation in clinical trials.<sup>115</sup>

As opposed to the combination therapies there are MTDLs, a single API in single-dosage forms. MTDLs are single molecular entities designed to potentially modulate more pathological pathways resulting in a synergic effect.<sup>123</sup> From a structural point of view, they can be divided into two main classes: codrugs and hybrids (Figure 17).<sup>115</sup>



**Figure 17.** Two different possibilities to apply the MTDL strategy. (Figure adapted from doi: 10.1002/med.21699)<sup>115</sup>

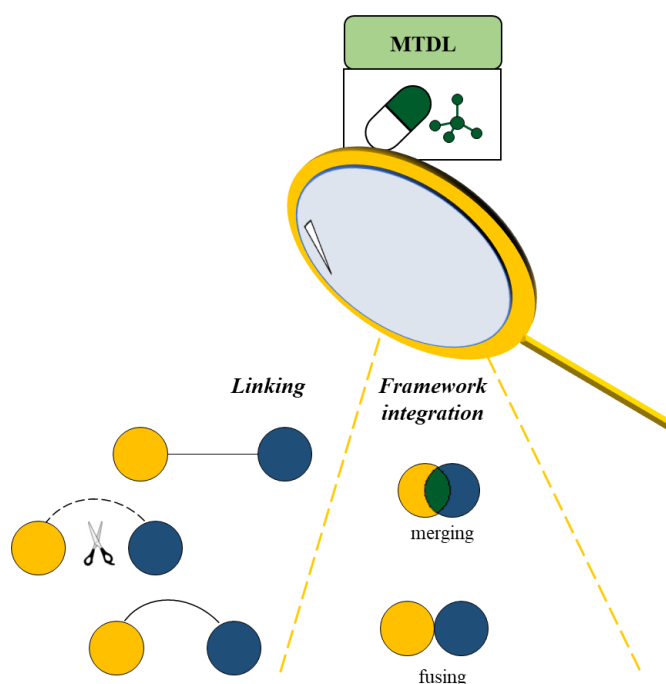
Codrugs consist of two-parent drugs chemically linked together, mainly with the aim of improving the drug delivery properties of one or both drugs.<sup>124</sup> Codrugs are inactive chemical entities until the parent drugs are released by hydrolysis. This could provide a high selectivity if codrugs show stability in the systemic blood circulation and then they are hydrolyzed where they should explicate the therapeutic effect.<sup>125</sup> In fact, the design of codrugs focuses on combining the starting chemical entities via bonds hydrolyzable by the drug metabolism. Thus, parent drugs, only after enzymatic biotransformation of the codrug, can individually modulate multiple pathways in the same target cells and at the same time. In this way, the polypharmacological effect can be produced by delivering at the same moment and directly at the site of action, the active APIs.<sup>125, 126</sup>

Hybrids are composed of the active pharmacophores of two or more diverse drugs via drug-structures overlap or permanent (non-cleavable) bonds.<sup>127</sup> They exhibit the multi-target effect by acting as a single chemical entity on multiple pathways simultaneously without undergoing hydrolysis.<sup>115</sup> In this case, only a single API is used for the modulation of multiple pathways thus, in addition to an easier therapeutic regimen, patient compliance is favored. Moreover, considering risk/benefit balance, the risk of drug-drug and protein-drug interactions is abolished and the study of pharmacokinetics and pharmacodynamics should be significantly easier when referring to a single API instead of a combination of two or more of them.<sup>120, 127</sup> Unfortunately, despite the great potential of the MTDL strategy, as demonstrated by various cases, MTDLs clinical translation is still challenging.<sup>115</sup>



### 3.3.1 Strategies to design multi-target-directed ligands

Although the MTDL approach is quite recent, many drugs in clinical use show a multi-target mode of action that was explained retrospectively.<sup>123</sup> Aiming at rationally designing potential MTDLs, one of the most exploited medicinal chemistry strategies is molecular hybridization.<sup>127</sup> Morphy and Rankovic were the first to comprehensively describe a rationale design of MTDLs based on combining molecular frameworks containing the pharmacophoric elements responsible for the modulation of each target of interest.<sup>114</sup> From a practical point of view, MTDLs can be obtained by linking strategy or framework integration (Figure 18).<sup>127</sup>



**Figure 18.** MTDL can be designed by linking or framework integration (*e.g.* merging or fusing) strategies. (Figure adapted from doi: 10.2174/1568026619666190619115735)<sup>127</sup>

For the linking strategy, the presence of a linker is key to connect by chemical bonds the selected pharmacophores. Depending on its chemical features, the linker can be a flexible chain or a rigid structure, linking the pharmacophores of interest by stable or hydrolyzable bonds.<sup>127</sup> In some cases, the linking strategy represents the only possibility of MTL design; this is the case of selected pharmacophores that don't present common features, in many cases giving rise to codrugs.<sup>115</sup> To note, if the MTDLs are designed to act against neurodegenerative diseases, the combination of two or more frameworks through

a linker leads to molecules with increased MW with respect to the starting structures. This is a crucial aspect to consider, as it can affect membrane permeation, especially BBB, compromising the reach of the desired targets.<sup>128</sup> Moreover, the privileged way of drug administration for patient compliance is oral thus, the influence of MW bioavailability can't be ignored.<sup>129</sup> Hybrids' design doesn't need a linker, so it overcomes the issue of a high MW and fusing or merging strategies can be applied (Figure 18).<sup>114</sup> Fusing strategy involved an overlapping of a common atom between the considered pharmacophores while the merging strategy can be applied only if the selected pharmacophores share a high grade of homology and can be extremely integrated.<sup>113</sup>

However, to design effective MTDLs is of crucial importance to select the right target combination. The selected targets should be validated by consistent investigation via *in vitro* and *in vivo* models, demonstrating additive or synergic effects resulting from a concomitant modulation of the targets.<sup>115</sup> Moreover, another critical factor is the achievement of a balanced modulation for each target excluding undesired interactions with the off-targets.<sup>130</sup>

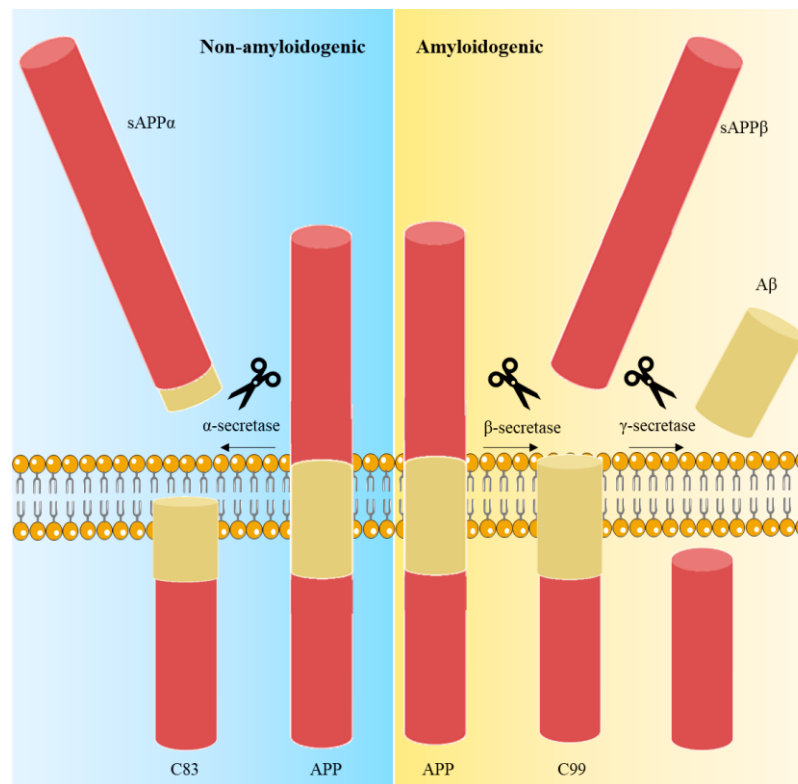
The concepts discussed in paragraphs 3.3 and 3.3.1 have been largely discussed in the following review articles:

- Ivasiv V, **Albertini C.**, Goncalves AE, Rossi M, Bolognesi M. L. Molecular hybridization as a tool for designing multitarget drug candidates for complex diseases. *Curr. Top. Med.Chem.* 2019, 19(19), 1694-1711.
- **Albertini C.**, Salerno A., De Sena Murteira Pinheiro P., Bolognesi M. L. From combinations to multitarget-directed ligands: A continuum in Alzheimer's disease polypharmacology. *Med. Res. Rev.* 2020, 41(5), 2606-2633.

### **3.4 Project 1: cromolyn-ibuprofen conjugates as potential “codrugs” for Alzheimer's disease treatment**

#### **3.4.1 The amyloidogenic pathway**

As already mentioned AD is a complex disease influenced by a multiplicity of pathways that cooperate toward disease progression. Amyloid plaques and NFTs of hyperphosphorylated tau are the two histopathological hallmarks of AD. Amyloid accumulation is the primary of a series of events that lead to neurofibrillary degeneration and dementia.<sup>33</sup> Amyloid plaques are generated by insoluble A $\beta$  peptides that deposit extracellularly. A $\beta$  precursor is usually processed in constitutive secretory pathways, thus, A $\beta$  deposits can also be found as an aging consequence in many cognitively normal people.<sup>131</sup> The imbalance between A $\beta$  production from APP processing and its clearance leads to A $\beta$  accumulation and the formation of plaques.<sup>132</sup> The main difference between these A $\beta$  deposits and those found in AD patients is their distribution. In cognitively normal individuals A $\beta$  deposits are limited to the cerebral cortex, the basal ganglia the thalamus, and the hypothalamus. In AD patients, A $\beta$  deposits are found in the midbrain, brain stem, and cerebellum, in addition to the previously mentioned regions.<sup>133</sup> However, the role of A $\beta$  deposits in AD is still controversial, because of their presence in the brain of healthy elderly people with normal cognition. A $\beta$  peptide is generated from the sequential cleavage of APP by enzymes called  $\alpha$ -,  $\beta$ - and  $\gamma$ -secretases.<sup>33</sup> The APP processing can involve a non-amyloidogenic pathway and an amyloidogenic pathway (Figure 19). That non-amyloidogenic is usually the prevalent pathway and involved APP cleavage by  $\alpha$ -secretase, it occurs within the A $\beta$  region, precluding the formation of A $\beta$  peptide. The  $\alpha$ -secretase activity forms the 83-amino-acid C-terminal fragment (C83), which is retained in the cell membrane, and a large amino (N)-terminal fragment (sAPP $\alpha$ ) which is secreted into the extracellular medium. Consequently, C83 is cleaved by the  $\gamma$ -secretase, producing a short fragment p3.<sup>33</sup> The alternative proteolysis site of APP leads to the amyloidogenic pathway and A $\beta$  generation. The initial step is mediated by the  $\beta$ -secretase that produces the 99-amino-acid C-terminal stub (C99) within the membrane and the sAPP $\beta$ , which is released into the extracellular space. The following cleavage of sAPP $\beta$  by the  $\gamma$ -secretase produces an A $\beta$  peptide of 40 or 42 residues depending on the cut position, giving the A $\beta$ <sub>40</sub> or A $\beta$ <sub>42</sub> peptides, respectively (Figure 19).<sup>33</sup>



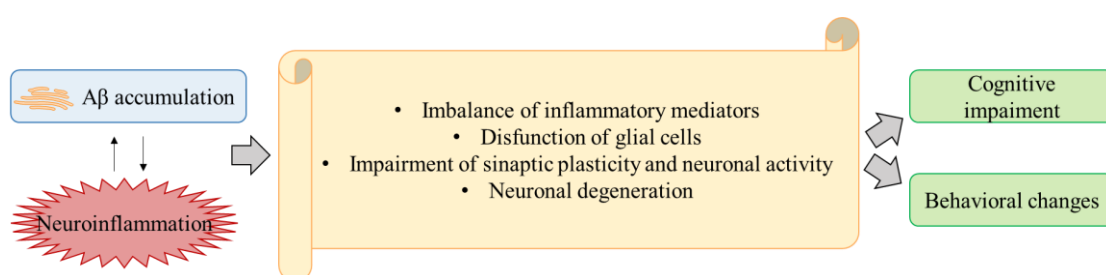
**Figure 19.** Non-amyloidogenic and amyloidogenic APP processing. (Figure adapted from doi: 10.1038/s41380-021-01249-0).<sup>33</sup>

The A $\beta$ <sub>42</sub> variant is more hydrophobic and more prone to fibril formation than A $\beta$ <sub>40</sub>. Moreover, it is also the more abundant isoform found in the cerebral plaques. Monomeric A $\beta$  is produced as a non-toxic monomer but, driven by misfolding processes, it easily aggregates to form oligomers, protofibrils, and insoluble fibrils that assemble in multimeric complexes.<sup>134</sup> Moreover, A $\beta$  fibril surfaces can catalyze the formation of A $\beta$  oligomers and A $\beta$  oligomers have been observed surrounding A $\beta$  fibrils. These are the most pathological form of A $\beta$ , and the main ones responsible for the neurodegenerative neurofibrillary pathology, the neuroinflammation, and the consequent disruption of learning, memory, and synaptic function.<sup>134</sup>

### 3.4.1.1 A $\beta$ pathophysiology and neuroinflammation

The relation between A $\beta$  and glial cells, which are the main players in the inflammatory responses, currently represents a hot research topic. Several efforts are devoted to determining whether neuroinflammation can activate and maintain the A $\beta$  dyshomeostasis development. *In vitro* microglia experiments have demonstrated a double

role in A $\beta$  clearance regulation. Microglia surround plaques and fibrils, creating a physical barrier to protect neurons from A $\beta$  toxicity. Microglia may contribute to A $\beta$  clearance (A $\beta$  protofibrils are more significantly internalized than monomers), as well as to limiting plaque growth and accumulation.<sup>135</sup> On the other hand, A $\beta$  protofibrils can be released from microglia microvesicles, increasing the extracellular A $\beta$  pool and the neuroinflammation.<sup>136</sup> Thus, A $\beta$  species stimulate the microglia release of proinflammatory cytokines and decrease the synthesis of anti-inflammatory cytokines.<sup>137</sup> In turn, proinflammatory cytokines increase the levels of extracellular A $\beta$  and the amyloid cleavage of APP, by increasing the  $\gamma$ -secretase activity (Figure 20).<sup>33</sup>



**Figure 20.** In AD A $\beta$  promotes neuroinflammation and consequently affects microglial function, neuronal function, and survival, driving the cognitive decline. Neuroinflammation, in turn, aggravates A $\beta$  accumulation and the consequent inflammatory response. (Figure adapted from doi: 10.1021/acchemneuro.8b00402)<sup>78</sup>

To remark on the microglia's role in AD, recent genetic studies highlighted that mutations in several genes, highly expressed in microglia, can be strictly related to AD late-onset insurgence. One of the strongest single-allele genetic risk factors is TREM2 R47H mutation, which leads to TREM2 loss-of-function.<sup>138</sup> Particularly, TREM2 modulates microglial functions by regulating the release of inflammatory cytokine in response to A $\beta$  plaques. Its expression increases microglia phagocytosis while TREM2 variants or downregulation reduce the A $\beta$  phagocytic ability of microglia.<sup>139</sup>

In light of the existing evidence, various commercial anti-inflammatory drugs, (*e.g.* NSAIDs), were tested to determine their microglia-mediated anti-inflammatory effect, and their reduced-A $\beta$  production and amyloid load in the brain, by  $\gamma$ -secretase inhibition.<sup>78</sup> Moreover, many clinical trials, still ongoing or completed, involved the administration of anti-inflammatory agents to modulate AD pathological processes by glial modulation, eicosanoid, and cytokine signaling (§ 3.1).<sup>78</sup>

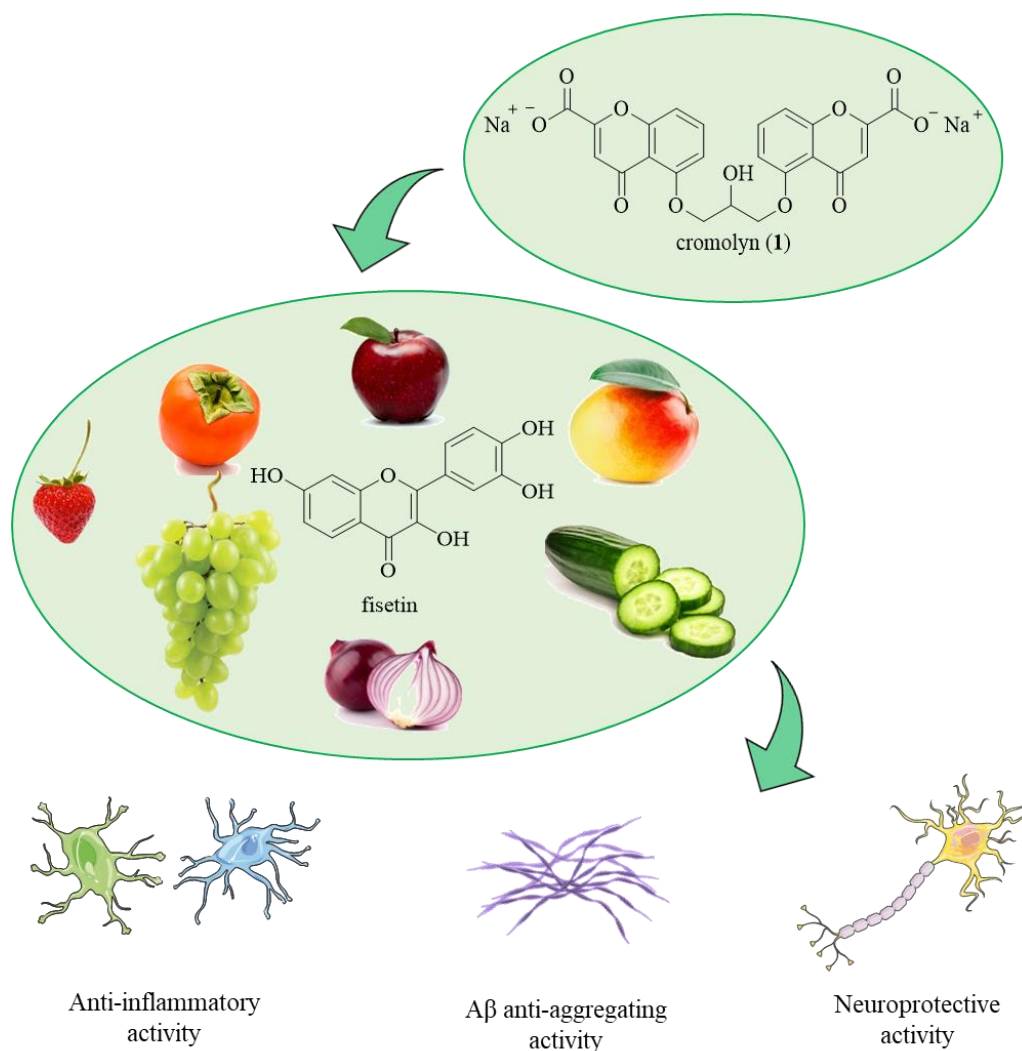
However, despite neuroinflammation has been extensively investigated and it is still considered a research priority by Alzheimer's Drug Discovery Foundation,<sup>140</sup> the

molecular control of microglia and astrocytes cell transition during the disease development is not completely understood, as well as the role of cytokines and complement factors in AD progression.<sup>78</sup> This lack of information contributes to hampering the design and the development of effective strategies to target neuroinflammatory glial processes. At the same time, unfocused anti-inflammatory strategies indiscriminately targeting glial cells failed to show effectiveness by globally attenuating glial cell functions.<sup>137</sup> Moreover, from the early AD stages complex pathogenesis and neuroinflammation occur. Despite the clear awareness of the existing correlation between A $\beta$  plaques formation, AD progression, and neuroinflammatory responses, the knowledge of the crucial mechanisms is still limited because of the difficult early-stage diagnosis and the lack of clinical validation of relevant biomarkers.<sup>139</sup>

### 3.4.2 Cromolyn and its potential application for AD treatment

Cromolyn (**1**, Figure 21), also known as disodium cromoglycate, is a drug currently approved to treat bronchial asthma, allergic rhinitis, and certain allergic eye conditions.<sup>141</sup> Because of its poor oral absorption (5%-0.5% of the administered dose), it was formulated as inhalation powder to improve its bioavailability.<sup>142</sup> Interestingly, **1**'s weak gastrointestinal membrane permeation has led to other therapeutic uses, which avoid any risk of systemic side effects. **1** is freely water-soluble and it is administered by oral capsules or solutions to treat food allergies. It transits unmodified in the gastric tract and accumulates at the bowel level, where it exerts the therapeutic effect.<sup>143</sup> The administration of **1** via collyrium is an effective treatment for allergic conjunctivitis. However, also in this case, **1**'s systemic absorption is negligible because of its low permeability of the eye's mucous membranes.<sup>144</sup>

Despite the mechanism of action of **1** is still not completely elucidated, it was observed to be effective as anti-inflammatory only when administered before antigen exposure. This evidence suggested that **1** acts as mast-cell stabilizer, by preventing the subsequent release of inflammatory mediators, including histamine and leukotrienes, usually responsible for allergic symptoms and bronchoconstriction.<sup>145</sup> **1** is a chromone heterocycle dimer with structural similarity to fisetin, a flavonoid found in various vegetables and fruits. Fisetin demonstrated multiple potential therapeutic effects in neurological disorders,<sup>146</sup> including neuroprotective, anti-inflammatory, and A $\beta$  anti-aggregating activities in AD *in vivo* models (Figure 21).<sup>147</sup>



**Figure 21.** Cromolyn (**1**), which is structurally related to fisetin, exerts anti-inflammatory, anti-aggregating, and neuroprotective effects in AD model.

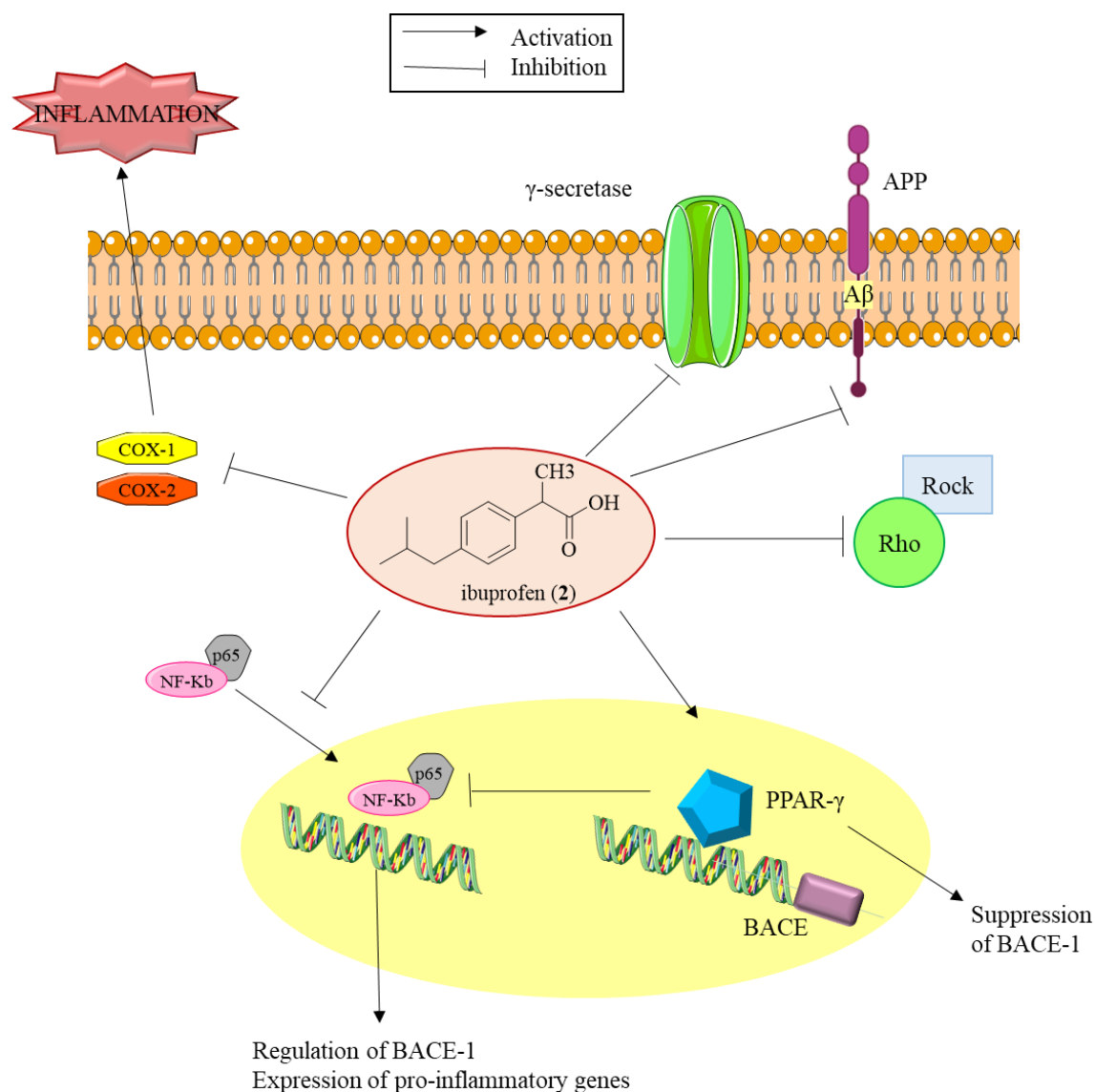
This evidence, together with the inhibition of multiple hematopoietic and phagocytic cells and anti-inflammatory activity demonstrated in an *in vivo* mast-cell-deficient mouse model, motivated the investigation of **1** for a potential application against AD.<sup>148</sup> Particularly, recent studies pointed out that **1** can prevent A $\beta$  aggregation and intensify the phagocytosis/clearance of neurotoxic A $\beta$ <sub>42</sub> by microglial cells with a consequent reduction in fibril-prone A $\beta$ <sub>42</sub>, anti-inflammatory, and neuroprotective effects.<sup>45,149</sup> Moreover, **1** was found to considerably reduce the microglia production of pro-inflammatory mediators,<sup>38</sup> such as cytokines and chemokines, and to promote neurite outgrowth.<sup>150</sup> The demonstrated ability of **1** in modulating multiple pathways involved in AD led to consider it a good candidate to be investigated in AD clinical trials.<sup>41, 42</sup>

### 3.4.3 Ibuprofen

Ibuprofen (**2**, Figure 22) is an NSAID commonly used to treat inflammatory conditions such as headache, dental pain, menstrual cramps, muscle aches, arthritis, common cold, or flu. It is a propionic acid derivative with analgesic and antipyretic effects by cyclooxygenase (COX) non-selective inhibition. The constitutive COX-1 and the inducible COX-2 isoforms are key enzymes in the anti-inflammatory response mediated by prostaglandin synthesis via the arachidonic acid pathway. To note, **2** presents a chiral center at C-2 adjacent to the carboxyl group, thus it exists as two enantiomeric forms.<sup>151</sup> Despite *S* is the only active enantiomer, while the *R* is inactive on COX-inhibition, ibuprofen is usually orally administered as a racemic mixture. In vivo it follows a rapid and complete absorption and the 2-arylpropionyl-coenzyme A epimerase converts a substantial amount of the *R* enantiomer (50-60% of the dose administered) in *S*.<sup>151</sup> Several NSAIDs, including **2**, demonstrated a trend in reducing AD risk (§ 3.1) via multiple mechanisms independent from COX inhibition, such as promoting non-amyloidogenic APP processing,<sup>79</sup> inhibiting of mitochondrial Ca<sup>2+</sup> overload. Particularly, epidemiological studies associated the treatment with NSAIDs with a reduced risk of developing AD.<sup>152</sup> For these reasons, and considering the crucial role of neuroinflammation in neurodegeneration, they were investigated as potential drug candidates in neurodegenerative diseases, including AD (§ 3.1).

The application of **2** for AD treatment, was largely investigated in *in vitro* and *in vivo* studies. In transgenic mouse models, it showed suppression of microglia activation and proinflammatory cytokines production, together with a reduced expression of the pro-inflammatory enzymes COX-2 and iNOS, and a reduced A $\beta$  accumulation.<sup>153, 154</sup> The modulation of the amyloids pathways by **2** seems to be due to multiple activities; (i) reduction of the A $\beta$  proteolytic enzymes  $\beta$ -secretase 1 (BACE1) and  $\gamma$ -secretase,<sup>153</sup> (ii) inhibition of the small GTP-binding protein Rho and its associated kinase ROCK<sup>155</sup> and (iii) agonism on the peroxisome proliferator-activated receptor- $\gamma$  (PPAR $\gamma$ ), a nuclear transcriptional regulator that reduces BACE1 expression (Figure 22).<sup>156</sup> These results were so encouraging that, together with the well-known safety profile, motivated the clinical investigation of **2** in AD patients alone (NCT00046358, NCT00239746 and NCT01436188)<sup>84,157,158</sup> or in combination with cromolyn (**1**) (NCT02547818 and NCT04570644).<sup>40,41,159</sup>





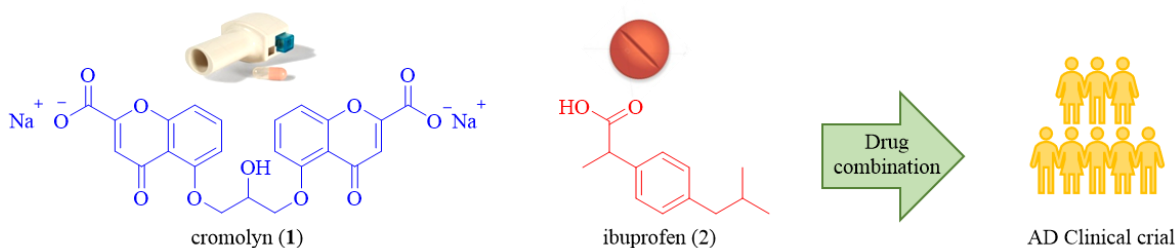
**Figure 22.** Molecular targets of ibuprofen in AD pathogenesis. (Figure adapted from doi: 10.1007/s00018-007-6516-1)<sup>160</sup>

Among the NSAIDs repurposed in AD clinical trials, from epidemiological and laboratory evidence **2** has one of the strongest rationales. The effect of the administration of **2** to AD patients started for the first time in a phase IV clinical trial in 2002 associated with active gastroprotection to minimize the risk of adverse gastrointestinal effects.<sup>157</sup> After 18 months of treatment **2** demonstrated to be well-tolerated, and a weak beneficial trend was observed. These results were considered not enough to consider **2** a disease-modifying drug but encouraging for further studies in the primary prevention of AD.<sup>157</sup> Subsequently, two clinical trials started the phase I intending to investigate if the expression of Aβ biomarker in the cerebrospinal fluid (CSF) could variate after the

administration of **2** (NCT00239746 and NCT01436188). Minimal fluctuations of the CSF level of A $\beta$  were observed.<sup>161</sup> More recently **2** was also investigated combined with **1**. Preclinical *in vivo* studies in an AD mouse model showed that **1+2** drug combination was able to increase the therapeutic effects provided by the two drugs alone. Particularly, the main effect observed involved the induction of the neuroprotective M2 microglia phenotype. The study demonstrated that **1** could promote A $\beta$ <sub>42</sub> uptake in microglia more efficiently when it is combined with **2**. Thus, A $\beta$  levels were reduced thanks to microglia by A $\beta$  phagocytosis activation. Then, thanks to the well-known profiles of both involved drugs, the quick switch from the preclinical studies to the clinical phase was obtained.<sup>39</sup> Thus, two clinical trials to define the pharmacokinetic/pharmacodynamic of **1+2** combination in healthy volunteers (NCT04570644) and its safety and efficacy profiles in AD patients (NCT02547818) were carried out.<sup>41, 159</sup>

### 3.4.4 Cromolyn-ibuprofen codrugs rationale of the project

As mentioned in the previous paragraphs (§ 3.4.2 and § 3.4.3) cromolyn (**1**) and ibuprofen (**2**) are two anti-inflammatory FDA-approved drugs, currently on the market and with a well-known safety profile. Both drugs, in *in vitro* and *in vivo* studies, showed potential in AD pathological pathways modulation, especially inflammatory and amyloid pathways.<sup>149, 162</sup> All these considerations, together with the evidence that the polypharmacological approach is one of the most promising ways to treat complex AD, laid the foundation for the investigation of a drug combination of **1** and **2**.<sup>39</sup> *In vivo* studies in an AD transgenic mouse model highlighted that **1**, alone or in combination with **2**, could be effective in both early- and later-stage cases of the disease. Particularly, the administration of **1** - and of **1** in combination with **2**- promoted anti-aggregation and pro-clearance mechanisms by enhancing microglia anti-inflammatory phenotype.<sup>39</sup>

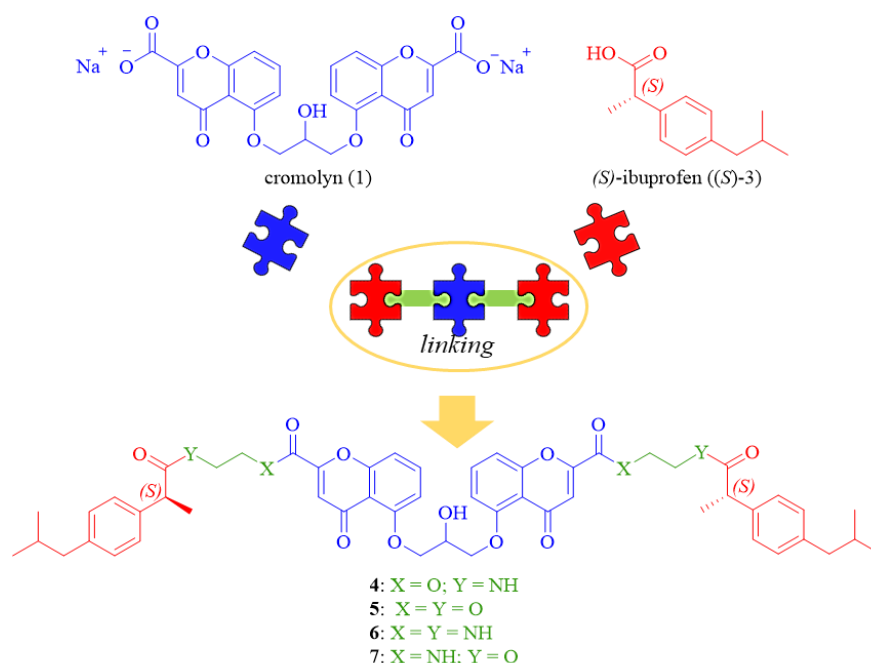


**Figure 23.** Cromolyn-ibuprofen drug combination was investigated at the clinical level in NCT04570644 and NCT02547818 clinical trials. (Figure adapted from doi: 10.1002/med.21699)<sup>115</sup>

Given that, **1** and **2** were very recently investigated in phase I and II clinical trials (NCT04570644) to explore pharmacokinetic/pharmacodynamic profiles in healthy volunteers,<sup>41</sup> and in phase III clinical trial (NCT02547818) to prove the safety of the drug combination in early AD patients.<sup>40,42</sup> In both clinical trials the two drugs were administrated in different pharmaceutical forms (Figure 23). The well orally adsorbed **2** was administrated by oral tablet while, considering the poor oral absorption, **1** was administrated by inhalation powder to enhance the amount of drug able to reach the CNS.<sup>41, 42</sup> Indeed, even if olfactory epithelium is present in only 3% of the nasal cavity, the intranasal administration through olfactory delivery provides an alternative for direct brain targeting.<sup>163</sup> However, the efficient assumption of an inhalation powder requires perfect coordination between deep exhalation-spray-inspiration, a sequence that may be compromised by the apraxia affecting most AD patients.<sup>164</sup> Thus, an alternative route of administration (*e.g.*, oral or transdermic) might provide a better patient compliance.<sup>165</sup> Taking inspiration from these promising clinical trials and with these pharmacokinetic limitations in mind, we designed and synthesized a small set of conjugates, aiming to convert the cromolyn-ibuprofen drug combination into MTDLs “codrugs”.<sup>115</sup> Codrugs are conjugates formed by two synergic therapeutic compounds chemically linked by *in vivo* metabolically cleavable bonds, to mainly improve the drug delivery properties and the pharmacokinetics profile of one or both parent drugs.<sup>124</sup> In this way, parent drugs may be released by codrug hydrolysis directly in the site of action simultaneously, overcoming the limits of drug combination (*e.g.* drug-drug interaction, multiple drug administrations, different concentrations or times of the drugs in the site of action) and reducing the gastrointestinal and cardiovascular side effects of chronic NSAIDs assumption.<sup>124, 166</sup> In this case, the conjugation strategy might improve the oral absorption of **1**, which presents high water solubility and low permeability by the gastrointestinal tract (bioavailability < 1%).<sup>167</sup> Particularly, the conversion of the two carboxylic acids into esters has been suggested as an effective prodrug strategy for oral delivery.<sup>167</sup> Moreover, the masking of conjugates’ acidic functionalities could enhance the BBB permeability of both parent drugs.<sup>44,45</sup>

### 3.4.4.1 Cromolyn-ibuprofen codrugs: design of a small set of 1:2 cromolyn-ibuprofen conjugates

With this in mind, we developed the first cromolyn-ibuprofen codrugs. We linked cromolyn (**1**) and the pharmacologically effective *S* enantiomer<sup>151</sup> of the racemic ibuprofen (*(S)*-**3**), with the aim of reducing the number of possible stereoisomers of the final compounds. Thus, we designed and synthesized a small set of cromolyn-*(S)*-ibuprofen conjugates (**4–7**) as potential codrugs to modulate neuroinflammatory and amyloid pathways in AD (Figure 24).<sup>43</sup>



**Figure 24.** Design of cromolyn-*(S)*-ibuprofen (1:2) conjugates by linking strategy. (Figure adapted from doi: 10.3390/molecules26041112)<sup>43</sup>

The new set of codrugs was designed by a linking approach. The carboxylic groups of the parent drugs **1** and *(S)*-**3** were coupled to form metabolically cleavable bonds (esters or amides) exploiting ethylene glycol, ethylenediamine, or ethanolamine linkers (Figure 24). The final conjugates **4–7** were designed as symmetrical conjugates that after their hydrolysis *in vivo* could produce a 1:2 parent drug ratio.<sup>43</sup> We were aware that **4–7** display a higher MW with respect to parent drugs, and physicochemical properties that might hamper drug-likeness.<sup>46</sup> Nevertheless, these disadvantages could be balanced by the increased lipophilicity by masking the carboxylic acid functions of the parent drugs.

Moreover, ester and amide prodrugs that are stable enough to allow their hydrolysis when they reach the brain level, demonstrated to increase CNS targeting.<sup>168</sup>

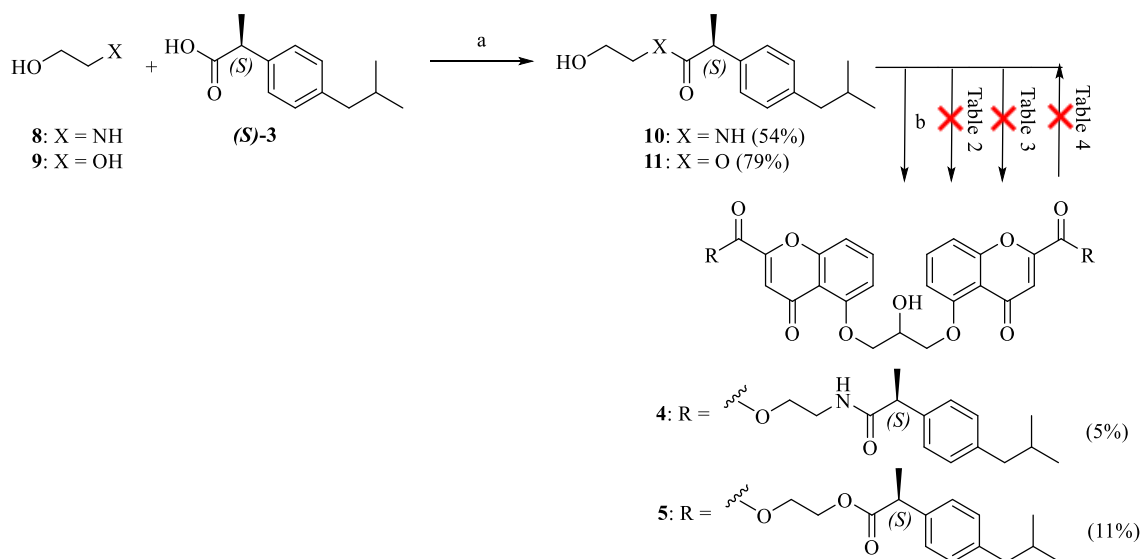
The concepts discussed in this paragraph and the data reported in the following paragraphs (§ 3.4.4.1, § 3.4.4.2, and § 3.4.4.3) have been fully discussed in the article:

- **Albertini C**, Naldi M., Petralla S., Strocchi S., Grifoni D., Monti B., Bartolini M. and Bolognesi M. L. From combinations to single-molecule polypharmacology— cromolyn-ibuprofen conjugates for Alzheimer’s disease. *Molecules*. 2021, 26, 1112.

### 3.4.4.2 Chemistry

Conjugates **4–5** were synthesized according to Scheme 1.<sup>43</sup> To obtain the desired diethanolamide **4** and diester **5**, intermediates **10** and **11** were synthesized. **10** was obtained by the selective formation of an amide between the amino group of the ethanolamine (**8**) and the carboxylic group of (**S**)-**3**. The reaction was performed by Steglich-type conditions in presence of 1-ethyl-3-(3-dimethylaminopropyl)carbodiimide) (EDC) as coupling reagent and 4-dimethylaminopyridine (DMAP) as catalyst.<sup>169</sup> To avoid the formation of dimers, **8** was used in large excess (7 equivalents). Moreover, despite both functions, hydroxyl and amine groups, might react with (**S**)-**3**’s carboxylic acid, ester formation was not observed. Indeed, the formation of the amide is preferred thanks to the highest nucleophilicity of the amine function with respect to the hydroxyl group.<sup>170</sup> **11** was synthesized by ethylene glycol (**9**) mono-esterification with the carboxylic group of (**S**)-**3**. The reaction was performed under similar EDC/DMAP Steglich coupling conditions;<sup>169</sup> also in this case, to prefer the monoesterification of **9** avoiding the OH monoprotection, the linker was added in substantial excess (7 equivalents).

**Scheme 1.** Synthetic strategy for the synthesis of conjugates **4-5**.



**Reagents and conditions:** a) EDC, DMAP, DCM, rt, 24 h; b) cromolyn (**1**), HOBt, EDC, DMF, cationic exchange resin [Amberlite IR120 (H<sup>+</sup>)], microwave irradiation (60 °C, 200W, 1 h).

With **10** and **11** in hand, we investigated the ideal conditions for linking them to **1**. Particularly, to obtain the final compound **5**, various synthetic strategies were explored. Firstly, the linking between intermediate **11** and **1** was investigated by activating the carboxylic acids of **1** under different coupling conditions in dimethylformamide (DMF) according to Table 2. Unfortunately, none of the reported strategies permitted to obtain the desired product.

**Table 2.** Coupling conditions investigated to link **11** to **1**.

Entry	Coupling reagent	T	t	Heating conditions
1	hydroxybenzotriazole (HOBt)/EDC	rt	22 h	/
2	1,1'-carbonyldiimidazole (CDI)	60 °C	2 h	conventional
3	CDI	60 °C	30 min	microwave

Subsequently, aiming to increase the reactivity of the carboxylic groups of **1**, their conversion into acyl chlorides was investigated. The reaction was performed at room temperature (rt) and in reflux conditions according to Table 3, using thionyl chloride (SOCl<sub>2</sub>) as both acylating agent and solvent. This allowed to overcome the insolubility of **1** in common organic solvents.<sup>171</sup> Then, the excess of SOCl<sub>2</sub> was removed, the residue was solubilized in dichloromethane (DCM) and 2 eq of intermediate **11** were added in presence of triethylamine (TEA) at rt.

**Table 3.** Activation conditions of **1** by thionyl chloride.

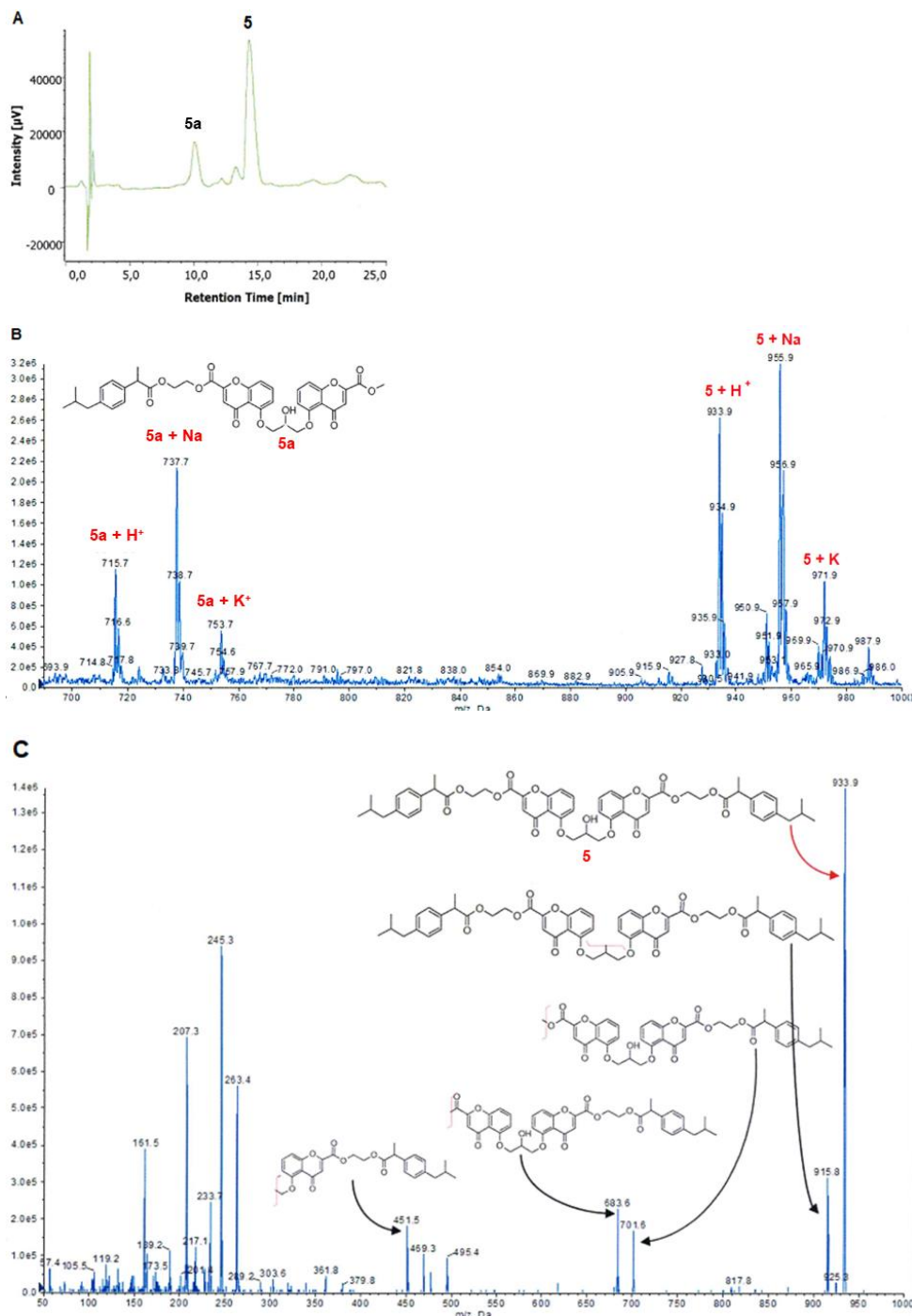
Entry	T	t	Reflux conditions
1	rt	22 h	/
2	80 °C	2 h	conventional reflux
3	80 °C	2 h	pressure tube

However, also these attempts revealed ineffective and didn't afford the desired compound **5**. Driven by the several unsuccessful results, an alternative synthetic strategy was explored. The introduction of the ethanolamide linkers on **1**'s carboxylic acid functionalities, was investigated by using bromoethanol.<sup>172</sup> Despite different reaction conditions were tested, even in this case, the desired intermediate was not obtained (Table 4).

**Table 4.** Conditions investigated for introducing the ethanolamide linkers on **1**'s carboxylic acids.

Entry	Solvent	T	t	Heating conditions
1	dimethylsulphoxide (DMSO)	70 °C	24 h	conventional
2	DMSO	120 °C	80 min	microwave
3	bromoethanol	60 °C	30 min	conventional
4	bromoethanol	60 °C	30 min	microwave

Finally, assuming that the low reactivity of **1** (sodium salt) could be due to its low solubility in organic solvents, including DMF, a cation-exchange resin was exploited to obtain, *in situ*, the cromoglycholic acid, a more soluble form of **1**. In this way, although in low yield, the target diester **5** was obtained by a coupling reaction catalyzed by hydroxy benzotriazole (HOBt) and EDC in DMF, in presence of cation-exchange resin,<sup>173</sup> under microwave irradiation.<sup>174</sup>



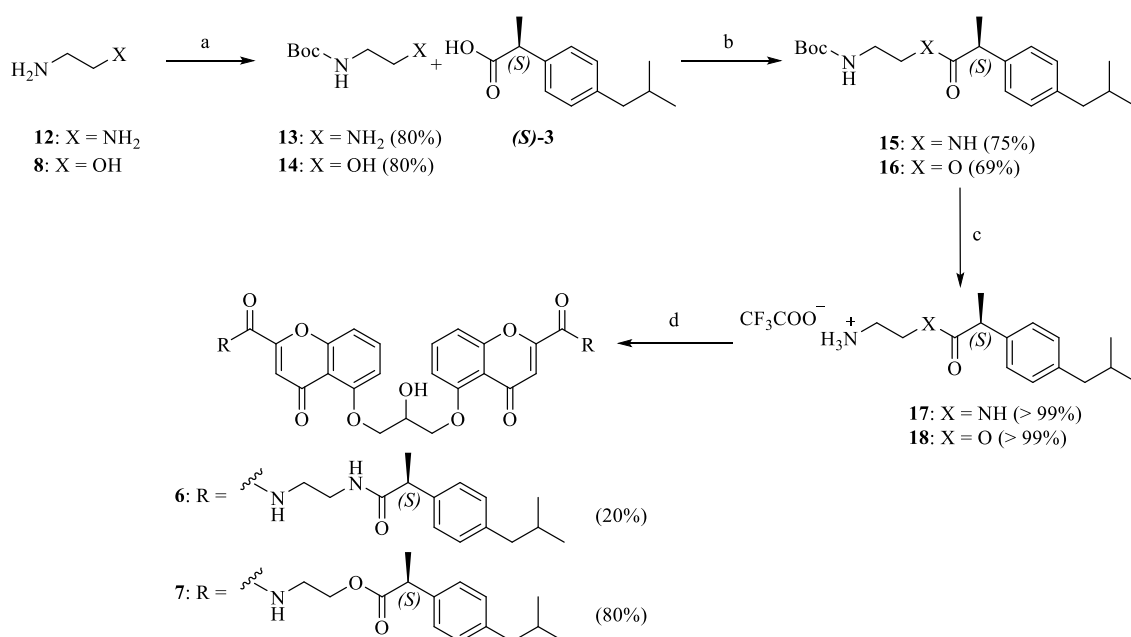
**Figure 25.** LC-UV (A), ESI-MS (B) and ESI-MS/MS (C) analysis of the coupling reaction to obtain compound **5**.

Compound **4**, in turn, was synthesized starting from intermediate **11** following the analog procedure of **5**. Also in this case ESI-MS confirmed the final product structure (Figure 25C). In both cases, compounds **4** and **5** demonstrated a tendency to degradation in the reaction environment, by the formation of the methylated side product (**5a** figure 25B, data not shown for compound **4**). This aspect probably negatively influenced the yield of the final reactions. Unfortunately, diethanolamide **4**, differently from **5**, couldn't be



obtained with more than 85% purity. In addition, HPLC analysis performed at different times showed a decreasing trend in **4**'s purity (from 85% to 75%), confirming its low stability. For this reason, it was excluded from the biological evaluation described in the following paragraph.

**Scheme 2.** Synthetic strategy for the synthesis of conjugates **6–7**.

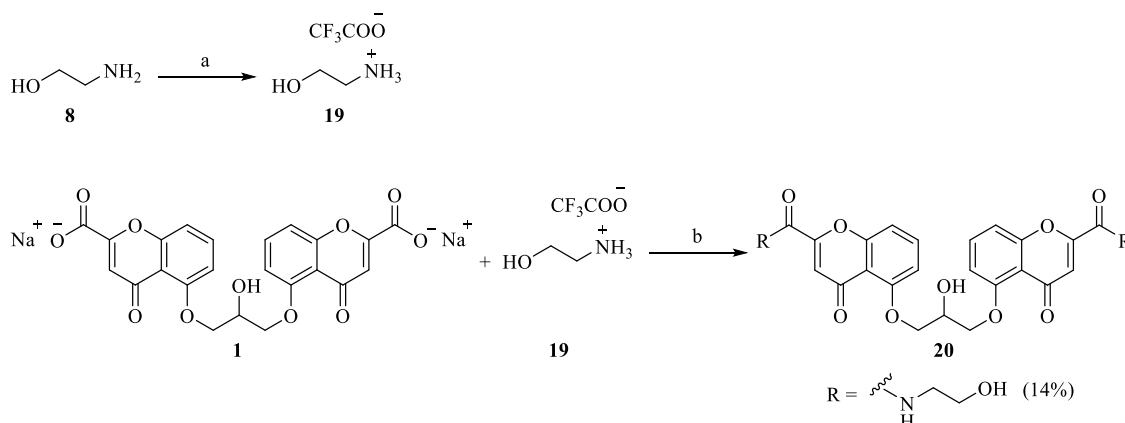


**Reagents and conditions:** a) (Boc)<sub>2</sub>O (0 °C), DCM, rt, 2 h; b) EDC, DMAP, DCM, rt, 24 h; c) TFA (0 °C), DCM, rt, 2 h; d) cromolyn (**1**), HOBT, EDC, DMF, rt, 24 h.

Compounds **6** and **7** were synthesized by following a similar route described in Scheme 2.<sup>43</sup> The amino group of ethylenediamine (**12**) or ethanolamine (**8**) was selectively protected by tert-butyloxycarbonyl (Boc) group, to give intermediates **13** or **14**. Then, the free reactive function, amine or hydroxyl, respectively, was linked to the carboxylic group of (**S**)-**3** by ester or amide bond formation via an EDC/DMAP Steglich coupling.<sup>169</sup> The obtained compounds **15** and **16** were quantitatively deprotected in acidic conditions by trifluoroacetic acid (TFA), to provide the corresponding **17** or **18** trifluoroacetate salts. These intermediates, reacting with **1** (sodium salt), by coupling reaction with HOBT and EDC in DMF, gave the desired compound **6** or **7**. In this case, we assume that the acid form of **1** (the cromoglycic acid) is formed *in situ* by **10** disodium ionic exchanges with the trifluoroacetate counterion of **15** or **16**. In a second moment, **20**, one of the possible hydrolysis products of the diethanolamide **7**, was synthesized to be used as control

compound in the A $\beta$ <sub>42</sub> self-aggregation assay (Scheme 3). As the first step ethanolamine **8** was treated with TFA to obtain the corresponding trifluoroacetic salt. This first step was necessary to generate the trifluoroacetate counter-ion (CF<sub>3</sub>COO<sup>-</sup>) to sequestrate the sodium in the following step. Then, compound **20** was synthesized by diammidation of **1** and the ethanolamine **19** under coupling conditions by HOBt and EDC in DMF. The desired compound was extracted with n-butanol.

**Scheme 3.** Synthetic strategy for the synthesis of metabolite **19**



Reagents and conditions: a) TFA, DCM, rt, 1.5 h; b) HOBt, EDC, DMF, rt, 24 h.

All the compounds were characterized by <sup>1</sup>H NMR and <sup>13</sup>C NMR. In addition, the tested compounds were analyzed by high-resolution mass spectrometry (HRMS) and HPLC demonstrating at least 95% purity  $\lambda = 254$  nm (see Chapter 6).

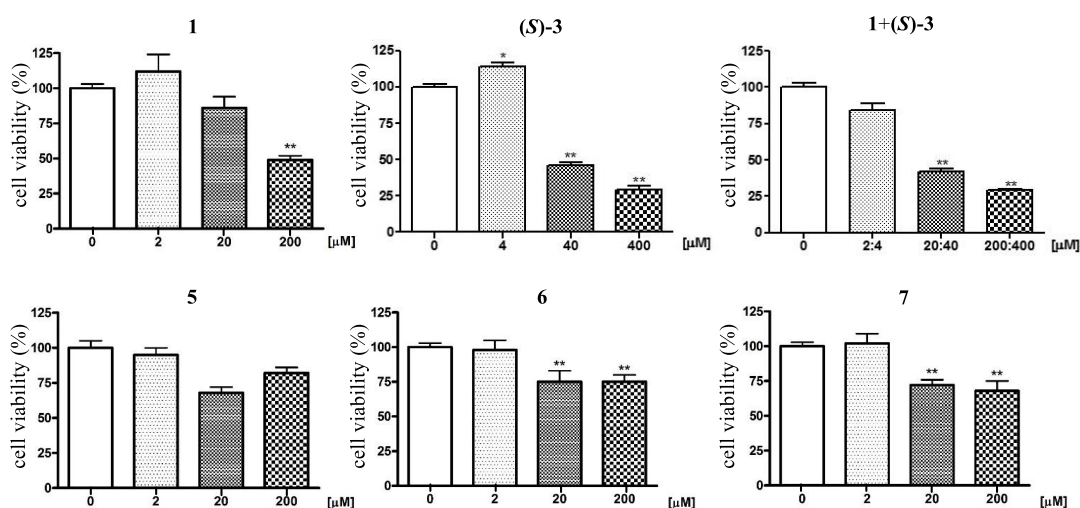
### 3.4.4.3 Results and discussion

The results discussed in the following were obtained by our collaborators at the Pharmacy and Biotechnology (FaBiT) Department of the University of Bologna, Prof. Bartolini's group (stability, permeation and A $\beta$  anti-aggregating assays), Prof. Monti's group (cellular assays) and Prof. Grifoni's group (*in vivo* assays).

#### Neurotoxicity evaluation in primary neurons

Considering the importance of drug cytotoxicity evaluation since the early step of drug development,<sup>175</sup> neurotoxicity assay in rat cerebellar granule neurons (CGNs) was assessed. Primary neurons were treated with increasing concentrations (0, 2, 20, 200  $\mu$ M) of **5-7** conjugates and the results were compared with those obtained treating cells with

parent drugs **1** and (*S*)-**3**. Moreover, to mimic the metabolites potentially released by codrugs' hydrolysis *in vivo*, the parent drug combination in 1:2 ratio (**1**+*(S)*-**3**) was also tested (Figure 26) and the cell viability was evaluated by MTT (3-(4,5-dimethylthiazol-2-yl)-2,5-diphenyltetrazolium bromide) assay.<sup>43</sup> While **1** showed toxicity only at 200  $\mu$ M concentration, (*S*)-**3** and their 1:2 combination (**1**+*(S)*-**3**) resulted toxic on CGNs cells already at respectively 40  $\mu$ M and 20:40  $\mu$ M concentrations. Particularly, conjugates **5–7** (2  $\mu$ M), as well as parent drugs **1** (2  $\mu$ M) and (*S*)-**3** (4  $\mu$ M), were not toxic, while the corresponding **1**+*(S)*-**3** combination (2:4  $\mu$ M) decreased cell viability of about 10%. At higher concentrations (20  $\mu$ M and 200  $\mu$ M), **5–7** demonstrated lower cytotoxicity (around 30%) than **1**+*(S)*-**3** combination (respectively 20:40  $\mu$ M and 200:400  $\mu$ M). Thus, in these experimental conditions, codrugs **5–7** showed lower neuronal toxicity better than **1**+*(S)*-**3** combination.<sup>43</sup>

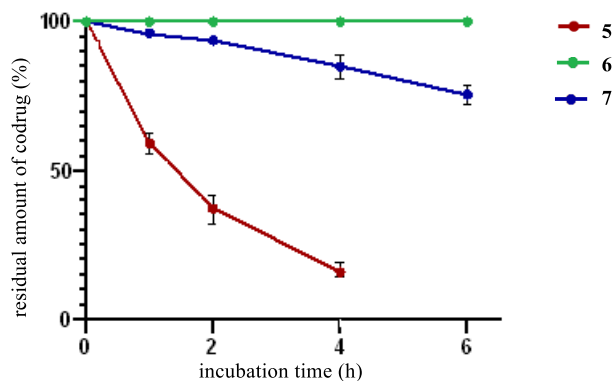


**Figure 26.** Neurotoxicity evaluation of conjugates **5–7** in comparison with controls **1**, (*S*)-**3** and their 1:2 combination in primary CGNs. Cell viability was determined by MTT assay. Results are expressed as percentages of controls and are the mean  $\pm$  SE of at least 3 independent experiments, each run in triplicate. \*  $p < 0.05$  \*\*  $p < 0.01$  compared to control conditions (0  $\mu$ M), Dunnett test after one-way ANOVA. (Figure adapted from doi: 10.3390/molecules26041112)<sup>43</sup>

### Stability in human plasma

Aiming to select codrugs potentially able to reach the CNS unmodified and to release the parent drugs (**1** and (*S*)-**3**) directly where AD pathogenetic pathways occur, **5–7**'s stability in human plasma was analyzed. Each conjugate was incubated in plasma at 37  $^{\circ}$ C and at selected times (0, 2, 4, 6 h) the samples were collected and analyzed by liquid

chromatography-mass spectrometry (LC-MS) (Figure 27). As expected from the literature, the nature of the chemical bonds between the linker and the parent drugs deeply influence the stabilities of the conjugates.<sup>125, 126, 176</sup>



**Figure 27.** Stability of **5-7** conjugates in human plasma. (Figure adapted from doi: 10.3390/molecules26041112)<sup>43</sup>

Consequently, diamide **6** exhibited the highest plasma stability at all time points, while diester **5** showed the lowest stability. Interestingly, ethanolamide **6** is stable for more than 75% after 6 h of incubation. On this basis and considering the no toxic profile of all the compounds, we selected the most stable diamide **6** and ethanolamide **7**, for the following studies.<sup>43</sup>

#### Internalization of compounds **6** and **7** in microglial cells

**Table 5.** Predicted pharmacokinetic parameters of compounds **6** and **7** in comparison with the parent drugs.<sup>43</sup>

Compound	MW	logP	logD	pKa	N°charges
<b>1</b>	512	1.92	-5.57	4.91	2
<b>(S)-3</b>	206	3.89	1.34	4.37	1
<b>6</b>	929	7.57	6.49	13.23	0
<b>7</b>	931	8.72	7.95	13.23	0

The tabulate properties were computed by FAF-Drugs4.<sup>177</sup>

Before investigating **6** and **7** immunomodulatory effects, diamide **6** and ethanolamide **7**'s capability to permeate the cell membranes and enter in microglia cells was evaluated. To exclude that the high MW and the physicochemical parameters (Table 5) could hamper their membrane permeation.<sup>43</sup> Thus, in the immortalized microglia cell line N9 the percentages of **6** and **7** internalization were measured by LC-UV. Cells were treated with 10  $\mu$ M concentration of **6** or **7** with and without LPS (100 ng/mL) inflammatory insult. Subsequently to cell lysis, both conjugates (**6** and **7**) demonstrated to permeate N9 microglial cells without significant differences in their internalization percentages with and without LPS insult (Table 6). Particularly, diamide **6** was more effectively internalized than ethanolamide **7** ( $17.90 \pm 11,77\%$  (average value) and  $1.91 \pm 1.26\%$  (average value), respectively). Notably, the LC-UV analysis did not reveal the presence of **1** or (*S*)-**3** as metabolites of **6** and **7** hydrolysis. Thus, despite **6** and **7** predicted pharmacokinetic parameters didn't respect Lipinski's rule,<sup>178</sup> both diamide **6** and ethanolamide **7** showed to effectively permeate in N9 cells.<sup>43</sup>

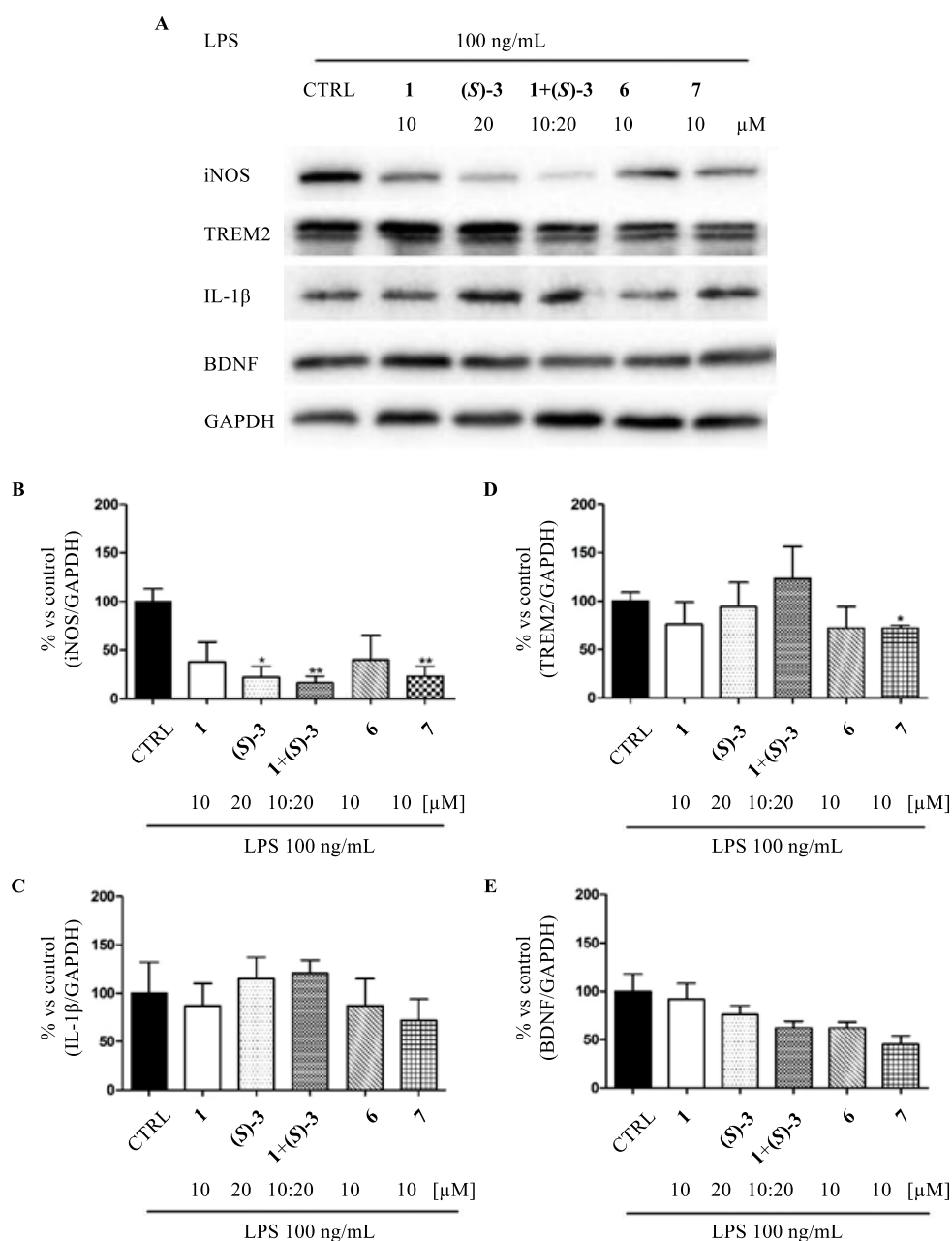
**Table 6.** Percentage of internalization of conjugates **6** and **7** in N9 microglial cells.<sup>43</sup>

Compound	Cell type	Sample	N° of cells	% compound internalized/cell $\pm$ SD (n = 3)	% compound internalized/cell mean $\pm$ SD <sup>1</sup>
<b>6</b>	N9 CTRL	CTRL-1	2,60E+06	9.03 $\pm$ 1.10	17.64 $\pm$ 12.81
		CTRL-2	1,48E+06	32.36 $\pm$ 2.49	
		CTRL-3	2,80E+06	11.54 $\pm$ 0.38	
	N9+LPS	LPS-1	2,13E+06	7.40 $\pm$ 0.59	16.15 $\pm$ 10.73
		LPS-2	1,48E+06	28.13 $\pm$ 0.35	
		LPS-3	2,40E+06	12.92 $\pm$ 0.40	
<b>7</b>	N9 CTRL	CTRL-1	2,18E+06	0.77 $\pm$ 0.05	1.35 $\pm$ 0.96
		CTRL-2	1,80E+06	0.82 $\pm$ 0.13	
		CTRL-3	1,90E+06	2.46 $\pm$ 0.03	
	N9+LPS	LPS-1	1,45E+06	1.76 $\pm$ 0.05	2.47 $\pm$ 1.56
		LPS-2	1,65E+06	1.39 $\pm$ 0.03	

<sup>1</sup>LC-UV analyses are the mean of three independent samples each analyzed in triplicate in triplicate experiments.

## Immunomodulation assay in microglia cells

Thanks to the positive permeation results, we tested whether diamide **6** and ethanolamide **7** could modulate microglia M1/M2 phenotype switch. Thus, the expression of different typical M1 and M2 biomarkers was evaluated by western blot (Figure 28A).



**Figure 28.** Evaluation of diamide **6** and diethanolamide **7** immunomodulatory effects in comparison with controls **1**, **(S)-3** and their 1:2 combination in immortalized microglia cells (N9) after LPS inflammatory insult. Characteristic M1 (iNOS (B) and IL-1β (C)) and M2 (TREM2 (D) and BDNF (E)) phenotype biomarkers were evaluated by western blot analysis. GAPDH was used as loading control. Densitometric results are expressed as a percentage of LPS only and are the mean ± SE of three different experiments. \*

$p < 0.05$  \*\*  $p < 0.01$  compared to LPS condition, Student's  $t$  test after ANOVA. (Figure adapted from doi: 10.3390/molecules26041112)<sup>43</sup>

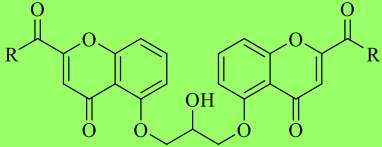
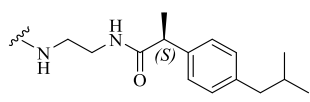
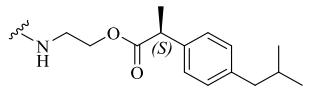
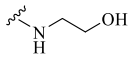
After insulting N9 microglial cells by inflammatory LPS (100 ng/mL) stimuli for 24 h, iNOS, TREM2, IL-1 $\beta$ , and brain-derived neurotrophic factor (BDNF) were assessed (Figure 28). LPS-treated microglial cells showed a substantial reduction of the M1 inflammatory biomarker iNOS by treatment with both **6** and **7** at 10  $\mu$ M and parent drugs (**1** and (**S**)-**3**) alone or combined in a 1:2 ratio (10:20  $\mu$ M). Particularly, diamide **6** (45% of residual iNOS) and diethanolamide **7** (30% of residual iNOS) maintained the anti-inflammatory activity of **1**+**(S)**-**3** parent drug combination, even though the combination was more effective (25% of residual iNOS) (Figure 27B).<sup>43</sup> As far as M2 anti-inflammatory biomarker evaluation is concerned, TREM2 expression, which promotes A $\beta$  phagocytosis by microglia, was evaluated. In this case, only the **1**+**(S)**-**3** 1:2 parent drug combination did not affect TREM2 expression (Figure 28D). Nevertheless, no statistically significant difference was observed for the M1-IL-1 $\beta$  and M2-BDNF biomarkers expression, even if a reduction of IL-1 $\beta$  was observed after treatment with **7** (Figure 28B and 28E).<sup>43</sup>

#### Anti-aggregating activity towards A $\beta$ <sub>42</sub> self-aggregation

Starting from the reported A $\beta$  anti-aggregating activity of parent drug **1**,<sup>39</sup> the possibility of diamide **6** and ethanolamide **7** to inhibit the A $\beta$ <sub>42</sub> self-aggregation was studied through thioflavin T (ThT) fluorescence assay (Table 7).<sup>179</sup> First, we confirmed the inhibition of A $\beta$ <sub>42</sub> aggregation by **1** in the ThT fluorescence assay experimental set-up (69.7 % inhibition, Table 7).<sup>149</sup> Then, **6** and **7** A $\beta$ <sub>42</sub> anti-aggregating activity was tested to define whether they could maintain the same profile of **1**. Unluckily, diamide **6** couldn't be analyzed because not soluble in the assay conditions. Interestingly, ethanolamide **7** exhibited a strong anti-aggregating activity (72.0 % inhibition, Table 7), similarly to that of **1**.<sup>43</sup> To note, **20** (a potential metabolite of **7**) did not inhibit A $\beta$ <sub>42</sub> self-aggregation activity (**20** = < 5% inhibition, Table 7).<sup>43</sup> This result could be motivated by the correlation showed by compounds with A $\beta$ <sub>42</sub> anti-aggregating activity and the possibility to establish ionic, hydrogen bond, and  $\pi$ -stacking interactions.<sup>180</sup> Differently from **1**, The masked carboxylic acid groups of **20** could avoid the establishment of ionic/hydrogen bond interactions with A $\beta$ <sub>42</sub> peptide. Contrariwise, the A $\beta$ <sub>42</sub> anti-aggregating profile of **7**,

which carries a complex molecular architecture, could positively influence the establishment of several positive hydrogen bonds and  $\pi$ -stacking contacts.<sup>43</sup>

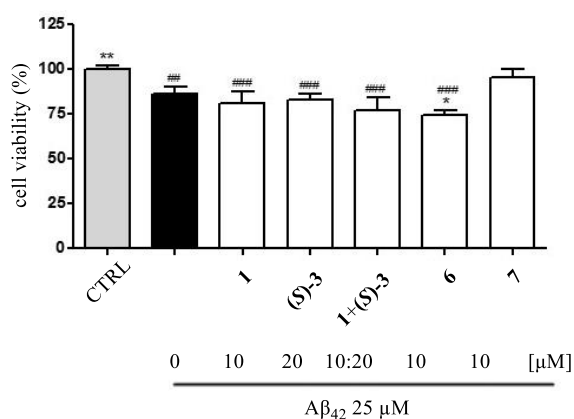
**Table 7.** Inhibition of A $\beta$ <sub>42</sub> self-aggregation of conjugates **6** and **7**.<sup>43</sup>

Compound		Inhibition of amyloid-self aggregation (%) [I] = 50 $\mu$ M
R		
<b>6</b>		Not soluble in the assay conditions
<b>7</b>		72.0 $\pm$ 0.3
<b>20</b>		< 5
<b>1</b> (cromolyn)	O <sup>-</sup> Na <sup>+</sup>	69.7 $\pm$ 5.3

#### Neuroprotective effect on A $\beta$ <sub>42</sub>-induced neurotoxicity in CGNs

Next, the neuroprotective profile of **6** and **7** against A $\beta$ <sub>42</sub> was evaluated in primary neurons (CGNs). After pretreatment with diamide **6**, diethanolamide **7**, parent drugs **1** or (*S*)-**3** at 10  $\mu$ M as well as their combination (10:20  $\mu$ M), cells were insulted with toxic A $\beta$ <sub>42</sub> (25  $\mu$ M) for 24 h (Figure 29).<sup>43</sup> Then, the cell viability was measured by MTT assay and, as expected, CGNs exposed to A $\beta$ <sub>42</sub> reduced their viability to 85% in comparison to the control. Notably, diethanolamide **7** reversed A $\beta$ <sub>42</sub>-induced neuronal death restoring the cell viability to 95%. On the other hand, **6**, parent drugs (**1** and (*S*)-**3**) alone or in 1:2 combination at the same concentration (10  $\mu$ M) didn't demonstrate the same neuroprotective effect.<sup>43</sup>



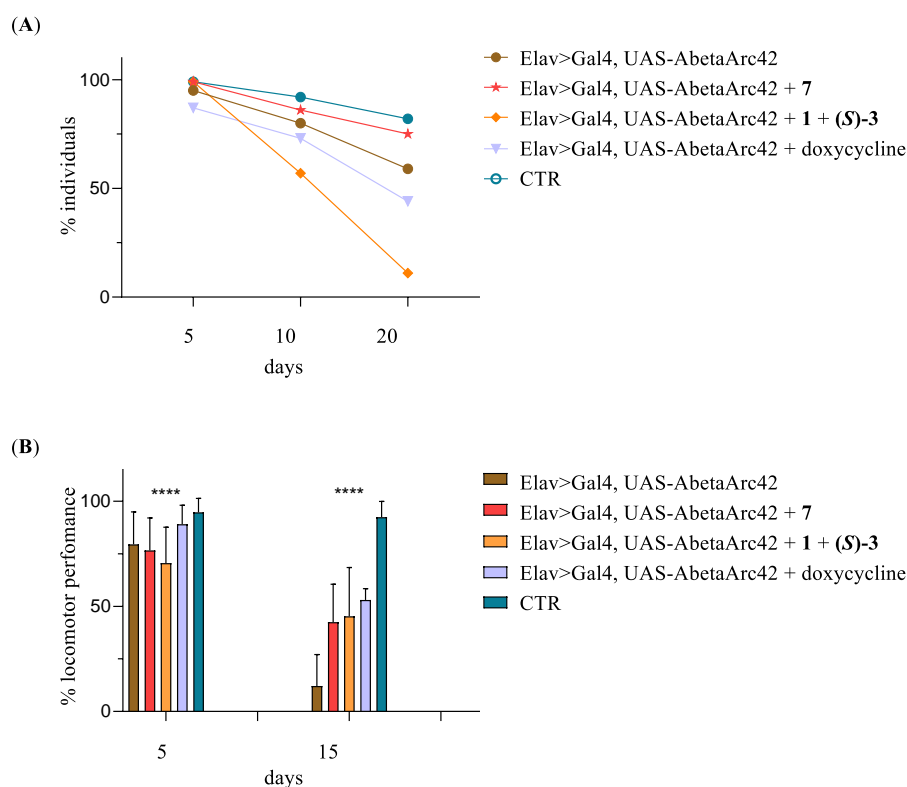


**Figure 29.** Neuroprotective effects of diamide **6** and diethanolamide **7** in comparison with controls **1**, (**S**)-**3** and their 1:2 combination in primary CGNs after A $\beta$ <sub>42</sub> neurotoxic insult. Cells were pretreated (6 h) at 10  $\mu$ M concentrations of the tested compounds in the presence of A $\beta$ <sub>42</sub> (25  $\mu$ M) for 24 h. Cell viability was evaluated by MTT assay. The results are expressed as a percentage of controls and each bar is the mean  $\pm$  SE of 2 different experiments, each run in quadruplicate. \*  $p < 0.05$ , \*\*  $p < 0.01$  compared to A $\beta$ <sub>42</sub>, ##  $p < 0.01$ , ###  $p < 0.001$  compared to control condition, Student's  $t$  test. (Figure adapted from doi: 10.3390/molecules26041112)<sup>43</sup>

### Lifespan and climbing evaluation in A $\beta$ <sub>42</sub>-expressing *Drosophila*

Integrating the promising anti-inflammatory effect, the A $\beta$ <sub>42</sub> anti-aggregating profile, and the neuroprotective result, **7** was selected for being evaluated in an AD *Drosophila in vivo* model. This is an inexpensive and accessible *in vivo* model that has already demonstrated its utility for studies in AD and related neurodegenerative diseases fields.<sup>181</sup> In particular, the behavioral analysis gives important information about flies' neuronal condition.<sup>181</sup> For example, a significant reduction in locomotor abilities or a shorter lifespan can be translated into a neurodegenerative phenotype. The capability of **7** to affect *Drosophila* longevity and locomotor performance was investigated in A $\beta$ <sub>42</sub>-expressing flies.<sup>43</sup> For 20 days, the lifespan and the climbing abilities of flies (E22G variant of A $\beta$ <sub>42</sub>) treated with **7** (20  $\mu$ M), with the parent drug combination (**1**+**(S)**-**3**, 20:40  $\mu$ M) or the reference drug doxycycline (50  $\mu$ M),<sup>182</sup> were compared. Notably, the lifespan (Figure 30A) of *Drosophila* treated with **7** (red curve) increased markedly after the 10<sup>th</sup> day of treatment compared to untreated A $\beta$ <sub>42</sub>-expressing flies (brown curve), reaching almost the value of the control healthy flies ( $w^{1118}$ —without transgenic mutation) (petrol blue curve), with more than 70% of flies still alive at 20<sup>th</sup> day of observation.<sup>43</sup> In line with the result published by Costa *et al.*,<sup>182</sup> we observed that the administration of doxycycline did not influence the longevity of A $\beta$ <sub>42</sub>-expressing flies.<sup>43</sup> In parallel to fly

lifespan evaluation, the fly climbing assay (Figure 30B) was performed. Ethanoloamide **7**, **1+(S)-3** or doxycycline (respectively 20  $\mu$ M, 20:40  $\mu$ M and 50  $\mu$ M) were administered to three cohorts of A $\beta$ <sub>42</sub>-expressing flies. Healthy control (*w*<sup>1118</sup>) flies, as we could expect (petrol blue columns), maintained the best locomotor ability for the whole analysis period (nearly 100%).



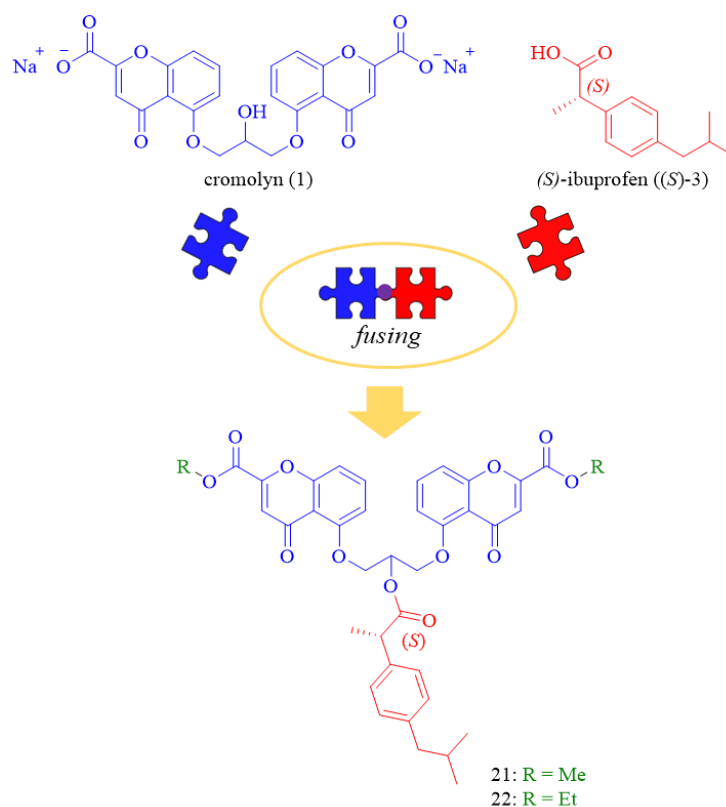
**Figure 30.** Behavioral studies in A $\beta$ <sub>42</sub>-expressing *Drosophila* compare the lifespan and the climbing performance of flies treated with diethanoamide **7** (20  $\mu$ M, in red) in comparison with two cohorts treated with controls: **1** and **(S)-3** combination (20:40  $\mu$ M, in orange) and doxycycline (50  $\mu$ M, in lilac). In addition, untreated-A $\beta$ <sub>42</sub>-expressing flies (in brown) as positive control and *w*<sup>1118</sup> healthy flies (in petrol blue) as negative control were evaluated. **(A)** The lifespan analysis compares the results at three different timepoints: 5, 10, and 20 days, **(B)** The climbing assay compares the climbing assay results at 5 and 15 days. Two-way ANOVA test, \*\*\*\* *p* value < 0.0001. (Figure adapted from doi: 10.3390/molecules26041112)<sup>43</sup>

Age-related decline in untreated flies' locomotor performance is associated with A $\beta$ <sub>42</sub> expression (brown columns). Compared to the untreated flies, the administration respectively of doxycycline (50  $\mu$ M, lilac column), ethanoloamide **7** (20  $\mu$ M, red column), or parent drug combination (**1+(S)-3**, 20:40  $\mu$ M, orange column) demonstrated to do not significantly affect fly cohorts' climbing capability at day 5 (climbing index of about 75%). Remarkably, on day 15, the locomotor performance of flies treated with **7** (red

column) and **1+(S)-3** combination (orange column) or doxycycline (lilac column) was similar (nearly to 50%) and significantly higher than the locomotor performance showed by untreated A $\beta$ <sub>42</sub>-expressing flies.<sup>43</sup> In conclusion, **7** can be considered a valid substitute for doxycycline, it demonstrated restoration of the locomotor abilities with comparable efficacy to that of doxycycline, but at a lower concentration and with lower toxicity.<sup>43</sup>

### 3.4.4.4 Cromolyn-ibuprofen codrugs: design of a small set of 1:1 cromolyn-ibuprofen conjugates

From the investigation of the (1:2) cromolyn-(S)-ibuprofen set of conjugates (**5-7**) promising results were obtained. Particularly, the best candidate diethanolamide **7** showed a potential AD disease-modifying profile acting on A $\beta$ , neuroinflammatory and neuroinflammatory pathways. Thus, a second small set of “codrugs” (**21** and **22**, Figure 31) was developed. These new molecules might maintain the multi-target profile of **5-7** and hopefully improve their biological activities.



**Figure 31.** Design of cromolyn-(S)-ibuprofen (1:1) conjugates by fusing strategy.

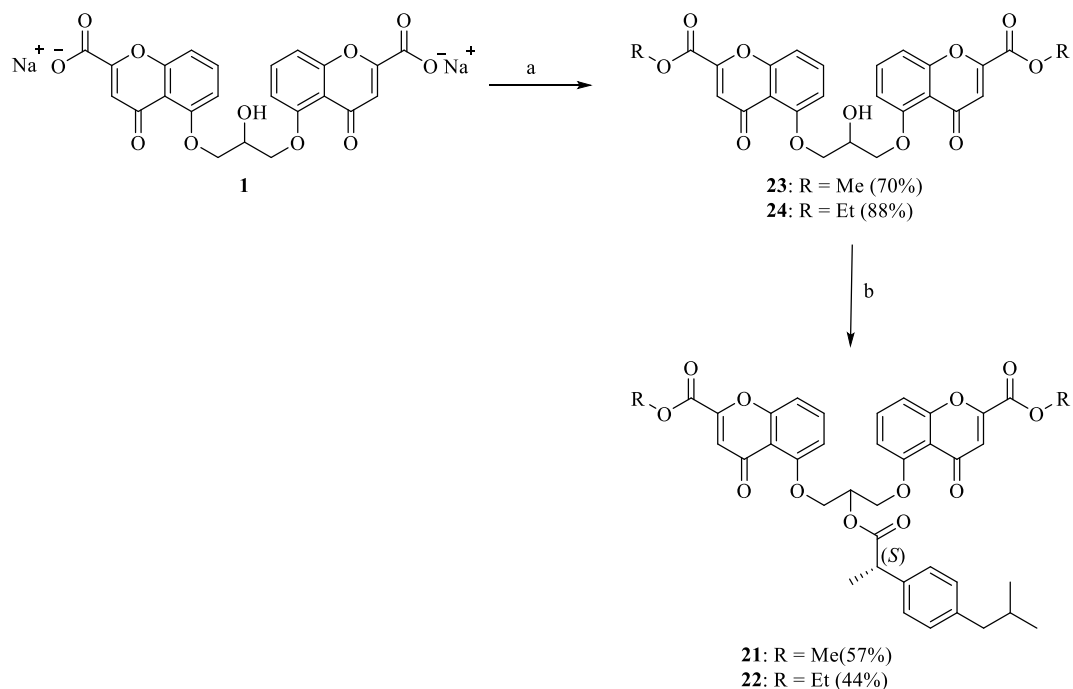
Importantly, codrugs **21** and **22** were designed by combining **1** and (S)-**3** in 1:1 ratio: thus, the resulting lower MW could improve their drug-likeness, BBB and membrane permeation.<sup>46</sup> As in the previous case, parent drugs were linked by cleavable bonds.

However, in this case, to favor codrugs' hydrolysis and the parent drugs' release only esters were introduced, since they are more easily hydrolyzed than the amides. In this case, **21** and **22** by their eventual *in vivo* hydrolyses could afford cromolyn-(*S*)-ibuprofen in 1:1 ratio. Particularly, **21** and **22** were designed by fusing strategy, linking the hydroxy group at the 2-carbon of the propane linker of **1** with (*S*)-**3**'s carboxylic function. As emerges from literature, cromolyn's 2-hydroxypropyl linker is a suitable portion to obtain cromolyn-conjugates, because hydroxyl function can well tolerate modifications without affecting **1**'s biological activity. For instance, amino acids were conjugates in that position, with the aim of improving the intestinal absorption of **1**.<sup>183</sup> Moreover, to improve **1** low membrane permeability and ameliorate cromolyn's features for BBB-permeation, in analogy with **5-7**, the carboxylic groups of **1** were masked to obtain prodrugs by methyl or ethyl esters (Figure 31).<sup>45</sup>

### 3.4.4.5 Chemistry

Conjugates **21** and **22** were synthesized according to Scheme 4. Firstly, **1**'s carboxylic acids were esterified by Fisher conditions.<sup>184</sup> **1** was respectively suspended in methanol (MeOH) or ethanol (EtOH) and refluxed in a reaction tube, in presence of concentrated hydrochloric acid (HCl) as catalyst, to afford intermediates **23** and **24** in good yields. Then, the desired codrugs **21** and **22** were synthesized by esterifying compound **23** or **24** to the carboxylic group of (*S*)-**3**, via EDC/DMAP Steglich coupling conditions. All the compounds were characterized by <sup>1</sup>H NMR and <sup>13</sup>C NMR. In addition, the tested compounds were analyzed by HRMS and HPLC demonstrating at least 95% purity  $\lambda = 254$  nm (see Chapter 6).

**Scheme 4.** Synthetic strategy for the synthesis of conjugates **21** and **22**.



Reagents and conditions: a) MeOH or EtOH, HCl (37%), 100 °C, 24 h; b) EDC, DMAP, DCM, (*S*)-ibuprofen (**3**) rt., 24 h.

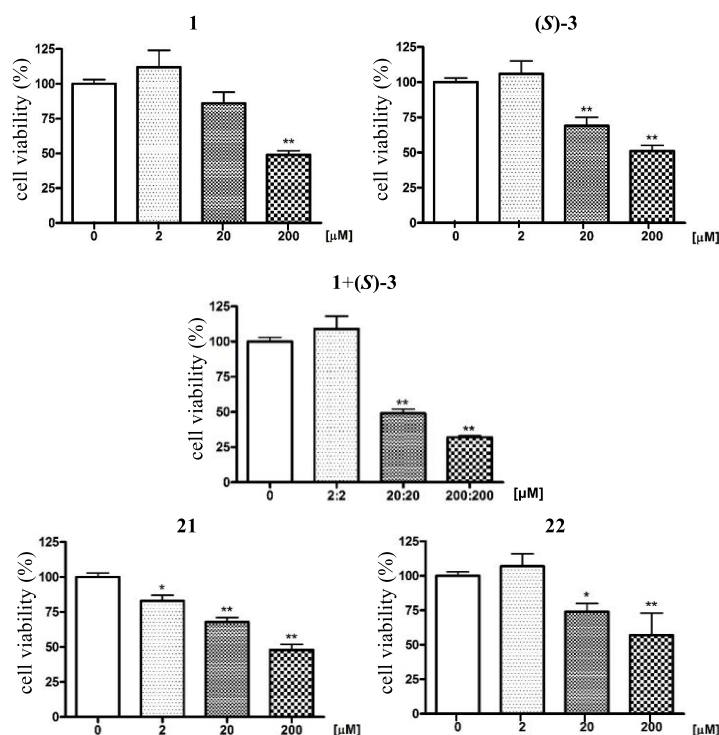
### 3.4.4.6 Results and discussion

The following results were obtained thanks to our collaborators of the Pharmacy and Biotechnology (FaBiT) Department-University of Bologna Prof. Bartolini's group (for the stability and the permeation assays); Prof. Monti's group (for the cellular assays).

#### Neurotoxicity evaluation in primary neurons

As for the first set of conjugates, the initial assay was the evaluation of **21** and **22** toxicity in primary CGNs. In analogy to the previous toxicity screening, primary neuron viability was evaluated by MTT assay after treatment with increasing concentrations (0, 2, 20, 200  $\mu$ M) of **21** and **22**. The results were compared to those of the parent drugs **1** and (*S*)-**3** and their combination in 1:1 ratio, to simulate the metabolites that could be released following codrugs' hydrolysis (Figure 32). As previously described, **1** showed toxicity only at 200  $\mu$ M concentration while (*S*)-**3** and **1**+(*S*)-**3** combination in 1:1 ratio resulted toxic already at 20  $\mu$ M and 20:20  $\mu$ M concentrations. Interestingly, conjugates **21** and **22**, the parent drugs **1** and (*S*)-**3**, as well as the corresponding **1**+(*S*)-**3** combination were not toxic at respectively 2  $\mu$ M and 2:2  $\mu$ M. However, the test compounds **21** and **22** at higher concentrations (20  $\mu$ M and 200  $\mu$ M) showed lower cytotoxicity than **1**+(*S*)-**3** combination

at the corresponding concentrations (respectively 20:20  $\mu\text{M}$  and 200:200  $\mu\text{M}$ ). Thus, considering that in the experimental conditions, codrugs **21** and **22** showed lower toxicity in CGNs than the corresponding parent drug combination, both tested compounds were progressed for the following studies.

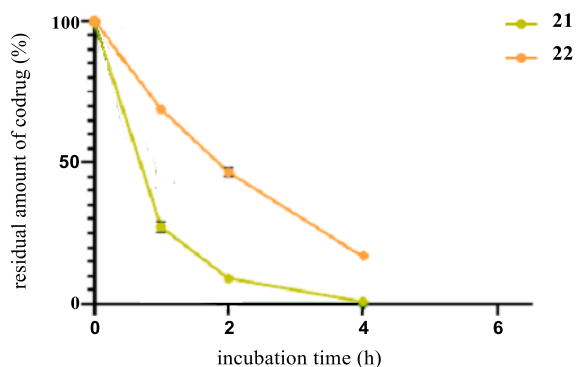


**Figure 32.** Neurotoxicity evaluation of conjugates **21** and **22** in comparison with controls **1**, **(S)-3** and their 1:1 combination in primary CGNs. Cell viability was determined by MTT assay. Results are expressed as percentages of controls and are the mean  $\pm$  SE of at least 3 independent experiments, each run in triplicate. \*  $p < 0.05$  \*\*  $p < 0.01$  compared to control conditions (0  $\mu\text{M}$ ), Dunnett test after one-way ANOVA.

### Stability in human plasma

After the investigation of the cytotoxicity profile, the stability of **21** and **22** in human plasma was evaluated (Figure 33). Our aim was to proceed with codrugs stable enough to potentially reach unmodified the CNS, where they could release the parent drugs. Following the same protocol used for **5-7** stability evaluation, **21** and **22** were incubated at 37  $^{\circ}\text{C}$  in human plasma and the samples were collected after 0, 2, 4, and 6 h. As expected, they demonstrated more lability of the diamide **6** and the diethanolamide **7**

codrugs, due to the presence of only ester bonds. Both codrugs **21** and **22**, analyzed by LC-MS, resulted in a human plasma concentration lower than about 25% after 4h.



**Figure 33.** Stability of **21** and **22** conjugates in human plasma.

Despite the lower plasma stability, we decided to consider for the following studies both compounds, **21** and **22**. Indeed, in agreement with the half-life time ( $t_{1/2}$ ) in human plasma of other CNS conjugates reported in the literature,<sup>185</sup> they showed a  $t_{1/2}$  major than 50 min, respectively (**21**  $t_{1/2}$  = 53 min and **22**  $t_{1/2}$  = 150 min).

## **3.5 Project 2: neflamapimod-rasagiline hybrids to target neuroinflammation in Alzheimer's disease**

### **3.5.1 Protein kinases as a druggable target for Alzheimer's disease**

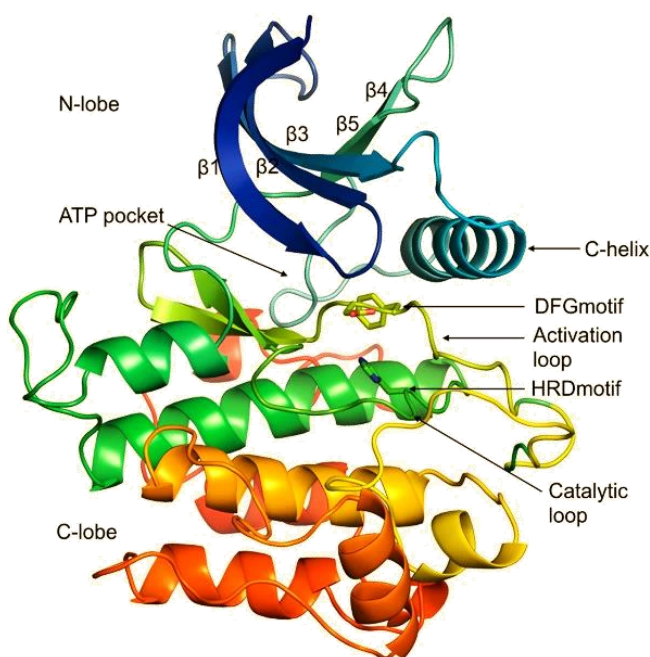
The protein kinase (PK) represents one of the major enzyme families of the human genome. Thanks to the complete human genome sequencing, 518 PKs codified by 575 genes were discovered and classified in a hierarchy of groups, families, and subfamilies.<sup>186</sup> However, due to the existing high complexity and variability, several PK classification schemes were proposed based on different kinds of similarities (*i.e.* conservation of the catalytic domain, domain structure similarities outside of the catalytic domain, biological function, biological function across organisms).<sup>187,188</sup> Focusing on PKs that phosphorylate protein substrates, the Nomenclature Committee of the International Union of Biochemists classified PKs on the basis of their substrate's acceptor amino acid, into 5 groups:<sup>189</sup>

1. Protein-serine/threonine (Ser/Thr) kinases (phosphotransferases with an alcohol group as acceptor)
2. Protein-tyrosine kinases (phosphotransferases with a phenolic group as acceptor)
3. Protein-histidine kinases (phosphotransferases with a histidine, arginine, or lysine group as acceptor)
4. Protein-cysteine kinases (phosphotransferases with a cysteine group as acceptor)
5. Protein-aspartyl or glutamyl kinases (phosphotransferases with an acyl group as acceptor)

PK family members are characterized by highly conserved amino acids sequence and three-dimensional structure of the catalytic domain. Interestingly, it can be considered the result of selective evolutionary pressure, aimed to preserve the primary function of the PK gene family: the phosphate transfer from adenosine triphosphate (ATP) to a protein substrate.<sup>190</sup> Particularly, PKs' catalytic function involves the covalent  $\gamma$  phosphate transfer from a phosphate donor, usually ATP (or other nucleoside triphosphates), onto an acceptor substrate (*i.e.* proteins, nucleotides, lipids ecc...). As far as PKs' catalytic domain structure is concerned, it shows a three-dimensional structure that comprises the



N-terminal lobe (N-lobe) and the C-terminal lobe (C-lobe) connected by a flexible region where is located the hinge motifs.<sup>191</sup> The N-lobe is constituted of a five-stranded  $\beta$ -sheet, with an  $\alpha$ -helix ( $\alpha$ C-helix). Moreover, it contains the consensual glycine-rich loop (G-loop), which controls ATP binding and phosphate transfer (Figure 33).<sup>191</sup> The C-lobe is comprised of six  $\alpha$ -helices and includes the activation segment. The N-terminus of the activation segment includes the Asp-Phe-Gly (DFG motif), which presents a magnesium binding site important for the interaction with an oxygen atom of the ATP  $\beta$ -phosphate. In addition, a short  $\beta$  sheet ( $\beta_9$ ), the activation loop (A-loop), and the P + 1 loop (Figure 34) are present.<sup>192</sup> The catalytic cleft between these two lobes involves two regions: the front cleft, and the back cleft. While the front cleft contains principally the ATP-binding site, the back cleft includes elements important for the regulation of kinase catalysis. In the gate between the front and the back clefts are located the gatekeeper residue in  $\beta_5$ , which allows the back cleft to be accessible, and a conserved lysine in the  $\beta_3$  strand.<sup>192</sup>



**Figure 34.** Structure of a typical protein kinase domain which shows the ATP binding site and the conserved close regions (Figure adapted from doi: 10.1073/pnas.1814279116).<sup>191</sup>

PKs are involved in many intercellular and intracellular signaling pathways by transducing, amplifying or integrating upstream signals.<sup>186</sup> Particularly, PKs include the enzymes that are most strongly implicated in the pathogenesis of neurodegenerative diseases and AD.<sup>193</sup> Thus, their modulation by selective protein kinase inhibitors (PKIs) is considered a promising therapeutic approach. In most cases, PKs are demonstrated to

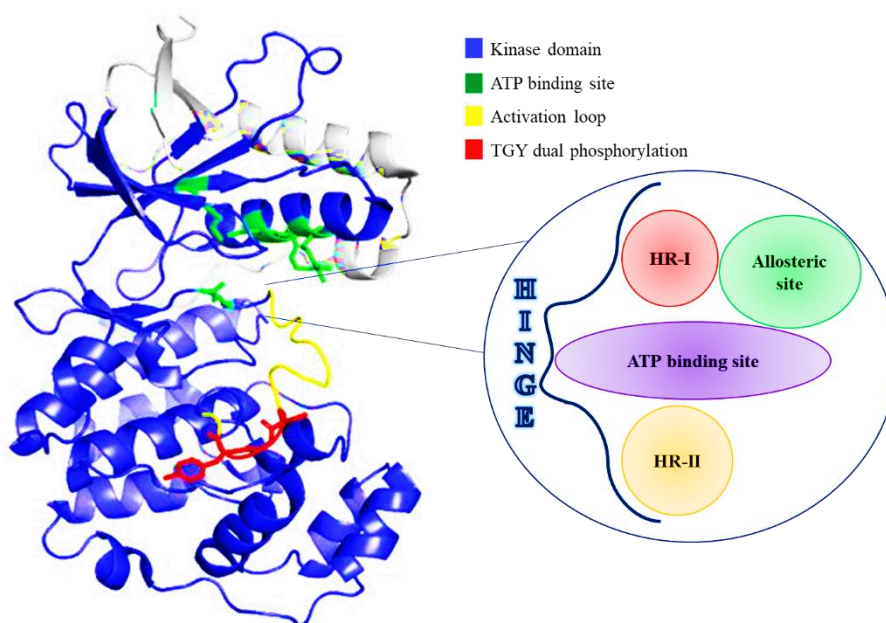
be successfully modulated by small molecules, that can bind to high-affinity specific pockets. In light of this, starting from the well-characterized structure of the catalytic domain, many protein kinase inhibitors (PKIs) have been developed as potential drug candidates. Almost all PKIs bind to the ATP-binding cleft. Nevertheless, due to PKs' considerable similarity, selectivity and minimal off-target effects represent two challenging aspects.<sup>194</sup> Focusing on AD, since drugs currently on the market are not able to effectively influence disease progression, PKIs for AD therapy may demonstrate a promising alternative.<sup>195</sup> Indeed, PKs are known to contribute to several of the toxic events involved in AD pathogenesis, especially tau hyperphosphorylation pathways. For instance, among PKs acting on tau cascade, there are glycogen synthase kinase (GSK)-3 $\beta$ , cyclin-dependent kinase 5 (CDK5), and dual-specificity tyrosine phosphorylation-regulating kinase 1A (DYRK1A). c-Jun N-terminal kinases (JNKs) and casein kinase isoforms (CKs) take part in tau phosphorylation but are also involved in  $\gamma$ -secretase modulation, stimulating the amyloidogenic cleavage of APP and the consequent increment of toxic A $\beta$  levels.<sup>195</sup>

Besides tau and amyloid pathways, inhibitors of mitogen-activated protein kinase (MAPK) family members have received attention, since MAPK contributes to neuroinflammatory pathways.

### **3.5.1.1 p38 $\alpha$ -MAPK: a member of MAPK family**

MAPK family is involved in signaling pathways that control cellular processes including proliferation, differentiation, apoptosis, and stress responses. MAPK is a group of serine/threonine intracellular kinases involved in crucial intracellular signals. In mammals 14 MAPKs have been characterized that are expressed across a variety of cell types, including cells of the central and peripheral nervous systems.<sup>50</sup> So far the most investigated MAPK members are the p38-MAPKs, which include p38 isoforms ( $\alpha$ ,  $\beta$ ,  $\gamma$ , and  $\delta$ ), the extracellular signal-regulated kinases (ERK 1 and ERK 2), and the c-Jun amino (N)-terminal kinases (JNK 1, JNK 2 and JNK 3).<sup>50</sup> Particularly, ERKs primarily are activated by growth factors and mitogens that induce cell growth and differentiation. JNKs are mainly stimulated by environmental stresses (ionizing radiation, heat, oxidative stress, and DNA damage), inflammatory cytokines, and growth factors. p38-MAPKs are strongly activated by environmental stresses and inflammatory cytokines, that promote p38-MAPKs contribution to inflammation, apoptosis, and cell differentiation.<sup>196</sup>

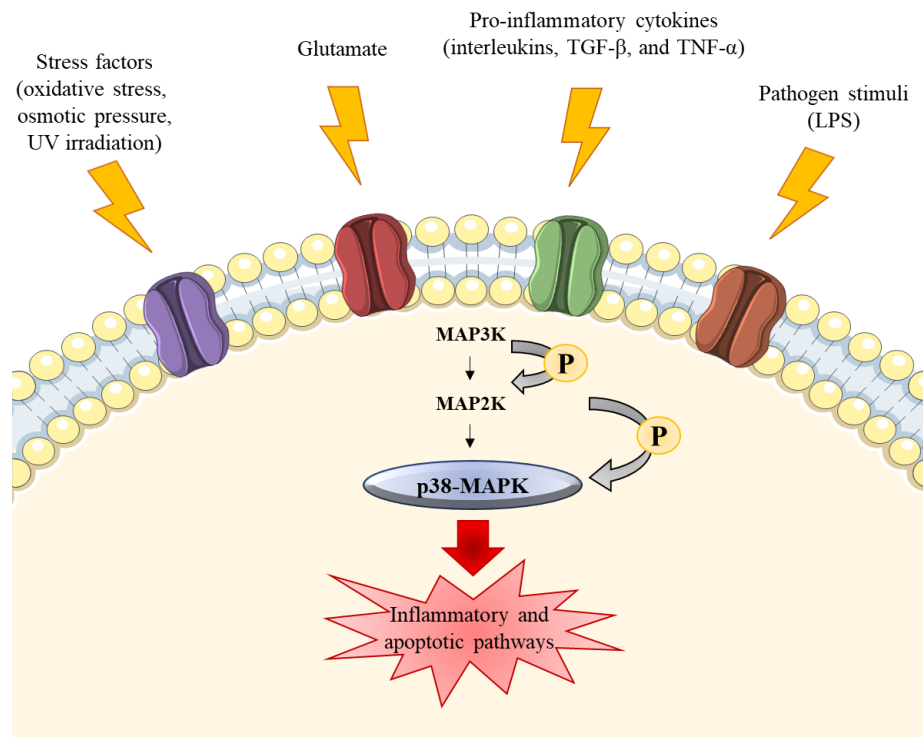
Considering the variety of the stimuli able to induce MAPK activation, their dysregulation is implicated in various pathological conditions. Persistent activation of the JNK or p38 signaling pathways has been suggested to be involved in neurodegenerative diseases, such as AD, PD, and ALS, whereas the ERK signaling pathways principally play a key role in tumorigenesis.<sup>197</sup> The external stimuli such as proinflammatory cytokines (*e.g.* IL-1 $\alpha$ , IL-2, IL-7, IL-17, IL-18, TGF- $\beta$ , and TNF- $\alpha$ ), growth factors, pathogenic stimuli, including LPS and oxidative stress induce a following three-tiered hierarchical phosphorylation cascade.<sup>198</sup> Thus, the sequential activation of a MAPK kinase (MAP3K), a MAP2K, and finally MAPK dual phosphorylation results in kinase activation and structural changes within the kinase domain.



**Figure 35.** Schematic representation of p38 $\alpha$ -MAPK ATP-binding site. The hydrophobic regions (HR-I and HR-II), the ATP binding site, and the allosteric site close to the ATP binding site are highlighted. (Figure adapted from doi: 10.3389/fnmol.2020.570586; doi: 10.3390/molecules200915842)<sup>50, 199</sup>

All MAPKs mainly share the common structure described in § 3.5.1. Particularly, p38-MAPKs present the N- and C-lobe of the kinase domain, the active site located between the ATP binding site and the TGY (threonine-glycine-tyrosine) dual phosphorylation site. The active site is covered by the activation loop. Moreover, focusing on p38-MAPKs, three additional less conserved regions are present. The two hydrophobic regions I and II (HR-I and HR-II) are located adjacently to the ATP binding site and an allosteric site (Figure 35).<sup>200</sup> Consequently to the dual MAPK phosphorylation, conformational changes occur, thanks to the induced rotation of the two kinase lobes. Such rotation is afforded by

the stabilization of the activation loop in a more open conformation that permits the access of the substrates to the active site.<sup>200</sup>

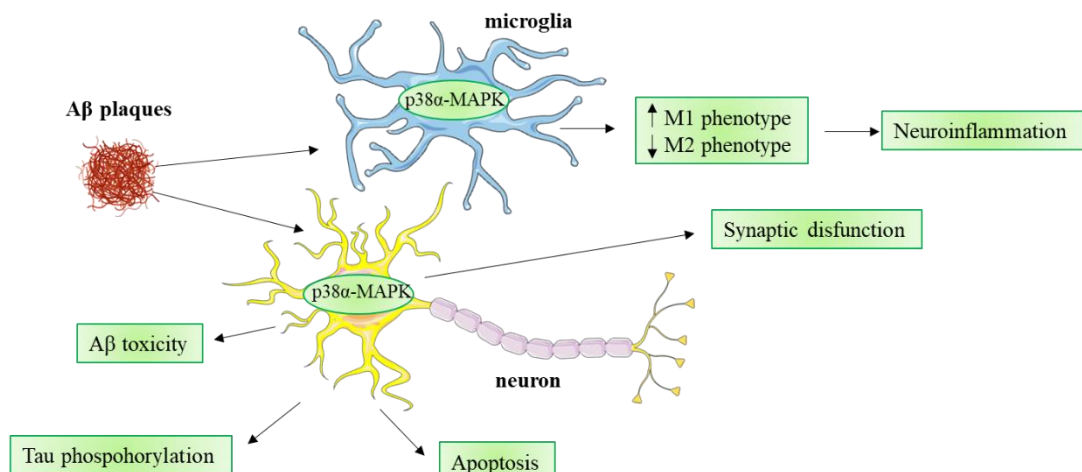


**Figure 36.** p38-MAPK activation cascade induced by external stimuli leads to the activation of apoptotic and inflammatory pathways. (Figure adapted from doi: 10.3389/fnmol.2020.570586)<sup>50</sup>

MAPK activation causes the transfer of the  $\gamma$ -phosphate of cosubstrate ATP to the hydroxyl group of serine and threonine side chains of their substrates.<sup>50</sup> The phosphorylated substrates initiate several signaling cascades that lead to pro-inflammatory cytokine biosynthesis and apoptotic and proliferative pathways modulation (Figure 36).<sup>198</sup> MAPK isoforms differ in their expression in the body. p38 $\alpha$ -MAPK is ubiquitously expressed with respect to the other isoforms. However, p38 $\alpha$  and p38 $\beta$ -MAPKs are the most present at the CNS level, including neurons, astrocytes, microglia, endothelial cells, and the spinal cord.<sup>198</sup> p38 $\alpha$ -MAPK is the major isoform activated under inflammatory conditions, and it is crucial for the production of inflammation mediators.<sup>201</sup> p38 $\gamma$ -MAPK is mainly peripheral and p38 $\delta$ -MAPK expression is more restricted in comparison with the other isoforms.<sup>198</sup>

### 3.5.1.2 p38 $\alpha$ -MAPK involvement in Alzheimer's disease development

Considering the p38 $\alpha$ -MAPK prevalence in neurons as well as glia cells, it has been principally studied in the context of CNS. It is implicated especially in neuroinflammatory pathway activation.<sup>201</sup> Inflammatory mediators induce p38 $\alpha$ -MAPK activation that leads to NF- $\kappa$ B-regulated transcription and the consequent release of inflammatory mediators (*e.g.* TNF- $\alpha$  and IL-1 $\beta$ ), up to an uncontrolled response by microglia and the consequent neuronal damage and death.<sup>201</sup> Particularly, p38 $\alpha$ -MAPK upregulation was found in AD, as well as MAPK phosphatase 1 (MKP-1) downregulation. MKP-1 is the negative modulator of MAPKs since it produces the dephosphorylation of tyrosine and threonine residues.<sup>201</sup> Additionally to the main contribution to AD neuroinflammation, p38 $\alpha$ -MAPK overactivation is also related to excitotoxicity (by accumulating glutamate in synapses) in astrocytes and inflammation-induced synaptic dysfunction.<sup>201</sup> Moreover, p38 $\alpha$ -MAPK contributes to tau phosphorylation, causing its dissociation from neuron cytoskeleton and self-aggregation. Interestingly, p38 $\alpha$ -MAPK activation and A $\beta$  deposition seem to be mutually influenced.<sup>201</sup> Particularly, A $\beta$  plaques stimulate microglia that, by p38 $\alpha$ -MAPK activity, up-regulates the production of pro-inflammatory cytokines, supporting chronic inflammation. In neurons, A $\beta$  can increase p38 $\alpha$ -MAPK activation and the consequent tau hyperphosphorylation. In turn, p38 $\alpha$ -MAPK is the most essential regulator of A $\beta$  deposition and neurotoxic effects.<sup>202</sup> Moreover, p38 $\alpha$ -MAPK expression promotes M1 microglia phenotype leading to pro-inflammatory mediator production and inhibition of A $\beta$  phagocytosis (Figure 37).<sup>202</sup>

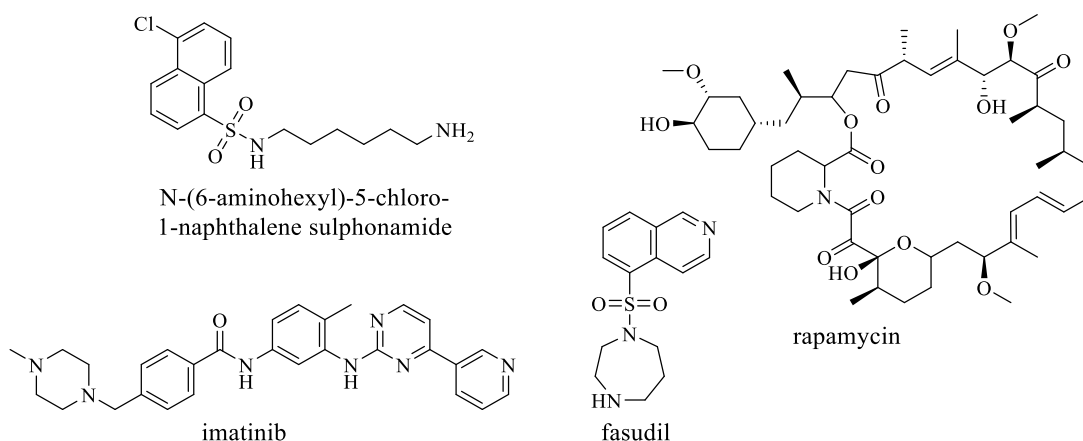


**Figure 37.** p38 $\alpha$ -MAPK implications in AD pathogenesis. (Figure adapted from doi: 10.3390/molecules22081287)<sup>203</sup>

To prove the relation between p38 $\alpha$ -MAPK and AD pathways, two independent *in vivo* AD mouse models were exploited in behavioral assays; the first model with a rapid pathophysiology disease progression, and the second with an age-related pathophysiology disease progression. In both cases, after the administration of a selective p38 $\alpha$ -MAPK inhibitor memory deficits were attenuated by a hippocampus-dependent mechanism.<sup>204</sup> All these considerations, together with the evidence that p38 $\alpha$ -MAPK is highly expressed in regions crucial for learning and memory, support p38 $\alpha$ -MAPK as a prominent drug target for AD.<sup>203</sup> Thus, brain-penetrant p38 $\alpha$ -MAPK inhibitors could lead to promising AD disease-modifying drugs.<sup>55, 205</sup>

### 3.5.2 Protein kinase inhibitors as a valuable strategy against Alzheimer's disease

The development of the first PKI goes back to the early 1980s, when Hiroyoshi Hidaka observed that sulphone amides, like the N-(6-aminohexyl)-5-chloro-1-naphthalene sulphonamide, already known as a calmodulin antagonist, could inhibit protein kinases at higher concentrations (Figure 38).<sup>206</sup> However, only in 2001, the first PKI drug was approved by Food and Drug Administration (FDA). Imatinib was the first drug targeting a specific PK, the Abelson tyrosine kinase (ABL), developed for the treatment of chronic myeloid leukemia (Figure 38).<sup>207</sup> Indeed, even if rapamycin (a TORC1 protein kinase inhibitor) and fasudil (a Rho-kinase inhibitor) were approved earlier than 2001, it happened before knowing the specific target proteins they acted on (Figure 38).<sup>207</sup>



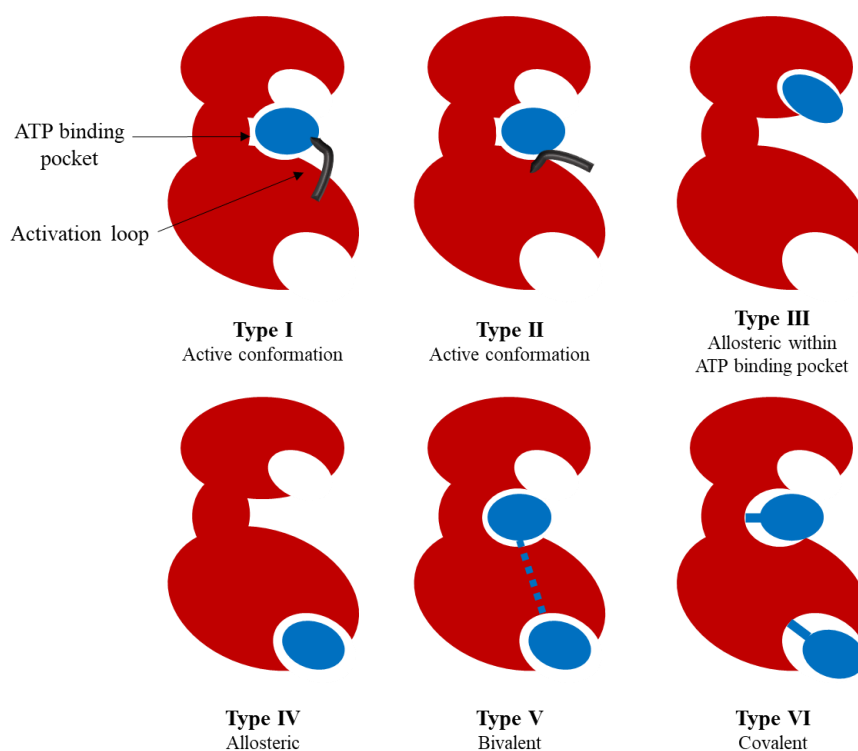
**Figure 38.** Structures of the first naphthalene sulphonamide discovered with protein kinases inhibitor activity and of the first three FDA-approved kinase inhibitors imatinib, rapamycin, and fasutidil.

Nowadays, more than 70 PKIs have been approved for clinical use,<sup>207</sup> and there are 1941 ongoing clinical trials involving PKIs as drug candidates.<sup>208</sup> Particularly, they are principally used in cancer, even if their application in inflammatory<sup>209</sup> and neurodegenerative diseases is expanding.<sup>193</sup> PKIs can bind their target reversibly or irreversibly. The reversible binding is an equilibrium and ligand potency is defined by the inhibition constant ( $K_i$ ), which represents the ratio between the rate constants of unbinding ( $k_{off}$ ) and binding ( $k_{on}$ ). In contrast, irreversible binding refers to the formation of a covalent interaction between the inhibitor and the PK. However, PKI-PK occurs in two steps. The first is a reversible step based on PKI-PK affinity and is defined by an inhibitory constant ( $K_i$ ). Then, it is followed by the irreversible reaction of PKI electrophilic warhead and an amino acid nucleophilic side chain which affords the covalent interaction.<sup>210</sup> Since, the covalently bounded protein is progressively removed from the equilibrium of the first reversible step, the full target occupancy by PKI can be obtained. Potentially, even moderately efficient PKIs can drive to the full target inhibition, if the incubation time is long enough. Overall, covalent binding can be considered a non-equilibrium process since, in most cases, the bounded protein can't be regenerated. However, the time-dependent nature of the first reversible step can influence the apparent potency of PKIs, which can change in function of the incubation time.<sup>211</sup>

This results in an incubation-time-dependent PKIs  $IC_{50}$ . The  $IC_{50}$  measurement indeed doesn't take into account the first equilibrium step of the process which precedes the bond formation. Therefore it should be warily interpreted in PKI's potency evaluation. To compare correctly the potency of different covalent PKIs against a target is the covalent inactivation constant ( $K_{inact}$ )/ $K_i$ .<sup>212</sup>

All PKIs can be classified into six groups (Figure 39): "Type I" inhibitors are PKIs that, binding the ATP binding site, induce an active conformation of the kinase or a conformation that is anyway favorable to ATP-binding. PKIs that bring to an outward of the DFG-motif preventing the stabilization of the active conformation are called "type II". Then, there are two classes of allosteric inhibitors, that bind a site different from the active site, which refers to the ATP binding site. They are the "type III" and "type IV".<sup>213</sup> "Type III" includes PKIs that bind a pocket adjacent to the ATP binding site, the "back pocket" of the kinase, without displacing ATP. "Type IV" comprises the inhibitors that exclusively bind kinases outside of the cleft, in the "phosphor acceptor region". In this

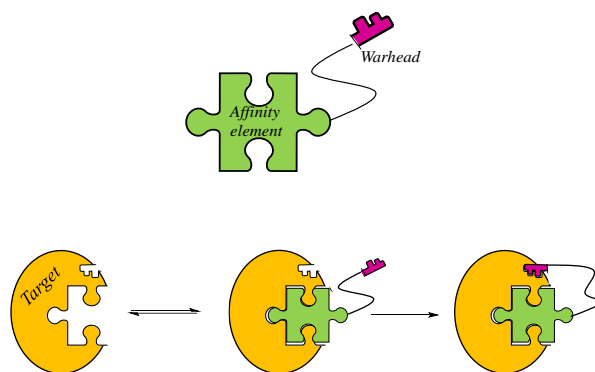
case, the inhibitor binding induces a conformational change in the activation loop that forces the  $\alpha$ C-helix to adopt an inactive conformation, preventing the proper glutamate aligning in the ATP binding site, which is essential for catalysis. “Type V”, are bivalent and bi-substrate inhibitors, which combine an active site-directed ligand and an allosteric effector or any protein kinase binding agent by using an appropriate synthetic linker. Types I-V include inhibitors that form exclusively reversible interaction with the target PK. In contrast, “Type VI” inhibitors are small molecules that form covalent adducts with the target enzyme (Figure 39).<sup>214</sup>



**Figure 39.** Schematic representation of the different kinds of PKIs. (Figure adapted from doi: 10.1007/978-3-030-48283-1\_3)<sup>215</sup>

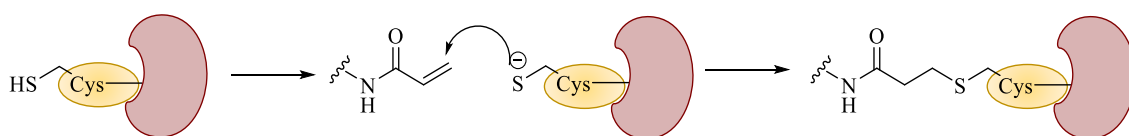
Covalent inhibitors usually present an affinity element and an electrophilic moiety (warhead) to address cysteine or other nucleophilic residues in proximity to the ATP-binding pocket (Figure 40).<sup>216</sup>





**Figure 40.** Structural outlines of a covalent inhibitor and schematic representation of the covalent mechanism of action. (Figure adapted from DOI: 10.4155/fmc-2020-0236)<sup>217</sup>

In detail, the two-step covalent inhibition mechanism required that the first non-covalent interaction with the target allows the correct orientation of the reactive electrophilic moiety (in Figure 41, the acrylamide) toward the nucleophilic amino acid. In this way, the covalent reaction (typically is a Michael addition) can occur (Figure 41).<sup>217</sup> At this point, the first equilibration step permanently shifts to the right inactivating the enzyme and potentially driving the reaction to completion. Thus, the kinase function can be restored only by expressing the protein *via de novo* protein synthesis.<sup>217</sup>



**Figure 41.** Example of a covalent irreversible binding mechanism by an electrophile warhead, (in this case an acrylamide) and Michael addition of the thiol of a cysteine side chain. (Figure adapted from DOI: 10.1002/ange.201707875)<sup>216</sup>

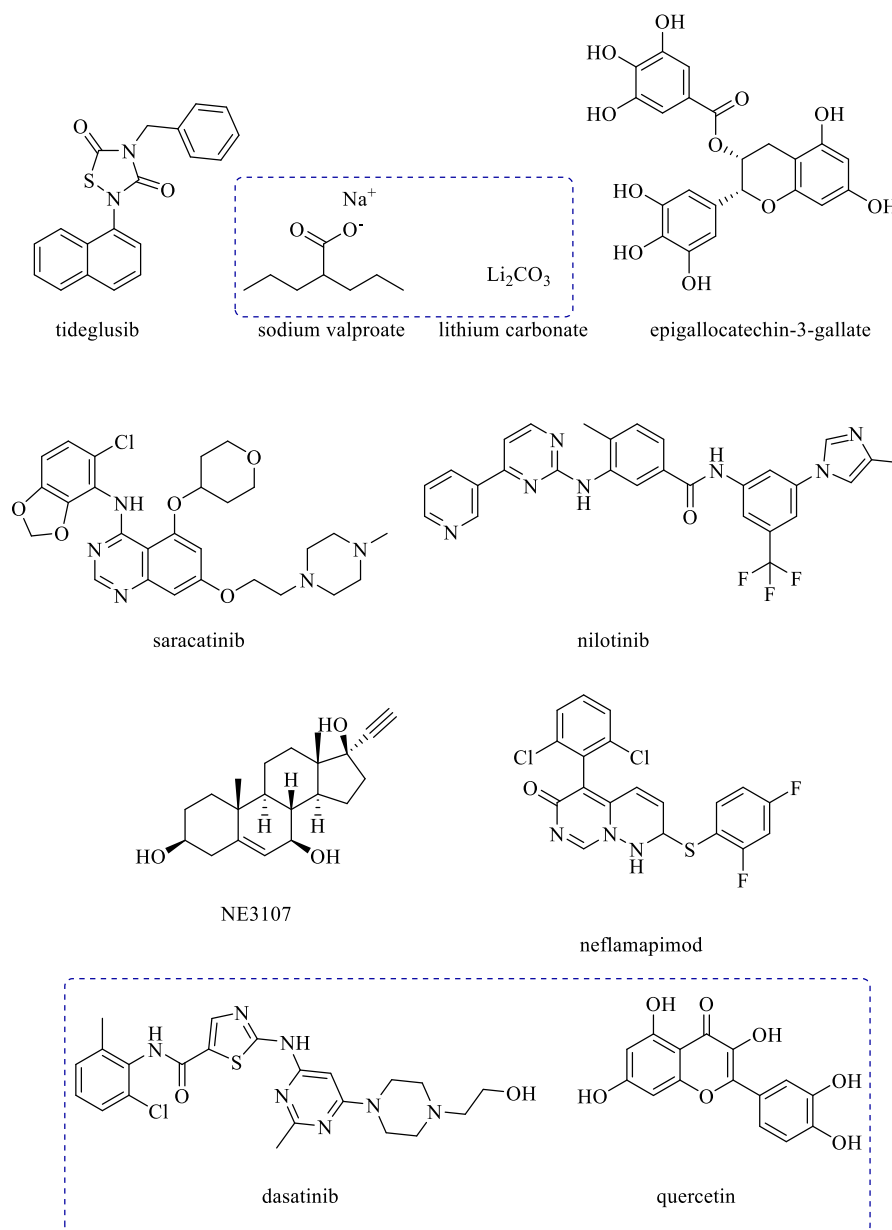
Traditionally, reactive molecules able to irreversibly bind their targets were associated with promiscuity, indiscriminate reactivity, and potential immune-mediated adverse effects.<sup>217</sup> Recently, the interest in the development of irreversible PKIs was renewed, focusing on the development of both chemical probes and potential drugs.<sup>218</sup> In contrast to the common opinion, thanks to the warhead, targeted covalent inhibitors can even increase the selectivity for the desired target. This is particularly the case when warhead reactivity is “low” enough and the target amino acid sequence is poorly conserved.<sup>217</sup> For example, promising covalent selective inhibitors can be designed by targeting the not conserved ‘cysteinome’.<sup>218</sup> Moreover, covalent inhibitors properly designed may offer multiple advantages leading to a favorable benefit–risk balance. They could (i) allow a

lower dose use by increasing the target occupancy, (ii) increase the time-dependent potency, (iii) overcome the obstacle of the ATP competition, and (iv) reduce the risk of side effects and off-target activities.<sup>210</sup>

### **3.5.2.1 Protein kinase inhibitors investigated in clinical trials for Alzheimer's disease**

PKIs have been longly considered a valuable strategy in cancer therapies since PKs' overactivity is principally involved in uncontrolled cell divisions, cell migration, and cellular invasion. With the expanding understanding of PK functions, the idea of developing PKIs as potential candidates for AD therapy is increasing. Indeed, PK overactivations seem to be involved in AD progression pathways, including pathophysiological tau protein phosphorylation and A $\beta$  toxicity. However, despite the large therapeutic success, anticancer PKIs show the critical issue of toxicity and side effects. Moreover, as an important determinant in CNS drug discovery, only 2% of small molecule inhibitors can effectively reach the CNS. Thus, developing PKIs with a good BBB permeability and limited side effects are two aspects of primary importance.<sup>195</sup> The majority of therapeutic strategies that included PKIs for AD, focused on the inhibition of the kinases that phosphorylate tau. These PKs are responsible for the irreversible hyperphosphorylation of the protein and the consequent imbalance between tau phosphorylation and dephosphorylation seen in AD brains. The two key kinases involved in tau phosphorylation are GSK-3 $\beta$  and CDK5.<sup>219</sup> Many GSK-3 $\beta$  inhibitors have been developed, but most of them never reached clinical studies due to their undesirable side effects, inadequate kinase specificities, or insufficient BBB permeability. A GSK-3 $\beta$  inhibitor developed against progressive supranuclear palsy (PSP), a progressive tauopathy, and AD, is tideglusib. In preclinical studies, tideglusib reduced a range of disease outcomes, including tau phosphorylation. Thus, it reached phase II (NCT00948259) in AD clinical trial, but the study was discontinued.<sup>219</sup> More success had lithium (administered as carbonate salt Li<sub>2</sub>CO<sub>3</sub>) that, together with valproate, is on the market for mood disorders treatment.<sup>220</sup> Lithium was repurposed, alone (NCT01055392) or in combination (NCT00088387) with valproate in two independent phase II clinical trials, to reduce AD tauopathy by GSK-3 $\beta$  inhibition.<sup>221</sup> Despite both trials have failed, lithium is still under investigation in phase IV clinical trial (NCT03185208) to evaluate

whether it can delay dementia onset, or slow its progression in patients affected by mild cognitive impairment (Table 7 and Figure 42).<sup>222</sup>



**Figure 42.** Chemical structures of kinase inhibitor drug candidates for AD treatment.

As far as CDK5 inhibitors are concerned, despite various small molecules have shown preclinical efficacy, none of them has been tested in a clinical trial. The low selectivity over other CDK family members, as well as the still not clearly elucidated risk associated with CDK5 inhibition in humans, negatively influenced the clinical development of these inhibitors.<sup>221</sup> Likewise, JNK and DYRK1A inhibitors showed disappointing results in clinical development. However, epigallocatechin-3-gallate, the major catechin in green tea, has been investigated in phase II clinical trial (NCT01699711) as a dietary

supplement able to modulate DYRK1A and APP functions and improve cognitive dysfunction in AD.<sup>223</sup> FYN, a member of SRC family also phosphorylates tau. Saracatinib is an SRC family kinase inhibitor with high potency for FYN and SRC kinase. Preclinical evidence demonstrated that it could rescue synaptic dysfunction and spatial memory impairment in AD transgenic mice. Thus, it was investigated in phase I, in which safety, tolerance profile, and good BBB permeability were confirmed (NCT01864655).<sup>224</sup> Then, a phase II clinical trial was started to evaluate the best dosage (NCT02167256) (Table 8 and Figure 42). Based on Cumming's 2021 review of the AD drug development pipeline, there are four kinase inhibitors in ongoing clinical trials.<sup>225</sup> Nilotinib is an oral ABL-tyrosine kinase inhibitor approved for the treatment of chronic myeloid leukemia. It has been repurposed against AD since it was demonstrated to reduce the accumulation of A $\beta$  in AD mouse models. This was confirmed in patients by a phase II clinical trial (NCT02947893)<sup>226</sup> that has paved the way to the currently ongoing phase III (NCT05143528).<sup>227</sup>

**Table 8.** Kinase inhibitors that were investigated in clinical trials as potential AD treatment.<sup>100</sup>

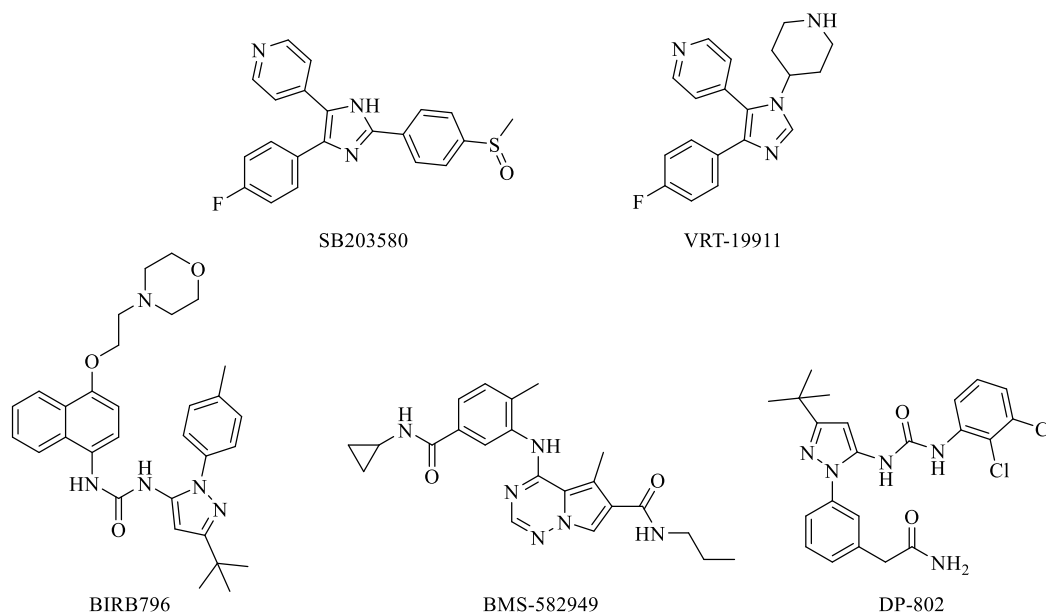
Drug candidate	NCT number	Target kinase	Status	Phase
tideglusib	NCT00948259	GSK-3 $\beta$	Completed	Phase II
lithium	NCT01055392	GSK-3 $\beta$	Completed	Phase II
lithium + valproate	NCT00088387	GSK-3 $\beta$	Completed	Phase II
epigallocatechin-3-gallate	NCT01699711	DYRK1A	Completed	Phase II
saracatinib	NCT02167256	SRC	Completed	Phase II
nilotinib	NCT05143528	ABL	Ongoing	Phase III
dasatinib + quercetin	NCT04063124	SRC/ABL	Ongoing	Phase I and II
dasatinib + quercetin	NCT04785300	SRC/ABL	Ongoing	Phase I and II
dasatinib + quercetin	NCT04685590	SRC/ABL	Ongoing	Phase II
NE3107	NCT04669028	ERK	Ongoing	Phase III
neflamapimod	NCT03435861	p38 $\alpha$ -MAPK	Ongoing	Phase II

Form the evidence that dasatinib and quercetin combination can enhance remaining health- and lifespan in old mice displaying a senolytic effect,<sup>228</sup> their combination skipped from the preclinical to the clinical investigation as AD disease-modifying treatment (NCT04063124,<sup>229</sup> NCT04785300,<sup>230</sup> NCT04685590<sup>231</sup>) (Table 8) (Figure 42). While quercetin is a flavonoid that demonstrated neuroprotective and antioxidant activity used as a dietary supplement for metabolic and inflammatory disorders, as well as AD.<sup>232</sup> Dasatinib is an SRC/ABL kinase inhibitor that is approved for the treatment of chronic

myelogenous leukemia. It was repurposed against AD because it induces apoptosis in senescent cells inhibiting SRC tyrosine kinases. This activity can be synergistically combined with that of quercetin, which inhibits the anti-apoptotic protein Bcl-xL.<sup>233</sup> NE3107 is a BBB permeable anti-inflammatory insulin sensitizer acting as ERK inhibitor. It modulates neuroinflammatory pathways in microglia by decreasing inflammation. In the phase III clinical trial (NCT04669028) the first endpoint has been satisfied.<sup>234</sup> After 30 weeks of treatment, it has demonstrated benefits in cognition. Neuropsychological deficits, functional performance, and glycemic control have not been evaluated yet.<sup>235</sup> MAPK, as previously explained (§ 3.5.1.1), is critically involved in AD neuroinflammatory pathways. Thus neflamapimod, a selective p38 $\alpha$ -MAPK inhibitor, is currently under investigation in a promising phase II clinical trial (NCT03435861) (Table 8) (Figure 42).<sup>225</sup> This point will be returned to later in this Chapter.

### 3.5.2.2 p38-MAPK inhibitors

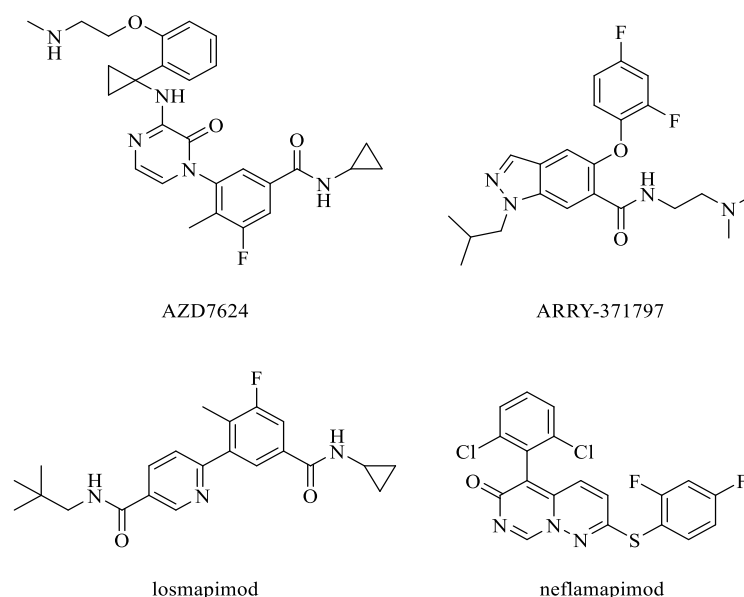
As previously said, p38-MAPK is a subgroup of the MAPK family. Since they are deeply involved in cellular responses to external stress signals and inflammatory cytokines, they are considered an attractive target in medicinal research. Particularly the  $\alpha$  isoform is the best characterized and it has a crucial role in the signal cascade of inflammatory pathways.<sup>236</sup>



**Figure 43.** Some examples of p38-MAPK inhibitors.

For this reason, the first p38-MAPK inhibitors were initially developed for the treatment of rheumatoid arthritis (RA). The first discovered p38-MAPK inhibitors date back to 1994. The two pyridinylimidazole derivatives SB203580 and VRT-19911 are ATP binding site p38-MAPK inhibitors, SB203580 is active on both  $\alpha$  and  $\beta$  isoforms, while VRT-19911 is a potent and selective p38 $\alpha$  inhibitor (Figure 43).<sup>237</sup> They have been demonstrated to reduce the release of TNF- $\alpha$  and IL-1 $\beta$ . However, their significant cytochrome P450 inhibition, attributed to the presence of the pyridyl moiety, was a critical issue.<sup>237</sup> To overcome this issue, many approaches and optimizations were investigated and other inhibitors were discovered. The pyrazole aryl urea class member BIRB796 was proved to efficiently reduce TNF $\alpha$  production stimulated by LPS and was investigated in a clinical trial for RA and Crohn's disease. It is a very potent and selective inhibitor of p38 $\alpha$  that inhibits allosterically. It binds with the morpholino ring, the unphosphorylated p38 $\alpha$ -MAPK activation loop, extending into the ATP pocket hinge where it makes hydrogen bond interactions with the hinge methionine.<sup>238</sup> The highly p38 $\alpha$ -MAPK selective aminobenzoic acid BMS-582949 inhibits both p38 $\alpha$ -MAPK activity and its activation. It induces a conformational change in the p38 $\alpha$ -MAPK activation loop which hampered p38 $\alpha$ -MAPK phosphorylation by upstream kinases.<sup>239</sup> The pyrazole urea p38 $\alpha$ -MAPK inhibitor DP-802 has an allosteric mechanism of action (Figure 43). It binds unphosphorylated inactive conformation of p38 $\alpha$ -MAPK.<sup>240</sup> More than 20 p38-MAPK inhibitor candidates have entered clinical trials but, among the 32 protein kinase inhibitors currently approved by the FDA, there is still no p38-MAPK inhibitor. The only exception is the weak and unselective p38 kinase inhibitor pirfenidone, approved by the FDA for the treatment of idiopathic pulmonary fibrosis, despite its severe adverse events.<sup>241</sup> However, in the last 5 years while big pharma didn't contribute significantly to the production of new patents involving p38-MAPK inhibitors, Universities, small companies, and other research institutions gave their important contribution.<sup>236</sup> The most recent clinical trials involving p38-MAPK inhibitors focus on inflammatory diseases, such as corticosteroid-resistant asthma, chronic obstructive pulmonary disease, AD, acute coronary syndrome, dementia with Lewy bodies, COVID-19, LMNA-Related Dilated Cardiomyopathy. The structures of these inhibitors are reported in Figure 44.<sup>200</sup> Pyrazinone AZD7624 (Figure 44) was investigated in two different phase II clinical trials, one for acute chronic obstructive pulmonary disease (NCT02238483)<sup>242</sup> and one for corticosteroid-resistant asthma (NCT02753764).<sup>243</sup> It was shown to specifically inhibit p38 $\alpha$  and p38 $\beta$  isoforms in human alveolar

macrophages, reduce cytokine release after LPS stimulation and decrease systemic and lung inflammation.<sup>200</sup> Losmapimod is an oral p38 $\alpha$ / $\beta$ -MAPK inhibitor that was investigated in patients affected by cardiovascular diseases and atherosclerosis. Recently, it was studied in an acute coronary syndrome phase III clinical trial (NCT02145468).<sup>244</sup> It targets p38-MAPKs activated in macrophages, myocardium, and endothelial cells inducing plaque reuptake.<sup>245</sup> The phenylpyridine Losmapimod (Figure 44) inhibits p38 $\alpha$ - and p38 $\beta$ -MAPK isoforms, it was investigated at clinical level in chronic obstructive pulmonary disease, and in 2020 it was repurposed in phase 3 clinical trial against COVID-19 (NCT04511819).<sup>246</sup> Indeed, p38-MAPK seems to be involved in the exaggerated acute inflammatory response caused by SARS-CoV-2 infection.<sup>200</sup> However, the only trial still ongoing focuses on losmapimod application for facioscapulohumeral muscular dystrophy treatment (NCT04264442).<sup>247</sup>



**Figure 44.** p38-MAPK inhibitors that were recently investigated in clinical trials.

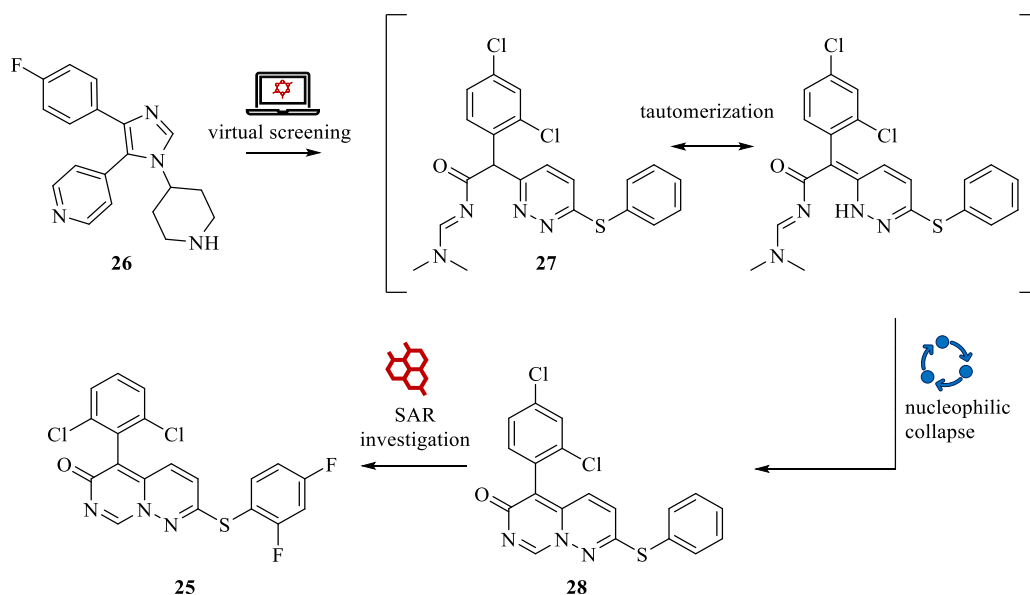
ARRY-371797 (Figure 44) is an indazole derivative that selectively inhibits p38 $\alpha$ -MAPK. It was investigated in several clinical trials against RA, dental pain, and osteoarthritis of the knee. Recently, *in vivo* studies showed that it prevents left ventricular dilatation and deterioration.<sup>248</sup> It was then investigated in phase II clinical trial (NCT03439514)<sup>249</sup> for the treatment of Lamin A/C gene (LMNA)-related dilated cardiomyopathy and it is still under investigation at phase III level (NCT02351856).<sup>200,</sup><sup>250</sup> Neflamapimod (Figure 44), which presents a diphenyl substituted pyrimidopyridazinone core, is an ATP competitive p38 $\alpha$ -MAPK inhibitor. It was

investigated in patients affected by RA, Huntington's disease (NCT03980938),<sup>251</sup> dementia with Lewy bodies (NCT04001517).<sup>252</sup> Particularly, since 2015 it is under investigation as a potential AD treatment (NCT03435861) (*vide infra*).<sup>253</sup>

To note, p38-MAPK inhibitors have failed at the clinical stage often owing to a lack of efficacy, poor pharmacokinetics, or unspecific toxicity.<sup>236</sup>

### 3.5.2.3 Neflamapimod

Neflamapimod (VX-745, **25**) is a selective p38 $\alpha$ -MAPK inhibitor recently discovered by Vertex Pharmaceuticals (Figure 45).<sup>55</sup> Particularly, starting from the previously discovered p38 $\alpha$ -MAPK inhibitor **26**, virtual screening and shape similarity methods were applied to a library of commercial molecules.<sup>55</sup> Thus, hit compound **27** was selected. In an attempt to resynthesize **27**, Duffy *et al.* observed the *in situ* tautomerization of **27** and the formation of the 5-phenyl-2-(phenylthio)-6H-pyrimido[1,6-b]pyridazin-6-one scaffold by the nucleophilic collapse of the pyridazine ring nitrogen on the ethanamide carbon, affording compound **28** (Figure 45).<sup>55</sup>

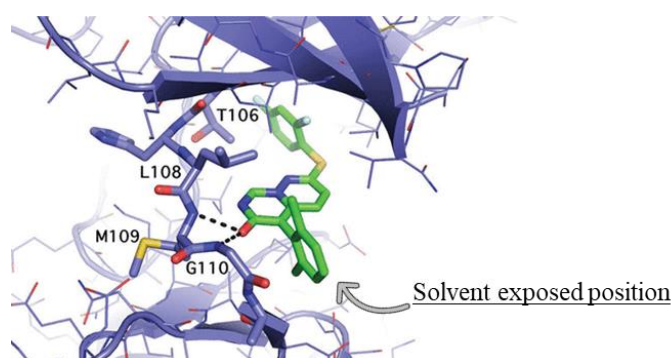


**Figure 45.** Hit to lead optimization of p38 $\alpha$ -MAPK inhibitors. (Figure adapted from doi: 10.1021/ml2001455)<sup>55</sup>

Thus, aiming to investigate the structure-activity relations (SAR) of the new pyridazine-containing class, the optimized lead **25** was discovered by changing the substituents of **28** on both the phenyl rings.<sup>55</sup> Interestingly, **25** showed an IC<sub>50</sub> in the nanomolar range



and every modification in terms of position or nature of phenyl ring substituents led to a considerable loss in p38 $\alpha$ -MAPK inhibition.<sup>55</sup> **25**-p38 $\alpha$ -MAPK crystal structure showed the interaction of the pyrimidopyridazinone moiety with the ATP binding site. The 2,4-fluorophenyl ring occupies a hydrophobic pocket (HR I) at the gatekeeper (Thr106) residue, while each chlorine of the 2,6-dichlorophenyl ring occupies a hydrophobic pocket (HR-II) and the phenyl itself makes favorable Van der Waals interactions with backbone residue atoms (Figure 46). The para position of the 2,6-dichlorophenyl ring is the only one that faces bulk solvent.<sup>55</sup>



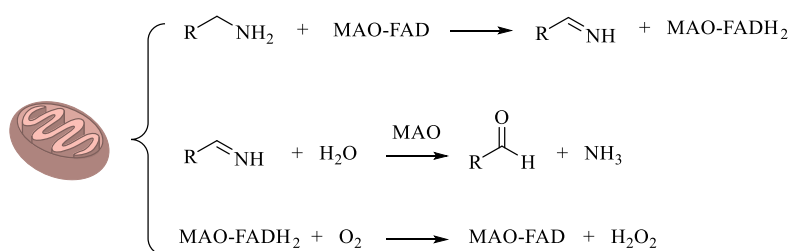
**Figure 46.** Structure of **25** bound to p38 $\alpha$ -MAPK complex. (Figure adapted from doi: 10.1021/ml2001455).<sup>55</sup>

Following, the pharmacokinetic parameters were evaluated and surprisingly **25** demonstrated to be a very well-absorbed oral small molecule.<sup>55</sup> As previously described, p38 $\alpha$ -MAPK is a kinase deeply involved in inflammation. Thus, aiming to explore the anti-inflammatory profile of **25**, it was investigated in an *in vivo* murine collagen-induced arthritis model of human RA. Considerable improvements in the inflammatory score were observed,<sup>55</sup> laying the foundations for a pilot phase II clinical trial in patients affected by RA.<sup>47</sup> However, **25** demonstrated to reach a concentration in the CSF twice as much as protein-unbonded fraction in plasma. This distribution profile produced CNS adverse effects,<sup>49</sup> which led to trial discontinuation; however, this was the trigger for repurposing **25** as a disease-modifying drug against AD.<sup>254</sup> *In vivo* studies in Tg2576 mice reported the immunomodulatory profile of **25**, able to induce microglia shift from the M1 pro-inflammatory phenotype to the M2 phagocytic state.<sup>48</sup> Consequently, improvements in mitochondrial function, synaptic transmission, and memory were observed.<sup>48</sup> Moreover, the administration of **25** to 2-year-old Tg2576 mice treated with 3 mg/kg for two weeks, reduced amyloid plaque load.<sup>48</sup> Thus, from 2015 (NCT02423200)<sup>255</sup> to today (NCT03435861)<sup>49, 253</sup> a series of clinical trials to evaluate cognitive improvement in AD

patients by neuroinflammatory pathways modulation, has started. Synaptic dysfunction,<sup>254,256</sup> neuronal death, amyloid deposition (NCT02423122)<sup>257</sup>, and immunomodulation were evaluated in patients.<sup>49</sup>

### 3.5.3 MAO-B and its implication as a therapeutic target in Alzheimer's disease

Monoamine oxidase (MAO) is an enzyme located on the external membrane of mitochondria; it mainly metabolizes monoamine neurotransmitters catalyzing their oxidative deamination. MAO exists in two isoforms, the monoamine oxidase-A (MAO-A) and the monoamine oxidase-B (MAO-B).<sup>258</sup> Both isoforms induce the oxidative deamination of primary, secondary, and tertiary amines (*e.g.* dopamine, serotonin, norepinephrine) where the flavin adenine dinucleotide (FAD) cofactor plays a crucial role. Amines act as electron donors to give the corresponding imines that are then oxidized to the corresponding aldehydes producing ammonia (NH<sub>3</sub>). Despite the physiological importance of MAO activity and the related biochemical reactions, several byproducts are produced, such as hydrogen peroxide (H<sub>2</sub>O<sub>2</sub>) and NH<sub>3</sub> which can result in neurotoxic effects (Figure 47).<sup>258</sup> In turn, H<sub>2</sub>O<sub>2</sub> can lead to ROS production increasing oxidative stress which is responsible for mitochondrial dysfunction and neuronal death.



**Figure 47.** Monoamine-oxidase-catalyzed reactions could generate reactive and toxic species. (Figure adapted from doi: 10.3390/molecules26123724)<sup>258</sup>

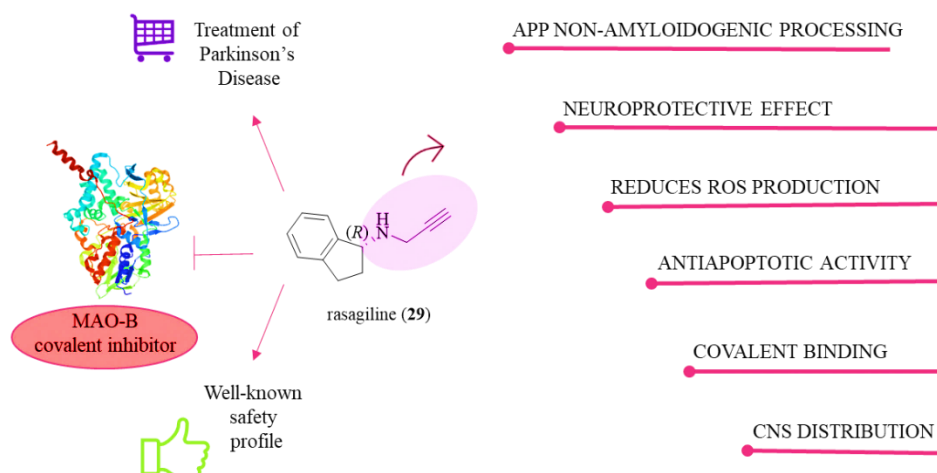
MAO-A and MAO-B are encoded by two different genes, and they exhibit different tissue distribution and substrate specificity. Particularly, MAO-B is the isoform principally expressed in the brain, especially in glial cells, but also in platelets and hepatic cells. It takes part in neurotransmitters deactivation and other neuro-modulatory amines like polyamines.<sup>258</sup> Altered levels of MAO isoenzymes are associated with the degeneration of biogenic amine neurotransmitters suggesting their involvement in multiple

neurodegenerative conditions. Typically, selective MAO-B inhibitors are used to treat Parkinson's disease (PD), since MAO-B was found overexpressed in the brains of these patients. Despite the correlation of MAO-B in AD is still not clear, MAO-B expression and activity are enhanced in the hippocampus and cerebral cortex of AD brains; for this reason, MAO-B inhibitors are currently investigated as a valuable strategy also in AD treatment.<sup>259</sup> It is speculated that this overexpression of MAO-B could produce an increased generation of free radicals and H<sub>2</sub>O<sub>2</sub> and thus may exacerbate the neurodegenerative mechanisms occurring in AD. The oxidative stress in AD patients contributes to A $\beta$  plaque generation.<sup>260</sup> Additionally, MAO may indirectly sustain neuroinflammation proinflammatory cytokine since it is primarily involved in ROS and free radical production. Furthermore, high levels of oxidative stress were found in the brains of AD patients.<sup>261</sup> In turn, oxidative stress can induce an active, self-preserving cycle of chronic neuroinflammation, which stimulates further oxidative stress and contributes to irreversible neuronal dysfunction and cell death.<sup>259</sup> Activation of MAO-B also contributes to the production of amyloid- $\beta$  plaques. The mechanism seems to be due to a relation between MAO-B,  $\gamma$ -secretase, and A $\beta$  in neurons.<sup>260</sup>

### 3.5.3.1 Rasagiline

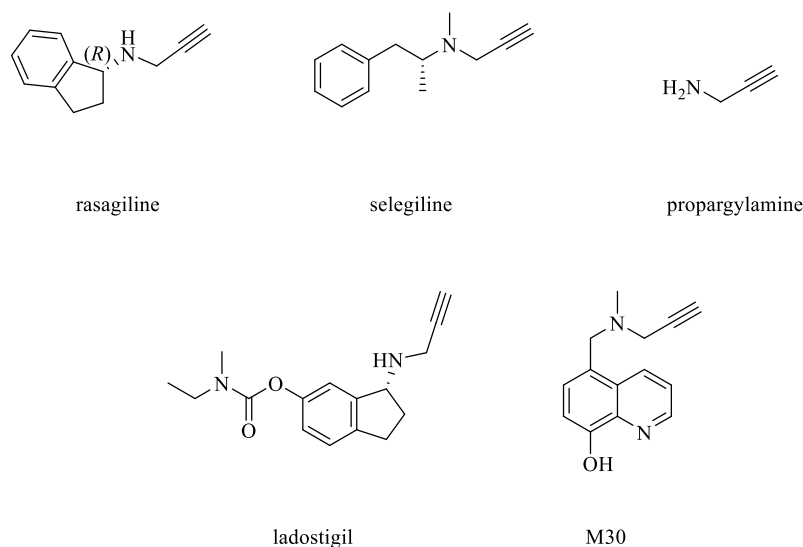
Rasagiline (**29**, Figure 48) is the *R*-isomer of the racemic AGN1135.<sup>51</sup> It is a drug currently on the market for the treatment of PD, which acts as a covalent and selective MAO-B inhibitor.<sup>262</sup> Indeed, the Michael acceptor propargyl fragment allows the formation of an adduct with the N5 atom of the FAD MAO cofactor.<sup>262</sup> MAO-B physiologically is involved in monoamine degradation. For this reason, MAO-B inhibitors, such as rasagiline and selegiline (Figure 49), are on the market for PD treatment, since MAO-B inhibition contributes to the dopamine deficiency restoration typical of PD.<sup>53</sup> However, dopamine mediates not only motor function and executive abilities, but also cognitive functions, including attention and reward.<sup>53</sup> Moreover, many evidences contribute to the idea that the effect of **29** are not exclusively related to MAO-B inhibition. To support this hypothesis, **29** demonstrated by *in vitro* and *in vivo* studies neuroprotective, anti-apoptotic and antioxidant effects by MAO-B independent mechanisms. In fact, similar properties were observed for **29**'s *S*-enantiomer (TVP1022), which has 1000-fold weaker MAO-B inhibitory activity than the *R*-enantiomer.<sup>51</sup> In the same way, various propargylamine derivatives have displayed neuroprotective action,

combined with anti-apoptotic properties by mitochondrial permeability transition pore regulation. These activities have been attributed to the N-propargyl group present in the structures. To further support, N-propargylamine itself, which is not a MAO inhibitor, seems to have intrinsic neuroprotective and neuro-rescue effects, similarly to propargylated MAO inhibitors.<sup>263</sup>



**Figure 48.** Description of rasagiline (**29**)’s main characteristics and the principal activities attributed to **29**’s propargylamine fragment.

Starting from this, many known propargylamine-derivatives such as the anti-PD drugs rasagiline and selegiline, the N-propargylamine fragment, the multi-target hybrid ladostigil (rasagiline-rivastigmine hybrid) and M30 (the rasagiline-VK-28 hybrid) were deeply investigated for AD application (Figure 49).



**Figure 49.** Structures of propargylated compounds studied against AD pathways.

All of them showed a reduction in amyloid production and accumulation, in tau hyperphosphorylation, and neurofibrillary tangle formation.<sup>264</sup> Moreover, neuroprotective/anti-apoptotic activities, together with nonamyloidogenic APP processing upregulation via PKC-MAPK- $\alpha$ -secretase pathway stimulation were observed.<sup>264</sup> The promising preclinical results obtained for the MTDL ladostigil led it to phase II clinical trials (NCT01429623<sup>265</sup> and NCT01354691<sup>266</sup>) that unfortunately didn't produce its approval by FDA.<sup>267</sup> Moreover, anti-PD drugs rasagiline (**29**) and selegiline, thanks to their well-known safety profile, were repurposed in clinical trials for AD<sup>52,53</sup> as well as other neurodegenerative diseases (Table 9).<sup>263</sup>

**Table 9.** Rasagiline and selegiline repositioning in neurodegenerative diseases.<sup>100</sup>

Drug candidate	Aim of repurposing	NCT number	Status	Phase
rasagiline	ALS	NCT01786603	Completed	Phase II
		NCT01879241	Completed	Phase II
		NCT01232738	Completed	Phase II
	multiple system atrophy	NCT00977665	Completed	Phase II
	sleep disturbances	NCT01442610	Completed	Phase IV
	AD dementia and AD	NCT02359552	Completed	Phase II
		NCT00104273	Completed	Phase II
	depressive symptoms	NCT01055379	Completed	Phase IV
	PSP	NCT01187888	Completed	Phase III
	schizophrenia	NCT00492336	Completed	Phase IV
depression	NCT04841798	Ongoing	Phase II Phase II	
brain injury	NCT02696512	Unknown	Phase I Phase II	
				restless legs syndrome
selegiline	bipolar depression	NCT00535262	Completed	Phase IV
	borderline personality disorder	NCT01912391	Completed	Phase III
		major depressive disorder	NCT00531947	Completed
	schizophrenia	NCT00285766	Completed	Phase III
		NCT00456976	Completed	Phase I
	cognition disorders in HIV infected patients	NCT00013585	Completed	Phase II
NCT00002154		Completed	Phase II	
NCT00027040		Completed	Not applicable	

Particularly, very recently **29** was investigated as AD add-on therapy to cholinesterase inhibitors or memantine, and an incremented effect of **29** by the co-administration of these drugs was observed. Then, taking glucose metabolism decline as a function of dementia, improvements were observed in comparison to placebo (NCT02359552).<sup>53, 268</sup> Concomitantly, for the first time, the beneficial effects on brain perfusion and on cerebral regional functions were observed following **29** and donepezil combination treatment, supporting **29**'s potential neuroprotective effects.<sup>52</sup>

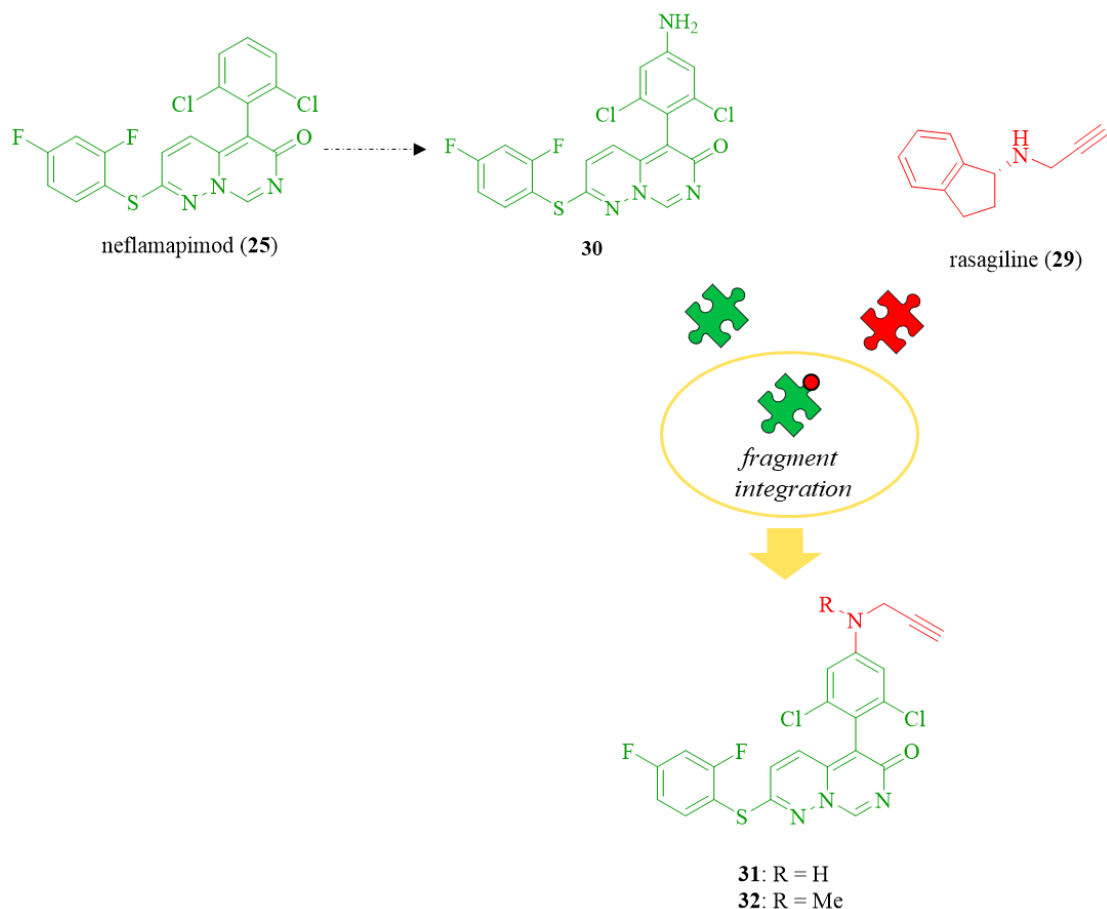
### 3.5.4 Neflamapimod-rasagiline hybrids: rationale of the project

This project aimed to design and synthesize potential MTDLs to combine in a single-molecule the promising anti-neuroinflammatory activity of neflamapimod (**25**) and the neuroprotective/anti-apoptotic effect of rasagiline (**29**). This builds on the notion that the simultaneous modulation of multiple pathways by MTDLs is a promising strategy to face the complexity of AD.<sup>115</sup> We were also particularly inspired by the repositioning of **25** in AD, due to its peculiar CNS delivery.<sup>49</sup> Taking advantage of **25**'s excellent BBB permeability and aiming to not lose p38 $\alpha$ -MAPK selectivity, we maintained the core structure of the selective p38 $\alpha$ -MAPK inhibitor **25**. As previously mentioned, **25** thanks to its neuroinflammatory activity, is under investigation in an ongoing phase II clinical trial (NCT03435861).<sup>253</sup> On the other side, we were attracted by the versatility of the anti-PD drug **29**. Besides a selective MAO-B inhibitory activity, **29** has demonstrated neuroprotective, anti-apoptotic, and  $\alpha$ -secretase potentials by *in vitro* and *in vivo* studies.<sup>263</sup> Thus, thanks to the well-known safety profile and its multiple-pathways modulation, **29** was very recently investigated for its neuroprotective profile in AD patients.<sup>52</sup> In light of this, aiming to apply polypharmacology by MTDLs, a small set of neflamapimod-rasagiline hybrids was designed and synthesized. By a fragment integration strategy, we introduced **29**'s propargylamine active fragment on **25**'s p38 $\alpha$ -MAPK binding scaffold. In principle, the introduction of a propargylamine can play many roles in fine-tuning biological activities. These include potency enhancement (by a complementary fit into a receptor binding pocket), reactive warhead (for irreversible inhibition of a target protein), interaction with additional biological targets, and modulation of drug-like properties profile. Indeed, propargylamine of **29** is essential not

only for MAO-B irreversible inhibition but also for conferring neuroprotective activity,<sup>51</sup> and improving BBB permeability and CNS distribution.<sup>269</sup>

### 3.5.4.1 Design of neflamapimod-rasagiline hybrids

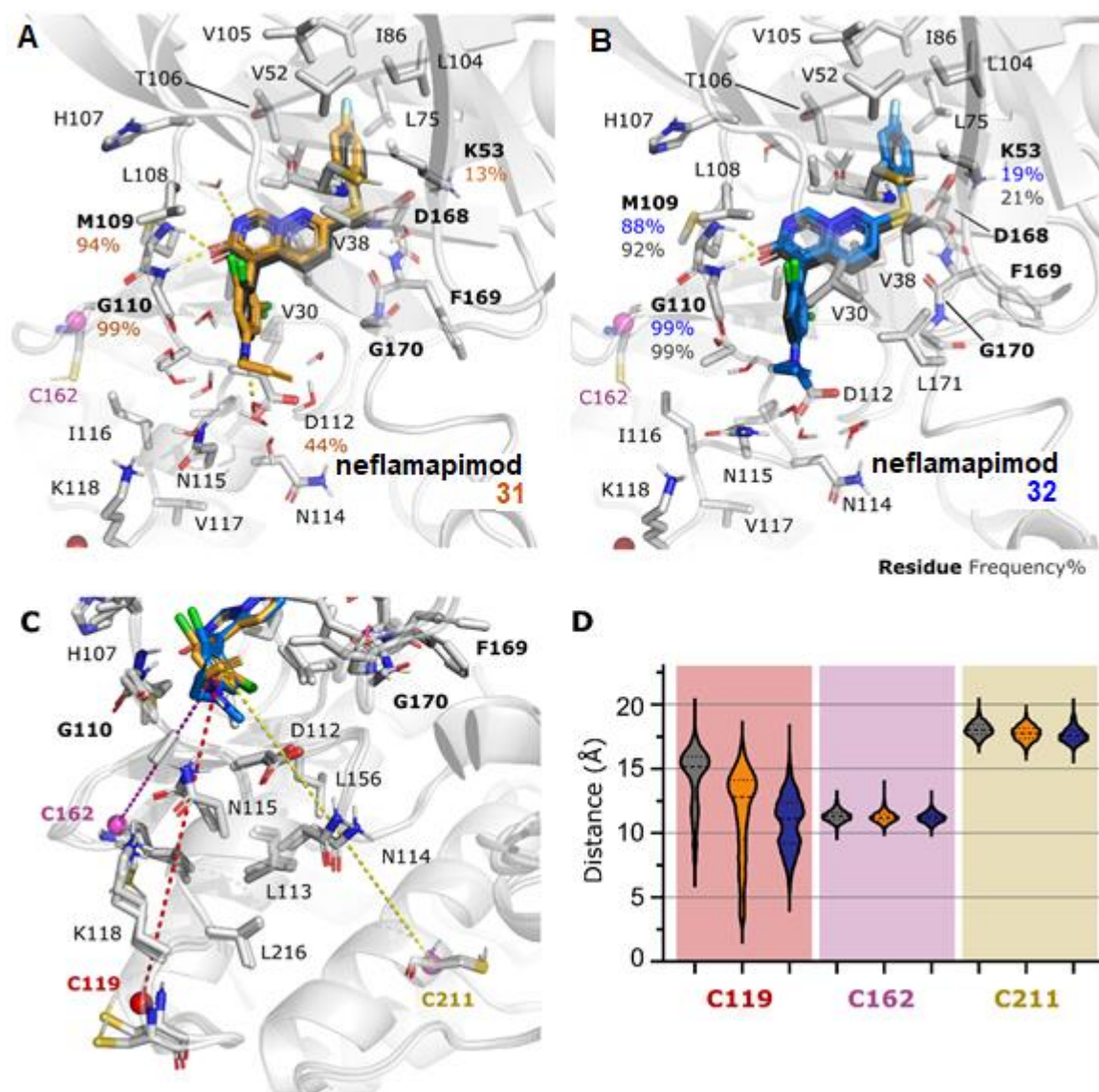
By following a ligand-based approach, the propargylamine fragment of **29** was introduced on **25**'s scaffold. Based on the SAR of neflamapimod derivatives investigated by Duffy *et al.*, every variation of substituents' nature or position negatively affected p38 $\alpha$ -MAPK inhibition.<sup>55</sup> Thus, N-propargyl moiety was introduced in the only position facing the bulk solvent (Figure 46), by adding an aniline NH<sub>2</sub> group to the 2,6-chlorophenyl ring.<sup>55</sup> Remarkably, a library of patented MAPK inhibitors (WO2001070695A1) based on **25**'s scaffold, were derivatized in the same position without loss of activity.<sup>56</sup> Moreover, despite in **29** the N-propargyl moiety is separated from the aromatic ring by a “methylene spacer”, in literature has been already reported the possibility to maintain an excellent MAO-B inhibition even by directly connecting the propargyl to the aniline NH<sub>2</sub>.<sup>270</sup> Thus, starting from the key scaffold **30**, hybrids **31** and **32** (Figure 50) were designed.



**Figure 50.** Design of neflamapimod-rasagiline hybrids **31** and **32** by fragment integration strategy.

First, the N-propargyl moiety was introduced on the aniline nitrogen to obtain compound **31**. Then, aiming to tune the propargyl nitrogen basicity and slightly increase the lipophilicity of the hybrid, the N-methyl derivative **32** was designed. Next, to preliminarily investigate whether **31** and **32** could bind to p38 $\alpha$ -MAPK and MAO-B, *in silico* studies were performed in Prof. Laufer's group. Docking studies were performed by Glide (protocol: induced-fit docking), while molecular dynamic (MD) simulations were carried out with Desmond. Considering the high similarity between the hybrids' structure and **25**, MD studies demonstrated with good reliability that **31** and **32** could reproduce the same binding mode of **25** to p38 $\alpha$ -MAPK (PDB: 3ZSI). Both analyses of key interacting residues and Root Mean Square deviation (RMSD) trend (Figure 51) pointed out that **31** and **32** could reproduce all the relevant interactions of **25** with the target, such as the Met109 and Gly110, from the hinge region, the catalytic lysine (K53) or the DFG motif (Asp168-Gly170) (Figure 51, A and B). Moreover, **31** seems to establish an additional H-interaction with a carbonyl group of the Asp112 in the hydrophobic region II (HR-II). Then, to preliminary evaluate whether p38 $\alpha$ -MAPK covalent binding could be provided by the propargyl reactive fragment, the distance between the **31** and **32**'s warhead and the cysteines close to the ATP binding pocket was considered. The docking analysis showed a conformational distribution of hybrids **31** and **32** where their most populated states displayed a distance from Cys119, Cys162, and Cys211 not allowing a covalent interaction (Figures 51 C and D).

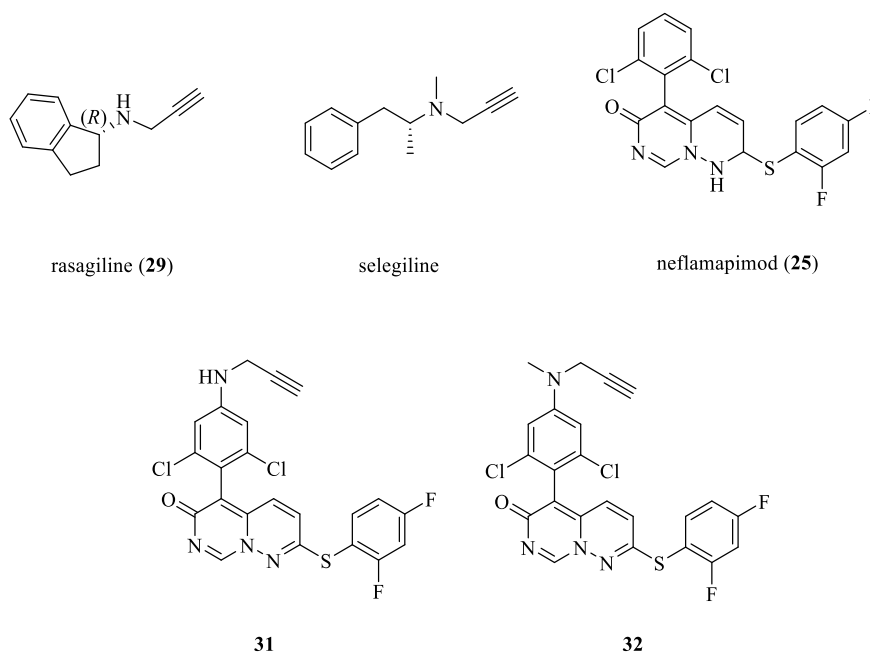




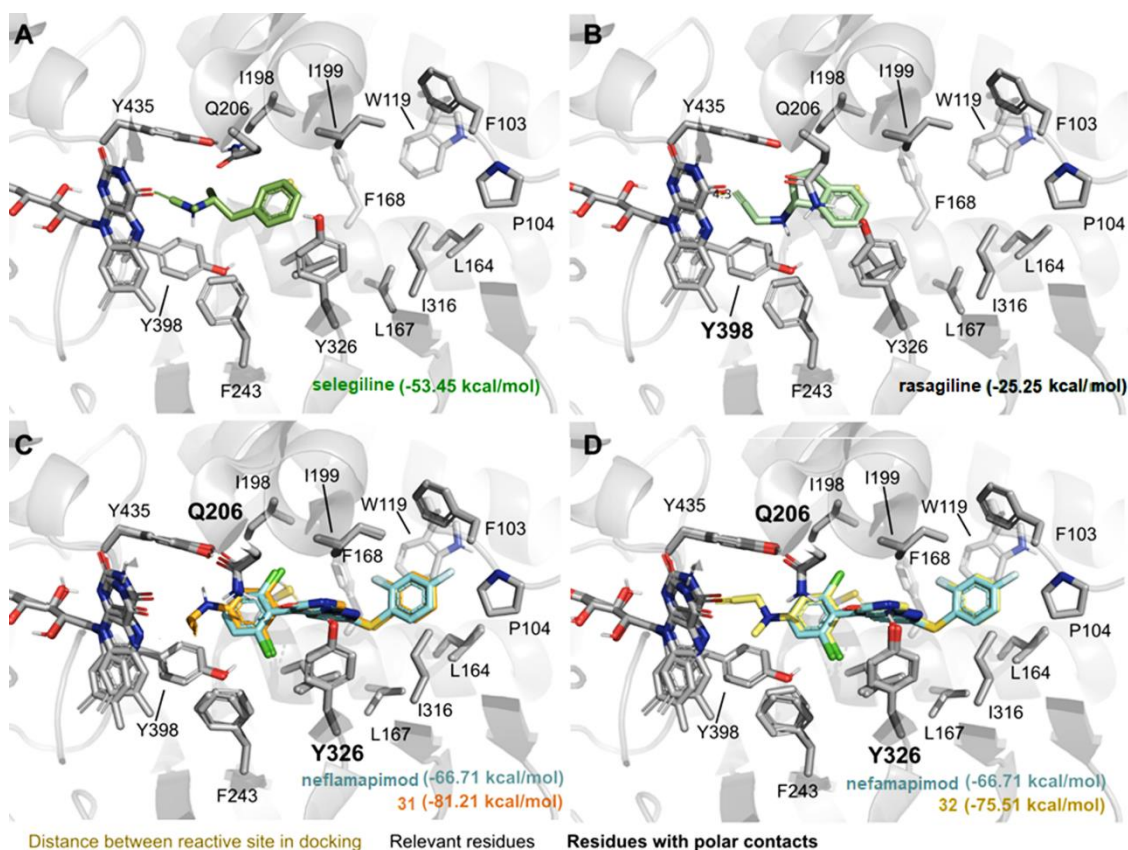
**Figure 51.** Representative frames from the MD simulations of **31** (A, in orange) and **32** (B, in blue) were superimposed on the conformation of neflamapimod (**25**) (dark grey). Residues performing relevant interactions are depicted as sticks labeled in bold. For these residues, the frequency of the interaction along the MD simulation (for each system total of 2.5  $\mu$ s) is shown as % for the reference ligand (grey) and coloured for the respective ligand. C) Representation of the HR-II from p38 $\alpha$ -MAPK highlighting not only the relevant interactions but also the position of cysteine residues (represented as coloured spheres). D) Representation of **25** (gray), **31** (orange) and **32** (blue) conformational distribution. The violin plot represents the distance between each cysteine residue sulfur atom and the propargyl moiety (centre of mass) along the simulation time.

In parallel, considering the N5(FAD)-adducts formed by **29**'s propargyl covalent binding to human MAO-B by, **25**, **31**, and **32** were docked on the same target. MAO-B-pioglitazone cocrystal was used (PDB 4A79)<sup>271</sup> because it is the highest resolution MAO-B-inhibitor co-crystal obtained with a molecule presenting a hindrance comparable to that

of our hybrids. FADH and FAD were considered as independent options during the docking assay. The highest scored docking pose underwent MM-GBSA post-docking energy minimization. Firstly, as positive controls, *N*-propargylated rasagiline and the *N*-methyl propargylated selegiline (Figure 52) were docked. Since both reference compounds showed a nice fit in the pocket (Figure 53 A and B), **25**, **31**, and **32** (Figure 52) were docked with the same protocol. All the three compounds demonstrated some sterical clashes, but both hybrids demonstrated to retrace the same conformation of **25** (Figure 53 C and D). Equally to rasagiline (**29**) and selegiline, once selected the highest-ranked pose of them, energy minimization was performed on a constant dielectric water molde (MM-GBSA). Despite the differences in size and structure of the two MAO-B inhibitors considered, reasonable **31/32**-MAO-B binding modes were obtained by energy minimization (Figure 53). Remarkably, the MAO-B binding mode of the two hybrids displayed lower energy than those of rasagiline, selegiline, and neflamapimod.



**Figure. 52.** Molecules docked on MAO-B.



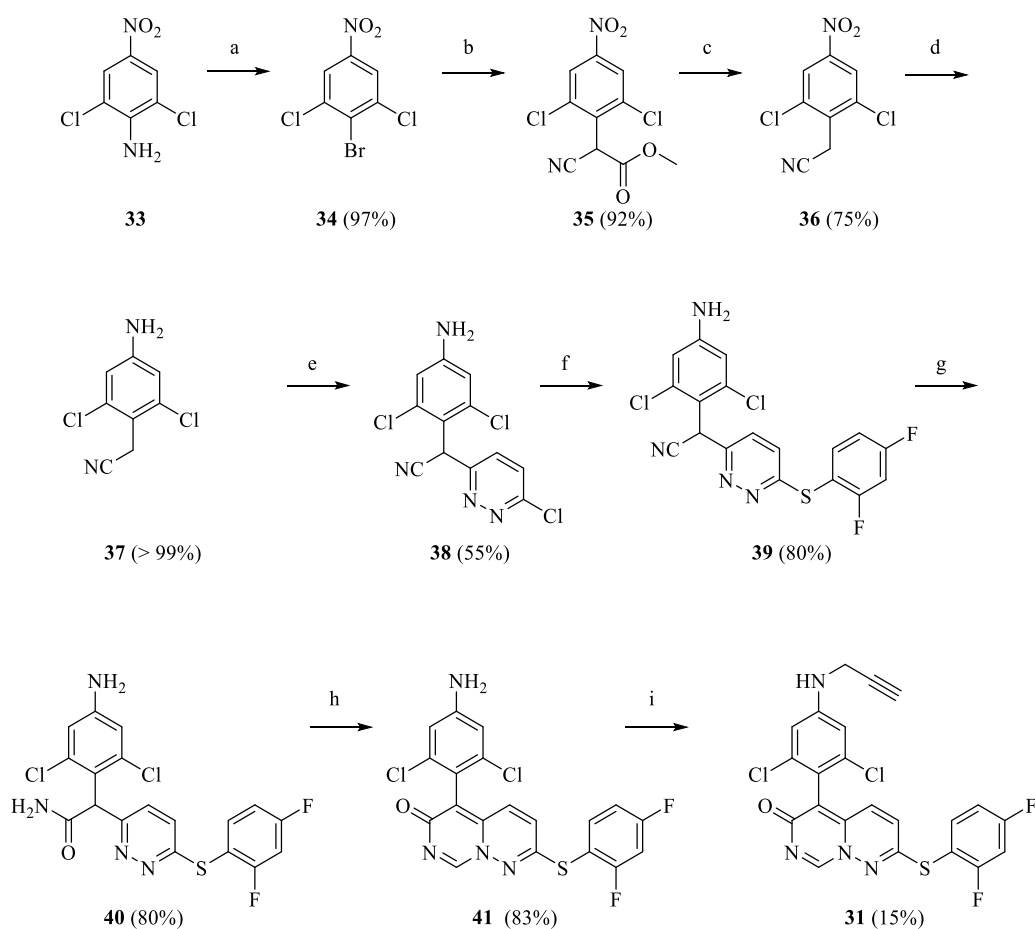
**Figure 53.** Representations were obtained after XP Glide docking simulation following the “induced fit docking” protocol. Representations of the best complexes of compounds **31** (C, in orange) and **32** (D, in yellow) superimposed to the conformation of neflamapimod (**25**) (cyan) with hMAO-B are shown. **31** and **32**’s binding mode has been predicted with respect to selegiline (A), rasagiline (**29**) (B) complexes with human MAO-B. Residues performing relevant interactions are depicted as sticks, while residues performing polar contacts are labeled in bold. Amino acid residues involved in the molecular interactions are shown as grey carbon sticks.

### 3.5.4.2 Chemistry

Hybrid **31** was synthesized according to Scheme 5. The key intermediate **37** was obtained starting from 2,6-dichloro-4-nitroaniline (**33**). As the first step, the Sandmeyer reaction was performed. The reaction proceeds by a radical-nucleophilic aromatic substitution mechanism. **33** was treated with a solution of hydrobromic acid (HBr 48%) and sodium nitrite (NaNO<sub>2</sub>) to form *in situ* the nitrous acid and the corresponding diazonium salt.<sup>272</sup> Particularly, the electrophile nitrosonium ion reacts with the aniline to afford, through a nitrosamine intermediate formation, the corresponding diazonium salt.<sup>273</sup> Then, a copper bromide/hydrobromic acid (CuBr/HBr) solution was added affording the intermediate **34** in good yield.<sup>56</sup> After CuBr/HBr addition the reaction proceeds thanks to the copper (Cu) catalyst that undergoes an oxidation-reduction cycle (Cu<sup>+1</sup> → Cu<sup>+2</sup> → Cu<sup>+1</sup>). In detail, by

the spontaneous decomposition of the unstable diazonium ion, one electron is transferred by copper (I) catalysis with loss of nitrogen gas, and an aryl radical is produced. The bromine ( $\text{Br}^-$ ) is directly transferred from the copper (II) to the aryl radical to produce the substituted arene and regenerate the copper (I).<sup>273</sup> Then, thanks to the acidity character of the  $\alpha$  proton of methyl cyanoacetate, the corresponding anion was formed *in situ* by treating with the weak base potassium carbonate ( $\text{K}_2\text{CO}_3$ ).<sup>56</sup>

**Scheme 5.** Synthetic strategy for obtaining the synthesis of hybrid **31**.



**Reagents and conditions:** a)  $\text{NaNO}_2/\text{H}_2\text{O}$ ,  $\text{CuBr}/\text{HBr}$ ,  $\text{MeCN}$ , rt, 30 min; b) methyl cyanoacetate,  $\text{K}_2\text{CO}_3$ ,  $\text{DMF}$ ,  $50^\circ\text{C}$ , 22 h; c)  $\text{H}_2\text{SO}_4/\text{AcOH}/\text{H}_2\text{O}$  (0,1/1/1),  $125^\circ\text{C}$ , 2.5 h; d)  $\text{SnCl}_2$ ,  $\text{HCl}$  (37%),  $\text{EtOH}$ ,  $75^\circ\text{C}$ , 30 min; e)  $t\text{BuOK}$ , 3,6-dichloropyridazine,  $\text{THF}$ , rt, 3 h; f)  $\text{NaH}$ , 2,4-difluorobenzenethiol,  $\text{THF}$ ,  $60^\circ\text{C}$ , 3 h; g)  $\text{H}_2\text{SO}_4$ ,  $100^\circ\text{C}$ , 30 min; h)  $\text{DMF-DMA}$ ,  $\text{THF}$ ,  $70^\circ\text{C}$ , 4h; i) propargyl bromide,  $\text{K}_2\text{CO}_3$ ,  $\text{DMF}$ , rt, 22 h.

Once formed the anion, **34** was added, and by  $\text{S}_{\text{N}}2$  mechanism a nucleophilic substitution was performed exploiting **34**'s bromine as a good leaving group. Thus intermediate **35** was obtained and used without further purification to obtain intermediate **36** by decarboxylation in strong acidic conditions.<sup>56</sup> Subsequently, **36**'s nitro group was

selectively reduced to an amine by SnCl<sub>2</sub> in presence of concentrated hydrochloric acid (HCl) under reflux conditions, to give intermediate **37** in quantitative yield.<sup>56</sup> With **37** in hands, two consequent SN<sub>2</sub> were carried out.<sup>56</sup> Firstly, the acid  $\alpha$  proton of **38** has been removed by a strong base. This step was optimized by trying different combinations of bases and solvents according to those reported in the literature (Table 9).<sup>55, 56, 274</sup> While most of the attempts didn't afford the desired compound, **38** was obtained in 55% yield by 3 eq of potassium ter-butoxide (*t*BuOK) and tetrahydrofuran (THF) (entry 6, Table 10). To study whether a higher yield could be obtained by increasing the temperature, the reaction was also performed at 40°C, but no changes were observed (entry 7, Table 10).

**Table 10.** Synthetic conditions investigated to obtain intermediate **38**.

Entry	Base (eq)	Solvent	3,6-dichloro-pyridazine (eq)	T (°C)	t (h)	Yield (%)
1	NaH (1.2 eq)	THF	1	rt	22 h	/
2	<i>t</i> BuOK (1.7 eq)	toluene	1	120 <sup>a</sup>	1.5 h	/
3	<i>t</i> BuOK (1.7 eq)	MeCN	1	rt	2 h	/
4	<i>t</i> BuOK (1.7 eq)	THF	1	65	3 h	5%
5	<i>t</i> BuOK (1.7eq)	THF	1.5	rt	3h	18%
6	<i>t</i> BuOK (3 eq)	THF	1.5	rt	3h	55 %
7	<i>t</i> BuOK(3 eq)	THF	1.5	40	3h	56 %

<sup>a</sup>Microwave irradiation (200 W).

Thus, **37** was deprotonated by *t*BuOK and the resulting anion, stabilized by resonance thanks to the presence of the nitrile group, was reacted with 3,6-dichloropyridazine (0.5 eq. excess was used) to afford intermediate **38** by monosubstitution.<sup>56</sup> The subsequent SN<sub>2</sub> reaction was performed with **38** and the 2,4-difluorothiophenol in presence of NaH to give intermediate **39**.<sup>56</sup> To obtain intermediate **40**, the nitrile group of **39** was hydrolyzed to amide by H<sub>2</sub>SO<sub>4</sub> under reflux conditions.<sup>56</sup> In turn, **40** treated with an excess of dimethylformamide dimethyl acetal (DMF-DMA) at 70°C led to the pyrimidopyridazinone ring formation.<sup>56</sup> Thus, **41** was obtained by the formation of an amidine intermediate followed by its cyclization to form the pyridazine ring.<sup>275</sup> Finally by nucleophilic substitution the propargyl fragment was introduced on **41**'s aniline group. The reaction was performed with propargyl bromide considering different conditions (Table 11).<sup>276</sup> The only successful strategy to afford the desired hybrid **31** was to perform the reaction in presence of K<sub>2</sub>CO<sub>3</sub> and a catalytic amount of potassium iodide (KI) in

dimethylformamide (DMF) (entry 6, Table 11).<sup>277</sup> However **31** was obtained in low yield, probably due to its low solubility and the poor nucleophilic nature of aniline nitrogen.

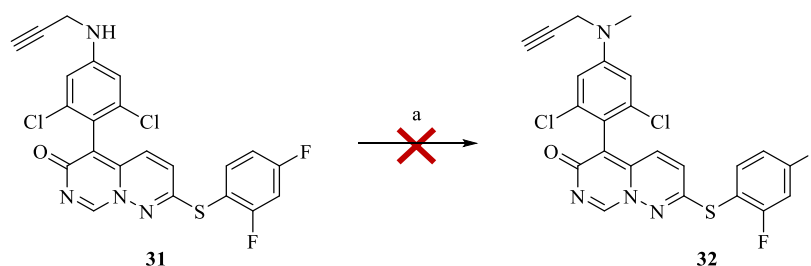
**Table 11.** Synthetic conditions investigated to obtain compound **31**.

Entry	Base	Solvent	KI (eq)	T (°C)	t (h)	Yield (%)
1	NaOH (10%)	DCM: H <sub>2</sub> O (7 :3)	/	140 <sup>a</sup>	10 min	/
2	Et <sub>3</sub> N	toluene	Reactions not performed because of the insolubility of intermediate <b>41</b>			
3	Et <sub>3</sub> N	THF				
4	Et <sub>3</sub> N	DMF	/	90 °C	5 h	traces of <b>31</b>
5	K <sub>2</sub> CO <sub>3</sub>	DMF	/	rt	22 h	/
6	K <sub>2</sub> CO <sub>3</sub>	DMF	1	rt	22 h	15%

<sup>a</sup> Microwave irradiation (200 W).

Once we optimized the synthetic strategy to afford **31**, the direct introduction of the methyl fragment on the **31** or **41**'s aniline was investigated according to Scheme 6 and Scheme 7.

**Scheme 6.** Synthesis of compound **32** by monomethylation of compound **31**.



Reagents and conditions: a) MeI, K<sub>2</sub>CO<sub>3</sub>, DMF, rt, 22h.

At first, the methylation by equimolar methyl iodide (MeI) was performed and the reaction was monitored by LC-MS (Scheme 6). After 24 h of stirring at room temperature the starting material **31** appeared unmodified, with no traces of byproducts (entry 1, Table 12), the same situation was observed in presence of an excess of MeI (entry 2, Table 12). Thus, to increase the aniline reactivity, the reaction was performed by increasing the temperature close to the MeI boiling point (T = 40 °C, entry 3, Table 12). However, the desired product didn't form but an increment of byproduct formation was observed. The unsuccess of the studied strategies can be reasonably attributed to the low aniline nucleophilicity and the steric hindrance of the propargyl moiety. To avoid these limits, the methyl fragment was introduced on **41**. To increase **41**'s aniline reactivity the

corresponding trifluoroacetamide derivative (**42**) was synthesized by trifluoroacetic anhydride (Scheme 7).


**Table 12. 31** monomethylation investigated conditions.

Entry	MeI (eq)	T (°C)	t (h)	Yield (%)
1	1	rt	24	/
2	2	rt	24	/
3	2	40 °C	3	/

Intermediate **42** was treated with  $K_2CO_3$  (2 eq), to remove the amide acid proton, and MeI (1.5 eq). Despite the expected product was **44**, LC-MS showed **43** (75%) as the main products, with a minor percentage of the unreacted **42** and **44** (25 %). Thus, for two times 1.5 eq excess of MeI and 2 eq of  $K_2CO_3$  were added every 24 h, until the LC-MS displayed the complete consumption of **42** and **44** (Table 13). **43** was obtained with traces of not-identified side products; however, the crude reaction was used without further purification.

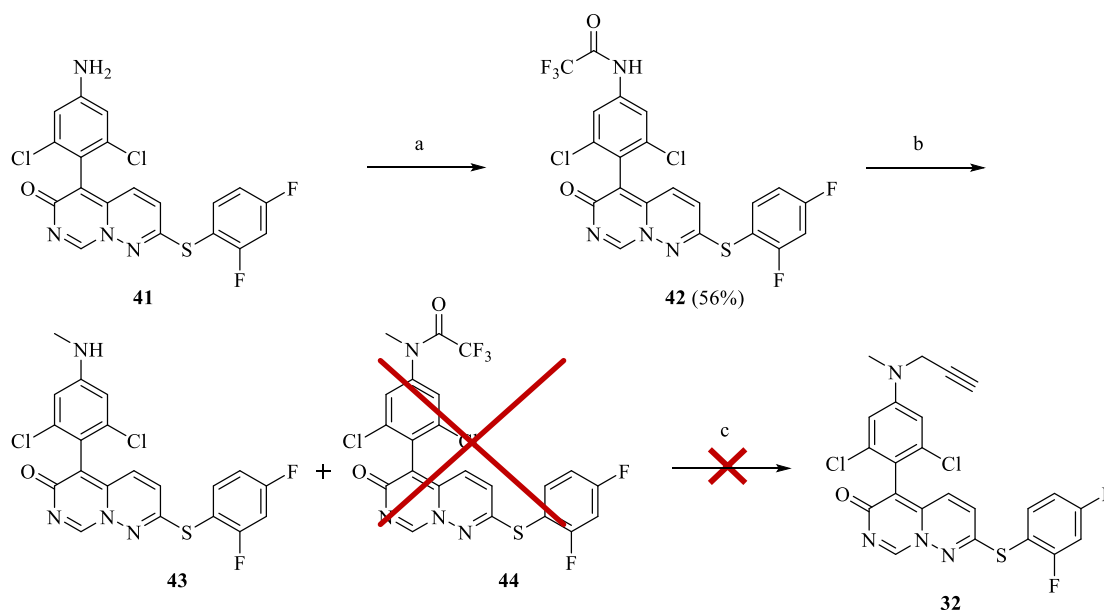
**Table 13.** Synthesis of **43**.

Entry	MeI (eq)	T (°C)	t(h)	
1	1.5	rt	24	1 <sup>st</sup> addition
2	1.5	rt	24	2 <sup>nd</sup> addition
3	1.5	rt	48	<b>43</b> + side products



Thus, a nucleophilic substitution was performed in presence of propargyl bromide and  $K_2CO_3$ , unfortunately, also in this case the desired product wasn't afforded (Scheme 7).

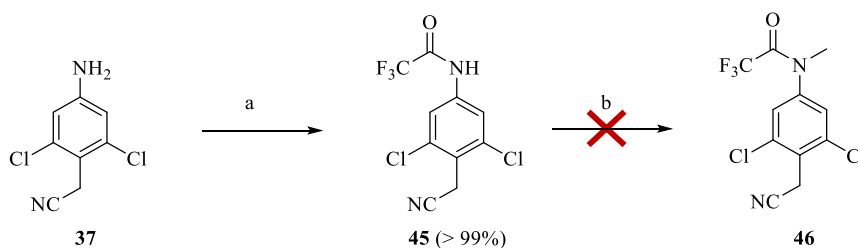
**Scheme 7.** Synthesis of compound **32** by monomethylation of compound **41**.



**Reagents and conditions:** a) trifluoroacetic anhydride,  $\text{NEt}_3$ , DMF, rt, 22h; b) MeI,  $\text{K}_2\text{CO}_3$ , DMF, rt, 72h; c) propargyl bromide,  $\text{K}_2\text{CO}_3$ , DMF, rt, 22h.

Taking advantage of the demonstrated aniline reactivity by trifluoroacetamide formation, the same strategy was used starting from intermediate **37** (Scheme 8). However, while intermediate **45** was quantitatively obtained, the introduction by MeI of the methyl substituent didn't afford the intermediate **46**, giving a complete recovery of **45**.

**Scheme 8.** **37** monomethylation by the synthesis of a trifluoroacetamide intermediate.



**Reagents and conditions:** a) trifluoroacetic anhydride,  $\text{NEt}_3$ , DCM, rt, 22h; b) MeI,  $\text{K}_2\text{CO}_3$ , DCM, rt, 22h.

The only successful strategy to afford hybrid **32** was the direct introduction of the methyl substituent on **37** aniline moiety by MeI under increased pressure (Table 14).<sup>278</sup> The reaction conditions were studied in both, conventional heating (entry 1, Table 14) and microwave irradiation (entry 2, Table 14). The reaction under microwave irradiation was selected since permitted to afford the same yield as the conventional heating in only 1.5 h.

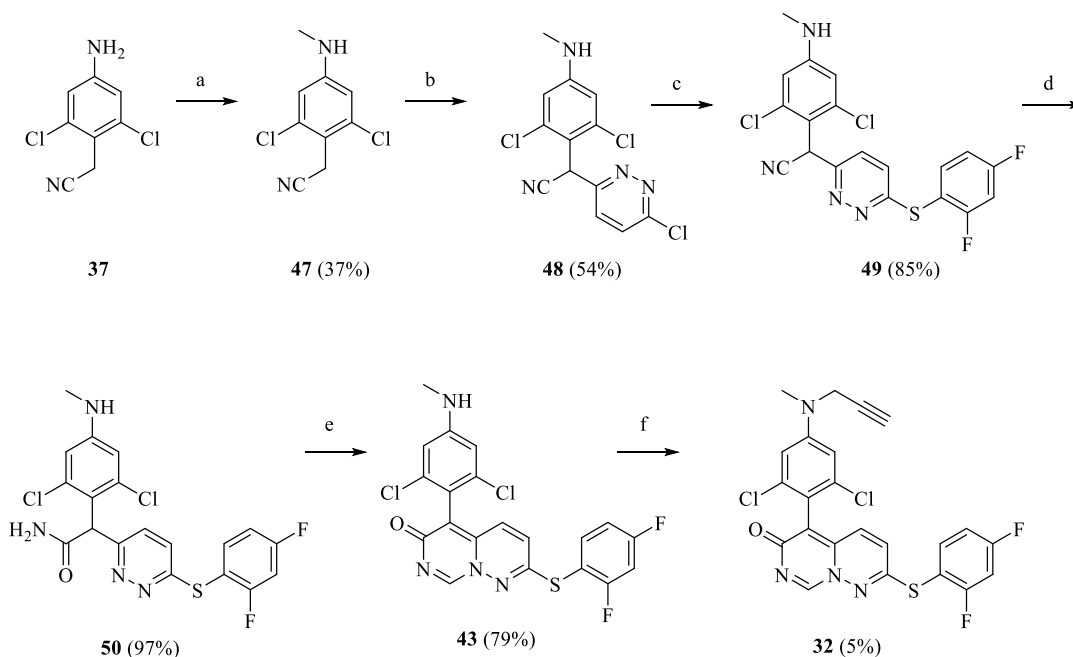


**Table 14.** Synthetic conditions investigated to optimize **37** monomethylation.

Entry	MeI (eq)	Heating system	T (°C)	t (h)	Yield (%)
1	1.2	pressure tube	55	24	35%
2	1.2	microwave	70° C	1.5	37%

Intermediate **47** was then used to synthesize the pyrimidopyridazinone core (Scheme 9). With **47** in hand, the same synthetic strategy optimized to obtain **31** was exploited, and the methylated intermediates **48-50** and **43** were obtained (Scheme 9) with yields in line with those obtained for the corresponding not methylated intermediates **38-41** (Scheme 5). Finally, the propargyl fragment was introduced on **43** by nucleophilic substitution in presence of  $K_2CO_3$  in agreement with **31** synthetic routes. The desired product **32** was afforded even if in a lower yield (5%) with respect to **31**. This difference in yield was probably due to the steric hindrance determined by the presence of the methyl substituents on **32**.

**Scheme 9.** Synthetic strategy for the synthesis of hybrids **32**.



**Reagents and conditions:** a) MeI,  $K_2CO_3$ , DMF, 70 °C microwave (200W), 1.5 h; b) *t*BuOK, 3,6-dichloropyridazine, THF, rt, 3 h; c) NaH, 2,4-difluorobenzenethiol, THF, 60 °C, 3 h; d)  $H_2SO_4$ , 100 °C, 30 min; e) DMF-DMA, THF, 70 °C, 4 h; f) propargyl bromide,  $K_2CO_3$ , DMF, rt, 22h.

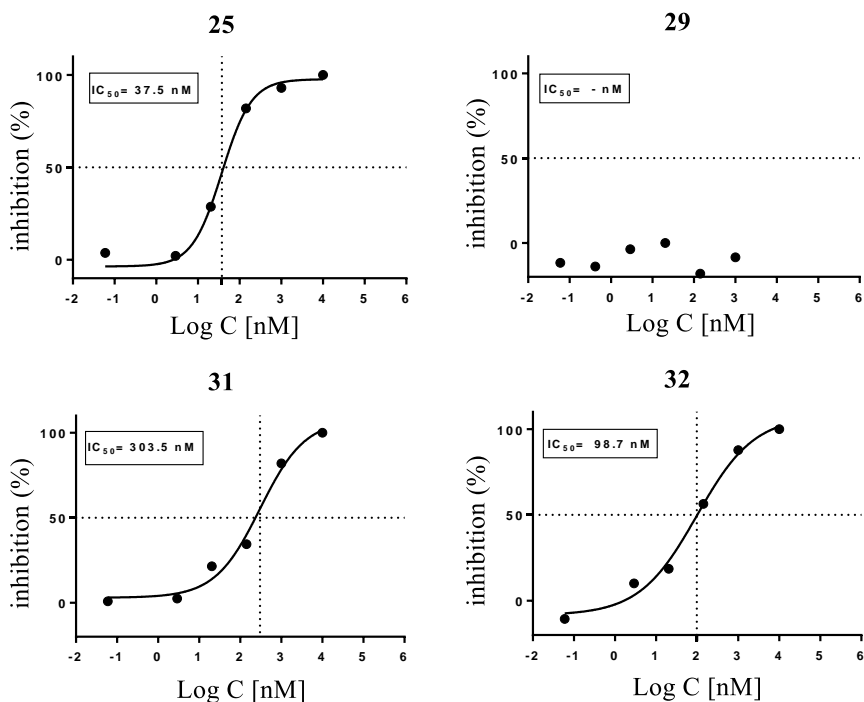
All the intermediates were characterized by  $^1\text{H}$  NMR and  $^{13}\text{C}$  NMR except for **50** which was characterized only by  $^1\text{H}$  NMR. The tested compound **31** was analyzed by  $^1\text{H}$  NMR,  $^{13}\text{C}$  NMR, and LC-MS. The tested compound **32** was analyzed by  $^1\text{H}$  NMR, HRMS, and LC-MS (see Chapter 6). In the case of **32**  $^{13}\text{C}$  NMR wasn't performed for the low quantity of final compound obtained. Both tested compounds demonstrated at least 95% purity at  $\lambda = 254$  nm.

### 3.5.4.3 Results and discussion

The following biological results were obtained by our collaborators at the Department of Pharmacy and Biotechnology (FaBiT)-University of Bologna: Prof. Monti's group for cellular assays in CGNs primary neurons and N9 microglia cells. *In silico* studies and p38 $\alpha$ -MAPK IC<sub>50</sub> evaluation were performed in Prof. Laufer's group at the Department of Medicinal Chemistry-University of Tübingen, while MAO-B inhibition was studied by Prof. Borges' group at the Department of Chemistry and Biochemistry-University of Porto. The cytotoxicity assay in HepG2 cells was performed in Prof. Fricker's group at the Institute of Pharmacy and Molecular Biotechnology-University of Heidelberg.

#### p38 $\alpha$ -MAPK inhibition

To verify whether hybrids **31** and **32** could retain p38 $\alpha$ -MAPK inhibitory activity of neflamapimod (**25**) their IC<sub>50</sub> values were evaluated. The controls and the compounds were diluted up to 10  $\mu\text{M}$ . Firstly, the good p38 $\alpha$ -MAPK inhibition of **25** was confirmed in our system. In agreement with the literature, **25** displayed an IC<sub>50</sub> in the low nanomolar range (IC<sub>50</sub> = 37.5 nM).<sup>55</sup> Notably, both hybrids **31** and **32** confirmed p38 $\alpha$ -MAPK inhibition (Figure 54) especially **32** maintained an IC<sub>50</sub> in the nanomolar range (IC<sub>50</sub> = 98.7 nM), without significant difference with respect to the reference compound **25**. To exclude any unspecific interaction caused by the reactive propargyl fragment rasagiline (**29**) was also tested. As expected, it didn't show p38 $\alpha$ -MAPK inhibition activity.



**Figure 54.** IC<sub>50</sub> values for p38α-MAPK inhibitory effects of compounds **31** and **32** in comparison with the parent compounds **25** and **29**.

### MAO enzymatic inhibition

Among the multiple activities attributed to **29**, the one currently exploited for therapeutic activity in PD is the MAO-B selective inhibition. Thus, to evaluate if hybrids **31** and **32** could display the same inhibitory activity of the parent compound **29** (IC<sub>50</sub> = 3.72 μM), they were tested at 10 μM against human recombinant MAO-B (*h*MAO-B). Unfortunately, they demonstrated negligible inhibitory activity on *h*MAO-B (Table 15).

**Table 15.** *h*MAO inhibition assay

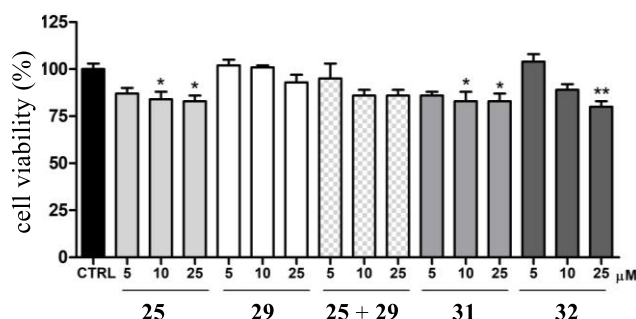
Compound	% inhibition at 10 μM or IC <sub>50</sub> (μM)		SI <sup>a</sup>
	<i>h</i> MAO-A	<i>h</i> MAO-B	
<b>25</b>	10.1 %	22.8 %	-
<b>29</b>	3.72 ± 0.38	0.149 ± 0.023	24.9
<b>31</b>	12.2 %	22.3 %	-
<b>32</b>	15.1 %	30.6 %	-

<sup>a</sup> SI: *h*MAO-B selectivity index = IC<sub>50</sub>(*h*MAO-A)/IC<sub>50</sub>(*h*MAO-B).

Considering the higher hindrance of **31** and **32** with respect to **29**, both hybrids were also tested against human recombinant MAO-A (*h*MAO-A), which presents higher substrate

permissiveness. However, also in this case no significant inhibitory activity was observed (Table 15).

#### Cytotoxicity in human hepatocyte carcinoma cells (HepG2)



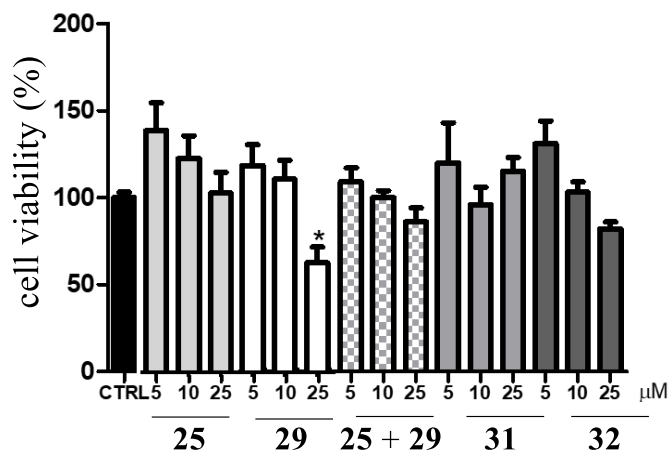
**Figure 55.** Cytotoxicity evaluation of hybrids **31** and **32** in comparison with the parent compounds **25**, **29** and their 1:1 combination (**25+29**) in HepG2 cells after 24 h treatment. Cell viability was determined by MTT assay. Results are expressed as a percentage of controls and are the mean  $\pm$  SE of 2 different experiments, each run-in quadruplicate; \* $p < 0,05$ ; \*\* $p < 0,01$  compared to control conditions (CTRL), Dunnett's test after one way ANOVA.

To preliminary evaluate whether **31** and **32** could exert a hepatotoxic effect a cytotoxicity assay in human hepatocyte carcinoma cells (HepG2) was performed. The cytotoxic profile of **31** and **32** was evaluated at 5, 10, and 25  $\mu$ M concentrations by fluorimetric MTT reduction assay. The two hybrids were compared with the cytotoxic effect of both parent compounds **25** and **29** together with their combination in 1:1 ratio (**25+29**). No toxicity was observed for **29** and **25+29** at all the tested concentrations (Figure 55). To note, **25** and **31** showed slight toxicity at 10 and 25  $\mu$ M, reducing the cell viability by around 20%. **32** showed toxicity only at the highest tested concentration (25  $\mu$ M) (Figure 55).

#### Neurotoxicity evaluation in primary neurons

To examine the neurotoxicity profile of the new hybrids **31** and **32**, primary neurons (CGNs) were employed. Both hybrids were tested at 5, 10, 25  $\mu$ M concentrations in comparison with the parent compounds **25**, **29**, and their combination in 1:1 ratio (**25+29**). Cell viability was assessed by MTT fluorimetric assay (Figure 56). All the compounds and the combination showed a trend of no toxicity at 5 and 10  $\mu$ M. To note, **25** and **31** showed no toxicity even at 25  $\mu$ M, while at the tested higher concentration, **29** and **32**

decreased cell viability respectively by about 40% and 25%. Interestingly, at 25  $\mu$ M the 1:1 combination of **25** and **29** resulted in lower cytotoxicity than **29** alone (cell viability about 75%).

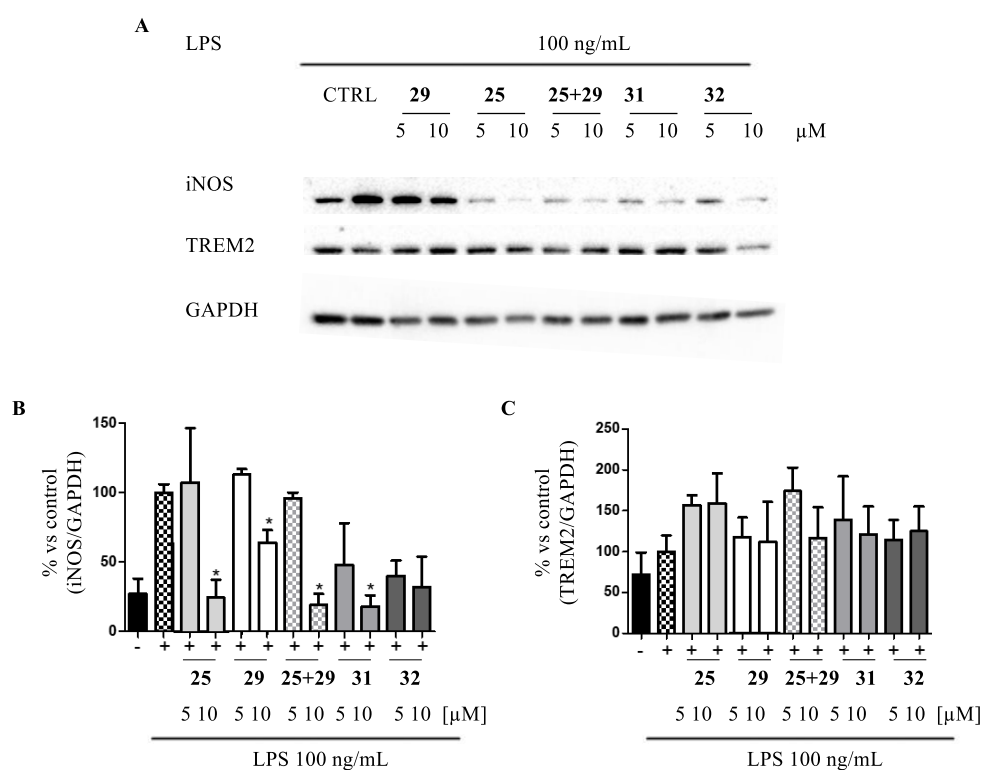


**Figure 56.** Neurotoxicity evaluation of conjugates **31** and **32** in comparison with controls **25**, **29** and their 1:1 combination (**25+29**) in primary CGNs. Cell viability was determined by MTT assay. Results are expressed as percentages of controls and are the mean  $\pm$  SE of at least 3 independent experiments, each run in triplicate. \*  $p < 0.05$  compared to control conditions (0  $\mu$ M), Dunnett test after one-way ANOVA.

#### Immunomodulation assay in microglia cells

Based on their positive neurotoxicity profiles and considering the known anti-inflammatory and immunomodulatory effect of **25**, we next evaluated whether hybrids **31** and **32** could maintain the same positive activities. Thus, the new hybrids were compared to parent compounds **25** and **29** and their combination in 1:1 ratio. Since **29**, **32** and **25+29** combination showed certain toxicity in CGNs at 25  $\mu$ M as well as **32** showed a cytotoxic effect in HepG2 concentration, immunomodulation was assessed only at 5 and 10  $\mu$ M. In immortalized microglia cell line N9, the expression of the typical M1 inflammatory biomarker iNOS and the M2 phagocytic biomarker TREM2 were evaluated (Figure 57B). The microglia cells were firstly insulted by inflammatory LPS (100 ng/mL) stimuli then, biomarker expression was evaluated through Western blot analysis (Figure 57A). LPS-treated microglial cells showed a substantial iNOS expression decrement by treatment with **31** and **32** at 5 and 10  $\mu$ M, while parent compounds and their combination significantly decreased iNOS expression only at 10  $\mu$ M. To note, **25+29** 10  $\mu$ M combination showed a stronger iNOS reduction than that observed by treatment with parent compounds alone at the same concentration. Moreover, at 10  $\mu$ M **31** reduced iNOS

expression comparably to the parent drug combination. Then, to evaluate whether **31** and **32** could modulate microglia M1/M2 phenotype switch, TREM2 expression was assessed. All the compounds tested demonstrated an immunomodulatory profile by maintaining or increasing TREM2 expression in comparison to the positive control (Figure 57C). **25** showed the most accentuated TREM2 increment, as well as **25+29** combination at 5 $\mu$ M. While slighter increment was observed for cells treated with **29**, **31** and **32** at 5 and 10  $\mu$ M. To note, **29** showed an immunomodulatory trend as well as **25**, which confirmed the expected immunomodulatory profile. Both hybrids **31** and **32** maintained the immunomodulatory trend of controls at the two tested concentrations.



**Figure 57.** Evaluation of hybrid **31** and **32** immunomodulatory effects in comparison with controls **25**, **29** and their 1:1 combination (**25+29**) in immortalized microglia cells (N9) after LPS inflammatory insult. Characteristic M1 (iNOS (B)) and M2 (TREM2 (C)) phenotype biomarkers were evaluated by western blot analysis. GAPDH was used as loading control. Densitometric results are expressed as a percentage of LPS only and are the mean  $\pm$  SE of three different experiments. \*  $p < 0.05$  compared to LPS condition, Student's  $t$  test after ANOVA.

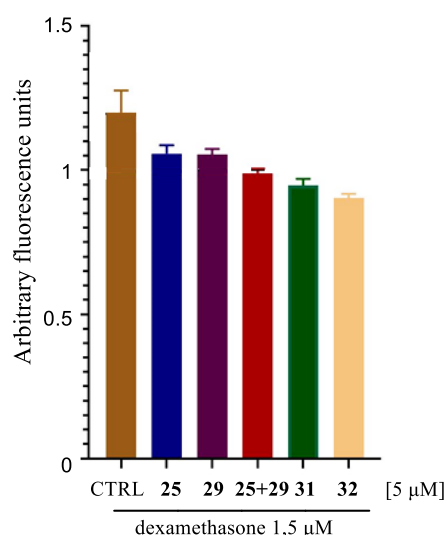
### Neuroprotective effect in CGNs

To prove whether hybrids **31** and **32** could show a neuroprotective effect thanks to the presence of the propargylamine fragment, their neuroprotective effect was assessed in

primary neurons (CGNs). Both hybrids were tested in comparison with parent compounds **25** and **29** and their 1:1 combination (**25+29**) at 5 and 10  $\mu\text{M}$  concentrations. Serum and potassium deprivation and 6-hydroxydopamine insults were used by following the protocol reported by Uliassi *et al.*<sup>279</sup>. Unfortunately, in both cases and at all the tested concentrations, the compounds didn't show any neuroprotective effect (data not shown).

#### Neuroprotective effect on dexamethasone-induced neurotoxicity in SH-SY5Y

Given the negative results in primary CGNs cells insulted with serum-potassium deprivation and 6-hydroxydopamine, neuroprotection was further tested in neuroblastoma cells (SH-SY5Y) after dexamethasone-induced stress. Dexamethasone is reported to increase MAO expression level and activity, with a consequent increment in ROS production.<sup>280</sup> Thus, neuroblastoma SH-SY5Y cells were respectively pretreated with 5  $\mu\text{M}$  of **31**, **32**, **25**, **29** or parent compound combination in 1:1 ratio (**25+29**). Subsequently, they were insulted by 1.5  $\mu\text{M}$  dexamethasone (Figure 58). After 1.5 h, ROS levels were quantified by fluorescence measurement.<sup>280</sup> Particularly, the non-fluorescent 2',7'-dichlorodihydrofluorescein (DCFH) dye was used since it is oxidized to the fluorescent 2',7'-dichlorofluorescein-diacetate (DCF) proportionally to the presence of ROS.<sup>280</sup>



**Figure 58.** Neuroprotective effects of hybrids **31** and **32** in comparison with controls **25** and **29** and their combination (**25+29**) in neuroblastoma SH-SY5Y cells after dexamethasone neurotoxic insult. Cells were pretreated (24h) at 5  $\mu\text{M}$  concentrations of the tested compounds in the presence of dexamethasone (1.5  $\mu\text{M}$ ) for 1.5 h. Protection from ROS insult was evaluated by DCF fluorescence. The results are expressed as fluorescence units  $\pm$  SE of 2 different experiments, each run in triplicate. Dunnett test after ANOVA was performed.

In agreement with the literature, **29** confirmed the reported neuroprotective effect after dexamethasone insult.<sup>281</sup> Interestingly, also **25** showed a similar protective effect against ROS toxicity. This result can be explained by the reported reduction of ROS levels after treatment with a p38 $\alpha$ -MAPK inhibitor.<sup>282</sup> To note, **25+29** combination showed a synergistic neuroprotective effect by parent compound combination, while hybrids **31** and **32** demonstrated a greater neuroprotection trend than **25**, **29**, and their combination. However, **32** seems to provide a slightly improved protection from ROS. This could be the result of a synergic effect between the neuroprotection given by the propargylamine fragment and the p38 $\alpha$ -MAPK inhibition. To note, **32** showed a higher p38 $\alpha$ -MAPK inhibition with respect to **31** (for **32** IC<sub>50</sub> = 98.7 nM, for **25** IC<sub>50</sub> = 37.5 nM, Figure 54).

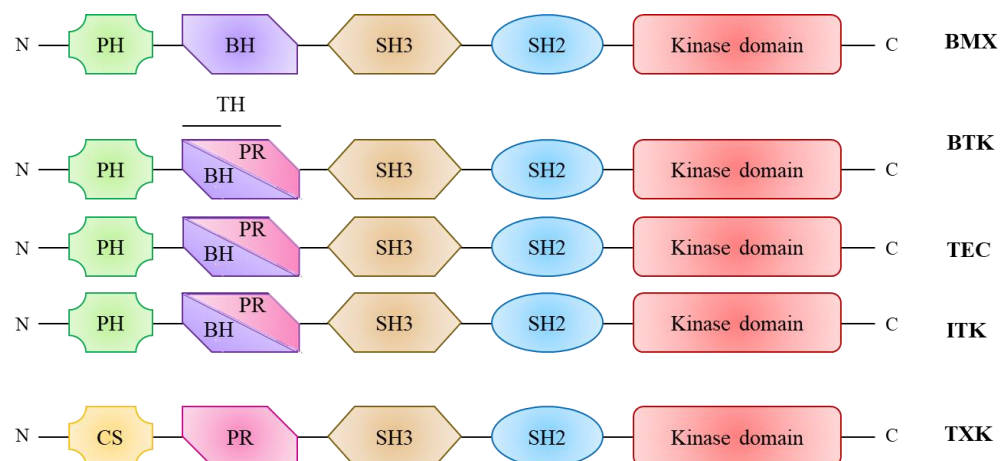


# Chapter 4



#### 4. BMX: a member of TEC protein kinase family

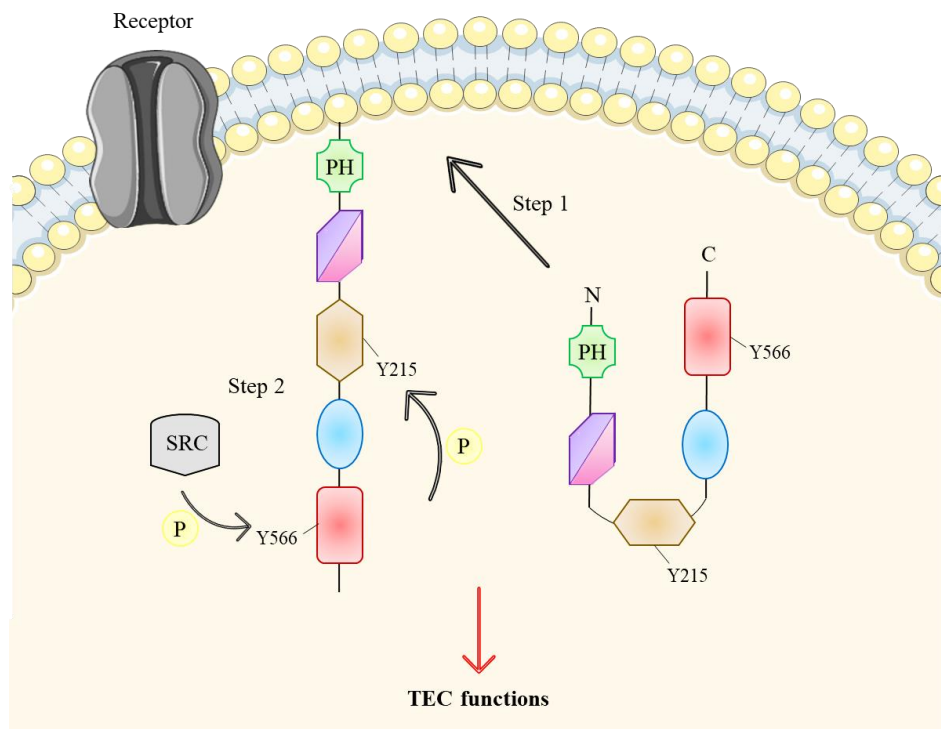
Among the families of protein-tyrosine kinases (PTKs) there is the so-called TEC family which constitutes the second-largest non-receptor tyrosine kinase family. The TEC family includes five members: the tyrosine kinase expressed in hepatocellular carcinoma (TEC), the Bruton's tyrosine kinase (BTK), the interleukin-2-inducible T-cell kinase (ITK or EMT/TSK), the bone marrow tyrosine kinase on chromosome X (BMX or ETK) and the tyrosine-protein kinase (TXK or RLK). Since they are “non-receptor-type” PTKs’ structure doesn't present a transmembrane domain. When they are inactive, they are located principally in the cytosol, upon ligand binding, TEC family member is recruited to the membrane where it binds phosphatidylinositol P<sub>3</sub>. Subsequently, it is phosphorylated on a tyrosine residue located in the catalytic domain by SRC kinase. This event allows the tyrosine autophosphorylation which starts the following signal pathway cascades.<sup>283, 284</sup> All the TEC family members, in addition to the similarities with the other PTK families (see § 3.5.1), share a further degree of homology in all their tridimensional and domain structures as well as their amino acid sequence. They possess a highly conserved C-terminal kinase domain, followed by the SRC-homology domains SH2 and SH3, in homology with the largest non-receptor-type PTKs family called SRC (Figure 59). The characteristic TEC homology domain (TH) is constituted by the Zn<sup>2+</sup>-binding region, the BTK-homology motif (BH), and the two proline-rich regions (PR) adjacent to the N-terminal pleckstrin homology (PH) domain.<sup>285, 286</sup>



**Figure 59.** Schematic representation of the TEC family kinases’ structural domains. Pleckstrin homology domain (PH); cysteine string motif (CS); BTK homology domain (BH); proline-rich region (PR); TEC homology (TH); SRC homology (SH). (Figure adapted from doi: 10.3109/08830185.2012.663838)<sup>287</sup>

However, some differences characterize the TEC family members. BMX presents a different TH domain where the proline-rich region is missing, and its SH3 domain shows a slightly differing sequence.<sup>287</sup> Moreover, TXK shows a TH domain devoid of the BH motif, and the PH domain is substituted by a cysteine string motif (CS) (Figure 59).<sup>285</sup> These mentioned domains mediate inter- and intramolecular protein interactions that play a role in regulating kinase activity and substrate access. Nevertheless, although the BH domain is considered essential for TEC family member's functions, it is not clear what the functional consequences of the differences in the BH motif are.<sup>287</sup>

BMX is the last of the five human TEC kinases discovered and the closest to the most investigated TEC family member BTK. They share the N-terminal PH domain, the SH2 and SH3 domains, and the C-terminal catalytic kinase domain, with a total of 71% of homology in amino acids for the human full-length proteins.<sup>288</sup> However, the BMX sequence differs from BTK for the TH domain structure which shows a low degree of conservation (Figure 59). Indeed, BMX diverges from BTK in the absence of the PR region. Despite the high similarity between BMX and BTK crystal structures with different ligands bound, significant differences between the two PTKs were discovered and highlighted.<sup>289</sup> Moreover, BMX differs from BTK in the hydrophobic pocket, behind the so-called "gatekeeper residue" (Thr489) between the  $\alpha$ C-helix and the  $\beta$ -strand 4. Here, BMX presents a phenylalanine (Phe475) while BTK shows a leucine (Leu460). Particularly, the steric hindrance of the Phe475 side chain in BMX forces the  $\alpha$ C-helix further away from  $\beta$ -strand 4 than does the smaller Leu460 side chain in BTK. This, not only affects the conformation of the DFG motif, but causes a greater outward tilt of BMX  $\alpha$ C-helix in comparison with BTK and a larger gatekeeper pocket in BMX.<sup>289</sup> BMX, as well as the other TEC family members' activities, is generally regulated by many cell-surface receptor pathways. They include receptor-type PTKs, cytokine receptors, antigen receptors, integrins, and G-protein-coupled receptors (GPCR).<sup>290</sup> The regulation of the active/inactive conformation is mediated by phosphorylation/dephosphorylation and protein-protein intermolecular interactions.<sup>291</sup> Particularly, for BMX, the activation occurs in two consecutive steps. At first, the kinase is translocated to the plasma membrane *via* the PH domains acting as a membrane anchor. Then, the phosphorylation of the tyrosine (Tyr566), located in the BMX catalytic domain occurs,<sup>292</sup> usually by one of the SRC kinases. Following, the autophosphorylation of BMX Tyr 215 of the SH3 domain (Figure 60).<sup>293</sup>



**Figure 60.** BMX kinase activation mechanism. (Figure adapted from doi: 10.1016/s1074-7613(00)80189-2)<sup>284</sup>

Consequently, several cellular pathways can be activated. BMX is mainly expressed in granulocytes, monocytes, epithelial and endothelial cells, as well as brain, prostate, lung, and heart.<sup>294</sup> Despite BMX's physiological and pathological role is still not fully elucidated, it seems to be involved in tumorigenicity, adhesion, motility, angiogenesis, proliferation, and differentiation. It was found overexpressed in numerous cancer types, such as breast, prostate, colon, and cervical carcinoma, suggesting a correlation between elevated levels of BMX and cancer-cell survival.<sup>294</sup> Moreover, BMX is involved in stem-cell homeostasis and survival, cardiac pressure regulation, ischemia-induced arteriogenesis and angiogenesis, and inflammatory signaling pathways.<sup>287</sup> Moreover, *in vivo* studies, demonstrated that homozygous BMX knockout mice displayed normal fertility and life span suggesting that BMX inhibition might cause few side effects. These considerations reinforced BMX inhibition as an attractive and promising therapeutic strategy.<sup>294</sup> Yet, proper validation of this kinase as a drug target will require highly specific inhibitors to be used as chemical probes in mechanistic and pharmacological experiments.

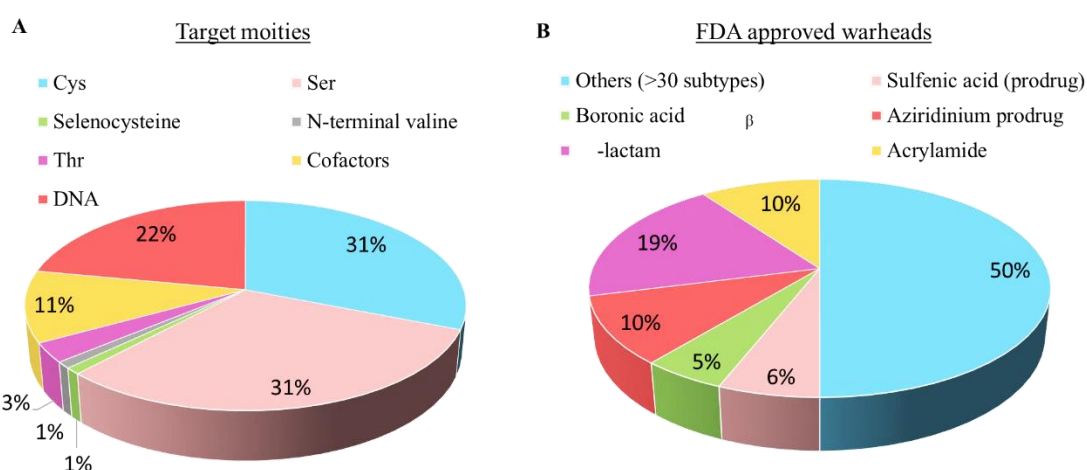
## 4.1 BMX as a potential target to modulate neuroinflammation

BMX functions have been still not completely understood however, one of the roles in which it seems to be essential is the activation of inflammatory pathways.<sup>287</sup> For instance, experimental studies demonstrated that BMX expression increased after LPS stimulation while BMX depletion reduced production of IL-8 in response to TNF- $\alpha$  and IL-1 $\beta$  stimulation in rheumatoid arthritis synovial fibroblasts.<sup>57</sup> Moreover, TLR-4, expressed peripherally, as well as in CNS (neurons, microglia, astrocytes), demonstrated to increase the release of critical pro-inflammatory cytokines, including TNF- $\alpha$  and IL-1 $\beta$ , after LPS stimulation. Particularly, BMX is activated by TLR-4 agonist and results are essential for p38-MAPK, c-Jun N-terminal Kinase (JNK), and NF-kB activation. In consequence, the pro-inflammatory cytokines TNF- $\alpha$  and IL-1 $\beta$  are released.<sup>57</sup> All these considerations together with the discovery of BMX expression in neurons led to consider its possible involvement in the pathogenesis of CNS inflammatory disorders.<sup>58</sup> So far, specific attention has been dedicated to BMX activation in response to traumatic brain injury. It is defined as a condition of altered brain functions caused by an external insult. This neuroinflammatory and neurodegenerative disorder leads to cognitive decline, increased BBB permeability, and microvascular damage in the brain.<sup>295</sup> BMX-dependent pathways seem to be crucial in the recruitment of inflammatory cells and angiogenesis after ischemic brain injury.<sup>58</sup> Particularly BMX was found overexpressed after traumatic brain injury in proportion to the severity of the trauma. Which can produce a disruption in the blood flow leading to an ischemic condition. To note, other tyrosine kinases and signal transduction proteins such as TEC, BTK, and SRC, appear unchanged after the trauma.<sup>58</sup> Ischemia induces neural degeneration through inflammation and apoptosis increasing the formation of ROS, and NO.<sup>296</sup> It was observed that ischemia enhanced BMX phosphorylation (activation). Moreover, *in vitro* neuronal models demonstrated that BMX suppression attenuates H<sub>2</sub>O<sub>2</sub>-induced cell death. Indeed, BMX phosphorylation seems to be an important mediator for cell death after free-radical damage.<sup>57</sup> From these evidences modulation of BMX activity by selective inhibitors might be a valuable strategy to control the neuroinflammatory response and protect against neurodegeneration in the ischemic brain.<sup>57</sup>

## 4.2 Project 3: optimization of covalent BMX inhibitors

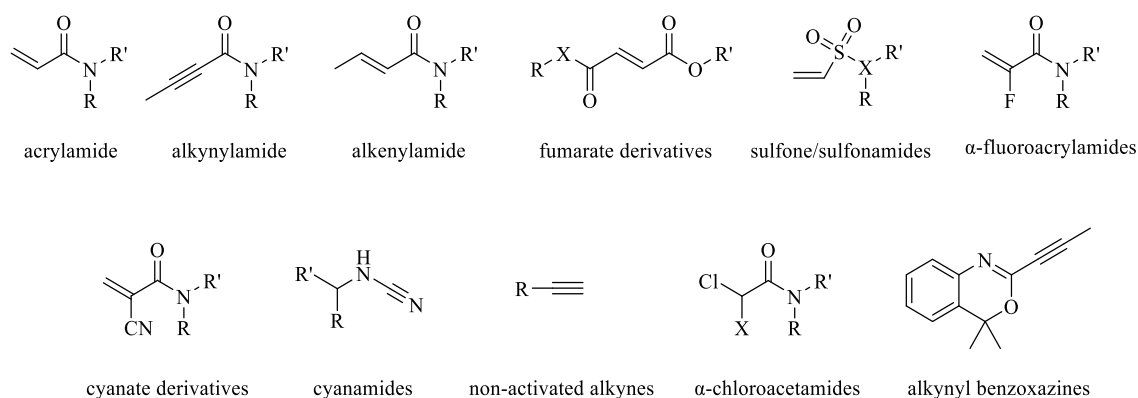
### 4.2.1 Design of covalent inhibitors targeting non-conserved cysteine residues

The covalent nature of many drugs, such as aspirin and penicillin, was only discovered after their regulatory approval. Covalent inhibition was often associated with promiscuity thus, covalent drug candidates were avoided for a long time. However, during the last 10 years, covalent drugs have seen a revival.<sup>217</sup> So far, more than 40 drugs with a covalent mechanism of action have been approved by FDA (Figure 61) and, even if most of them were discovered serendipitously, considerable advancements were done in this field.<sup>217</sup> The emerging idea of "Targeted Covalent Inhibitor" (TCI) underlines the possibility to develop inhibitors aiming to covalently address poorly conserved amino acids. These inhibitors present a covalent bond-forming functional group with “low” reactivity that can rapidly react with a non-catalytic residue after affording the right position thanks to the target binding of the reversible recognition element.<sup>217</sup> In this way, on-target reactivity can be enhanced by affinity-driven proximity and proper orientation of the reactive moiety toward a nucleophilic amino acid residue.<sup>217</sup> Importantly, the warheads required to design TCIs need a well-balanced reactivity profile. They should be reactive enough to form a covalent bond with the target residue but only after the proper alignment of both reaction partners by the reversible binding event.<sup>218</sup>



**Figure 61.** (A) Amino acids covalently targeted by FDA-approved drugs, (“DNA” includes all the nonspecific alkylating agents and “cofactors” include pyridoxal phosphate, heme groups, flavin adenine dinucleotide (FAD), and nicotinamide adenine dinucleotide (NADH)). (B) Main warheads present in FDA-approved drugs. (Figure adapted from doi: 10.4155/fmc-2020-0236 )<sup>217</sup>

TCIs are typically generated by a structure-based design strategy starting from reversible ligands. The ligand's structures are usually designed by introducing on an optimized affinity element a relatively “unreactive” electrophilic covalent group, the “warhead”, to address a nucleophilic amino acid, classically a cysteine.<sup>216</sup> In protein kinases cysteines don't take part in the catalysis but may be involved in regulatory functions resulting in a low degree of conservation. Notably, cysteine is a relatively rare amino acid with a prevalence of only 1.9%. Consequently, the targeting of cysteines located in proximity to the kinase ATP binding site is a suitable strategy for covalent inhibitor development. However, compared to catalytic cysteines in cysteine protease, non-catalytic cysteines are less reactive and prone to mutations, which has a significant impact on covalent inhibitor design efforts.<sup>218</sup> The particular reactivity of cysteine arises from the presence of a thiol group in the side chain. Compared to hydroxy groups found for example in serine, such thiols can easily be deprotonated and represent the strongest nucleophile among the 20 canonical amino acids.<sup>297</sup> Thus, the development of selective cys-targeting inhibitors not only as potential drug candidates but also as chemical probes is a valuable strategy. Specific covalent kinase inhibitors can serve as fundamental tools for mechanistic investigation of understudied kinases such as TEC family members and their validation as drug targets.<sup>217</sup> Many different Cys-targeting warheads are reported in the literature.<sup>218</sup> However, only some of them possess favorable properties that could be exploited in the clinic, such as stability and selectivity.



**Figure 62.** Examples of cysteine-targeted warheads used for covalent inhibitor design.



For example, most of the recent FDA-approved cysteine-targeting covalent inhibitors use an acrylamide moiety (Figure 62) as the warhead.<sup>217</sup> It is, together with other  $\alpha,\beta$ -unsaturated carbonyl compounds, the predominant covalent-reactive group to target non-conserved non-catalytic cysteine residues. The greatest success of acrylamide is due to its well-balanced reactivity as a Michael acceptor. Indeed it demonstrated to avoid promiscuous interactions because it is sufficiently reactive only brought in proximity to a nucleophilic cysteine by a reversible binding event.<sup>298, 299</sup> Thus, reactivity tuning plays an important role, not only in preventing promiscuity but also in enhancing on-target efficacy.<sup>299</sup> The reactivity of the cysteine's thiol group depends on steric and electronic factors as well as on solvation; however, the ease of thiol deprotonation (i.e. the cysteine's  $pK_a$  value) is generally the main element that influences its reactivity toward electrophiles.<sup>300</sup> The reaction mechanism of Michael's addition includes cysteine thiol deprotonation to form a thiolate before it reacts with an acrylamide functional group of the inhibitor (Figure 41).<sup>300</sup> Thus, more reactive cysteines tend to have lower  $pK_a$ 's increasing the probability of the cysteine being in the thiolate state.<sup>300</sup> Other representative Michael's acceptors are alkynyl or alkenyl amides, which are supposed to react with thiols via a similar conjugate addition,<sup>301</sup> fumarate derivatives, that demonstrated to minimize time-dependent off-target modification due to metabolic inactivation<sup>302</sup> and vinyl sulfones/sulfonamides that react with cysteine but also showed significant reactivity towards lysine (Figure 62).<sup>218, 303</sup> Moreover, to tune the warhead reactivity, alternative warheads can be used, such as  $\alpha$ -fluoroacrylamides. Despite it is becoming a common warhead, the chemical reason behind its reduced reactivity is not yet clear.<sup>304</sup> One possibility is that the observed "less reactivity" can be the result of a reversible covalent bond formation.<sup>217</sup> The replacement of the fluorine with a stronger electron-withdrawer such as the cyanate<sup>305</sup> could be a strategy to design covalent reversible inhibitors where the increased acidity of the  $\alpha$ -proton in the adduct favors retro-Michael's addition. Pinner-type additions<sup>306</sup> were exploited to design reversible covalent inhibitors with cyanamides.<sup>305</sup> In alternative, reactions related to Michael's additions are also described for compounds presenting activated heteroaryl alkynes, in which the intermediate negative charge created upon thiol addition is stabilized by the heteroarene and non-activated alkynes (Figure 62). One of the most recently investigated cysteine-targeting warheads is the alkynyl benzoxazines,<sup>307</sup> but it's not well studied in terms of applicability (Figure 62).

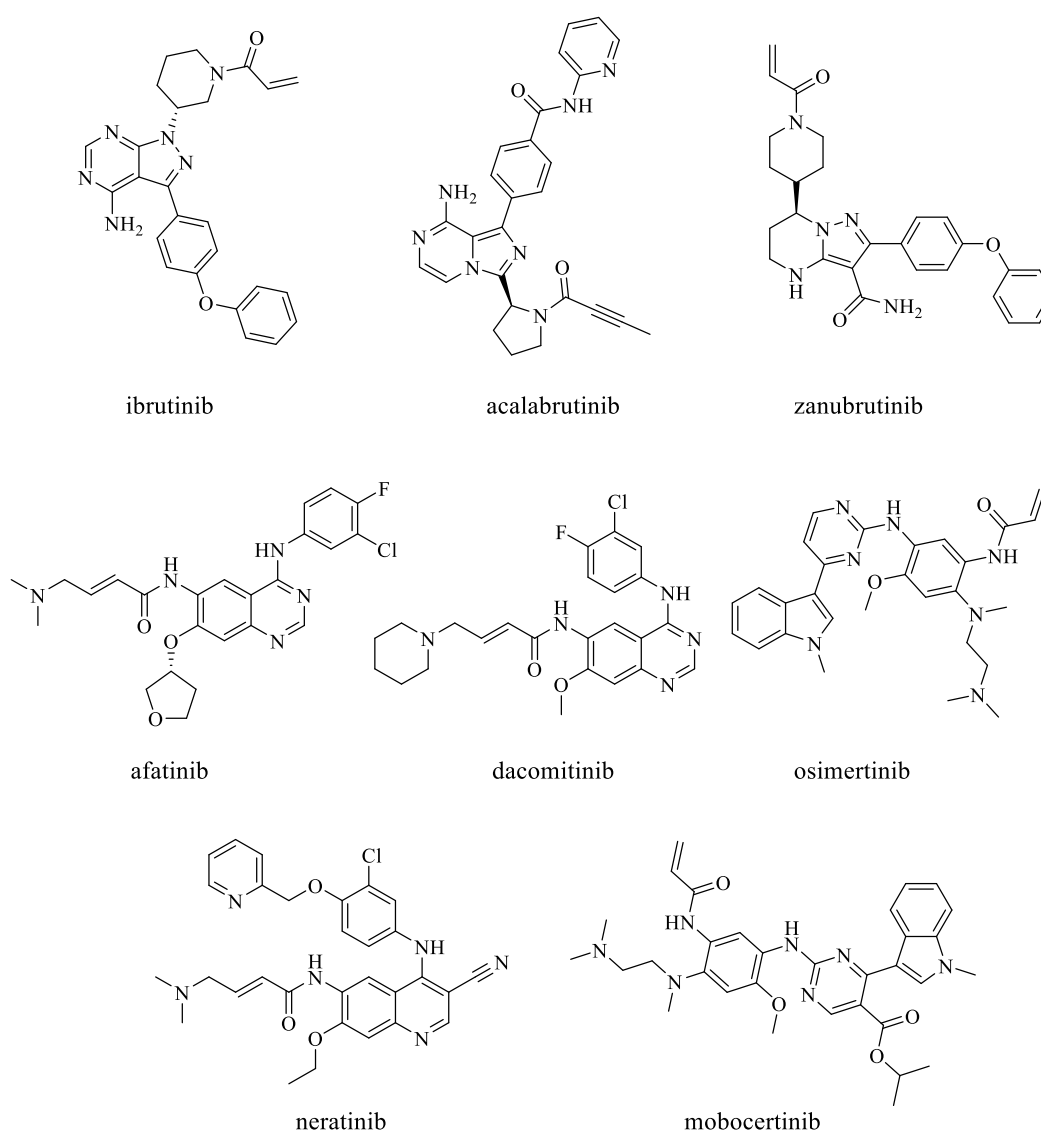
Moreover, non-activated alkynes can also undergo an addition reaction. However, this reaction is very rare and limited to highly activated nucleophiles (*e.g.* in certain cysteine proteases) and thus considered to be highly specific.<sup>308</sup> Nucleophilic substitution mechanisms ( $S_N2$ ) as described for  $\alpha$ -chloroacetamides, are frequently used in fragment-based covalent drug ligand and chemical biology but are usually considered too promiscuous for drug design.<sup>309</sup> Thus, the introduction of a substituent such as a sterically hindering  $\alpha$ -methyl group ( $\alpha$ -chloroacetamides, X = Me) or an additional fluoride ( $\alpha$ -fluorochloroacetamides, X = F), was investigated. In both cases, the introduced modifications resulted in the desired decrease in intrinsic reactivity.<sup>309</sup>

#### 4.2.2 TEC kinase FDA approved inhibitors

Among the TEC kinase family, BTK is the most studied member due to its important function in B-cell receptor signaling essential for B-cell development. Recently, three covalent BTK inhibitors targeting a non-conserved cysteine, namely ibrutinib,<sup>310</sup> acalabrutinib<sup>311</sup>, and zanubrutinib<sup>312</sup> were approved by FDA for the treatment of different B-cell lymphomas, while ibrutinib was also approved for chronic graft-versus-host disease treatment (Figure 63).<sup>313</sup> Despite the different selectivity profiles, all these share the same mode of inhibition *i.e.*, covalent binding to BTK's non-catalytic Cys481 located in the front pocket of the ATP binding site close to the  $\alpha$ D-helix ( $\alpha$ D-1 position).<sup>314</sup> However, despite strong evidence suggesting the crucial roles of the other TEC family members in different disease conditions, the effort on specific inhibitor development is still limited, especially for BTK's closest relative BMX.<sup>315</sup>

By comparison, it was discovered that also all the other TEC family members and few additional kinases have the same non-conserved cysteine as found in BTK. Besides its presence in all the five TEC kinases (Cys496 in BMX; Cys481 in BTK, this  $\alpha$ D-1 cysteine is found in the epidermal growth factor receptor (HER) family (except HER3), JAK3, B-lymphoid tyrosine kinase (BLK) and the mitogen-activated protein kinase MKK7 (MAP2K7). On the one hand, the presence of the  $\alpha$ D-1 cysteine gives a possibility for an irreversible targeting in all the mentioned kinases. On the other hand, it can give rise to covalent inhibitors targeting that cysteine showing cross-reactivity with other family members.<sup>216</sup> However BTK inhibitors are not the only drugs targeting the  $\alpha$ D-1 cysteine currently approved. The HER family inhibitors afatinib,<sup>316</sup> dacomitinib<sup>317</sup>, and osimertinib,<sup>318</sup> the HER2 inhibitor neratinib<sup>319</sup> (Figure 63) have been also authorized by

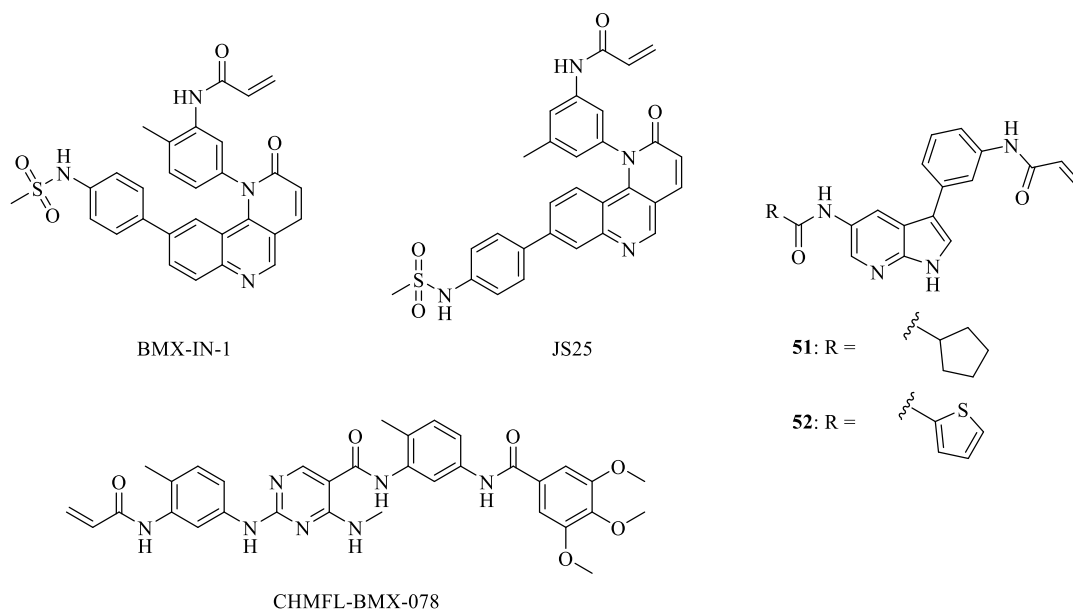
FDA, and the recently approved mobocertinib that targets epidermal growth factor receptor (EGFR).<sup>320</sup> However, focusing on the TEC family, the most explored example of investigating kinases by chemical probes is BTK. Unfortunately, the little difference in TEC family members' binding sites and the lack of understanding of these pockets, make the development of highly selective covalent TEC inhibitors still challenging. For example, the research in specific ITK inhibitors is struggled by lower cysteine reactivity<sup>321, 322</sup> and the larger gatekeeper residue while only few examples of selective inhibitors are published regarding the less studied BMX and no inhibitors specifically addressing TXK or TEC have been discovered.



**Figure 63.** Structure of covalent protein kinase inhibitors approved by FDA that act targeting the  $\alpha$ D-1 cysteine in HER or BTK kinases.

### 4.2.2.1 BMX inhibitors

Despite the limited knowledge about the pathological roles of BMX, its involvement in various disorders has been suggested, even if it is not completely understood. Aiming to develop selective BMX inhibitors, several small molecules or peptides were developed as potential chemical probes. Unsurprisingly, however, they often showed a promiscuous activity inhibiting, besides BMX, other TEC kinase family members or other kinases.<sup>323</sup> So far only few structural series of covalent BMX inhibitors targeting the non-conserved Cys496 in  $\alpha$ D-1 position were discovered. The first inhibitor discovered was BMX-IN-1 (Figure 64), a benzonaphthyridinone scaffold with an acrylamide warhead.<sup>323</sup> BMX-IN-1 inhibited the proliferation of prostate cancer cell lines with a balanced activity on both, BMX and BTK ( $IC_{50}$  in the nanomolar range).<sup>323</sup>



**Figure 64.** Structure of BMX inhibitors that target covalently the non-conserved cysteine in  $\alpha$ D-1 position (Cys496).

Nevertheless, BMX-IN-1 showed to be one of the most potent BMX inhibitors reported in the literature (BMX  $IC_{50}$  = 25 nM).<sup>3</sup> The benzonaphthyridinone core was later investigated in more detail by Seixas *et al.* who developed a small follow-up series of BMX inhibitors closely related to BMX-IN-1's structure.<sup>294</sup> All the compounds maintained the strong BMX inhibitory potency of BMX-IN-1 and analog JS25 (Figure 64) proved to be the most potent compound in a cellular context (JS25  $IC_{50}$ : 44.8 nM vs BMX-IN-1  $IC_{50}$ : 495 nM).<sup>294</sup> A different series of covalent BMX inhibitors was

discovered by Liang *et al.*<sup>324</sup> These compounds with a 2,6-diaminopyrimidine scaffold can be exemplified by CHMFL-BMX-078 (Figure 64). CHMFL-BMX-078 is a highly selective type II irreversible BMX inhibitor. It addresses BMX hydrophobic back-pocket which is only accessible in the DFG-out conformation. Indeed, CHMFL-BMX-078 showed a major affinity for the BMX inactive conformation while the affinity for the active (phosphorylated) kinase was weak (apparent  $K_d > 10 \mu\text{M}$ ).<sup>324</sup> Very recently, Foster *et al.* presented a new series of potential BMX covalent inhibitor with a 7-azaindole core derivatized in the 3 and 5 positions.<sup>61</sup> This series, illustrated by the most promising compounds **51** and **52**, demonstrated a dual inhibitory profile against BMX and BTK with a low nanomolar  $\text{IC}_{50}$  value against both kinases (Figure 64).<sup>61</sup>

### **4.2.3 The importance of the chemical probes in chemical biology and drug discovery**

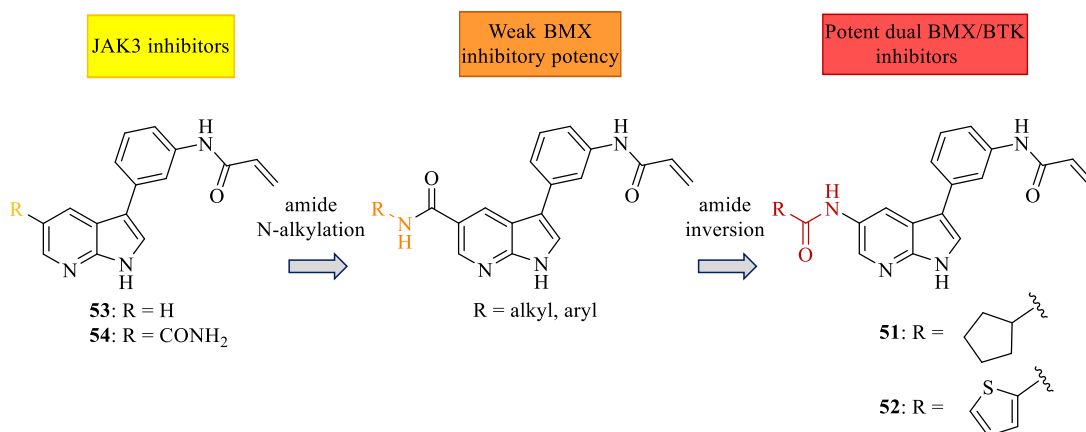
The decoding of the entire human genome sequence raised expectations for the identification of many novel targets explorable in drug discovery. Nevertheless, the number of drug approvals did not increase at the expected rate, especially since many compounds in clinical trials failed to achieve clinical efficacy.<sup>325</sup> Among the main reasons for attrition there was poor target selection which plays a pivotal role in the early steps of drug discovery. Indeed, the often insufficient target validation at the preclinical level and the lack of understanding of the molecular pathological mechanisms hampered the discovery of new drugs.<sup>326</sup> Thus, the experimental validation of new clinically relevant targets is of primary importance. For this purpose, the production of selective chemical probes is a major requirement to avoid pharmacological promiscuity or insufficient target engagement. Indeed, an erroneous interpretation of the data can convert into inappropriate conclusions with respect to the potential of a target.<sup>327</sup> Thus, well-validated high-quality chemical probes are of utmost importance. They are defined as selective small-molecule that, by protein function modulation, give information about the mechanistic and phenotypic roles of a protein in biochemical, cell-based, or animal studies.<sup>325</sup> Chemical probes are mainly exploited to study the biological tractability and functional profile of a target. This includes the understanding of the relationship between a target and its phenotype as well as the possibility to modulate that phenotype by a small molecule.<sup>325</sup> Overall, these small molecules are fundamental tools to investigate the potential for efficacy, mode-of-action, and on-target safety can be addressed as well. Moreover, they

may be further developed into therapeutic agents.<sup>325</sup> Pharmaceutical industry also exploits chemical probes to establish the clinical translatability of a target from the basic scientific findings in a laboratory setting to the potential human applications. Translatability can finally result in potential new treatments or biomarkers for disease.<sup>326</sup> In the end, it is important to consider that even if chemical probes can be a good starting point for drug development, drugs, and chemical probes can be very different. A drug does not always need to have an exquisitely selective activity profile since many drugs owe their success to their multiple target modulation. However, they need to be safe and effective.<sup>324</sup> In turn, chemical probes do not need to meet the same good pharmacokinetics and pharmacodynamics as drugs. While having less stringent requirements for drug-likeness, chemical probes must demonstrate a clear mechanism of action, high potency, and selectivity to be useful for investigation of target biology.<sup>325</sup> So far, nearly 25% of the protein kinases discovered have no known function and about 50% are not well characterized. Thus, despite the complete kinome having been decrypted, the knowledge about protein function did not change substantially in recent years.<sup>315</sup> Notably, the inadequate protein kinases' characterization is often due to the unavailability of high-quality chemical probes (potency against the target < 100 nM, cellular potency < 1  $\mu$ M,  $\geq$ 30-fold selectivity against other kinases) to study the target biology and not to the absence of interest.<sup>315</sup> In light of this, covalent kinase inhibitors can be a very successful strategy since the covalent mode of action can promote high potency and durable target engagement.<sup>216</sup> However, the high similarity shared by kinases influences the achievement of selectivity, which is particularly challenging. As previously mentioned, targeting noncatalytic cysteines, which are poorly conserved around the ATP binding site is a valuable strategy.<sup>315</sup>

#### **4.2.4 The discovery of a new series of covalent BMX inhibitors: rationale of the project**

As mentioned, BMX is the last-discovered member of the TEC family and it is also one of the members least understood in terms of its physiological/pathological role. For this purpose, the discovery of selective BMX inhibitors as chemical probes is of primary importance since they represent a fundamental tool in chemical biology and drug discovery fields. Selective BMX chemical probes could permit a deeper understanding of the mechanistic and phenotypic role of this kinase, which in turn can drive important information regarding its pathological involvement. As previously said, a further step for

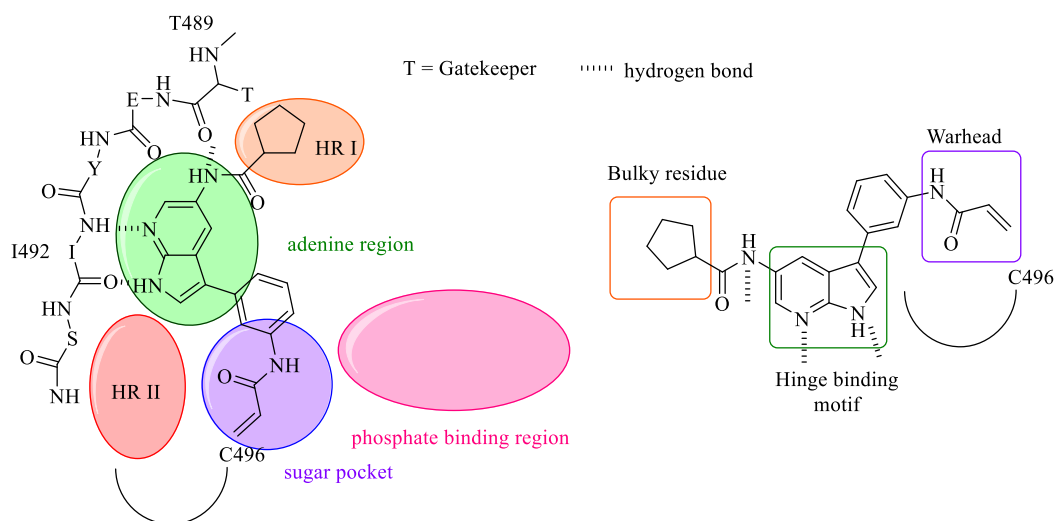
obtaining high-quality chemical probes is the possibility to form a covalent binding. Since covalent binding can provide several advantages such as prolonged duration of action, improved potency, and exquisite selectivity when they target a non-conserved amino acid.<sup>216</sup> However, the discovery of selective covalent inhibitors is still considered challenging since the electrophilic warhead can be a source of unspecific reactions and intrinsic non-selectivity. Moreover, affording the selectivity in kinases is even more challenging due to the high similarity grade shared by kinases, especially among kinases belonging to the same family. A valuable strategy to avoid the unspecific binding of covalent kinase inhibitors is the development of TCI targeting non-conserved amino acids. For this purpose, TEC family members present the useful non-conserved cysteine in  $\alpha$ D-1 position.<sup>314</sup> Recently, the groups of Prof. Laufer and Prof. Gehring discovered a small set of JAK3 covalent inhibitors that share a 7-azaindole core and an acrylamide as the reactive warhead (**53** and **54**, Figure 65).<sup>61</sup> Both compounds demonstrated that by the H-bonds interaction of their 7-azaindole's nitrogens with the JAK3 hinge region, their warheads were positioned for the efficient covalent reaction of the acrylamide Michael acceptor with the  $\alpha$ D-1 cysteine.<sup>61</sup> While **53** and **54** demonstrated a high JAK3 selectivity ( $IC_{50} < 0.1$  nM) over most of the kinases featuring this non-conserved cysteine (EGFR, HER2, HER4, BLK, MAP2K7), they showed a strong inhibition against two TEC family members, BMX and TXK.<sup>61</sup> These evidences offered a good starting point for the development of new BMX covalent inhibitors.



**Figure 65.** Development of covalent BMX inhibitors with a 7-azaindole scaffold.

Aiming on this, the gatekeeper residue was exploited as an additional selectivity filter and several N-substituents were introduced at the 5-carboxamide's nitrogen. Indeed, JAK3 presents a methionine gatekeeper residue, which is relatively “big” with respect to the

smaller threonine gatekeeper residue of BMX and other TEC kinases (except ITK). Thus a new series of compounds was developed that, as expected, switched the selectivity from JAK3 to BMX. However, this modification resulted in a strong loss in inhibitory potency (Figure 65).<sup>61</sup> Based on this result, molecular modeling studies were performed aiming to maintain the preferential BMX inhibition while increasing the potency of the inhibitors. Docking simulations suggested that inversion of the 5-carboxamide could allow for an additional hydrogen bond between the NH of the inhibitors' carboxamide and the hydroxy group of the BMX threonine gatekeeper residue (Figure 66). Thus, a third series of covalent inhibitors was developed exemplified by the best compounds **51** (BMX IC<sub>50</sub> = 2.2 nM / BTK IC<sub>50</sub> = 2.2 nM) and **52** (BMX IC<sub>50</sub> = 1.1 nM / BTK IC<sub>50</sub> = < 1 nM). Both strongly inhibit BMX showing an IC<sub>50</sub> in the nanomolar range. Particularly **51**, showed a balanced inhibitory activity on BMX and the closest TEC family member BTK while sparing most other kinases with an equivalent cysteine.<sup>61</sup>



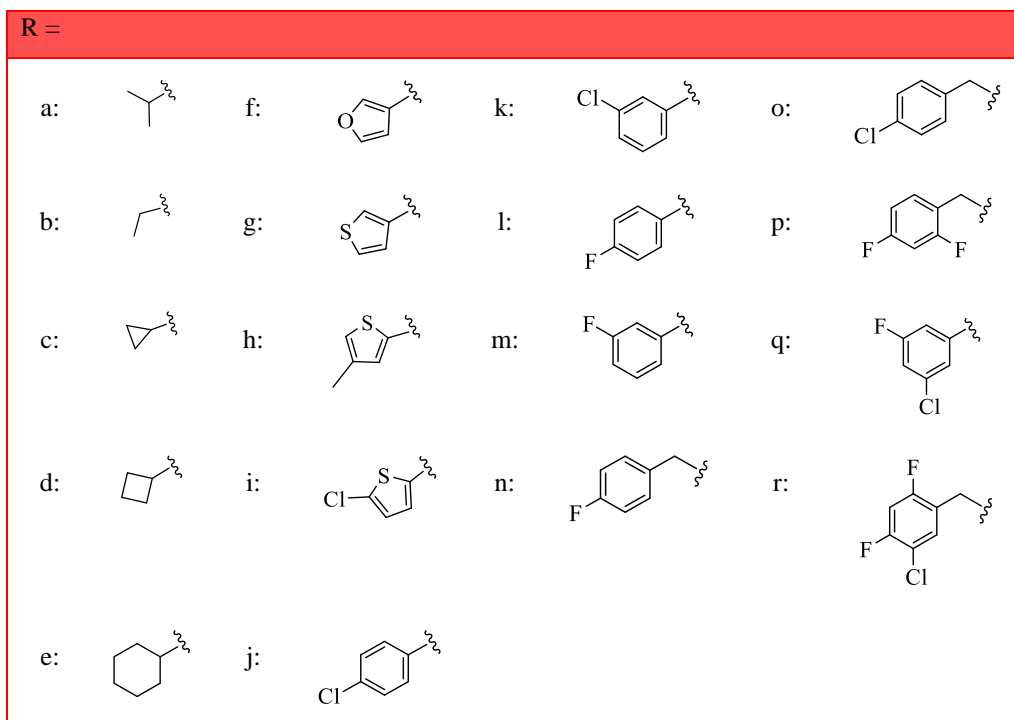
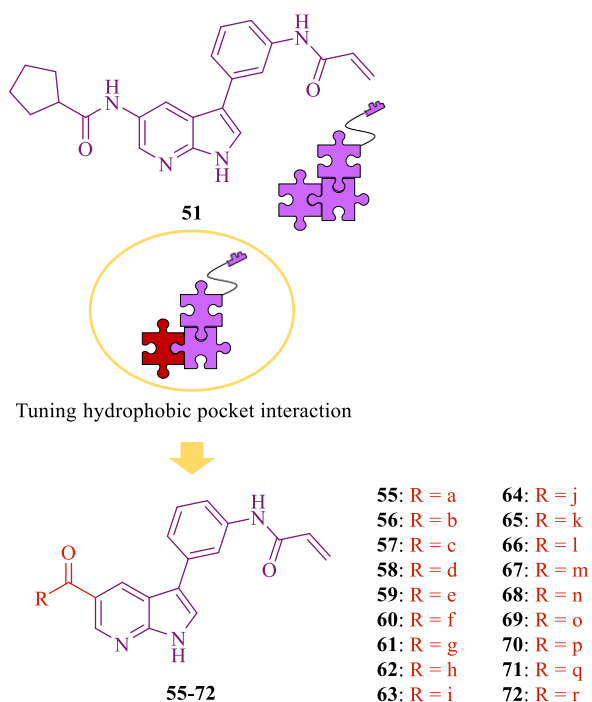
**Figure 66.** Schematic illustration of the expected binding mode of inverse amide derivative **51**.

#### 4.2.4 Hit to lead optimization: design of new series of BMX inhibitors

Taking advantage of the previously established structure-activity relationships, the aim of this project was to design and synthesize optimized covalent BMX with improved selectivity over BTK as potential chemical probes. This project conducted at the Institute of Pharmaceutical Sciences at the University of Tübingen resulted in the development of two small series of compounds. The first series was developed focusing on tuning BMX selectivity by modulating the interaction of the 5-carboxamide substituent with the

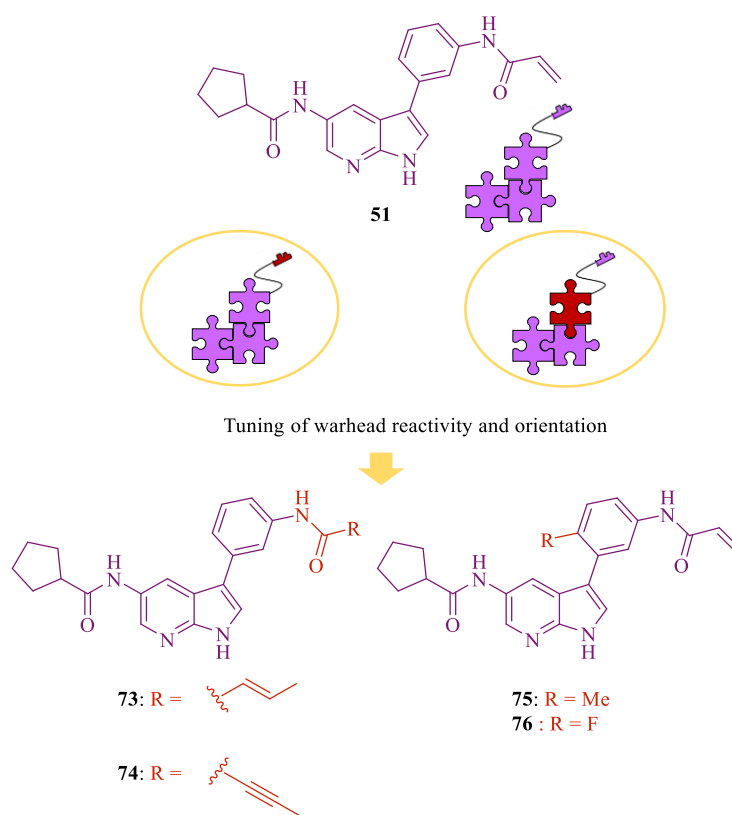


hydrophobic pocket located behind the threonine gatekeeper residue (also called hydrophobic region I; HR I). Notably, as explained above, the HR I is slightly different between BMX and BTK because the Phe475 of BMX is replaced by the Leu460 in BTK. Thus, to expand the already developed series, the N-(3-(1H-pyrrolo[2,3-b]pyridin-3-yl)phenyl)acrylamide structure was maintained (see **51** and **52** Figure 65) and several alkyl, aryl, and haloaryl substituents were introduced with or without a methylene spacer, to give compound **55-72** (Figure 67).



**Figure 67.** Design of an optimized series of 7-azaindole-derived BMX inhibitors tuning the interaction with the hydrophobic pocket behind the gatekeeper residue.

Particularly, the introduction of the aryl and haloaryl substituents aimed to investigate whether an additional  $\pi$ - $\pi$  or halogen- $\pi$  interaction with Phe475 of BMX could be exploited to improve selectivity over BTK. The second small series of molecules focused on the design and the synthesis of new covalent inhibitors exploring the effect of different warheads and the warhead orientation in relation to the  $\alpha$ D-1 cysteine. In the first case, the overall structure of the previously discovered BMX/BTK dual inhibitor **51** (Figure 65) was maintained but the acrylamide fragment was replaced with two alternative electrophilic warheads *i.e.* 2-butenamide and 2-butyneamide to afford compounds **73** and **74** (Figure 68). To fine-tune the selectivity by modifying the warhead orientation, small substituents such as methyl or fluoro were introduced on *ortho*-position of compound **51**'s phenyl ring (with respect to the linkage with the 7-azaindole scaffold). This led to compounds **75** and **76** (Figure 68). Here, sterical repulsion may induce the rotation of the phenyl ring changing the warhead orientation.

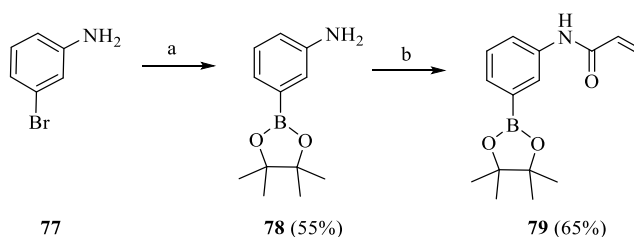


**Figure 68.** Design of a new optimized series of 7-azaindole-derived BMX inhibitors with modified warhead reactivity and orientation.

## 4.2.5 Chemistry

The first series of new BMX inhibitors (**55-72**) were synthesized based on the synthetic route already investigated by Forsters *et al.*<sup>61</sup> The steps are described below in Schemes 10, 11, and 12.

**Scheme 10.** Synthetic strategy for obtaining the N-acetylated pinacol ester **79**.

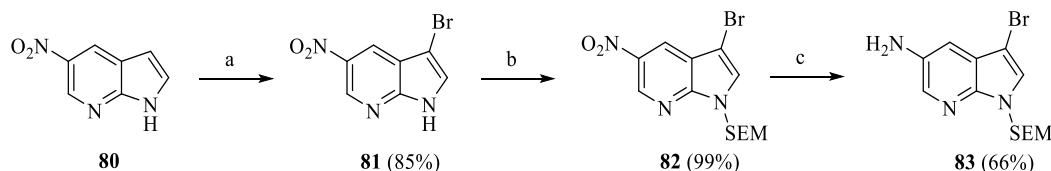


**Reagents and conditions:** a) B<sub>2</sub>pin<sub>2</sub>, XPhos, Pd(OAc)<sub>2</sub>, KOAc, dioxane, 90 °C, 24h; b) acryloyl chloride, Et<sub>3</sub>N, DCM, 0°C to rt, 1h.

Aryl boronic ester **79** was synthesized starting from 3-bromoaniline (**77**) (Scheme 10). First, the pinacol boronate **78** was obtained by cross-coupling under Miyaura condition. Bis(pinacolato)diboron was used as the boron source since the corresponding pinacol ester products (**78**) are easier to handle and more stable in comparison to free boronic acids.<sup>328</sup> The reaction was carried out using a 2-dicyclohexylphosphino-2',4',6'-triisopropylbiphenyl (XPhos)/palladium acetate (Pd(OAc)<sub>2</sub>) catalyst system. Initially, Pd(OAc)<sub>2</sub> associates with XPhos to form Pd<sup>II</sup>(OAc)<sub>2</sub>(XPhos) complex. Then, Pd<sup>II</sup> is reduced to the Pd<sup>0</sup>(XPhos)<sub>2</sub> species by an intramolecular process.<sup>329</sup> Subsequently, the Pd<sup>0</sup>(XPhos)<sub>2</sub> complex undergoes the oxidative addition-transmetallation-reductive boration Miyaura catalytic cycle.<sup>329</sup> The transmetallation is a base-mediated process. However, a competitive Suzuki-coupling reaction between the resulting boronic ester and the organohalide can be a critical issue. Particularly, when the reaction presents an amount of the formed boronic ester is prevalent with respect to the organohalide. It was found that weak bases such as potassium acetate (KOAc) gave the best selectivity.<sup>330</sup> Subsequently, the amino group of aniline **78** was acylated by acryloyl chloride to afford intermediate **79**. In parallel, the 5-nitro-7-azaindole (**80**) was selectively brominated in position 3 by N-bromosuccinimide to obtain the intermediate **81** which was used without further purification. Then, to ameliorate **81** solubility in organic solvents, the indole nitrogen was protected in quantitative yield by 2-(trimethylsilyl)ethoxymethyl chloride (SEM-Cl) to afford intermediate **82**. The reaction was promoted by sodium hydride

(NaH), necessary to deprotonate the indole's NH, in dimethylformamide (DMF) and conducted using a slight excess of SEM-Cl. Finally, the nitro group of **82** was reduced by treatment with zinc and ammonium formate to obtain the key intermediate **83** (Scheme 11).

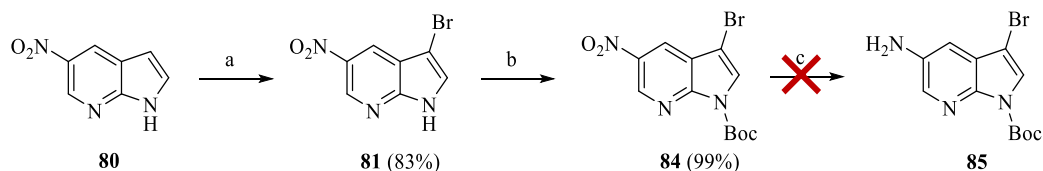
**Scheme 11.** Synthetic strategy for obtaining the SEM-protected intermediate **83**.



Reagents and conditions: a) NBS, DMF, rt, 3h; b) NaH, SEM-Cl, DMF, 0°C to 22 h, c) Zn<sup>0</sup>, ammonium formate, EtOH, 50 °C, 22 h.

Alternatively, a Boc protecting group was also evaluated. However, it didn't demonstrate sufficient stability to the nitro reductive conditions (Scheme 12) highlighting the lower stability of this protection group on N-heterocycles.

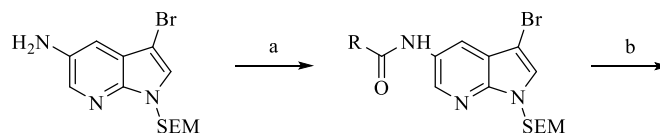
**Scheme 12.** Synthetic strategy investigated for obtaining the Boc-protected intermediate **85**.



Reagents and conditions: a) NBS, DMF, rt, 3h; b) Boc anhydride, DMAP (cat.), MeCN, rt, 2 h; c) Zn<sup>0</sup>, ammonium formate, EtOH, 50 °C, 22 h.

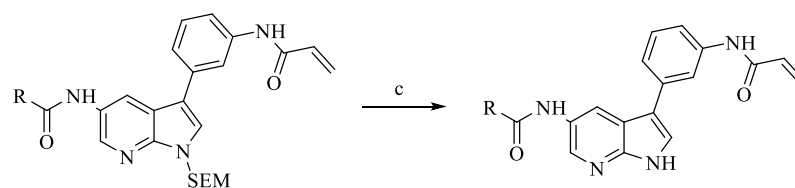
Subsequently, the obtained intermediate **83** (Scheme 13) was acetylated in position 5 by treatment with the appropriate acyl chloride, to afford intermediates **86-103**. Then, intermediates **86-103** and the boronate ester **79** were linked under optimized Suzuki cross-coupling conditions to afford the SEM-protected prefinal intermediates **104-121**.<sup>61</sup>

**Scheme 13.** Synthetic strategy for obtaining final compounds **55-72**.

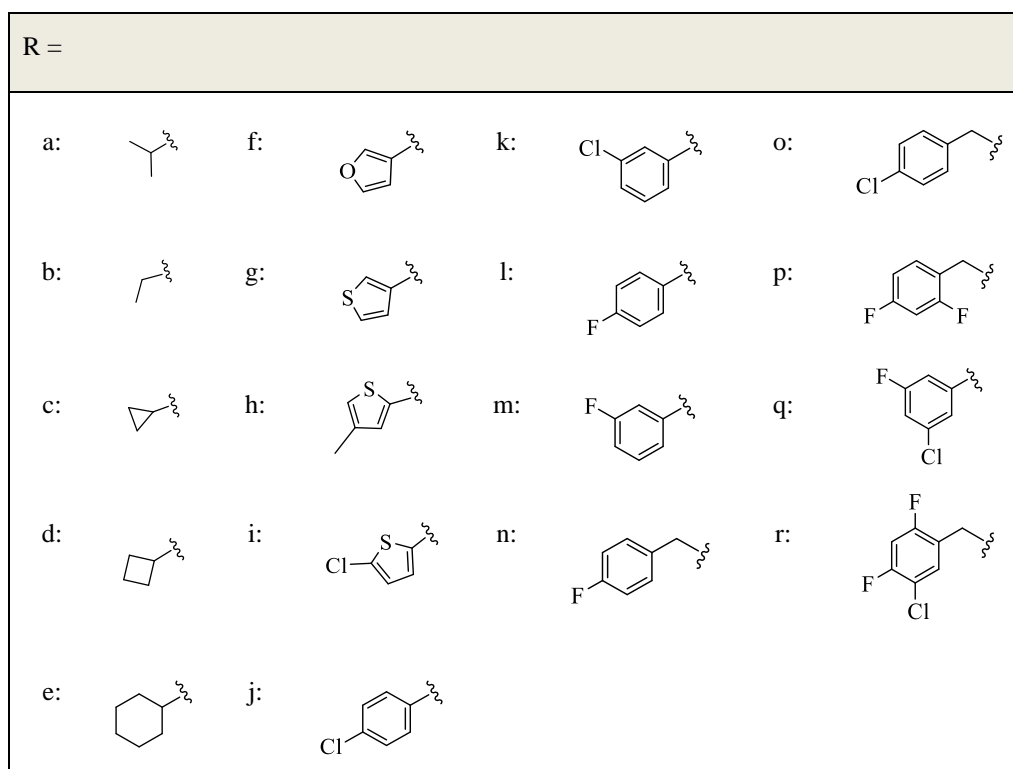


**83**

<b>86:</b> R = a (99%)	<b>95:</b> R = j (100%)
<b>87:</b> R = b (90%)	<b>96:</b> R = k (86%)
<b>88:</b> R = c (100%)	<b>97:</b> R = l (100%)
<b>89:</b> R = d (88%)	<b>98:</b> R = m (94%)
<b>90:</b> R = e (93%)	<b>99:</b> R = n (72%)
<b>91:</b> R = f (69%)	<b>100:</b> R = o (59%)
<b>92:</b> R = g (51%)	<b>101:</b> R = p (81%)
<b>93:</b> R = h (84%)	<b>102:</b> R = q (88%)
<b>94:</b> R = i (93%)	<b>103:</b> R = r (93%)



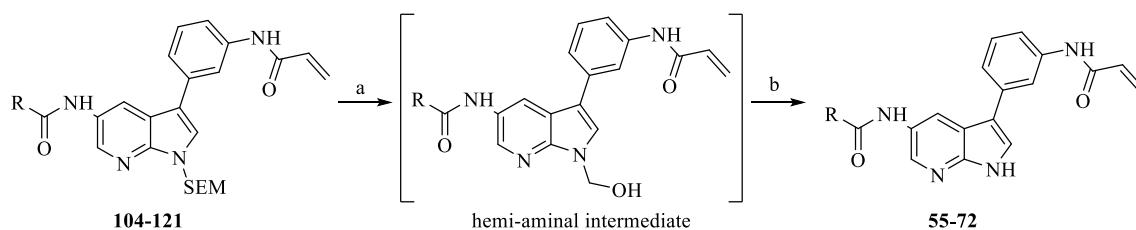
<b>104:</b> R = a (49%)	<b>113:</b> R = j (75%)	<b>55:</b> R = a (36%)	<b>64:</b> R = j (42%)
<b>105:</b> R = b (35%)	<b>114:</b> R = k (49%)	<b>56:</b> R = b (63%)	<b>65:</b> R = k (98%)
<b>106:</b> R = c (69%)	<b>115:</b> R = l (63%)	<b>57:</b> R = c (85%)	<b>66:</b> R = l (74%)
<b>107:</b> R = d (68%)	<b>116:</b> R = m (58%)	<b>58:</b> R = d (70%)	<b>67:</b> R = m (56%)
<b>108:</b> R = e (42%)	<b>117:</b> R = n (54%)	<b>59:</b> R = e (62%)	<b>68:</b> R = n (73%)
<b>109:</b> R = f (38%)	<b>118:</b> R = o (47%)	<b>60:</b> R = f (52%)	<b>69:</b> R = o (48%)
<b>110:</b> R = g (57X%)	<b>119:</b> R = p (49%)	<b>61:</b> R = g (94%)	<b>70:</b> R = p (72%)
<b>111:</b> R = h (82%)	<b>120:</b> R = q (57%)	<b>62:</b> R = h (99%)	<b>71:</b> R = q (56%)
<b>112:</b> R = i (60%)	<b>121:</b> R = r (47%)	<b>63:</b> R = i (81%)	<b>72:</b> R = r (85%)



**Reagents and conditions:** a) corresponding acyl chloride, Et<sub>3</sub>N, DCM, r.t., 1h; b) **79**, Pd-*t*Bu<sub>3</sub>P, K<sub>2</sub>CO<sub>3</sub> (0,5M), dioxane, rt or T = 80 °C, 22h; c) (i) TFA, DCM, rt, 8h; (ii) NH<sub>3</sub> (25%), EtOH, rt, 24 h.

Similarly to the aforementioned Miyaura-borylation, the mechanism of the cross-coupling reaction involves an oxidative addition-transmetalation-reductive elimination sequence. To prevent eventual side reactions caused by the Michael-acceptor-system of the acrylamide, a Buchwald's 3<sup>rd</sup> generation tri-*tert*-butyl phosphine palladium (Pd-*t*Bu<sub>3</sub>P) precatalyst was used, which allowed very mild reaction conditions.<sup>331</sup> Thus, the reaction was carried out in presence of the mild base K<sub>2</sub>CO<sub>3</sub> that activates the palladium precatalyst forming an active Pd<sup>0</sup> complex through reductive elimination. In addition, another advantage of using K<sub>2</sub>CO<sub>3</sub> is that it accelerates the reaction by mild transmetalation. Indeed, the transmetalation is likely to occur between the aryl boronic ester and the metalloid adduct Pd<sup>II</sup>-79-HCO<sub>3</sub> which presents low nucleophilicity.<sup>332</sup> Finally, SEM-deprotection was performed under acidic conditions by means of trifluoroacetic acid (TFA). The deprotection usually first showed the formation of an intermediate with slightly different polarity in HPLC from the desired product. This product, which was not separable by TLC was shown by mass spectrometry and NMR to be N-hydroxymethyl hemiaminal intermediate. The elimination of the hemi-aminal was achieved at basic pH values by an excess of ammonia aqueous solution (NH<sub>3</sub> 25%) in EtOH (Scheme 14). In this way, the first series of desired final compounds **55-72** was obtained (Scheme 13).

**Scheme 14.** Acid-promoted SEM deprotection via the formation of a hydroxymethyl intermediate

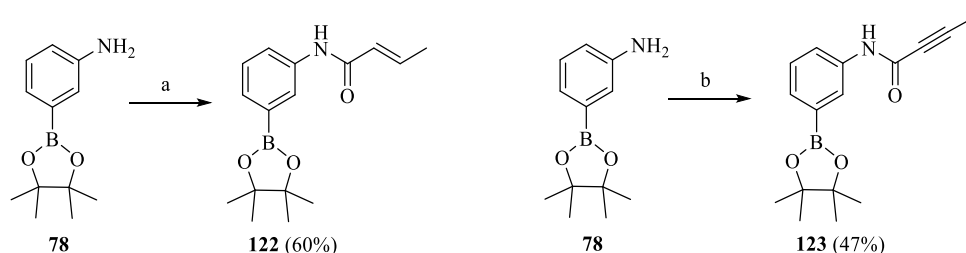


Reagents and conditions: a) TFA, DCM, rt, 8h; b) NH<sub>3</sub> (25%), EtOH, rt, 24h.

The second series of compounds **73-76** (Scheme 16) was obtained starting with the synthesis of the boronate esters **122**, **123**, **129**, and **130**. 3-bromoaniline, 3-bromo-4-methylaniline, and 3-bromo-4-fluoroaniline respectively were converted to the respective boronates under Miyaura cross-coupling conditions (see step a) Scheme 10 for the conditions). Then, intermediate **78**, **127**, and **128** were acylated to afford **122**, **123**, **129**, and **130** (Scheme 15, Scheme 16). Particularly, intermediate **122** and **123** were synthesized under peptide coupling conditions. Intermediate **78** and (*E*)-2-butenic were treated with 1H-1,2,3-Triazolo[4,5-b]pyridinium, 1-[bis(dimethylamino)methylene]-, 3-

oxide hexafluorophosphate (HATU) and N-ethyldiisopropylamine (DIPEA) to provide intermediate **122**. On the other side, intermediate **123** was obtained under Steglich coupling conditions. **78** and 2-butyric acid were treated with *N,N'*-dicyclohexylcarbodiimide (DCC), and DMAP to give the desired compound (Scheme 15). The synthesis of both intermediates was also investigated through the (*E*)-2-butyric acid and 2-butyric acyl chloride produced by treatment with thionyl chloride treatment. However, in both cases, the desired intermediates weren't obtained, probably because of the rapid degradation of the mentioned acyl chloride.

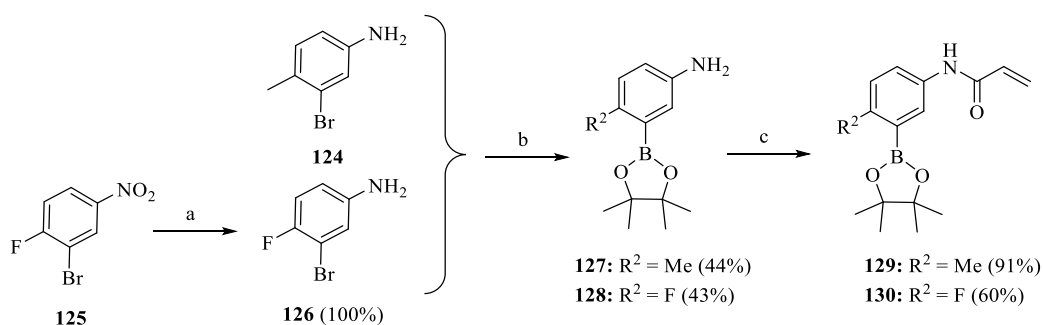
**Scheme 15.** Synthetic strategy for obtaining the acetylated pinacol boronates **122** and **123**.



**Reagents and conditions:** a) (*E*)-2-butyric acid, HATU, DIPEA, THF, 0°C to rt, 22 h; b) 2-butyric acid, DCC, DMAP, DCM, 0°C to rt, 22 h.

In contrast, intermediate **129** and **130** were synthesized by acylating boronic esters **127** and **128** with acryloyl chloride (Scheme 16).

**Scheme 16.** Synthetic strategy for obtaining the acetylated pinacol boronates **129** and **130**.

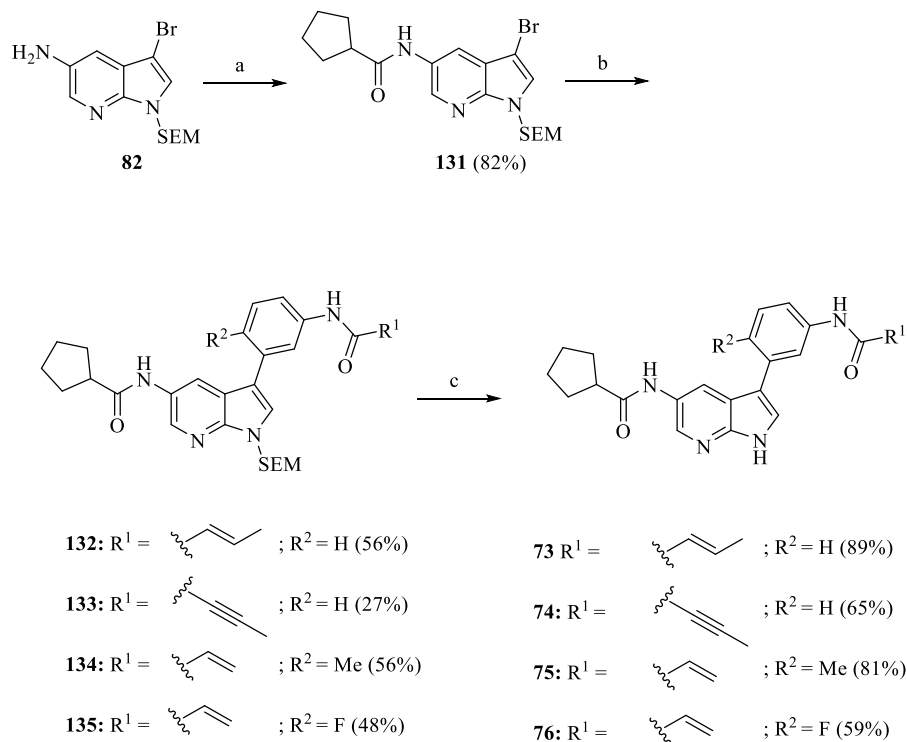


**Reagents and conditions:** a) SnCl<sub>2</sub>/HCl (37%), EtOH, 75 °C, 30 min; b) B<sub>2</sub>pin<sub>2</sub>, Xphos, Pd(OAc)<sub>2</sub>, KOAc, dioxane, 90 °C, 24h; c) acryloyl chloride, Et<sub>3</sub>N, DCM, 0°C to rt, 1h.

Simultaneously, intermediate **83** (see Scheme 11 for its synthesis) was derivatized in position 5 by acylation with cyclopentanecarbonyl chloride to give the key intermediate

**131.** In turn, Suzuki cross-coupling between **83** and respectively boronic acid esters **122**, **123**, **129**, **130** in presence of Pd-*t*Bu<sub>3</sub>P and K<sub>2</sub>CO<sub>3</sub> afforded the SEM-protected prefinal compounds **132-135**. Subsequently, the SEM-group was cleaved under acidic conditions by TFA and the following treatment with NH<sub>3</sub> (25%) in EtOH.

**Scheme 16.** Synthetic strategy for obtaining the final compounds **73-76**.



**Reagents and conditions** a) cyclopentanecarbonyl chloride, Et<sub>3</sub>N, DCM, rt, 1h; b) corresponding boronic ester (**122,123,129,130**), Pd-*t*Bu<sub>3</sub>P, K<sub>2</sub>CO<sub>3</sub> (0,5M), dioxane, rt or T = 80 °C, 22h; c) TFA, DCM, rt.

All the compounds were characterized by <sup>1</sup>H NMR, <sup>13</sup>C NMR, HPLC and MS. In addition, the tested compounds were analyzed by HRMS demonstrating at least 95% purity at λ = 254 nm and λ = 365 nm (see Chapter 6).

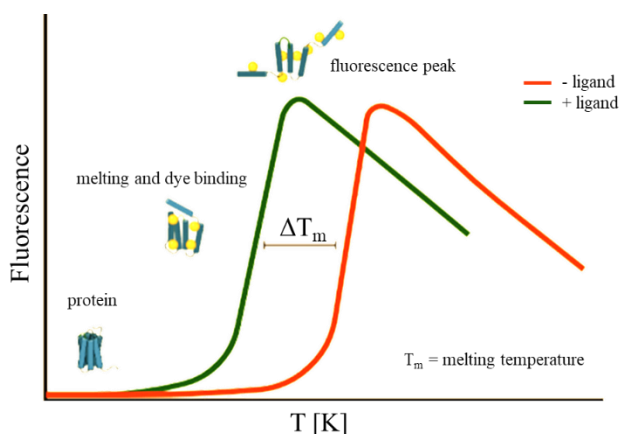
#### 4.2.6 Results and discussion

The following results were developed thanks to Prof. Knapp's group (for the thermal shift assay) Institute of Pharmaceutical Chemistry, Goethe University Frankfurt, and Reaction Biology Corporation (US) (for the IC<sub>50</sub> evaluation).



## Thermal shift assay

To preliminarily evaluate the affinities of final compounds **55-76** for BMX, a thermal shift assay was performed. This test gave preliminary useful information about the preference of the compounds for BMX compared to the closely related BTK and the MAP kinase kinase 7 (MKK7) holding an equivalent cysteine. The thermal shift ( $\Delta T_m$ ) assay was assessed by Prof. Knapp's group (University / Structural Genomics Consortium Frankfurt, Germany). This simple and cost-effective screening method is based on the stabilization of a protein, (here the kinase domain of the target kinase) upon ligand binding which leads to a shift in the "melting point", i.e. the temperature of thermal denaturation (Figure 69).

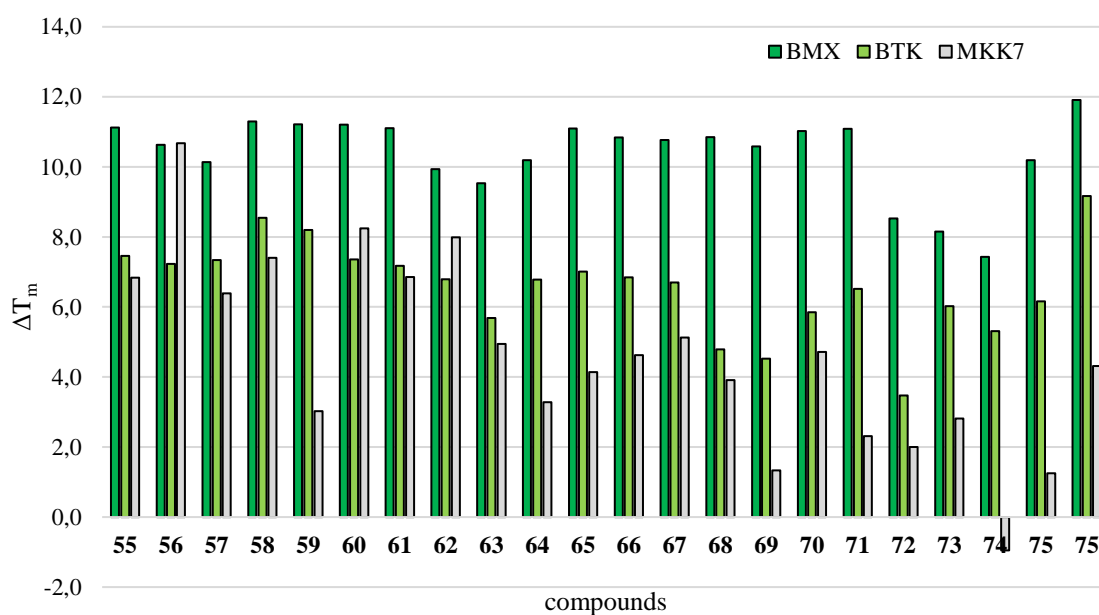


**Figure 69.** Schematic representation of the thermal shift analysis.

Consequently, the stabilized protein kinase domain required a higher temperature to be denaturated than that necessary for unbonded protein domain denaturation.<sup>333</sup> Compounds **55-76** were tested at 10  $\mu\text{M}$  concentration. The difference between the melting temperature of the native protein domain and the melting temperature of the ligand stabilized domain is the thermal shift ( $\Delta T_m$ ) measured for compounds **55-76** (Figure 70). The  $\Delta T_m$  was evaluated by fluorescent measurement exploiting the spiro orange dye and it is proportional to the affinity of the ligands for the kinase domain of the considered protein.<sup>333</sup>

Interestingly, among all the compounds tested some displayed a stronger stabilization of BMX with respect to BTK and MKK7 suggesting a higher affinity for BMX. However, all compounds were also screened in activity-based assay on isolated BMX for complementary validation. Moreover, based on thermal shift difference vs BTK and

MKK7 (Table 16) and using structural features as additional selection criteria, compounds **68**, **69**, **71**, **72**, and **75** were selected to be tested also on BTK. The selected compounds at least showed a  $\Delta T_m$  BMX/BTK > 1.70 and a  $\Delta T_m$  BMX/MKK7 > 2.7. According to their structural characteristics, **68**, **69**, **71**, and **72** present a halogenated bulky substituent in position 5 of the azaindole scaffold that may afford an additional interaction with the Phe475 in the HRI of BMX. Compound **75** with the warhead showing a different orientation because of the methyl *ortho*-substituent on the phenyl ring may give information about possible discrimination among the cysteines in  $\alpha$ D-1 position present in both the kinases.



**Figure 70.** Thermal stabilization of BMX, the close relative BTK and MKK7's kinase domains by compounds **55-76** on.

**Table 16.**  $\Delta T_m$  values of the compounds selected to evaluate the  $IC_{50}$  against BTK.

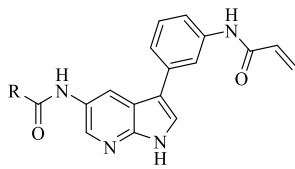
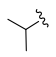
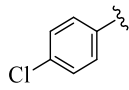

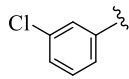

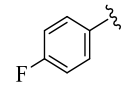
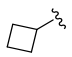
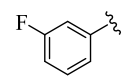
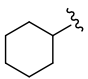
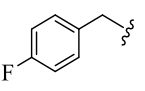
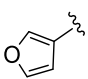
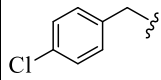
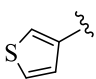
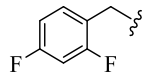
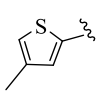
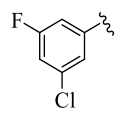
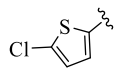
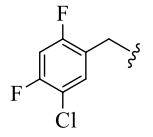
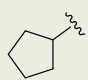
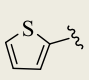
Compound	$\Delta T_m$				
	BMX <sup>a</sup>	BTK <sup>a</sup>	MKK7 <sup>a</sup>	BMX/BTK	BMX/MKK7
<b>68</b>	10.9	4.8	3.9	2.27	2.78
<b>69</b>	10.6	4.5	1.3	2.34	7.96
<b>71</b>	11.1	6.5	3.3	1.70	4.81
<b>72</b>	8.5	3.5	2.0	2.46	4.27
<b>75</b>	10.2	6.2	1.3	1.65	8.13

<sup>a</sup> Mean of three independent measurements

## Evaluation of BMX inhibitory activity

The IC<sub>50</sub> values of the final compounds **55-76** were evaluated on BMX to define whether they could improve the inhibitory potency of the hit compounds **51** (IC<sub>50</sub> = 2 nM) and **52** (IC<sub>50</sub> = 1 nM).<sup>61</sup>

**Table 17.** IC<sub>50</sub> evaluation of compounds **54-71** on BMX.

					
Compound	R	IC <sub>50</sub> [nM]	Compound	R	IC <sub>50</sub> [nM]
<b>55</b>		< 0.5 <sup>b</sup>	<b>64</b>		0.63
<b>56</b>		< 0.5 <sup>b</sup>	<b>65</b>		5.56
<b>57</b>		< 0.5 <sup>b</sup>	<b>66</b>		< 0.5 <sup>b</sup>
<b>58</b>		< 0.5 <sup>b</sup>	<b>67</b>		< 0.5 <sup>b</sup>
<b>59</b>		< 0.5 <sup>b</sup>	<b>68</b>		16.4 <sup>c</sup>
<b>60</b>		< 0.5 <sup>b</sup>	<b>69</b>		no inhibition <sup>c</sup>
<b>61</b>		< 0.5 <sup>b</sup>	<b>70</b>		10.6
<b>62</b>		2.31	<b>71</b>		16.5 <sup>c</sup>
<b>63</b>		< 0.5 <sup>b</sup>	<b>72</b>		no inhibition
<b>51<sup>a</sup></b>		2	<b>52<sup>a</sup></b>		1

<sup>a</sup>IC<sub>50</sub> of the hit compounds published by Forster *et al.*<sup>61</sup>; <sup>b</sup>IC<sub>50</sub> < than the lowest concentration tested (0.5

nM); ° The IC<sub>50</sub> curves showed a deviation from the expected sigmoid curve maybe because of the poor solubility in the buffer of the assay

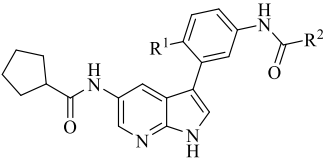
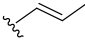

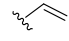
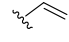
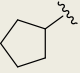
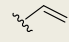
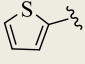

All the IC<sub>50</sub> values were determined commercially at Reaction Biology Corporation using the “HotSpot” assay platform. This platform relies on a radiometric assay format employing <sup>33</sup>P ATP. Compounds were tested in 5-dose IC<sub>50</sub> scheme with a 10-fold serial dilution starting at 5 μM and all kinase reactions were carried out at 10 μM ATP.

All the compounds inhibited BMX with at least double-digit nanomolar IC<sub>50</sub> values with exception of **73** that showed a micromolar IC<sub>50</sub>, while **69** and **72** were demonstrated not active on BMX (Table 17). Notably, both of those compounds had shown a significant thermal shift in the preliminary assay. Among the first series of compounds **55-76** potential BMX inhibitors **55-61**, **63**, **66**, and **67** demonstrated extremely potent on BMX inhibition, showing IC<sub>50</sub> values below the lowest concentration tested (0.5 nM) and the resolution limit of the assay.

**55-61** feature flexible aliphatic substituent (ethyl, cyclobutyl, cyclohexyl) or small aromatic rings such as furan-3-carboxamide (**60**) and thiophene-3-carboxamide (**61**) directly linked to the amide in position 5 of the azaindole scaffold, which can favorably interact with the HR I of BMX. Also compounds **63-67** which present a bulky chloro/fluoro-aromatic substituent demonstrated very potent inhibitory activity, especially compounds **63**, **65**, and **66**. In this case, the increased potency with respect to the hit compounds could be due to additional interaction by π-π or halogen-π interaction that the bulky substituent in position 5 of the azaindole can establish with the mentioned Phe745 in the HR I region of BMX.

In the end, the presence of a methyl spacer between the bulky substituent and the amide as for **68** and **70** seems to reduce BMX inhibition. However, **68** and **70** which possess a 2-(4-fluorophenyl)acetamide and a 3,5- difluorophenyl)acetamide moiety respectively maintained an IC<sub>50</sub> in the double-digit nanomolar range. Conversely, the presence of a 2-(4-chlorophenyl)acetamide (**69**) leads to a complete loss of activity. The introduction of bulky tri-halogenated phenylacetamides (**72**) led as well to an underprivileged interaction with HR I and loss of activity, probably due to the presence of too cluttered fragments. On the other side, di-halogenated benzamide (**71**) directly linked to the azaindole scaffold maintain a nanomolar inhibitory potency. It should also be noted here that some of the inactive compounds showed very low solubility, which may also have influenced the IC<sub>50</sub> measurements, at least at higher concentrations.

**Table 18.** IC<sub>50</sub> evaluation of compounds **73-76** on BMX.

			
Compound	R <sup>1</sup>	R <sup>2</sup>	IC <sub>50</sub> [nM]
<b>73</b>	H		236.9
<b>74</b>	H		< 0.5
<b>75</b>	Me		40.7
<b>76</b>	F		< 0.5
<b>51<sup>a</sup></b>			2
<b>52<sup>a</sup></b>			1

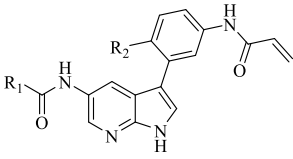
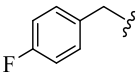
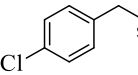
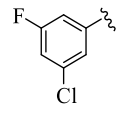
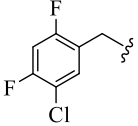
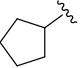
<sup>a</sup> IC<sub>50</sub> of the hit compounds published by Forster *et al.*<sup>61</sup>

Considering the second series of compounds (**73-76**, Table 18), we can assume to reproduce the Van der Waals interactions of **53** within the HR I of BMX.<sup>61</sup> Thus, the IC<sub>50</sub> differences can be attributed to the different nature of the warheads introduced or the different warhead orientations. While the introduction of the (*E*)-but-2-enamide warhead (**73**) resulted in a weaker BMX inhibition with respect to **53**, the presence of the 2-butyneamide **74** showed an improved IC<sub>50</sub> value (< 0.5 nM). The induction of a different warhead orientation by the introduction of methyl (**75**) and fluoro (**76**) substituents on the phenyl ring showed to maintain BMX inhibition. However, the presence of the electron-withdrawing fluorine significantly increased the inhibitory potency driving the IC<sub>50</sub> value of compound **76** down to the picomolar range.

### Evaluation of BTK Inhibitory Activity

Concomitantly, based on thermal shift differences and structural features compounds **68-72** and **75** were also tested on BTK, to have preliminary information about their ability to discriminate between the two closest relatives among the TEC family members.

**Table 19.** IC<sub>50</sub> evaluation of compounds **68-72** and **75** on BTK.

				
Compound	R <sup>1</sup>	R <sup>2</sup>	BTK IC <sub>50</sub> [nM]	BMX IC <sub>50</sub> [nM]
<b>68</b>		H	86.2 <sup>a</sup>	16.35
<b>69</b>		H	no inhibition <sup>a</sup>	no inhibition
<b>71</b>		H	1,07 <sup>a</sup>	16.5
<b>72</b>		H	4760	no inhibition
<b>75</b>		Me	1010	40.7

<sup>a</sup> The IC<sub>50</sub> curves showed a deviation from the expected sigmoid curve maybe because of the poor solubility in the buffer of the assay.

Similarly to the results on BMX, compounds **68** and **71** showed a BTK IC<sub>50</sub> in the nanomolar range, while **69** demonstrated to not inhibit the enzyme. Compound **72**, which was not active on BMX showed a low micromolar inhibition of BTK. Interestingly, **75** which displayed a nanomolar IC<sub>50</sub> on BMX showed only micromolar inhibition of BTK, suggesting modification of the linker/warhead orientation as a promising strategy to discriminate these two highly homologous kinases (Table 19).

However, since IC<sub>50</sub> of covalent inhibitors is time-dependent is possible it doesn't reflect exactly the potency of the compounds. Considering that it doesn't take into account the two steps required for a covalent inhibition (the affinity-driven non-covalent interaction step and the following covalent inactivation step), these promising results should be cautiously considered.

# Chapter 5





## 5. Conclusions and Perspectives

Inflammation represents the first response of the innate immune system aiming to protect and defend the body. Particularly, in the context of the CNS, it is one of the major contributors to traumatic brain injury damage and to the onset and progression of neurodegenerative diseases.<sup>5</sup> Over the last years, the awareness of the central role of neuroinflammation in neurodegenerative diseases has been consolidated. Thus, many drug candidates have been investigated as neuroinflammatory modulators in clinical trials, although they have often failed.<sup>334</sup> One of the causes of the clinical failures of neuroinflammatory drugs is the limited understanding of the neuroinflammatory pathways synergistically contributing to neurodegeneration. However, the importance of the microglia's role in sustaining chronic neuroinflammation has been deemed crucial for neurodegenerative progression. To note, the M1 microglia pro-inflammatory phenotype pathways can be physiologically antagonized by alternative microglia activation. Thus, the idea of exploiting M2 microglia anti-inflammatory phenotype polarization as a therapeutic strategy is increasingly gaining a broad consensus. For this reason, immunomodulatory agents that could stimulate the M1/M2 microglia shift embody an attractive therapeutic strategy for various inflammatory-related diseases. The first part of this thesis focused on modulating neuroinflammatory pathways in AD by a polypharmacological approach based on MTDLs. AD is a neurodegenerative disease so far incurable with currently available drugs on the market showing only a symptomatic effect. Currently, polypharmacology is considered the most promising strategy to face the multifactorial nature of neurodegenerative diseases, including AD. In this respect, the most ambitious opportunity is the development of MTDLs, since they provide the possibility to modulate synergistically multiple pathological pathways by the use of single chemical entities. Thus, aiming to design and synthesize potential MTDLs targeting neuroinflammation in AD, we started from promising drug candidates under investigation at clinical level. In the first case, we took inspiration from an AD clinical trial that involved the co-administration of cromolyn and ibuprofen (NCT04570644),<sup>42</sup> two repurposed anti-inflammatory drugs.<sup>115</sup> The parent drugs were combined by a linking strategy in 1:2 ratio to provide the small set of cromolyn-(S)-ibuprofen codrugs (**5-7**) that were evaluated *in vitro/in vivo*. All conjugates demonstrated a non-cytotoxic profile in primary neurons and **6** and **7** showed also good plasma stability. Thus, assuming that **6** and **7** could be stable enough to reach unmodified the CNS, we progressed them to further

studies. Firstly, their possibility to be internalized in microglia cells N9 was proved. Then, their immunomodulatory profile was assessed by evaluating classical M1 and M2 biomarkers. **7** showed a good anti-inflammatory profile, by decreasing the expression of the pro-inflammatory biomarker iNOS after LPS insult. Moreover, it showed a good A $\beta$ <sub>42</sub> anti-aggregating profile and a neuroprotective effect against A $\beta$ <sub>42</sub>-induced neurotoxicity in primary neurons. Thus, **7** was selected for behavioral studies in A $\beta$ <sub>42</sub>-expressing *Drosophila*. This is a simple and versatile *in vivo* AD model. Interestingly, flies treated with **7** significantly increased their longevity and improved their locomotor performance after 7 days of treatment.<sup>43</sup> Motivated from the promising results obtained by **5-7** investigation, a further set of cromolyn-(S)-ibuprofen codrugs was developed. In this case, the parent drugs were combined in 1:1 ratio by a fusing strategy affording **21** and **22**, both with a lower molecular weight with respect to **5-7**. Thus, given the rigid physico-chemical parameters required for BBB permeation, **21** and **22** could show a more favorable CNS penetrating profile. Thus, MW was reduced with respect to the first series (**5-7**), in addition to having the free carboxylic acid groups masked in the ester form. Both codrugs showed a non-toxic profile in primary neurons, in line with the results obtained for cromolyn-(S)-ibuprofen 1:2 neurotoxicity. Moreover, they displayed plasma stability lower than **6** and **7**, but in agreement with codrugs' stability designed for CNS reported in the literature.<sup>185</sup> However, further studies to evaluate their anti-inflammatory and anti-aggregating profile are still ongoing, as well as the evaluation of the possible metabolite that could form by codrug hydrolysis.

Subsequently, considering the role of some PK in neuroinflammatory pathways, such as p38 $\alpha$ -MAPK, we were attracted by another clinical trial (NCT03435861),<sup>253</sup> where neflamapimod was investigated as a potential AD treatment. Neflamapimod is a selective p38 $\alpha$ -MAPK inhibitor developed for rheumatoid arthritis, which was repurposed against AD since it was demonstrated to be prevalently distributed at central level. Moreover, we considered the well-known and versatile anti-PD drug rasagiline. This drug has been many times repurposed in neurodegenerative diseases, thanks to the neuroprotective properties of its propargylamine fragment and its covalent MAO-B inhibition, responsible for antioxidant and neuroprotective effects.<sup>263</sup> Thus, aiming to exploit polypharmacology and combining the p38 $\alpha$ -MAPK inhibition of neflamapimod with the neuroprotective profile of rasagiline, hybrids **31** and **32** were designed and synthesized. Particularly, the propargylamine fragment was introduced on neflamapimod's scaffold, in a solvent-exposed position. Interestingly, both compounds, **31** and **32**, demonstrated the possibility

to interact with p38 $\alpha$ -MAPK and MAO-B by docking studies. Efficiently, **31** and **32** retained p38 $\alpha$ -MAPK inhibition, especially **32** which showed an IC<sub>50</sub> in the nanomolar range, similarly to the reference compound neflamapimod. On the other side, none of them demonstrated the ability to significantly inhibit MAO-B at 10  $\mu$ M. Before proceeding to the investigation of the immunomodulatory and neuroprotective profile of both hybrids, **31** and **32** cytotoxic profile was assessed. In human liver cancer HepG2 cells, both compounds showed no toxicity, except for **31** at 10  $\mu$ M which showed slight cell viability decrement. Interestingly, in primary neurons, no toxic effect was observed at the mentioned concentrations. **31** and **32** showed a good immunomodulatory profile, by reducing the expression of the pro-inflammatory iNOS and showing an unmodified level of the pro-phagocytic TREM2 in microglia cells after LPS stimulation. Moreover, both hybrids showed a neuroprotective effect against dexamethasone-induced ROS production in SH-SY5Y neuroblastoma cells. Interestingly, they displayed an improved effect with respect to the **25+29** combination. A BBB permeability assay to predict whether hybrids could reach CNS is still under investigation. Additional studies are needed to investigate whether **31** and **32** retain neflamapimod's selectivity in a kinase panel. Moreover, focusing on **31** and **32** inhibition-mode, preliminarily *in silico* studies have excluded the possibility of a covalent p38 $\alpha$ -MAPK inhibition, since the absence of nucleophilic amino acid side chains at a suitable distance from the propargyl moiety. In addition, **31** and **32**'s IC<sub>50</sub> didn't show an improvement with respect to that of the non-propargylated neflamapimod. However, more studies are needed to confirm the supposed inhibition mode.

The last part of the thesis focused on the development of BMX covalent chemical probes. Particularly, covalent and selective inhibitors could be a powerful tool to explore this underexplored PK and as a starting point for the development of drug candidates.<sup>218</sup> However, BMX potential involvement in neuroinflammatory pathways has already been considered since BMX was demonstrated to mediate cytokine production,<sup>57</sup> and was overexpressed in neuroinflammatory pathways in *in vivo* rat model.<sup>58, 59</sup> Starting from a potent BMX-BTK covalent dual inhibitor (**51**) discovered in Prof. Laufer's and Prof. Gehring's groups, two series of optimized BMX selective inhibitors were developed maintaining **51**'s azaindole core. **55-72** were designed and synthesized with the aim of tuning BMX selectivity by amide substituent modification in position 5 of the azaindole scaffold, by exploiting the interaction with the hydrophobic pocket behind the gatekeeper residue as a selectivity filter. While **73-76** were designed and synthesized by tuning BMX

selectivity by changing warhead or acrylamide warhead orientation. All compounds were preliminarily tested by thermal shift assay on BMX, BTK, and MKK7. All compounds (**55-76**) showed a good affinity for BMX and were evaluated for their IC<sub>50</sub>, where most of them showed values lower than 0.5 nM (**55-61**, **72**, **66**, and **67**). Moreover, compounds **68**, **69**, **71**, **72**, and **75** which showed a more significant thermal shift difference vs BTK and MKK7 were also tested for BTK IC<sub>50</sub>. To note, compounds **68** and **71** showed a nanomolar IC<sub>50</sub> on both, BMX and BTK, while **75** showed a higher potency in BMX (nanomolar IC<sub>50</sub>) with respect to BTK (micromolar IC<sub>50</sub>). From this evidence, a preference for BMX inhibition at the nanomolar range with respect to BTK could be assumed. However, the promising data obtained should be integrated with NanoBRET assays, to effectively evaluate the target engagement in cells. Then, the best candidates will be selected, and BMX selectivity assays will be performed.

# Chapter 6



## 6. Experimental part

All starting materials and reagents were purchased from Sigma-Aldrich, TCI, Alpha Aesar, Acros Organic (Italy or Germany) and used without further purification. Thin-layer chromatography (TLC) was carried out on precoated TLC plates (0.20 mm silica gel 60 with UV254 fluorescent indicator, Merck). Developed plates were air-dried and were visualized by exposure to UV light ( $\lambda = 254$  nm and 365 nm) or by an appropriate staining reagent. Column chromatography purifications were performed under flash conditions using Sigma-Aldrich silica gel (grade 9385, 60 Å, 230–400 mesh) (Merck Life Science S.r.l. Milan, Italy). Alternatively, automated flash column chromatography was performed by an Interchim PuriFlash 430 or PuriFlash XS420 system on silica gel (Grace Davison Davisil LC60A 20–45 micron) (W.R. Grace and Company, Columbia, MD, USA) or Merck Geduran Si60 63–200-micron silica gel (Merck KGaA, Darmstadt, Germany). Nuclear magnetic resonance (NMR) spectral analysis was performed on Varian VXR400 (400 MHz), Bruker Avance (200 MHz), or Bruker Avance (400 MHz) instruments. The samples were dissolved in deuterated solvents and chemical shifts ( $\delta$ ) are given in parts per million (ppm) in relation to tetramethylsilane (TMS). Spectra were calibrated using the residual peaks of the used solvent.  $^1\text{H}$  and  $^{13}\text{C}$  NMR spectra were acquired at 300 K and coupling constants (J) are reported in hertz (Hz). Spin multiplicity is reported as: s = singlet, br s = broad singlet, d = doublet, dd = doublet of doublets, t = triplet, td = triplet of doublets, q = quartet, m = multiplet. Thin layer chromatography-mass spectrometry (TLC-MS) was carried out with an Advion TLC-MS interface (Advion, Ithaca, NY, USA) with electron spray ionization (ESI) in positive and/or negative mode. Instrument settings were as follows: ESI voltage 3.50 kV, capillary voltage 187 V, source voltage 44 V, capillary temperature 250 °C, desolvation gas temperature 250 °C, gas flow 5 L/min nitrogen. Purities of final compounds were determined via Ultra-high performance liquid chromatography-mass spectrometry (UHPLC-MS) or high-performance liquid chromatography (HPLC). HUPLC-MS chromatograms were recorded on Acquity arc-QDA HUPLC-MS. The system consists of a QDa mass spectrometer equipped with an electrospray ionization interface and a 2489 UV/Vis detector. The detected wavelengths were 254 nm and 365 nm. The analyses were performed on an XBridge BEH C18 column (10 × 2.1 mm i.d., particle size 2.5  $\mu\text{m}$ ) with an XBridge BEH C18 VanGuard Cartridge precolumn (5 mm × 2.1 mm i.d., particle size 1.8  $\mu\text{m}$ ). Electrospray ionization in positive and negative modes was applied in the mass

scan range 50–1200. Mass spectrometry (MS) Q-ToF spectrometer (Micromass, Manchester, UK) equipped with a Z-spray ion source operating in a positive ion mode. Mobile phase A: [H<sub>2</sub>O/HCOOH (95/5) (v/v)]; Mobile phase B: MeCN. Eluting method : Linear gradient: 0–0.78 min, 40% B; 0.78-2.87 min, 40–95% B; 2.87-3.54 min, 95% B; 3.54-3.65 min, 95-40% B; 3.65-5-73, 40% B. Flow rate: 0.8 mL/min. (Method A).

Otherwise, HPLC was performed by different eluting methods.

- A C18 (Eclipse XDB-C18, 3.5  $\mu$ m; 2.1 x 150 mm; Agilent) column thermostated at 50°C was used. A gradient elution was optimized with the mobile phase A [H<sub>2</sub>O/MeCN/HCOOH (95/5/0.1) (v/v/v)] and B [acetonitrile/water/ formic acid (95/5/0.1) (v/v/v)]. Analyses were carried out employing the following gradient: mobile phase B was increased from 20 to 80% in 10 min and remained at 80% for 7 min. The column was equilibrated with the starting condition for 10 min before the next injection. The flow rate was set at 0.3 mL/min and the injection volume was 20  $\mu$ L. UV detection was performed at 254 nm. (Method B)
- An Agilent 1100 Series LC system (Agilent Technologies, Santa Clara, CA, USA) with a Phenomenex Luna C8 column (150  $\times$  4.6 mm, 5  $\mu$ m) (Phenomenex Inc. Torrance, CA, USA) and detection was performed with a UV DAD at 254 nm and 230 nm wavelength. Elution was carried out with the following gradient: mobile phase A: [H<sub>2</sub>O/KH<sub>2</sub>PO<sub>4</sub> (solution 0.01 M), pH 2.30]; mobile phase B: [MeOH], 40% B to 85% B in 8 min, 85% B for 5 min, 85% to 40% B in 1 min, 40% B for 2 min, stop time 16 min, flow 1.5 mL/min. (Method C)
- Agilent 1100 Series LC system (Agilent Technologies, Santa Clara, CA, USA) with a Phenomenex Kinetex C8 100A column (150  $\times$  4.6 mm, 2.6  $\mu$ m) (Phenomenex Inc. Torrance, CA, USA) and detection was performed with a UV DAD at 254 nm and 230 nm wavelength. Elution was carried out with the following gradients: mobile phase A: [H<sub>2</sub>O/KH<sub>2</sub>PO<sub>4</sub> (solution 0.01 M) (v/v), pH 2.30 (solvent A)], mobile phase B: [MeOH]. 40 % B to 95% in 9 min, 95%B for 1 min, 95% B to 40% B in 1 min, 40% B for 5 min, flow 0.5 mL/min. (Method C)

All compounds were found endowed with a purity degree  $\geq$  95% except for compounds **4** and **62**.



## 6.1 Synthesis of cromolyn-ibuprofen codrugs (1:2)

*bis(2-((S)-2-(4-isobutylphenyl)propanamido)ethyl) 5,5'-((2-hydroxypropane-1,3-diyl)bis(oxy))bis(4-oxo-4H-chromene-2-carboxylate) (4):*

77 mg of **1** (0.15 mmol) and about 40 mg of amberlite IR120 (H<sup>+</sup>) were suspended in 1.5 mL of DMF. Using a bath of ice (T = 0 °C), a solution of 85 mg of **10** (0.35 mmol) in DMF (1.5 mL) together with 56 mg of EDC (0.36 mmol) and 49 mg of HOBt (0.36 mmol) were added to the previously prepared suspension. The reaction was performed under microwave irradiation at 60 °C (200 W) for 1 h. Then, 5 mL of DCM were added to the reaction and the mixture was washed with an aqueous solution of LiCl 5% (3 × 15 mL). The organic phase was dried over anhydrous Na<sub>2</sub>SO<sub>4</sub>, filtered and the organic solvent was evaporated. The crude obtained was purified by flash column chromatography by eluting with CHCl<sub>3</sub>/MeOH/toluene (8.2/0.9/0.9) to afford 7 mg (5%) of the title compound **4** as colorless oil. <sup>1</sup>H NMR (400 MHz, CDCl<sub>3</sub>) δ 7.62 (t, *J* = 8.4 Hz, 2H), 7.22 – 7.10 (m, 8H), 7.07 (d, *J* = 8.0 Hz, 2H), 6.99 (d, *J* = 8.2 Hz, 2H), 6.86 (s, 2H), 5.77 (bs, 1H), 5.63 (t, *J* = 5.7 Hz, 2H), 4.63 – 4.55 (m, 2H), 4.55 – 4.46 (m, 1H), 4.44 – 4.31 (m, 4H), 3.66– 3.51 (m, 6H), 3.41 – 3.29 (m, 2H), 2.35 (d, *J* = 7.2 Hz, 4H), 1.80 – 1.70 (m, 2H), 1.51 (d, *J* = 7.2 Hz, 6H), 0.82 (d, *J* = 6.6 Hz, 12H) ppm; <sup>13</sup>C NMR (100 MHz, CDCl<sub>3</sub>) δ 178.0, 174.8, 160.3, 159.0, 158.0, 150.2, 141.2, 138.3, 135.2, 129.9, 127.5, 116.6, 115.9, 111.3, 109.8, 70.5, 67.9, 65.4, 46.8, 45.0, 38.7, 30.3, 22.5, 18.5 ppm. HRMS (ESI) *m/z*: [M + H]<sup>+</sup> calcd for C<sub>53</sub>H<sub>56</sub>O<sub>15</sub> 933.3697; found 933.3685. HPLC *t*<sub>ret</sub> = 14.11 min. (Method B)

*bis(2-(((S)-2-(4-isobutylphenyl)propanoyl)oxy)ethyl) 5,5'-((2-hydroxypropane-1,3-diyl)bis(oxy)) bis(4-oxo-4H-chromene-2-carboxylate) (5):*

100 mg of **1** (0.20 mmol) and about 40 mg of amberlite IR120 (H<sup>+</sup>) were suspended in 1.5 mL of DMF. Using a bath of ice (T = 0 °C), 75 mg of EDC (0.48 mmol), 65 mg of HOBt (0.48 mmol) and a solution of 110 mg of **11** (0.44 mmol) in DMF (1.5 mL) were added to the suspension previously prepared. The reaction was performed under microwave irradiation at 60 °C (200 W) for 1 h. Then, 5 mL of DCM were added to the reaction and the mixture was washed with an aqueous solution of LiCl 5% (3 × 15 mL). The organic phase was dried over anhydrous Na<sub>2</sub>SO<sub>4</sub>, filtered and the solvent was evaporated. The crude obtained was purified by flash column chromatography, by eluting with CHCl<sub>3</sub>/MeOH/toluene (9.5/0.3/0.2) to afford 20 mg (11%) of the title compound **5** as colorless oil. <sup>1</sup>H NMR (400 MHz, CDCl<sub>3</sub>) δ 7.62 (t, *J* = 8.4 Hz, 2H), 7.21–7.13 (m,

6H), 7.03 (d,  $J = 8.1$  Hz, 4H), 6.99 (d,  $J = 8.2$  Hz, 2H), 6.89 (s, 2H), 4.70–4.66 (m, 1H), 4.62–4.50 (m, 6H), 4.43–4.34 (m, 6H), 3.73 (q,  $J = 7.1$  Hz, 2H), 2.33 (d,  $J = 7.2$  Hz, 4H), 1.82–1.70 (m 2H), 1.50 (d,  $J = 7.2$  Hz, 6H), 0.82 (d,  $J = 6.6$  Hz, 12H) ppm;  $^{13}\text{C}$  NMR (100 MHz,  $\text{CDCl}_3$ )  $\delta$  178.2, 174.6, 160.3, 158.6, 157.8, 150.1, 140.8, 137.4, 135.2, 129.5, 127.2, 116.7, 115.8, 111.3, 109.8, 70.5, 67.9, 64.4, 61.8, 45.1, 45.1, 30.2, 22.5, 18.5 ppm. HRMS (ESI)  $m/z$ :  $[\text{M} + \text{H}]^+$  calcd for  $\text{C}_{53}\text{H}_{56}\text{O}_{15}$  933.3697; found 933.3685. HPLC  $t_{\text{ret}} = 18.17$  min. (Method B)

*5,5'-((2-hydroxypropane-1,3-diyl)bis(oxy))bis(N-(2-((S)-2-(4-isobutylphenyl)propanamido)ethyl)-4-oxo-4H-chromene-2-carboxamide) (6):*

78 mg of EDC (0.50 mmol) and a solution of 173 mg of **17** (0.47 mmol) in DMF (3 mL) were added to a suspension of 67 mg of HOBt (0.50 mmol) and 106 mg of **1** (0.21 mmol) in DMF (3 mL) with a bath of ice ( $T = 0$  °C). The mixture was stirred at rt overnight. Then, 5 mL of DCM were added to the reaction and the mixture was washed with a solution of LiCl 5% ( $3 \times 15$  mL). The organic phase was dried over anhydrous  $\text{Na}_2\text{SO}_4$ , filtered and the organic phase was evaporated. The obtained crude material was purified by silica gel flash column chromatography, by eluting with DCM/MeOH/ $\text{NH}_3$  (9/0.9/0.1) to afford 39 mg (20%) of the title compound **6** as white solid.  $^1\text{H}$  NMR (400 MHz,  $\text{CDCl}_3$ )  $\delta$  8.15 (bs, 2H), 7.58 (t,  $J = 8.4$  Hz, 2H), 7.21–6.77 (m, 14H), 6.10 (bs, 2H), 4.52 (d,  $J = 30.2$  Hz, 3H), 4.35 (s, 2H), 3.66–3.33 (m, 10H), 2.49–2.28 (m, Hz, 4H), 1.84–1.69 (m, 2H), 1.50 (d,  $J = 6.9$  Hz, 6H), 0.95–0.70 (m, 12H) ppm;  $^{13}\text{C}$  NMR (100 MHz,  $\text{CDCl}_3$ )  $\delta$  178.4, 177.0, 160.0, 159.1, 157.2, 153.1, 141.1, 138.1, 135.0, 129.8, 127.4, 115.5, 113.3, 111.0, 110.0, 70.5, 68.0, 46.8, 45.1, 41.8, 39.2, 30.2, 22.5, 18.6 ppm. Monoisotopic MS (ESI)  $m/z$ :  $[\text{M} + \text{H}]^+$  calcd for  $\text{C}_{53}\text{H}_{60}\text{N}_4\text{O}_{11}$ , 929.4337; found 929.4557. HPLC  $t_{\text{ret}} = 15.72$  min. (Method B)

*((5,5'-((2-hydroxypropane-1,3-diyl)bis(oxy))bis(4-oxo-4H-chromene-5,2-diyl-2-carbonyl))bis(azanediy))bis(ethane-2,1-diyl)(2S,2'S)-bis(2-(4-isobutylphenyl)propanoate) (7):*

48 mg of EDC (0.31 mmol) and a solution of 70 mg of **18** (0.28 mmol) in 2 mL of DMF were added to a suspension of 42 mg of HOBt (0.31 mmol) and 67 mg of **1** (0.13 mmol) in 2 mL of DMF with a bath of ice ( $T = 0$  °C). The mixture was stirred at rt overnight. Then, 5 mL of DCM were added to the reaction and the mixture was washed with an aqueous solution of LiCl 5% ( $3 \times 15$  mL). The organic phase was dried over anhydrous

Na<sub>2</sub>SO<sub>4</sub>, filtered and the organic solvent was evaporated. The obtained crude material was purified by silica gel flash column chromatography, by eluting with DCM/MeOH (9/1) to afford 97 mg (80%) of the title compound **7** as a colorless oil.

<sup>1</sup>H NMR (400 MHz, CDCl<sub>3</sub>) δ 7.60 (t, *J* = 8.4 Hz, 2H), 7.15–7.08 (m, Hz, 6H), 6.98–6.94 (m, 8H), 4.66–4.53 (m, 2H), 4.53–4.44 (m, 1H), 4.41–4.13 (m, 6H), 3.76–3.50 (m, 6H), 2.44 (d, *J* = 7.2 Hz, 1H), 2.33 (d, *J* = 7.2 Hz, 3H), 1.88–1.70 (m, 2H), 1.49 (dd, *J* = 7.2, 2.3 Hz, 6H), 0.88 (d, *J* = 6.6 Hz, 3H), 0.82 (d, *J* = 6.6 Hz, 9H) ppm; <sup>13</sup>C NMR (100 MHz, CDCl<sub>3</sub>) δ 178.1, 175.3, 159.4, 159.2, 157.0, 152.8, 140.9, 137.4, 134.9, 129.7, 129.5, 127.1, 127.1, 115.5, 113.6, 110.6, 110.0, 70.4, 67.9, 62.8, 62.4, 45.2, 45.0, 39.6, 39.4, 30.2, 22.5, 22.4, 18.5, 18.2 ppm. Monoisotopic MS (ESI) *m/z*: [M + H]<sup>+</sup> calcd for C<sub>53</sub>H<sub>58</sub>N<sub>2</sub>O<sub>13</sub>, 931.4017; found 931.4017. HPLC *t*<sub>ret</sub> = 18.17 min. (Method B)

*(S)*-*N*-(2-hydroxyethyl)-2-(4-isobutylphenyl)propanamide (**10**):

340 mg of EDC (2.19 mmol) and a catalytic amount of DMAP (9 mg, 0.073 mmol) were added to a solution of 300 mg of (*S*)-**3** (1.46 mmol) in 5 mL of DCM with a bath of ice (*T* = 0 °C). The solution was stirred at 0 °C for 30 min, then it was diluted to 30 mL and added dropwise to a solution of 0.7 mL of ethane-1,2-diol (**9**) (8.17 mmol) in 30 mL of DCM. After the addition, the reaction mixture was stirred at rt for 2 h. The solvent was evaporated, and the crude obtained was purified by silica gel flash column chromatography, by eluting with DCM/MeOH/toluene (8.4/0.8/0.8) to afford 195 mg (54%) of the title compound **10** as yellowish oil. <sup>1</sup>H NMR (400 MHz, CDCl<sub>3</sub>) δ 7.18 (d, *J* = 8.1 Hz, 2H), 7.10 (d, *J* = 8.1 Hz, 2H), 6.02 (bs, 1H), 3.61 (t, *J* = 5.1 Hz, 2H), 3.55 (q, *J* = 7.2 Hz, 1H), 3.42 – 3.23 (m, 2H), 2.77 (s, 1H), 2.44 (d, *J* = 7.2 Hz, 2H), 1.92 – 1.76 (m, 1H), 1.49 (d, *J* = 7.2 Hz, 3H), 0.89 (d, *J* = 6.6 Hz, 6H) ppm; <sup>13</sup>C NMR (100 MHz, CDCl<sub>3</sub>) δ 176.2, 140.8, 138.4, 129.8, 127.4, 62.4, 46.76, 45.1, 42.6, 30.1, 22.5, 19.0 ppm.

2-hydroxyethyl (*S*)-2-(4-isobutylphenyl)propanoate (**11**):

470 mg of EDC (3.03 mmol) and a catalytic amount of DMAP (5%) were added to a solution of 250 mg of (*S*)-**3** (1.21 mmol) in 3 mL DCM with a bath of ice (*T* = 0 °C). The solution was stirred at 0 °C for 30 min, then it was diluted to 30 mL and added dropwise to a solution of 510 mg of ethane-1,2-diol (**9**) (0.54 mL, 8.17 mmol) in 30 mL DCM. After the addition, the reaction mixture was stirred at rt for 2 h. The solvent was evaporated and the crude obtained was purified by silica gel flash column chromatography, by eluting with DCM/MeOH (9.8/0.2) to afford 238 mg (79%) the title compound **11** as colorless

oil. <sup>1</sup>H NMR (400 MHz, CDCl<sub>3</sub>) δ 7.20 (d, *J* = 8.0 Hz, 2H), 7.09 (d, *J* = 8.0 Hz, 2H), 4.17–4.15 (m, 2H), 3.75–3.71 (m, 3H), 2.44 (d, *J* = 7.2 Hz, 2H), 2.41 (d, 1H), 1.83–1.70 (m, 1H), 1.42 (d, *J* = 7.2 Hz, 3H), 0.82 (d, *J* = 6.6 Hz, 6H) ppm; <sup>13</sup>C NMR (100 MHz, CDCl<sub>3</sub>) δ 175.2, 140.7, 137.7, 129.4, 127.1, 66.3, 60.9, 45.1, 45.0, 30.2, 22.4, 18.5 ppm.

*tert*-butyl (2-aminoethyl)carbamate (**13**):

A solution of 408 mg of di-*tert*-butyl dicarbonate (1.9 mmol) in 9 mL DCM was added dropwise with a bath of ice (*T* = 0 °C) to a solution of 564 mg of **12** (9.4 mmol) in 6 mL DCM. After the addition, the resulting mixture was stirred at rt for 1.40 h. The organic solvent was evaporated, and the crude obtained was purified by silica gel flash column chromatography, by eluting with DCM/MeOH/NH<sub>3</sub> (7.8/2/0.2) to afford 243 mg (80%) of the title compound **13** as colorless oil. <sup>1</sup>H NMR (400 MHz, CDCl<sub>3</sub>) δ 5.19 (bs, 1H), 3.06 (t, *J* = 5.3 Hz, 2H), 2.68 (t, *J* = 5.8 Hz, 2H), 1.99 (bs, 2H), 1.32 (s, 9H) ppm; <sup>13</sup>C NMR (100 MHz, CDCl<sub>3</sub>) δ 156.9, 79.7, 43.4, 41.7, 28.5 ppm.

*tert*-butyl (2-hydroxyethyl)carbamate (**14**):

497 mg of di-*tert*-butyl dicarbonate (2.3 mmol) were added to a solution of 116 mg of **8** (1.9 mmol) in 5 mL DCM with a bath of ice (*T* = 0 °C). The resulting mixture was stirred at r.t. for 1.40 h. The organic solvent was evaporated and the crude obtained was purified by silica gel flash column chromatography, by eluting with DCM/MeOH/NH<sub>3</sub> (9.2/0.8/0.1) to afford 245 mg (80%) of the title compound **14** as colorless oil. <sup>1</sup>H NMR (400 MHz, CDCl<sub>3</sub>) δ 5.08 (bs, 1H), 3.69 (d, *J* = 4.8 Hz, 2H), 3.28 (d, *J* = 5.0 Hz, 2H), 2.89 (bs, 1H), 1.45 (s, 9H) ppm; <sup>13</sup>C NMR (100 MHz, CDCl<sub>3</sub>) δ 156.7, 79.8, 62.6, 43.3, 28.5 ppm.

*tert*-butyl (*S*)-(2-(2-(4-isobutylphenyl)propanamido)ethyl)carbamate (**15**):

To a solution of 150 mg of (*S*)-**3** (0.73 mmol) in 3 mL of DCM were added 113 mg of EDC (0.73 mmol) and a catalytic amount of DMAP with a bath of ice (*T* = 0 °C). After stirring the mixture at 0 °C for 30 min, keeping the reaction at the same temperature, a solution of 97 mg of **13** (0.61 mmol) in 2 mL of DCM was added. The resulting mixture was stirred at rt for 2.30 h. The solvent was evaporated and the crude obtained was purified by silica gel flash column chromatography, by eluting with DCM/toluene/MeOH/NH<sub>3</sub> (8.7/0.87/0.43/0.04) to afford 159 mg (75%) of the title compound **15** as colorless oil. <sup>1</sup>H NMR (400 MHz, CDCl<sub>3</sub>) δ 7.18 (d, *J* = 8.0 Hz, 2H),

7.09 (d,  $J = 8.0$  Hz, 2H), 6.11 (bs, 1H), 4.95 (bs, 1H), 3.50 (m, 1H), 3.35–3.12 (m, 4H), 2.43 (d,  $J = 7.2$  Hz, 2H), 1.84 (m, 1H), 1.48 (d,  $J = 7.2$  Hz, 3H), 1.41 (s, 9H), 0.89 (d,  $J = 6.6$  Hz, 6H) ppm;  $^{13}\text{C}$  NMR (100 MHz,  $\text{CDCl}_3$ )  $\delta$  174.7, 155.8, 140.7, 137.8, 129.5, 127.2, 79.8, 63.8, 45.2, 45.2, 39.8, 30.3, 28.5, 22.5, 18.5 ppm.

*2-((tert-butoxycarbonyl)amino)ethyl (S)-2-(4-isobutylphenyl)propanoate (16):*

186 mg of EDC (1.20 mmol) and a catalytic amount of DMAP were added with a bath of ice ( $T = 0$  °C) to a solution of 200 mg of (**S**)-**3** (0.97 mmol) in 4 mL of DCM. After stirring the solution at 0 °C for 30 min, a solution of 128 mg of **14** (0.80 mmol) in 1.5 mL of DCM was added at  $T = 0$  °C. The resulting mixture was stirred at rt for 4 h. The solvent was evaporated and the crude obtained was purified by silica gel flash column chromatography, by eluting with DCM/MeOH (9.6/0.4) to afford 191 mg (69%) of the title compound **16** as colorless oil.  $^1\text{H}$  NMR (400 MHz,  $\text{CDCl}_3$ )  $\delta$  7.18 (d,  $J = 8.0$  Hz, 2H), 7.08 (d,  $J = 8.0$  Hz, 2H), 4.57 (bs, 1H), 4.11–4.06 (m, 2H), 3.73–3.67 (m, 1H), 3.29 (bs, 2H), 2.44 (d,  $J = 7.2$  Hz, 2H), 1.83 (m, 1H), 1.48 (d,  $J = 7.2$  Hz, 3H), 1.42 (s, 9H), 0.88 (d,  $J = 6.6$  Hz, 6H) ppm;  $^{13}\text{C}$  NMR (100 MHz,  $\text{CDCl}_3$ )  $\delta$  174.9, 174.2, 140.0, 137.8, 137.2, 128.5, 126.7, 61.0, 46.3, 44.5, 42.1, 29.6, 22.1, 18.3, 17.9 ppm.

*(S)-N-(2-aminoethyl)-2-(4-isobutylphenyl)propenamide (17):*

0.7 mL of trifluoroacetic acid (9.14 mmol) was added to a solution of 159 mg of **15** (0.46 mmol) in 10 mL of DCM with a bath of ice ( $T = 0$  °C). The resulting mixture was stirred at rt for 2.5 h. The organic phase was evaporated. 173 mg (> 99%) of compound **17** were obtained and used without any further purification.  $^1\text{H}$  NMR (400 MHz,  $\text{CDCl}_3$ )  $\delta$  7.16 (d,  $J = 8.0$  Hz, 2H), 7.05 (d,  $J = 8.0$  Hz, 2H), 6.46 (bs, 1H), 3.52 (q,  $J = 7.1$  Hz, 1H), 3.33–3.13 (m, 4H), 2.75 (bs, 2H), 2.40 (d,  $J = 7.2$  Hz, 2H), 1.80 (m, 1H), 1.43 (d,  $J = 7.1$  Hz, 3H), 0.85 (d,  $J = 6.6$  Hz, 6H) ppm;  $^{13}\text{C}$  NMR (100 MHz,  $\text{CDCl}_3$ )  $\delta$  175.3, 140.6, 138.6, 129.6, 127.3, 77.4, 77.1, 76.8, 46.7, 45.1, 40.6, 30.2, 28.4, 22.4, 18.5 ppm.

*2-aminoethyl (S)-2-(4-isobutylphenyl)propanoate (18):*

0.1 mL trifluoroacetic acid (1.26 mmol) was added to a solution of 98 mg of **16** (0.28 mmol) in 2 mL of DCM with a bath of ice ( $T = 0$  °C). The resulting mixture was stirred at rt for 6 h. The organic phase was evaporated. 70 mg (> 99%) of compound **18** were used without any further purification.  $^1\text{H}$  NMR (400 MHz,  $\text{CDCl}_3$ )  $\delta$  7.17 (d,  $J = 8.0$  Hz, 2H), 7.05 (d,  $J = 8.0$  Hz, 2H), 4.40 (bs, 2H), 3.53 (q,  $J = 7.1$  Hz, 1H), 3.33–3.16 (m, 4H),

2.41 (d,  $J = 7.2$  Hz, 2H), 1.87–1.76 (m, 1H), 1.45 (d,  $J = 7.1$  Hz, 3H), 0.87 (d,  $J = 6.6$  Hz, 6H) ppm;  $^{13}\text{C}$  NMR (100 MHz,  $\text{CDCl}_3$ )  $\delta$  175.2, 140.7, 137.7, 129.5, 127.1, 66.3, 61.0, 45.1, 45.1, 30.2, 22.4, 18.6 ppm.

*5,5'-((2-hydroxypropane-1,3-diyl)bis(oxy))bis(N-(2-hydroxyethyl)-4-oxo-4H-chromene-2-carboxamide)* (**20**):

1.4 mL TFA (18.1 mmol) were added dropwise to a solution of 1 g of **8** (16.4 mmol) in 2 mL of DCM. The reaction mixture was stirred at rt for 1.5 h until an orange precipitate formed. The solvent was evaporated and intermediate **19** was obtained and triturated by heptane (205 mg, 1.17 mmol). 205 mg of **19** were solubilized in 1.5 mL DMF. Following, with a bath of ice ( $T = 0$  °C), this solution and 199 mg of EDC (1.29 mmol) were added to a suspension of 174 mg of HOBt (1.29 mmol) and 100 mg of **1** (0.20 mmol) in 1.5 mL of DMF. The mixture was stirred at rt overnight. Then, 5 mL of n-butanol were added to the reaction and the mixture was washed with an aqueous solution of LiCl 5% (3 x 10 mL). The organic phase was dried over anhydrous  $\text{Na}_2\text{SO}_4$ , filtered and the solvent was evaporated. The solid obtained was purified by triturating by DCM to afford 15 mg (14%) of the title compound **20** as white solid.  $^1\text{H}$  NMR (400 MHz,  $\text{DMSO}-d_6$ )  $\delta$  9.15 (s, 2H), 7.72 (t,  $J = 8.4$  Hz, 2H), 7.30 (d,  $J = 8.4$  Hz, 2H), 7.10 (d,  $J = 8.3$  Hz, 2H), 6.62 (s, 2H), 5.44 (d,  $J = 3.9$  Hz, 1H), 4.98 (t,  $J = 5.5$  Hz, 2H), 4.42 – 4.22 (m, 5H), 3.56 – 3.51 (m,  $J = 5.7$  Hz, 3H), 3.36 – 3.30 (m,  $J = 5.8$  Hz, 3H) ppm;  $^{13}\text{C}$  NMR (100 MHz, DMSO)  $\delta$  176.8, 159.1, 158.3, 157.0, 153.6, 135.0, 114.4, 112.0, 110.5, 108.9, 70.1, 67.4, 59.2, 42.3 ppm. MS (ESI)  $m/z$ :  $[\text{M}+\text{H}]^+$  555.3

## 6.2 Synthesis of cromolyn-ibuprofen codrugs (1:1)

*dimethyl 5,5'-((2-((2-(4-isobutylphenyl)propanoyl)oxy)propane-1,3-diyl)bis(oxy))(S)-bis(4-oxo-4H-chromene-2-carboxylate) (21):*

80 mg of (S)-**3** (0.39 mmol), 61 mg of EDC (0.39 mmol) and a catalytic amount of DMAP were solubilized in 2 mL of DCM and stirred at rt for 40 min. Following, this solution was added dropwise to a suspension of 127 mg of **23** (0.26 mmol) in 5 mL of DCM. The reaction mixture was stirred at rt overnight. Then, the solvent was evaporated and the crude obtained was purified by silica gel flash column chromatography, by eluting with DCM/MeOH (9.2/0.8) to afford 103 mg (57%) of the title compound **21** as white solid. <sup>1</sup>H NMR (400 MHz, CDCl<sub>3</sub>) δ 7.57 (t, *J* = 8.4 Hz, 1H), 7.52 (t, *J* = 8.4 Hz, 1H), 7.18 (d, *J* = 8.1 Hz, 2H), 7.09 (t, *J* = 9.0 Hz, 2H), 6.96 (dd, *J* = 8.3, 2.6 Hz, 3H), 6.87 (d, *J* = 5.5 Hz, 2H), 6.83 (d, *J* = 8.2 Hz, 1H), 5.65 – 5.54 (m, 1H), 4.67 (dd, *J* = 9.9, 5.1 Hz, 1H), 4.56 (dd, *J* = 9.9, 4.8 Hz, 1H), 4.47 (qd, *J* = 14.3, 9.8, 5.0 Hz, 2H), 3.97 (s, 6H), 3.78 (q, *J* = 7.1 Hz, 1H), 2.36 (d, *J* = 7.2 Hz, 2H), 1.83 – 1.71 (m, *J* = 13.4, 6.7 Hz, 1H), 1.49 (d, *J* = 7.2 Hz, 3H), 0.84 (d, *J* = 6.6 Hz, 6H) ppt; <sup>13</sup>C NMR (100 MHz, CDCl<sub>3</sub>) δ 177.24, 177.15, 174.20, 161.08, 158.52, 158.44, 157.69, 157.63, 149.94, 149.91, 140.37, 137.30, 134.75, 134.67, 129.18, 127.19, 116.44, 115.45, 115.37, 110.76, 110.70, 108.70, 108.61, 70.06, 66.94, 66.73, 53.37, 44.98, 30.11, 22.33, 18.35 ppt. HRMS (ESI) *m/z*: [M + H]<sup>+</sup> calcd for C<sub>38</sub>H<sub>37</sub>O<sub>12</sub> 685,2285; found 685.2234. HPLC *t*<sub>ret</sub> = 14.56 min. (Method B)

*diethyl 5,5'-((2-((2-(4-isobutylphenyl)propanoyl)oxy)propane-1,3-diyl)bis(oxy))(S)-bis(4-oxo-4H-chromene-2-carboxylate) (22):*

43 mg of (S)-**3** (0.21 mmol), 32 mg of EDC (0.21 mmol) and a catalytic amount of DMAP were solubilized in 1 mL of DCM and stirred at rt for 40 min. Following, this solution was added dropwise to a suspension of 73 mg of **24** (0.14 mmol) in 2.5 mL of DCM. The solution obtained was stirred at rt overnight. Then, the solvent was evaporated and the crude obtained was purified by silica gel flash column chromatography, by eluting with DCM/MeOH/toluene (8.7/0.4/0.9) to afford 44 mg (44%) of the title compound **22** as white solid. <sup>1</sup>H NMR (400 MHz, CDCl<sub>3</sub>) δ 7.57 (t, *J* = 8.4 Hz, 1H), 7.51 (t, *J* = 8.4 Hz, 1H), 7.18 (d, *J* = 8.0 Hz, 2H), 7.10 (t, *J* = 9.1 Hz, 2H), 6.96 (dd, 3H), 6.87 (d, *J* = 5.5 Hz, 2H), 6.83 (d, *J* = 8.3 Hz, 1H), 5.64 – 5.56 (m, *J* = 9.6, 4.8 Hz, 1H), 4.67 (dd, *J* = 10.0, 5.1 Hz, 1H), 4.56 (dd, *J* = 10.0, 4.8 Hz, 1H), 4.53 – 4.36 (m, 6H), 3.78 (q, *J* = 7.1 Hz, 1H),

2.36 (d,  $J = 7.2$  Hz, 2H), 1.83 – 1.71 (m,  $J = 13.5, 6.7$  Hz, 1H), 1.49 (d,  $J = 7.2$  Hz, 3H), 1.41 (t,  $J = 7.1$  Hz, 6H), 0.84 (d,  $J = 6.6$  Hz, 6H) ppm;  $^{13}\text{C}$  NMR (100 MHz,  $\text{CDCl}_3$ )  $\delta$  177.41, 177.31, 174.24, 160.63, 158.54, 158.46, 157.77, 157.71, 150.20, 140.40, 137.34, 134.72, 134.64, 129.20, 127.22, 116.31, 115.42, 110.85, 110.79, 108.68, 108.59, 70.09, 66.98, 66.76, 62.84, 45.01, 30.15, 22.37, 18.38, 14.11 ppm. HRMS (ESI)  $m/z$ :  $[\text{M} + \text{H}]^+$  calcd for  $\text{C}_{40}\text{H}_{41}\text{O}_{12}$  713,2595; found 713.2601. HPLC  $t_{\text{ret}} = 16.24$  min. (Method B)

*dimethyl 5,5'-((2-hydroxypropane-1,3-diyl)bis(oxy))bis(4-oxo-4H-chromene-2-carboxylate) (23):*

150 mg of **1** (0.29 mmol) were solubilized in 14 mL of MeOH and 0.15 mL of HCl (37%) in a pressure tube. The resulting mixture was refluxed under pressure overnight ( $T = 100^\circ\text{C}$ ). Subsequently, the solvent was removed under reduced pressure, and the crude was solubilized in 10 mL of DCM and washed with a basic aqueous solution (NaOH 10% 3 x 15 mL). The organic phase was dried over anhydrous  $\text{Na}_2\text{SO}_4$ , filtered and the solvent evaporated. The obtained crude material was purified by silica gel flash column chromatography, by eluting with DCM/MeOH (9.5/0.5) to afford 73 mg (70%) of the title compound **23** as a white solid. Compound **23** was characterized in agreement with the literature<sup>167, 335</sup>  $^1\text{H}$  NMR (400 MHz,  $\text{CDCl}_3$ )  $\delta$  7.60 (t,  $J = 8.4$  Hz, 2H), 7.16 (d,  $J = 8.4$  Hz, 2H), 6.96 (t,  $J = 4.0$  Hz, 4H), 4.58 (dd,  $J = 8.9, 4.6$  Hz, 2H), 4.53 – 4.41 (m, 1H), 4.35 (dd,  $J = 8.9, 6.0$  Hz, 2H), 3.99 (s, 6H) ppm.

*diethyl 5,5'-((2-hydroxypropane-1,3-diyl)bis(oxy))bis(4-oxo-4H-chromene-2-carboxylate) (24):*

100 mg of **1** (0.20 mmol) were solubilized in 10 mL of EtOH and HCl (37%) (0.10 mL) in a pressure tube. The resulting mixture was refluxed overnight ( $T = 100^\circ\text{C}$ ). Then, the solvent was evaporated and the crude was solubilized in DCM (10 mL) and washed with basic water (NaOH 10% 3 x 15 mL). The organic phase was dried over anhydrous  $\text{Na}_2\text{SO}_4$ , filtered and the organic solvent was evaporated under reduced pressure. The obtained crude material was purified by silica gel flash column chromatography, by eluting with DCM/MeOH (9.5/0.5) to afford 127 mg (88%) of the title compound **24** as a white solid that was characterized by  $^1\text{H}$  NMR in agreement with the literature<sup>167, 336, 337</sup>.  $^1\text{H}$  NMR (400 MHz,  $\text{CDCl}_3$ )  $\delta$  7.56 (t,  $J = 8.4$  Hz, 2H), 7.12 (d,  $J = 8.4$  Hz, 2H), 6.93 (t, 4H), 4.59 – 4.25 (m, 9H), 1.39 (t,  $J = 7.1$  Hz, 6H) ppm.



### 6.3 Synthesis of p38 MAPK/MAO-B potential dual inhibitors

*5-(2,6-dichloro-4-(prop-2-yn-1-ylamino)phenyl)-2-((2,4-difluorophenyl)thio)-6H-pyrimido[1,6-b]pyridazin-6-one (31):*

100 mg of **41** (0.22 mmol), 46 mg of K<sub>2</sub>CO<sub>3</sub> (0.33 mmol) and 37 mg of KI (0.22 mmol) were suspended in 0.6 mL of DMF. Then, 39 mg of propargyl bromide (80% in toluene) (45  $\mu$ L, 0.33 mmol) were added dropwise. The reaction was stirred rt overnight. 2 mL of H<sub>2</sub>O were added to the reaction and a red precipitate formed. The obtained precipitate was filtered and washed 2 times with EtOAc, a yellow precipitate was obtained and filtered. The obtained crude material was purified by silica gel flash column chromatography, by eluting with DCM/MeOH (9.6/0.4) to afford 16 mg (15%) of the title compound **31** as a yellow solid. <sup>1</sup>H NMR (400 MHz, DMSO-*d*<sub>6</sub>)  $\delta$  8.80 (s, 1H), 7.86 (dd, *J* = 14.9, 8.5 Hz, 1H), 7.56 (td, *J* = 9.3, 2.7 Hz, 1H), 7.30 (dd, *J* = 8.5, 6.1 Hz, 1H), 7.08 (d, *J* = 9.8 Hz, 1H), 7.00 (d, *J* = 9.9 Hz, 1H), 6.81 (s, 2H), 6.78 (bs, 1H), 3.97 (s, 2H), 3.17 (t, *J* = 2.3 Hz, 1H) ppm; <sup>13</sup>C NMR (100 MHz, DMSO-*d*<sub>6</sub>)  $\delta$  165.4, 153.4, 149.7, 149.5, 138.7, 138.6, 137.7, 135.6, 129.4, 122.9, 113.6, 113.1, 112.0, 111.7, 105.8, 105.5, 105.4, 81.2, 73.7, 31.7 ppm. MS (ESI) *m/z*: 489.2 [M + H]<sup>+</sup>. HPLC *T*<sub>ret</sub> = 2.53 min. (Method A)

*5-(2,6-dichloro-4-(methyl(prop-2-yn-1-yl)amino)phenyl)-2-((2,4-difluorophenyl)thio)-6H-pyrimido[1,6-b]pyridazin-6-one (32):*

192 mg of **43** (0.41 mmol), 141 mg of K<sub>2</sub>CO<sub>3</sub> (1.03 mmol) and 68 mg of KI (0.41 mmol) were suspended in 2 mL of DMF. Then, 98 mg of propargyl bromide (80% in toluene) (113  $\mu$ L, 0.82 mmol) were added dropwise. The reaction was stirred rt overnight. 2 mL of H<sub>2</sub>O were added to the reaction and a red precipitate formed. The obtained precipitate was filtered and washed 2 times with EtOAc, a yellow precipitate was obtained and filtered. The obtained crude material was purified by silica gel flash column chromatography, by eluting with DCM/MeOH (9.8/0.2) to afford 10 mg (5%) of the title compound **32** as a yellowish solid. <sup>1</sup>H NMR (400 MHz, DMSO-*d*<sub>6</sub>)  $\delta$  7.82 (td, *J* = 8.5, 6.4 Hz, 1H), 7.53 (td, *J* = 9.3, 2.7 Hz, 1H), 7.26 (td, *J* = 8.3, 2.2 Hz, 1H), 7.03 (d, *J* = 9.8 Hz, 1H), 6.97 (d, *J* = 9.8 Hz, 1H), 6.95 (s, 2H), 4.20 (d, *J* = 2.2 Hz, 2H), 3.16 (t, *J* = 2.3 Hz, 1H), 2.94 (s, 3H) ppm. MS (ESI) *m/z*: 503.1 [M + H]<sup>+</sup>. Calcd for C<sub>23</sub>H<sub>15</sub>C<sub>12</sub>F<sub>2</sub>N<sub>4</sub>OS 503.0312; found 503.0306. HPLC *t*<sub>ret</sub> = 2.63 min. (Method A)

*2-bromo-1,3-dichloro-5-nitrobenzene (34):*

1g of **33** (4.83 mmol) was solubilized in 30 mL of MeCN and 7.5 mL of HBr. The mixture was stirred for 20 min at rt. Then, 20 mL of an aqueous solution of 343 mg of NaNO<sub>2</sub> (4.79 mmol) were added dropwise in 70 min using a bath of ice (T = 0 °C). Following, a solution of 970 mg of CuBr (6.67 mmol) in 4 mL of HBr was prepared and added dropwise in 20 min to the reaction. After the addition, the mixture was stirred at rt for 30 min. The organic phase was evaporated and the remaining solution was extracted with DCM (3 x 25 mL). The organic phases were combined and washed with a basic aqueous solution (NaOH 10%). Then, they were dried over anhydrous Na<sub>2</sub>SO<sub>4</sub>, filtered and the organic solvent was evaporated under reduced pressure. 1.26 g (97%) of compound **34** were obtained as red solid and used without any further purification. <sup>1</sup>H NMR (400 MHz, CDCl<sub>3</sub>) δ 8.24 (s, 2H) ppm; <sup>13</sup>C NMR (100 MHz, CDCl<sub>3</sub>) δ 147.3, 137.8, 131.5, 123.2 ppm.

*methyl 2-cyano-2-(2,6-dichloro-4-nitrophenyl)acetate (35):*

500 mg of **34** (1.85 mmol) and 183 mg of methyl cyanoacetate (1.85 mmol) were solubilized in 6 mL of DMF and the solution was warmed to 50 °C. Then 510 mg of K<sub>2</sub>CO<sub>3</sub> (3.69 mmol) were added. The reaction mixture was stirred overnight at 50 °C. Then, the reaction was adjusted to pH = 2 by HCl (37%), 15 mL of DCM were added to the reaction and the mixture was washed with an aqueous solution of LiCl 5% (3 x 20 mL). The organic phase was dried over anhydrous Na<sub>2</sub>SO<sub>4</sub>, filtered and the organic solvent was evaporated under reduced pressure. 504 g (92%) of compound **35** were obtained as yellow solid and used without any further purification. <sup>1</sup>H NMR (400 MHz, CDCl<sub>3</sub>) δ 8.29 (s, 2H), 5.72 (s, 1H), 3.89 (s, 3H) ppm; <sup>13</sup>C NMR (100 MHz, CDCl<sub>3</sub>) δ 163.8, 137.1, 134.0, 124.0, 112.8, 55.1, 39.2 ppm.

*2-(2,6-dichloro-4-nitrophenyl)acetonitrile (36):*

2.63g of **35** (9.10 mmol) were solubilized in a mixture of 5 mL of H<sub>2</sub>SO<sub>4</sub>, 50 mL of AcOH, and 50 mL of H<sub>2</sub>O. The resulting solution was refluxed at T = 125 °C for 5 h. When the complete consumption of **35** was observed the reaction was cooled to rt and, using a bath of ice, about 100 mL of H<sub>2</sub>O were added, and a reddish precipitate formed. The precipitate was filtered, washed with water, and dried. The title compound **36** was obtained as 1.56 g (75%) of an orange solid that was used without further purification. <sup>1</sup>H

NMR (400 MHz, CDCl<sub>3</sub>) δ 8.27 (s, 2H), 4.10 (s, 2H) ppm; <sup>13</sup>C NMR (100 MHz, CDCl<sub>3</sub>) δ 146.8, 137.8, 131.6, 129.1, 128.4, 125.2, 123.2 ppm.

*2-(4-amino-2,6-dichlorophenyl)acetonitrile (37):*

350 mg of **36** (1.50 mmol) were solubilized in 26 mL of EtOH. The solution was warmed to 75 °C and a solution previously prepared of SnCl<sub>2</sub> in 9 mL of HCl (37%) was added dropwise. The reaction mixture was stirred at T = 75°C for 30 min. When the complete consumption of the starting compound **36** was observed the reaction was cooled to rt and basified by the addition of an aqueous solution of NaOH 10%. The organic phase was evaporated and the aqueous layer was extracted by DCM (3 x 25 mL). The organic phase was dried over anhydrous Na<sub>2</sub>SO<sub>4</sub>, filtered, and the organic solvent was evaporated under reduced pressure. 301 mg (> 99%) of compound **37** were obtained as orange solid and used without any further purification. <sup>1</sup>H NMR (400 MHz, CDCl<sub>3</sub>) δ 6.64 (s, 2H), 3.91 (bs, 2H), 3.86 (s, 2H) ppm; <sup>13</sup>C NMR (100 MHz, CDCl<sub>3</sub>) δ 148.1, 136.1, 116.6, 115.6, 114.5, 19.1 ppm.

*2-(4-amino-2,6-dichlorophenyl)-2-(6-chloropyridazin-3-yl)acetonitrile (38):*

In a dry three-neck round-bottom flask, 2.32 g of *t*BuOK (20.70 mmol) were suspended in 26 mL of THF under a nitrogen atmosphere. Using a bath of ice, a solution of 1.40 g of **37** (6.90 mmol) in 20 mL of THF was added. The resulting mixture was stirred at T = 0 °C for 30 min. Then, 1.54 g of 3,6-dichloropyridazine (20.70 mmol) were added and the reaction was stirred at rt for 3h. Following, the pH was adjusted to 7 by the addition of a solution of HCl (2N), the organic phase was evaporated and the remaining aqueous layer was extracted by EtOAc (3 x 30 mL). The organic phase was dried over anhydrous Na<sub>2</sub>SO<sub>4</sub>, filtered, and the obtained crude material was purified by silica gel flash column chromatography, by eluting with petroleum ether/EtOAc/ toluene (4/4/2) to afford 1.20 g (55%) of the title compound **38** as orange solid. <sup>1</sup>H NMR (400 MHz, CDCl<sub>3</sub>) δ 7.63 (d, *J* = 8.9 Hz, 1H), 7.53 (d, *J* = 8.9 Hz, 1H), 6.67 (s, 2H), 6.32 (s, 1H) ppm; <sup>13</sup>C NMR (100 MHz, CDCl<sub>3</sub>) δ 156.2, 148.5, 136.4, 130.5, 116.6, 115.5, 114.5, 19.1 ppm.

*2-(4-amino-2,6-dichlorophenyl)-2-(6-((2,4-difluorophenyl)thio)pyridazin-3-yl)acetonitrile (39):*

In a dry three-neck round-bottom flask, 210 mg of NaH 60 % dispersion in mineral oil (6.3 mmol) were suspended in 2 mL of THF under an inert atmosphere. Using a bath of

ice ( $T = 0\text{ }^{\circ}\text{C}$ ) 811 mg of 2,4-difluorobenzenethiol (25 mL, 5.55 mmol) were added dropwise to the reaction and the resulting mixture was stirred for 30 min at  $0\text{ }^{\circ}\text{C}$ . Subsequently, the reaction was warmed to  $60\text{ }^{\circ}\text{C}$  and a previously prepared solution of 1.18 g of **38** (5.90 mmol) solubilized in 18 mL of THF was added dropwise. The reaction was stirred at  $60\text{ }^{\circ}\text{C}$  for 3h. When the complete consumption of the starting compound **38** was observed by TLC, the reaction was cooled to rt and neutralized by the addition of some drops of HCl (2N). The organic solvent was evaporated and the obtained crude material was purified by silica gel flash column chromatography, by eluting with petroleum ether/EtOAc (5/5) to afford 1.24g (80%) of the title compound **39** as orange oil.  $^1\text{H}$  NMR (400 MHz,  $\text{CDCl}_3$ )  $\delta$  7.67 – 7.55 (m, 1H), 7.41 (d,  $J = 9.0$  Hz, 1H), 7.22 (d,  $J = 9.0$  Hz, 1H), 7.03 – 6.87 (m, 2H), 6.62 (s, 2H), 6.23 (s, 1H), 3.97 (bs, 2H) ppm;  $^{13}\text{C}$  NMR (100 MHz,  $\text{CDCl}_3$ )  $\delta$  162.4, 154.4, 148.5, 138.8, 138.6, 136.0, 125.3, 117.9, 116.2, 115.1, 113.0, 113.0, 112.8, 112.8, 105.7, 105.5, 105.2, 38.1 ppm.

*2-(4-amino-2,6-dichlorophenyl)-2-(6-((2,4-difluorophenyl)thio)pyridazin-3-yl)acetamide (40):*

500 mg of **39** (1.20 mmol) were solubilized in 15 mL of  $\text{H}_2\text{SO}_4$ . The reaction was stirred for 30 min at  $100\text{ }^{\circ}\text{C}$  and the complete consumption of compound **39** was observed. Following, the reaction mixture was neutralized by the addition of an aqueous solution of NaOH (10%), and a yellowish precipitate formed. The title compound was filtered under reduced pressure and dried. 520 mg (80%) of compound **40** were obtained as a yellowish solid, used without further purification.  $^1\text{H}$  NMR (400 MHz,  $\text{CDCl}_3$ )  $\delta$  8.46 (bs, 2H), 7.67 – 7.57 (m, 1H), 7.00 – 6.92 (m, 2H), 6.75 (s, 2H), 6.45 (d,  $J = 9.8$  Hz, 1H), 6.24 (d,  $J = 9.9$  Hz, 1H), 5.81 (s, 2H), 5.29 (s, 1H) ppm;  $^{13}\text{C}$  NMR (100 MHz,  $\text{CDCl}_3$ )  $\delta$  170.4, 161.8, 157.6, 139.5, 138.1, 136.7, 128.5, 127.7, 126.3, 125.3, 115.5, 115.1, 113.1, 112.9, 105.5, 51.6 ppm.

*5-(4-amino-2,6-dichlorophenyl)-2-((2,4-difluorophenyl)thio)-6H-pyrimido[1,6-b]pyridazin-6-one (41):*

550 mg of **40** (1.30 mmol) were solubilized in 10 mL of THF and 300 mg of DMF-DMA (0.34 mL, 2.60 mmol) were added. The resulting mixture was stirred at  $70\text{ }^{\circ}\text{C}$  for 4h. Following, the organic solvent was evaporated the residue was suspended in 20 mL of  $\text{H}_2\text{O}$  and extracted by DCM (3 x 15 mL). The organic phase was dried over anhydrous  $\text{Na}_2\text{SO}_4$ , filtered, and the obtained crude material was purified by silica gel flash column

chromatography, by eluting with DCM/MeOH (9.1/0.9) to afford 586 mg (83%) of the title compound **40** as yellow solid. <sup>1</sup>H NMR (400 MHz, DMSO-*d*<sub>6</sub>) δ 8.78 (s, 1H), 7.85 (dd, *J* = 14.9, 8.4 Hz, 1H), 7.55 (td, *J* = 9.3, 2.6 Hz, 1H), 7.29 (t, *J* = 7.3 Hz, 1H), 7.06 (d, *J* = 9.8 Hz, 1H), 6.98 (d, *J* = 9.8 Hz, 2H), 6.70 (s, 2H), 5.85 (s, 2H) ppm; <sup>13</sup>C NMR (100 MHz, DMSO-*d*<sub>6</sub>) δ 170.2, 165.4, 153.6, 150.8, 149.7, 138.7, 138.6, 137.8, 137.7, 135.5, 135.4, 129.5, 122.7, 115.3, 113.4, 113.1, 112.6, 112.1, 105.8, 105.5, 105.2 ppm.

*5-(2,6-dichloro-4-(methylamino)phenyl)-2-((2,4-difluorophenyl)thio)-6H-pyrimido[1,6-*b*]pyridazin-6-one (43):*

237 mg of **50** (0.52 mmol) were solubilized in 4 mL of THF and 124 mg of DMF-DMA (140 μL, 1.04 mmol) were added. The resulting mixture was stirred at 70°C for 4h. Following, the mixture was cooled to rt and a yellow precipitate formed. It was filtered under reduced pressure and washed by EtOAc. The title compound **43** was obtained as 192 mg (79%) of yellow solid and used without further purification. <sup>1</sup>H NMR (400 MHz, DMSO-*d*<sub>6</sub>) δ 8.79 (s, 1H), 7.92 – 7.79 (m, 1H), 7.56 (td, *J* = 9.3, 2.7 Hz, 1H), 7.30 (dd, *J* = 8.5, 5.7 Hz, 1H), 7.07 (d, *J* = 9.8 Hz, 1H), 6.99 (d, *J* = 9.8 Hz, 1H), 6.67 (s, 2H), 6.42 (d, *J* = 5.0 Hz, 1H), 2.71 (d, *J* = 4.9 Hz, 3H) ppm; <sup>13</sup>C NMR (100 MHz, DMSO-*d*<sub>6</sub>) δ 165.5, 153.5, 151.4, 149.6, 138.9, 137.8, 135.7, 129.8, 123.3, 115.3, 113.6, 112.5, 110.6, 109.6, 109.3, 109.1, 105.8, 105.5, 105.3, 29.4 ppm.

*2-(2,6-dichloro-4-(methylamino)phenyl)acetonitrile (47):*

In a microwave tube, 300 mg of **37** (1.49 mmol), 248 mg of K<sub>2</sub>CO<sub>3</sub> (1.83 mmol), and 241 mg of MeI (106 μL, 1.71 mmol) were added to 1.5 mL of DMF. The reaction was stirred under microwave irradiation at 70 °C at 200 W for 1.5 h. Then, 5 mL of DCM were added to the reaction and the mixture was washed with an aqueous solution of LiCl 5% (3 × 15 mL). The organic phase was dried over anhydrous Na<sub>2</sub>SO<sub>4</sub>, filtered and the organic solvent was evaporated. The crude obtained was purified by flash column chromatography by eluting with petroleum ether/EtOAc (8.6/1.4) to afford 117 mg (37%) of the title compound **47** as yellowish oil. <sup>1</sup>H NMR (400 MHz, CDCl<sub>3</sub>) δ 6.54 (s, 2H), 4.02 (bs, 1H), 3.85 (s, 2H), 3.28 (s, 3H) ppm; <sup>13</sup>C NMR (100 MHz, CDCl<sub>3</sub>) δ 150.0, 135.8, 116.6, 113.9, 111.7, 30.25, 18.94 ppm.

*2-(6-chloropyridazin-3-yl)-2-(2,6-dichloro-4-(methylamino)phenyl)acetonitrile (48):*

In a dry three-neck round-bottom flask, 393 mg of *t*BuOK (3.51 mmol) were suspended in 3 mL of THF under a nitrogen atmosphere. Using a bath of ice, a solution of 250 mg of **47** (1.17 mmol) in 3 mL of THF was added. The resulting mixture was stirred at T = 0 °C for 30 min. Then, 262 mg of 3,6-dichloropyridazine (1.76 mmol) were added and the reaction was stirred at rt for 3h. Following, the pH was adjusted to 7 by the addition of a solution of HCl (2N), the organic phase was evaporated and the remaining aqueous layer was extracted by EtOAc (3 x 30 mL). The organic phase was dried over anhydrous Na<sub>2</sub>SO<sub>4</sub>, filtered, and the obtained crude material was purified by silica gel flash column chromatography, by eluting with petroleum ether/EtOAc (7.5/2.5) to afford 204 mg (54%) of the title compound **48** as orange solid. <sup>1</sup>H NMR (400 MHz, CDCl<sub>3</sub>) δ 7.62 (d, *J* = 8.9 Hz, 1H), 7.53 (d, *J* = 8.9 Hz, 1H), 6.61 (s, 2H), 6.32 (s, 1H), 2.85 (s, 3H) ppm; <sup>13</sup>C NMR (100 MHz, CDCl<sub>3</sub>) δ 156.2, 150.9, 137.8, 136.4, 128.8, 127.4, 116.2, 116.1, 112.4, 38.1, 30.1 ppm.

*2-(2,6-dichloro-4-(methylamino)phenyl)-2-(6-((2,4-difluorophenyl)thio)pyridazin-3-yl)acetonitrile (49):*

In a dry three-neck round-bottom flask, 26 mg of NaH 60 % dispersion in mineral oil (1.1 mmol) were solubilized in 1 mL of THF under an inert atmosphere. Using a bath of ice (T = 0 °C) 138 mg of 2,4-difluorobenzenethiol (105 μL, 0.95 mmol) were added dropwise to the reaction and the resulting mixture was stirred for 30 min at 0 °C. Subsequently, the reaction was warmed to 60 °C and a previously prepared solution of 204 mg of **48** (0.63 mmol) solubilized in 2.5 mL of THF was added dropwise. The reaction was stirred at 60 °C for 3h. When the complete consumption of the starting compound **48** was observed the reaction was cooled to rt and neutralized by the addition of some drops of HCl (2N). The organic solvent was evaporated and the obtained crude material was purified by silica gel flash column chromatography, by eluting with petroleum ether/EtOAc (6.7/3.3) to afford 233 mg (85%) of the title compound **49** as orange oil. <sup>1</sup>H NMR (400 MHz, CDCl<sub>3</sub>) δ 7.67 – 7.55 (m, 1H), 7.41 (d, *J* = 9.0 Hz, 1H), 7.22 (d, *J* = 9.0 Hz, 1H), 7.03 – 6.87 (m, 2H), 6.62 (s, 2H), 6.23 (s, 1H), 2.76 (s, 3H) ppm; <sup>13</sup>C NMR (100 MHz, CDCl<sub>3</sub>) δ 162.4, 154.4, 148.5, 138.8, 138.6, 136.0, 125.3, 117.9, 116.2, 115.1, 113.0, 113.0, 112.8, 112.8, 105.7, 105.5, 105.2, 38.1, 29.5 ppm.

*2-(2,6-dichloro-4-(methylamino)phenyl)-2-(6-((2,4-difluorophenyl)thio)pyridazin-3-yl)acetamide (50):*

233 mg of **49** (0.54 mmol) were solubilized in 7 mL of H<sub>2</sub>SO<sub>4</sub>. The reaction was stirred for 30 min at 100 °C and the complete consumption of compound **49** was observed. Following, the reaction mixture was neutralized by the addition of an aqueous solution of NaOH (10%), and a yellowish precipitate formed. The title compound was filtered under reduced pressure and dried. 237 mg (97%) of compound **50** were obtained as a yellowish solid, used without further purification. <sup>1</sup>H NMR (400 MHz, CDCl<sub>3</sub>) δ 8.37 (s, 1H), 7.69 – 7.58 (m, 1H), 7.11 (s, 2H), 7.03 – 6.91 (m, 2H), 6.70 (s, 1H), 6.52 (d, *J* = 9.9 Hz, 1H), 6.30 (d, *J* = 9.8 Hz, 1H), 5.84 (s, 1H), 5.75 (s, 1H), 2.81 (s, 3H) ppm.

## 6.4 Synthesis of BMX covalent inhibitors

*General procedure A (the boronic ester formation):* in a flame-dried Schlenk flask the corresponding aniline (1 eq), KOAc (3 eq.), and bis(pinacolato)diboron (1 eq.) were suspended in dry dioxane. After three degas cycles vacuum/argon Pd(OAc)<sub>2</sub> (5%) and X Phos (10%) were added to the reaction mixture. The degassing procedure was repeated three times and then the reaction was stirred overnight at 90 °C. After cooling to room temperature, the mixture was diluted with EtOAc and filtered over a layer of celite. The filtrate was washed two times with water before drying over Na<sub>2</sub>SO<sub>4</sub> and evaporation. The residue was purified via automated flash column chromatography on silica gel using an appropriate solvent system.

*General procedure B (boronic ester acylation):* To a solution of the corresponding boronic ester (1 eq.) and Et<sub>3</sub>N (1.1 eq.) in DCM acryloyl chloride (1.1 eq.) was added dropwise with a bath of ice. The reaction mixture was stirred for 1 h. at room temperature. The solvent was evaporated, and the residue was purified via automated flash column chromatography on silica gel and an appropriate solvent system.

*General procedure C (7-azaindole acylation by commercial acyl chloride):* The corresponding acyl chloride (2 eq) was added dropwise to an ice-cooled solution of **11** and Et<sub>3</sub>N (3 eq.) in DCM. Then the reaction was warmed to room temperature and was stirred for 1 h. The organic solvent was evaporated, and the residue was purified via automated flash column chromatography on silica gel an appropriate solvent system.

*General procedure D (7-azaindole acylation activating a carboxylic acid):* The thionyl chloride (3 eq.) was added dropwise to a 0.37 M ice-cooled solution of the corresponding

carboxylic acid in DCM, in presence of a catalytic amount of DMF (1 or 2 drops). The mixture was warmed to 40 °C and stirred for 3 h. Then the organic layer was evaporated and a 0.24 M solution in DCM of the acyl chloride formed was added dropwise to a solution of **11** and Et<sub>3</sub>N (3.6 eq.) in DCM. The reaction was stirred at room temperature for 1 h. Then, the solvent was evaporated, and the residue was purified via automated flash column chromatography on silica gel and an appropriate solvent system.

*General procedure E (Suzuki coupling):* The corresponding boronic acid (1.5 eq.) and aryl bromide (1 eq.) were solubilized in dioxane in a dry flask to obtain a 0.14 M solution. The mixture was degassed for 7 min. Then the tBu<sub>3</sub>PPd G3 (5%) was added, and the mixture was degassed for another 5 min. Finally, a solution previously degassed of 0.5 M of K<sub>2</sub>CO<sub>3</sub> was added and the mixture was degassed for another 5 min. All the degas cycles were done by sonication. The reaction was stirred overnight at room temperature or at 80 °C under an argon atmosphere. The reaction mixture was evaporated, and the residue was purified by automated flash column chromatography on silica gel and an appropriate solvent system.

*General procedure F (SEM cleavage):* TFA was added to a 0.037 M solution of the SEM-protected compound dissolved in DCM, and the solution was stirred until the TLC showed the complete consumption of the starting compound (5h-overnight). Then, the organic layer was evaporated, and the residue was suspended in EtOH, basified by NH<sub>3</sub> (25%), and stirred at room temperature until HPLC indicated complete consumption of the hydroxymethyl intermediate (usually overnight). The volatile layer was evaporated under reduced pressure and the residue was purified by automated flash column chromatography on silica gel and an appropriate solvent system.

*N-(3-(5-isobutyramido-1H-pyrrolo[2,3-b]pyridin-3-yl)phenyl)acrylamide (55):*

The preparation was carried out following *General Procedure F* starting from 36 mg of **104** (0.075 mmol). Flash purification by eluting with DCM/MeOH (gradient: 2-5% of MeOH) afforded 10 mg (36%) of the title compound as a white solid. <sup>1</sup>H NMR (400 MHz, DMSO-*d*<sub>6</sub>) δ 11.83 (s, 1H), 10.22 (s, 1H), 9.91 (s, 1H), 8.52 (d, *J* = 2.1 Hz, 1H), 8.44 (d, *J* = 2.2 Hz, 1H), 7.93 (s, 1H), 7.75 (d, *J* = 2.6 Hz, 1H), 7.62 (d, *J* = 7.9 Hz, 1H), 7.43 – 7.34 (m, 2H), 6.49 (dd, *J* = 17.0, 10.1 Hz, 1H), 6.29 (dd, *J* = 17.0, 2.0 Hz, 1H), 5.78 (dd, *J* = 10.1, 2.0 Hz, 1H), 2.71 – 2.60 (m, 1H), 1.14 (d, *J* = 6.8 Hz, 6H) ppm; <sup>13</sup>C NMR (100



MHz, DMSO-*d*<sub>6</sub>) δ 175.2, 163.2, 145.7, 139.5, 136.7, 135.5, 131.9, 129.6, 129.2, 126.8, 124.3, 121.7, 118.3, 117.3, 116.9, 116.7, 114.2, 34.7, 19.5 ppm. TLC-MS (ESI) *m/z*: 349.4 [M + H]<sup>+</sup>; 371.3 [M + Na]<sup>+</sup>; 347.2 [M - H]<sup>-</sup>. HRMS ESI-TOF [M + H]<sup>+</sup> *m/z* calcd. for C<sub>20</sub>H<sub>20</sub>N<sub>4</sub>O<sub>2</sub>: 349.1665, found: 349.1662. HPLC *t*<sub>ret</sub> = 6.02 min. (Method C)

*N*-(3-(5-propionamido-1*H*-pyrrolo[2,3-*b*]pyridin-3-yl)phenyl)acrylamide (**56**):

The preparation was carried out following *General Procedure F* starting from 42 mg of **105** (0.09 mmol). Flash purification by eluting with DCM/MeOH (gradient: 2-5% of MeOH) afforded 19 mg (63%) of the title compound as a white solid. <sup>1</sup>H NMR (400 MHz, DMSO-*d*<sub>6</sub>) δ 11.83 (bs, 1H), 10.22 (s, 1H), 9.95 (s, 1H), 8.49 (d, *J* = 2.0 Hz, 1H), 8.41 (d, *J* = 2.1 Hz, 1H), 7.94 (s, 1H), 7.75 (d, *J* = 2.5 Hz, 1H), 7.61 (d, *J* = 7.8 Hz, 1H), 7.49 – 7.31 (m, 2H), 6.48 (dd, *J* = 17.0, 10.1 Hz, 1H), 6.28 (dd, *J* = 17.0, 1.9 Hz, 1H), 5.78 (dd, *J* = 10.1, 1.9 Hz, 1H), 2.36 (q, *J* = 7.5 Hz, 2H), 1.12 (t, *J* = 7.5 Hz, 3H) ppm; <sup>13</sup>C NMR (101 MHz, DMSO-*d*<sub>6</sub>) δ 172.0, 163.2, 145.8, 139.5, 136.7, 135.6, 131.9, 129.6, 129.3, 126.9, 124.4, 121.7, 118.3, 117.3, 116.9, 116.7, 114.2, 29.3, 9.7 ppm. TLC-MS (ESI) *m/z*: 357.3 [M + Na]<sup>+</sup>; 333.2 [M - H]<sup>-</sup>. HRMS ESI-TOF [M + H]<sup>+</sup> *m/z* calcd. for C<sub>19</sub>H<sub>18</sub>N<sub>4</sub>O<sub>2</sub>: 335.1508, found: 335.1504. HPLC *t*<sub>ret</sub> = 5.74 min. (Method C)

*N*-(3-(3-acrylamidophenyl)-1*H*-pyrrolo[2,3-*b*]pyridin-5-yl)cyclopropanecarboxamide (**57**):

The preparation was carried out following *General Procedure F* starting from 32 mg of **106** (0.067 mmol). Flash purification by eluting with DCM/MeOH (gradient: 3-5% of MeOH) afforded 50 mg (85%) of the title compound as a white solid. <sup>1</sup>H NMR (400 MHz, DMSO-*d*<sub>6</sub>) δ 11.82 (bs, 1H), 10.26 (s, 1H), 10.20 (s, 1H), 8.48 (d, *J* = 2.1 Hz, 1H), 8.41 (d, *J* = 2.2 Hz, 1H), 7.92 (s, 1H), 7.75 (d, *J* = 2.6 Hz, 1H), 7.61 (d, *J* = 7.9 Hz, 1H), 7.43 – 7.30 (m, 2H), 6.47 (dd, *J* = 17.0, 10.1 Hz, 1H), 6.28 (dd, *J* = 17.0, 2.0 Hz, 1H), 5.77 (dd, *J* = 10.1, 2.0 Hz, 1H), 2.09 – 1.58 (m, 1H), 0.96 – 0.57 (m, Hz, 4H) ppm; <sup>13</sup>C NMR (100 MHz, DMSO-*d*<sub>6</sub>) δ 171.8, 163.2, 145.7, 139.5, 136.7, 135.5, 131.9, 129.6, 129.3, 126.9, 124.4, 121.7, 118.3, 117.21, 116.9, 116.7, 114.2, 56.0, 18.5, 14.4, 7.0 ppm. TLC-MS (ESI) *m/z*: 369.2 [M + Na]<sup>+</sup>; 345.0 [M - H]<sup>-</sup>. HRMS ESI-TOF [M + H]<sup>+</sup> *m/z* calcd. for C<sub>20</sub>H<sub>18</sub>N<sub>4</sub>O<sub>2</sub>: 347.1508, found: 347.1506. HPLC *t*<sub>ret</sub> = 9.46 min. (Method D)

*N*-(3-(3-acrylamidophenyl)-1*H*-pyrrolo[2,3-*b*]pyridin-5-yl)cyclobutanecarboxamide (**58**):

The preparation was carried out following *General Procedure F* starting from 75 mg of **107** (0.15 mmol). Flash purification by eluting with DCM/MeOH (gradient: 1-6% of MeOH) afforded 38 mg (70%) of the title compound as a white solid. <sup>1</sup>H NMR (400 MHz, DMSO-*d*<sub>6</sub>) δ 11.84 (s, 1H), 10.23 (s, 1H), 9.83 (s, 1H), 8.51 (d, *J* = 1.8 Hz, 1H), 8.43 (d, *J* = 2.0 Hz, 1H), 7.93 (s, 1H), 7.76 (d, *J* = 2.4 Hz, 1H), 7.63 (d, *J* = 7.7 Hz, 1H), 7.43 – 7.35 (m, 2H), 6.49 (dd, *J* = 17.0, 10.1 Hz, 1H), 6.29 (dd, *J* = 16.9, 1.7 Hz, 1H), 5.79 (dd, *J* = 10.1, 1.8 Hz, 1H), 3.29 – 3.23 (m, 1H), 2.29 – 1.81 (m, 6H) ppm; <sup>13</sup>C NMR (100 MHz, DMSO-*d*<sub>6</sub>) δ 172.9, 163.2, 145.7, 139.4, 136.78, 135.5, 131.9, 129.5, 129.2, 126.7, 124.3, 121.6, 118.3, 117.2, 116.9, 116.6, 114.2, 24.6, 17.7 ppm. TLC-MS (ESI) *m/z*: 383.1 [M + Na]<sup>+</sup>; 415.1 [M + Na + MeOH]<sup>+</sup>; 359.1 [M - H]<sup>-</sup>. HRMS ESI-TOF [M + H]<sup>+</sup> *m/z* calcd. for C<sub>21</sub>H<sub>20</sub>N<sub>4</sub>O<sub>2</sub>: 361.1665, found: 361.1664. HPLC *t*<sub>ret</sub> = 6.40 min. (Method C)

*N*-(3-(3-acrylamidophenyl)-1*H*-pyrrolo[2,3-*b*]pyridin-5-yl)cyclohexanecarboxamide (**59**):

The preparation was carried out following *General Procedure F* starting from 69 mg of **108** (0.13 mmol). Flash purification by eluting with DCM/MeOH (gradient: 2-3% of MeOH) afforded 32 mg (62%) of the title compound as a white solid. <sup>1</sup>H NMR (400 MHz, DMSO-*d*<sub>6</sub>) 11.81 (bs 1H), 10.22 (s, 1H), 9.88 (s, 1H), 8.51 (d, *J* = 2.1 Hz, 1H), 8.42 (d, *J* = 2.2 Hz, 1H), 7.92 (s, 1H), 7.74 (d, *J* = 2.5 Hz, 1H), 7.61 (d, *J* = 8.0 Hz, 1H), 7.40 (t, *J* = 7.8 Hz, 1H), 7.34 (d, *J* = 7.7 Hz, 1H), 6.48 (dd, *J* = 17.0, 10.1 Hz, 1H), 6.28 (dd, *J* = 17.0, 1.9 Hz, 1H), 5.77 (dd, *J* = 10.1, 1.9 Hz, 1H), 2.42 – 2.23 (m 1H), 1.89 – 1.60 (m, 5H), 1.54 – 1.12 (m, 5H) ppm; <sup>13</sup>C NMR (100 MHz, DMSO-*d*<sub>6</sub>) δ 174.3, 163.2, 145.7, 139.5, 136.7, 135.6, 131.9, 129.7, 129.3, 126.9, 124.3, 121.7, 118.1, 117.3, 116.9, 116.7, 114.2, 44.7, 29.2, 25.4, 25.3 ppm. TLC-MS (ESI) *m/z*: 411.3 [M + Na]<sup>+</sup>; 387.3 [M - H]<sup>-</sup>. HRMS ESI-TOF [M + H]<sup>+</sup> *m/z* calcd. for C<sub>23</sub>H<sub>24</sub>N<sub>4</sub>O<sub>2</sub>: 389,1978, found:389.1976. HPLC *t*<sub>ret</sub> = 10.97 min. (Method D)

*N*-(3-(3-acrylamidophenyl)-1*H*-pyrrolo[2,3-*b*]pyridin-5-yl)furan-3-carboxamide (**60**):

The preparation was carried out following *General Procedure F* starting from 47 mg of **109** (0.093 mmol). Flash purification by eluting with DCM/MeOH (gradient: 1-7% of MeOH) afforded 17 mg (52%) of the title compound as a white solid. <sup>1</sup>H NMR (400 MHz, DMSO-*d*<sub>6</sub>) δ 11.89 (s, 1H), 10.22 (s, 1H), 10.07 (s, 1H), 8.52 (d, *J* = 4.9 Hz, 2H), 8.38 (s, 1H), 7.95 (s, 1H), 7.81 – 7.79 (m, 2H), 7.62 (d, *J* = 6.9 Hz, 1H), 7.39 (d, *J* = 6.9 Hz, 2H),

7.03 (s, 1H), 6.47 (dd,  $J = 17.0, 10.1$  Hz, 1H), 6.27 (dd,  $J = 17.0, 1.9$  Hz, 1H), 5.77 (dd,  $J = 10.1, 1.9$  Hz, 1H) ppm;  $^{13}\text{C}$  NMR (100 MHz, DMSO- $d_6$ )  $\delta$  163.2, 160.6, 146.1, 145.7, 144.2, 139.5, 137.9, 135.4, 131.9, 129.2, 128.70, 126.8, 124.5, 122.9, 121.6, 120.0, 117.2, 117.0, 116.7, 114.3, 109.1 ppm. TLC-MS (ESI)  $m/z$ : 395.2  $[\text{M} + \text{Na}]^+$ ; 371.1  $[\text{M} - 1]^-$ . HRMS ESI-TOF  $[\text{M} + \text{H}]^+$   $m/z$  calcd. for  $\text{C}_{21}\text{H}_{16}\text{N}_4\text{O}_3$ : 373.1301, found: 373.1298. HPLC  $t_{\text{ret}} = 6.82$  min. (Method C)

*N*-(3-(3-acrylamidophenyl)-1*H*-pyrrolo[2,3-*b*]pyridin-5-yl)thiophene-3-carboxamide (61):

The preparation was carried out following *General Procedure F* starting from 40 mg of **110** (0.077 mmol). Flash purification by eluting with DCM/MeOH (gradient: 1-7% of MeOH) afforded 29 mg (94%) of the title compound as a white solid.  $^1\text{H}$  NMR (400 MHz, DMSO- $d_6$ )  $\delta$  11.90 (s, 1H), 10.20 (d,  $J = 9.8$  Hz, 2H), 8.56 (d,  $J = 5.6$  Hz, 2H), 8.37 (s, 1H), 7.96 (s, 1H), 7.80 (d,  $J = 2.4$  Hz, 1H), 7.67 (d,  $J = 1.9$  Hz, 2H), 7.63 (d,  $J = 6.7$  Hz, 1H), 7.40 (d,  $J = 6.6$  Hz, 2H), 6.47 (dd,  $J = 16.9, 10.1$  Hz, 1H), 6.27 (dd,  $J = 17.0, 1.8$  Hz, 1H), 5.77 (dd,  $J = 11.0, 0.8$  Hz, 1H) ppm;  $^{13}\text{C}$  NMR (100 MHz, DMSO- $d_6$ )  $\delta$  163.2, 161.0, 146.1, 139.5, 138.01, 137.6, 135.43, 131.9, 129.5, 129.2, 128.9, 127.0, 126.9, 126.8, 124.4, 121.6, 120.0, 117.2, 116.9, 116.7, 114.2 ppm. TLC-MS (ESI)  $m/z$  411.2  $[\text{M} + \text{Na}]^+$ ; 387.2  $[\text{M} - 1]^-$ . HRMS ESI-TOF  $[\text{M} + \text{H}]^+$   $m/z$  calcd. for  $\text{C}_{21}\text{H}_{16}\text{N}_4\text{O}_2\text{S}$ : 389.1072, found: 389.1068. HPLC  $t_{\text{ret}} = 7.52$  min. (Method C)

*N*-(3-(3-acrylamidophenyl)-1*H*-pyrrolo[2,3-*b*]pyridin-5-yl)-4-methylthiophene-2-carboxamide (62):

The preparation was carried out following *General Procedure F* starting from 100 mg of **111** (0.21 mmol). Flash purification by eluting with DCM/MeOH (gradient: 2-6% of MeOH) afforded 75 mg (99%) of the title compound as a yellowish solid.  $^1\text{H}$  NMR (400 MHz, DMSO- $d_6$ )  $\delta$  11.91 (s, 1H), 10.30 (s, 1H), 10.23 (s, 1H), 8.55 (s, 2H), 7.96 (s, 1H), 7.87 (s, 1H), 7.80 (s, 1H), 7.63 (d,  $J = 6.8$  Hz, 1H), 7.45 – 7.39 (m, 4H), 6.48 (dd,  $J = 16.9, 10.1$  Hz, 1H), 6.28 (d,  $J = 16.9$  Hz, 1H), 5.77 (d,  $J = 12.0$  Hz, 2H), 2.29 (s, 3H) ppm;  $^{13}\text{C}$  NMR (100 MHz, DMSO- $d_6$ )  $\delta$  163.2, 160.1, 146.1, 139.5, 139.3, 137.9, 137.8, 135.4, 131.9, 130.9, 129.2, 128.7, 126.9, 126.7, 124.5, 121.6, 119.9, 117.2, 116.9, 116.7, 114.3, 15.4 ppm. TLC-MS (ESI)  $m/z$ : 425.3  $[\text{M} + \text{Na}]^+$ ; 401.2  $[\text{M} - \text{H}]^-$ . HRMS ESI-TOF  $[\text{M} + \text{H}]^+$   $m/z$  calcd. for  $\text{C}_{22}\text{H}_{18}\text{N}_4\text{O}_2\text{S}$ : 403.1229, found: 403.1228. HPLC  $t_{\text{ret}} = 10.61$  min. (Method D)

*N*-(3-(3-acrylamidophenyl)-1*H*-pyrrolo[2,3-*b*]pyridin-5-yl)-5-chlorothiophene-2-carboxamide (**63**):

The preparation was carried out following *General Procedure F* starting from 88 mg of **112** (0.15 mmol). Flash purification by eluting with DCM/MeOH (gradient: 1-7% of MeOH) afforded 54 mg (81%) of the title compound as a yellowish solid. <sup>1</sup>H NMR (400 MHz, DMSO-*d*<sub>6</sub>) δ 11.95 (s, 1H), 10.47 (s, 1H), 10.23 (s, 1H), 8.51 (s, 2H), 8.02 – 7.88 (m, 2H), 7.82 (d, *J* = 2.3 Hz, 1H), 7.62 (d, *J* = 7.1 Hz, 1H), 7.48 – 7.34 (m, 2H), 7.29 (d, *J* = 4.0 Hz, 1H), 6.47 (dd, *J* = 16.9, 10.1 Hz, 1H), 6.27 (dd, *J* = 17.0, 1.4 Hz, 1H), 5.77 (dd, *J* = 10.2, 1.4 Hz, 1H) ppm; <sup>13</sup>C NMR (100 MHz, DMSO-*d*<sub>6</sub>) δ 163.3, 159.2, 146.31, 139.6, 139.0, 138.0, 135.4, 133.9, 132.0, 129.4, 129.1, 128.4, 128.3, 127.1, 124.8, 121.7, 120.3, 117.3, 117.0, 116.8, 114.4 ppm. TLC-MS (ESI) *m/z*: 445.0 [M + Na]<sup>+</sup>; 421.0 [M - H]<sup>-</sup>. HRMS ESI-TOF [M + H]<sup>+</sup> *m/z* calcd. for C<sub>21</sub>H<sub>15</sub>ClN<sub>4</sub>O<sub>2</sub>S: 423.0682, found:423.0684. HPLC *t*<sub>ret</sub> = 11.23 min. (Method D)

*N*-(3-(3-acrylamidophenyl)-1*H*-pyrrolo[2,3-*b*]pyridin-5-yl)-4-chlorobenzamide (**64**):

The preparation was carried out following *General Procedure F* starting from 90 mg of **113** (0.16 mmol). Flash purification by eluting with DCM/MeOH (gradient: 1-6% of MeOH) afforded 28 mg (42%) of the title compound as a white solid. <sup>1</sup>H NMR (400 MHz, DMSO-*d*<sub>6</sub>) δ 11.92 (s, 1H), 10.45 (s, 1H), 10.21 (s, 1H), 8.58 (dd, *J* = 7.5, 2.0 Hz, 2H), 8.04 (d, *J* = 8.5 Hz, 2H), 7.96 (s, 1H), 7.80 (d, *J* = 2.5 Hz, 1H), 7.69 – 7.55 (m, 3H), 7.44 – 7.34 (m, 2H), 6.46 (dd, *J* = 17.0, 10.1 Hz, 1H), 6.27 (dd, *J* = 17.0, 1.9 Hz, 1H), 5.76 (dd, *J* = 10.1, 1.9 Hz, 1H) ppm; <sup>13</sup>C NMR (100 MHz, DMSO-*d*<sub>6</sub>) δ 164.5, 163.2, 146.2, 139.6, 138.1, 136.44, 135.5, 133.3, 131.9, 129.6, 129.3, 129.0, 128.5, 127.0, 124.6, 121.6, 120.2, 117.3, 117.0, 116.7, 114.3 ppm. TLC-MS (ESI) *m/z*: 439.3 [M + Na]<sup>+</sup>; 415.0 [M - H]<sup>-</sup>. HRMS ESI-TOF [M + H]<sup>+</sup> *m/z* calcd. for C<sub>23</sub>H<sub>17</sub>ClN<sub>4</sub>O<sub>2</sub>: 417.1118, found: 417.1115. HPLC *t*<sub>ret</sub> = 10.99 min. (Method D)

*N*-(3-(3-acrylamidophenyl)-1*H*-pyrrolo[2,3-*b*]pyridin-5-yl)-3-chlorobenzamide (**65**):

The preparation was carried out following *General Procedure F* starting from 62 mg of **114** (0.11 mmol). Flash purification by eluting with DCM/MeOH (gradient: 1-7% of MeOH) afforded 45 mg (98%) of the title compound as a white solid. <sup>1</sup>H NMR (400 MHz, DMSO-*d*<sub>6</sub>) δ 11.94 (s, 1H), 10.50 (s, 1H), 10.24 (s, 1H), 8.60 (d, *J* = 2.7 Hz, 2H), 8.08 (s, 1H), 7.98 (d, *J* = 6.9 Hz, 2H), 7.82 (d, *J* = 2.5 Hz, 1H), 7.69 (d, *J* = 8.0 Hz, 1H), 7.66

– 7.57 (m 2H), 7.43 – 7.36 (m 2H), 6.48 (dd,  $J = 16.9, 10.1$  Hz, 1H), 6.28 (dd,  $J = 17.0, 1.8$  Hz, 1H), 5.82 – 5.70 (m, 1H) ppm;  $^{13}\text{C}$  NMR (100 MHz, DMSO- $d_6$ )  $\delta$  164.2, 163.3, 146.3, 139.6, 138.0, 136.7, 135.5, 133.3, 131.9, 131.5, 129.4, 128.9, 127.4, 127.0, 126.5, 124.7, 121.7, 120.2, 117.3, 117.0, 116.7, 114.4 ppm. TLC-MS (ESI)  $m/z$ : 439.0  $[\text{M} + \text{Na}]^+$ ; 415.1  $[\text{M} - 1]^-$ . HRMS ESI-TOF  $[\text{M} + \text{H}]^+$   $m/z$  calcd. for  $\text{C}_{23}\text{H}_{17}\text{ClN}_4\text{O}_2$ : 417.1118, found: 417.1114. HPLC  $t_{\text{ret}} = 11.13$  min. (Method D)

*N*-(3-(3-acrylamidophenyl)-1*H*-pyrrolo[2,3-*b*]pyridin-5-yl)-4-fluorobenzamide (**66**):

The preparation was carried out following *General Procedure F* starting from 85 mg of **115** (0.16 mmol). Flash purification by eluting with DCM/MeOH (gradient: 1-7% of MeOH) afforded 37 mg (56%) of the title compound as a yellowish solid.  $^1\text{H}$  NMR (400 MHz, DMSO- $d_6$ )  $\delta$  11.92 (s, 1H), 10.40 (s, 1H), 10.23 (s, 1H), 8.58 (d,  $J = 6.7$  Hz, 2H), 8.09 (dd,  $J = 8.6, 5.6$  Hz, 2H), 7.96 (s, 1H), 7.80 (d,  $J = 1.7$  Hz, 1H), 7.62 (d,  $J = 6.6$  Hz, 1H), 7.43 – 7.37 (m, 4H), 6.46 (dd,  $J = 17.0, 10.1$  Hz, 1H), 6.27 (dd,  $J = 17.0, 1.7$  Hz, 1H), 5.77 (dd,  $J = 10.1, 1.7$  Hz, 1H) ppm;  $^{13}\text{C}$  NMR (100 MHz, DMSO- $d_6$ )  $\delta$  172.8, 165.4, 164.6, 163.3, 162.9, 146.2, 139.6, 138.1, 135.5, 131.9, 131.1, 131.1, 130.4, 130.3, 129.4, 129.1, 127.0, 124.6, 121.7, 120.2, 117.3, 117.0, 116.7, 115.5, 115.3, 114.3 ppm. TLC-MS (ESI)  $m/z$ : 423.0  $[\text{M} + \text{Na}]^+$ ; 399.1  $[\text{M} - \text{H}]^-$ . HRMS ESI-TOF  $[\text{M} + \text{H}]^+$   $m/z$  calcd. for  $\text{C}_{23}\text{H}_{17}\text{FN}_4\text{O}_2$ : 401.1414, found: 401.1411. HPLC  $t_{\text{ret}} = 10.50$  min. (Method D)

*N*-(3-(3-acrylamidophenyl)-1*H*-pyrrolo[2,3-*b*]pyridin-5-yl)-3-fluorobenzamide (**67**):

The preparation was carried out following *General Procedure F* starting from 90 mg of **116** (0.17 mmol). Flash purification by eluting with DCM/MeOH (gradient: 1-7% of MeOH) afforded 50 mg (74%) of the title compound as a white solid.  $^1\text{H}$  NMR (400 MHz, DMSO- $d_6$ )  $\delta$  11.93 (s, 1H), 10.46 (s, 1H), 10.23 (s, 1H), 8.58 (dd,  $J = 9.0, 2.1$  Hz, 2H), 7.96 (s, 1H), 7.86 (d,  $J = 7.8$  Hz, 1H), 7.84 – 7.78 (m 2H), 7.64 – 7.56 (m 2H), 7.45 (td,  $J = 8.4, 2.1$  Hz, 1H), 7.42 – 7.35 (m 2H), 6.45 (dd,  $J = 17.0, 10.1$  Hz, 1H), 6.26 (dd,  $J = 17.0, 1.9$  Hz, 1H), 5.76 (dd,  $J = 10.1, 1.9$  Hz, 1H) ppm;  $^{13}\text{C}$  NMR (100 MHz, DMSO- $d_6$ )  $\delta$  164.3, 163.4, 163.3, 160.96, 146.3, 139.6, 138.1, 137.1, 137.0, 135.5, 132.0, 130.8, 130.7, 129.4, 128.9, 127.1, 124.7, 123.9, 123.9, 121.8, 120.3, 118.7, 118.5, 117.3, 117.1, 116.8, 114.6, 114.4 ppm. TLC-MS (ESI)  $m/z$ : 423.0  $[\text{M} + \text{Na}]^+$ ; 455.0  $[\text{M} + \text{Na} + \text{MeOH}]^+$ ; 399.1  $[\text{M} - \text{H}]^-$ . HRMS ESI-TOF  $[\text{M} + \text{H}]^+$   $m/z$  calcd. for  $\text{C}_{23}\text{H}_{17}\text{FN}_4\text{O}_2$ : 401.1414, found: 401.1409. HPLC  $t_{\text{ret}} = 10.56$  min. (Method D)

*N*-(3-(5-(2-(4-fluorophenyl)acetamido)-1*H*-pyrrolo[2,3-*b*]pyridin-3-yl)phenyl)acrylamide (**68**):

The preparation was carried out following *General Procedure F* starting from 56 mg of **117** (0.10 mmol). Flash purification by eluting with DCM/MeOH (gradient: 1-7% of MeOH) afforded 30 mg (73%) of the title compound as a white solid. <sup>1</sup>H NMR (400 MHz, DMSO-*d*<sub>6</sub>) δ 11.86 (s, 1H), 10.28 (s, 1H), 10.22 (s, 1H), 8.49 (d, *J* = 2.2 Hz, 1H), 8.41 (d, *J* = 2.2 Hz, 1H), 7.93 (s, 1H), 7.76 (s, 1H), 7.58 (d, *J* = 7.9 Hz, 1H), 7.43 – 7.35 (m, 3H), 7.33 (d, *J* = 7.7 Hz, 1H), 7.15 (t, *J* = 8.9 Hz, 2H), 6.46 (dd, *J* = 17.0, 10.1 Hz, 1H), 6.27 (dd, *J* = 17.0, 1.9 Hz, 1H), 5.77 (dd, *J* = 10.1, 1.9 Hz, 1H), 3.67 (s, 2H) ppm; <sup>13</sup>C NMR (100 MHz, DMSO-*d*<sub>6</sub>) δ 193.0, 192.7, 187.7, 169.1, 163.2, 162.3, 161.7, 159.9, 145.9, 139.5, 136.7, 135.5, 132.1, 132.1, 131.9, 131.1, 131.0, 129.3, 129.2, 126.8, 124.4, 121.6, 118.4, 117.3, 117.0, 116.7, 115.1, 114.9, 114.3, 42.0 ppm. TLC-MS (ESI) *m/z*: 437.1 [M + Na]<sup>+</sup>; 469.0 [M + Na + MeOH]<sup>+</sup>; 413.2 [M - H]<sup>-</sup>. HRMS ESI-TOF [M + H]<sup>+</sup> *m/z* calcd. for C<sub>24</sub>H<sub>19</sub>FN<sub>4</sub>O<sub>2</sub>: 415.1570, found: 415.1565. HPLC *t*<sub>ret</sub> = 10.51 min. (Method D)

*N*-(3-(5-(2-(4-chlorophenyl)acetamido)-1*H*-pyrrolo[2,3-*b*]pyridin-3-yl)phenyl)acrylamide (**69**):

The preparation was carried out following *General Procedure F* starting from 32 mg of **118** (0.057 mmol). Flash purification by eluting with DCM/MeOH (gradient: 2-6% of MeOH) afforded 22 mg (85%) of the title compound as a white solid. <sup>1</sup>H NMR (400 MHz, DMSO-*d*<sub>6</sub>) δ 11.86 (s, 1H), 10.29 (s, 1H), 10.21 (s, 1H), 8.48 (d, *J* = 2.1 Hz, 1H), 8.41 (d, *J* = 2.2 Hz, 1H), 7.93 (s, 1H), 7.75 (d, *J* = 1.9 Hz, 1H), 7.58 (d, *J* = 7.9 Hz, 1H), 7.44 – 7.29 (m, 6H), 6.47 (dd, *J* = 17.0, 10.1 Hz, 1H), 6.27 (dd, *J* = 17.0, 1.9 Hz, 1H), 5.77 (dd, *J* = 10.1, 1.9 Hz, 1H), 3.69 (s, 2H) ppm; <sup>13</sup>C NMR (100 MHz, DMSO-*d*<sub>6</sub>) δ 168.8, 163.2, 145.9, 139.5, 136.6, 135.5, 135.0, 131.9, 131.3, 131.1, 129.3, 128.2, 126.9, 124.5, 121.7, 118.4, 117.3, 116.9, 116.6, 114.3, 42.2 ppm. TLC-MS (ESI) *m/z*: 453.2 [M + Na]<sup>+</sup>; 429.1 [M - H]<sup>-</sup>. HRMS ESI-TOF [M + H]<sup>+</sup> *m/z* calcd. for C<sub>24</sub>H<sub>19</sub>ClN<sub>4</sub>O<sub>2</sub>: 431.1275, found: 431.1271. HPLC *t*<sub>ret</sub> = 11.04 min. (Method D)

*N*-(3-(5-(2-(2,4-difluorophenyl)acetamido)-1*H*-pyrrolo[2,3-*b*]pyridin-3-yl)phenyl)acrylamide (**70**):

The preparation was carried out following *General Procedure F* starting from 67 mg of **119** (0.12 mmol). Flash purification by eluting with DCM/MeOH (gradient: 2-6% of MeOH) afforded 25 mg (48%) of the title compound as a white solid. <sup>1</sup>H NMR (400 MHz,

DMSO-*d*<sub>6</sub>) δ 11.86 (s, 1H), 10.30 (s, 1H), 10.20 (s, 1H), 8.46 (d, *J* = 29.6 Hz, 2H), 7.93 (s, 1H), 7.76 (s, 1H), 7.60 – 7.07 (m, 6H), 6.47 (dd, *J* = 16.8, 10.1 Hz, 1H), 6.27 (d, *J* = 16.8 Hz, 1H), 5.77 (d, *J* = 9.9 Hz, 1H), 3.76 (s, 2H) ppm; <sup>13</sup>C NMR (100 MHz, DMSO-*d*<sub>6</sub>) δ 167.9, 163.2, 145.8, 139.4, 136.6, 135.4, 133.0, 132.9, 131.9, 129.3, 129.2, 126.7, 124.4, 121.6, 119.3, 119.2, 118.3, 117.2, 116.9, 116.6, 114.2, 111.3, 111.2, 111.0, 110.9, 103.7, 103.4, 103.2, 54.8, 48.5, 35.3 ppm. TLC-MS (ESI) *m/z*: 455.4 [M + Na]<sup>+</sup>; 431.3 [M - 1]<sup>-</sup>. HRMS ESI-TOF [M + H]<sup>+</sup> *m/z* calcd. for C<sub>24</sub>H<sub>18</sub>F<sub>2</sub>N<sub>4</sub>O<sub>2</sub>: 433.1476, found:433.1474. HPLC *t*<sub>ret</sub> = 6.40 min. (Method C)

*N*-(3-(3-acrylamidophenyl)-1*H*-pyrrolo[2,3-*b*]pyridin-5-yl)-3-chloro-5-fluorobenzamide (71):

The preparation was carried out following *General Procedure F* starting from 74 mg of **120** (0.13 mmol). Flash purification by eluting with DCM/MeOH (gradient: 1-10% of MeOH) afforded 41 mg (72%) of the title compound as a white solid. <sup>1</sup>H NMR (400 MHz, DMSO-*d*<sub>6</sub>) δ 11.94 (s, 1H), 10.54 (s, 1H), 10.23 (s, 1H), 8.58 (s, 2H), 7.96 (d, *J* = 6.4 Hz, 2H), 7.82 (d, *J* = 5.7 Hz, 2H), 7.80 – 7.68 (m, 1H), 7.60 (d, *J* = 7.1 Hz, 1H), 7.45 – 7.34 (m, 2H), 6.46 (dd, *J* = 17.0, 10.1 Hz, 1H), 6.27 (dd, *J* = 17.0, 1.9 Hz, 1H), 5.76 (dd, *J* = 10.1, 1.9 Hz, 1H) ppm; <sup>13</sup>C NMR (100 MHz, DMSO-*d*<sub>6</sub>) δ 163.3, 162.9, 162.9, 160.8, 146.3, 139.6, 138.2, 138.1, 138.0, 135.5, 134.4, 134.3, 131.9, 129.4, 128.7, 127.0, 124.7, 124.0, 121.8, 120.2, 119.2, 119.0, 117.3, 117.1, 116.7, 114.4, 113.9, 113.7 ppm. TLC-MS (ESI) *m/z*: 457.0 [M + Na]<sup>+</sup>; 489.2 [M + Na + MeOH]<sup>+</sup>; 433.0 [M - H]<sup>-</sup>. HRMS ESI-TOF [M + H]<sup>+</sup> *m/z* calcd. for C<sub>23</sub>H<sub>16</sub>ClFN<sub>4</sub>O<sub>2</sub>: 435.1024, found: 435.1017. HPLC *t*<sub>ret</sub> = 11.45 min. (Method D)

*N*-(3-(5-(2-(5-chloro-2,4-difluorophenyl)acetamido)-1*H*-pyrrolo[2,3-*b*]pyridin-3-yl)phenyl)acrylamide (72):

The preparation was carried out following *General Procedure F* starting from 45 mg of **121** (0.075 mmol). Flash purification by eluting with DCM/MeOH (gradient: 2-5% of MeOH) afforded 19 mg (56%) of the title compound as a white solid. <sup>1</sup>H NMR (400 MHz, DMSO-*d*<sub>6</sub>) δ 11.86 (s, 1H), 10.28 (s, 1H), 10.22 (s, 1H), 8.49 (d, *J* = 2.2 Hz, 1H), 8.41 (d, *J* = 2.2 Hz, 1H), 7.93 (s, 1H), 7.76 (s, 1H), 7.58 (d, *J* = 7.9 Hz, 1H), 7.43 – 7.35 (m, 3H), 7.33 (d, *J* = 7.7 Hz, 1H), 7.15 (t, *J* = 8.9 Hz, 2H), 6.46 (dd, *J* = 17.0, 10.1 Hz, 1H), 6.27 (dd, *J* = 17.0, 1.9 Hz, 1H), 5.77 (dd, *J* = 10.1, 1.9 Hz, 1H), 3.67 (s, 2H) ppm; <sup>13</sup>C NMR (100 MHz, DMSO-*d*<sub>6</sub>) δ 193.0, 192.7, 187.7, 169.1, 163.2, 162.3, 161.7, 159.9, 145.9,

139.5, 136.7, 135.5, 132.1, 132.1, 131.9, 131.1, 131.0, 129.3, 129.2, 126.8, 124.4, 121.6, 118.4, 117.3, 117.0, 116.7, 115.1, 114.9, 114.3, 42.0 ppm. TLC-MS (ESI) m/z: 489.2 [M + Na]<sup>+</sup>; 521.3 [M + Na + MeOH]<sup>+</sup>; 465.3 [M - H]<sup>-</sup>. HRMS ESI-TOF [M + H]<sup>+</sup> m/z calcd. for C<sub>24</sub>H<sub>17</sub>ClF<sub>2</sub>N<sub>4</sub>O<sub>2</sub>: 467.1086, found: 467.1082. HPLC t<sub>ret</sub> = 11.16 min. (Method D)

*(E)-N-(3-(3-(but-2-enamido)phenyl)-1H-pyrrolo[2,3-b]pyridin-5-yl)cyclopentanecarboxamide (73):*

The preparation was carried out following *General Procedure F* starting from 111 mg of **132** (0.21 mmol). Flash purification by eluting with DCM/MeOH (gradient: 2-5% of MeOH) afforded 72 mg (89%) of the title compound as a white solid. <sup>1</sup>H NMR (400 MHz, DMSO-*d*<sub>6</sub>) δ 11.81 (s, 1H), 10.01 (s, 1H), 9.94 (s, 1H), 8.51 (d, *J* = 2.2 Hz, 1H), 8.43 (d, *J* = 2.2 Hz, 1H), 7.91 (s, 1H), 7.73 (d, *J* = 2.6 Hz, 1H), 7.60 (d, *J* = 8.1 Hz, 1H), 7.40 – 7.31 (m, 2H), 6.82 (dd, *J* = 15.2, 6.9 Hz, 1H), 6.17 (dd, *J* = 15.2, 1.7 Hz, 1H), 2.86 – 2.78 (m, *J* = 7.9 Hz, 1H), 1.90 – 1.56 (m, 11H) ppm; <sup>13</sup>C NMR (100 MHz, DMSO-*d*<sub>6</sub>) δ 174.4, 163.5, 145.7, 139.8, 136.7, 135.5, 129.6, 129.2, 126.1, 124.2, 121.4, 118.3, 117.2, 116.8, 116.7, 114.3, 45.1, 30.1, 25.7, 17.5 ppm. TLC-MS (ESI) m/z: 411.3 [M + Na]<sup>+</sup>; 387.2 [M - H]<sup>-</sup>. HRMS ESI-TOF [M + H]<sup>+</sup> m/z calcd. for C<sub>23</sub>H<sub>24</sub>N<sub>4</sub>O<sub>2</sub>: 389.1978, found: 389.1973. HPLC t<sub>ret</sub> = 7.66 min. (Method C)

*N-(3-(3-(but-2-ynamido)phenyl)-1H-pyrrolo[2,3-b]pyridin-5-yl)cyclopentane carboxamide (74):*

The preparation was carried out following *General Procedure F* starting from 44 mg of **133** (0.085 mmol). Flash purification by eluting with DCM/MeOH (gradient: 2-5% of MeOH) afforded 20 mg (65%) of the title compound as a white solid. <sup>1</sup>H NMR (400 MHz, DMSO-*d*<sub>6</sub>) δ 11.82 (s, 1H), 10.66 (s, 1H), 9.93 (s, 1H), 8.50 (d, *J* = 2.0 Hz, 1H), 8.40 (d, *J* = 2.2 Hz, 1H), 7.85 (s, 1H), 7.73 (d, *J* = 2.6 Hz, 1H), 7.53 (d, *J* = 7.4 Hz, 1H), 7.54 – 7.33 (m, 2H), 2.83 – 2.79 (m, 1H), 2.06 (s, 3H), 1.90 – 1.55 (m, 8H) ppm; <sup>13</sup>C NMR (100 MHz, DMSO-*d*<sub>6</sub>) δ 174.4, 150.6, 145.7, 139.1, 136.8, 135.5, 129.7, 129.2, 124.4, 121.9, 118.3, 117.4, 117.0, 116.6, 114.1, 84.1, 76.0, 45.1, 30.1, 25.7, 3.2 ppm. TLC-MS (ESI) m/z: 409.3 [M + Na]<sup>+</sup>; 385.1 [M - H]<sup>-</sup>. HRMS ESI-TOF [M + H]<sup>+</sup> m/z calcd. for C<sub>23</sub>H<sub>22</sub>N<sub>4</sub>O<sub>2</sub>: 387.1821, found: 387.1817. HPLC t<sub>ret</sub> = 7.46 min. (Method C)

*N-(3-(5-acrylamido-2-methylphenyl)-1H-pyrrolo[2,3-b]pyridin-5-yl)cyclopentane carboxamide (75):*



The preparation was carried out following *General Procedure F* starting from 38 mg of **134** (0.073 mmol). Flash purification by eluting with DCM/MeOH (gradient: 0.2-1.5% of MeOH) afforded 22 mg (81%) of the title compound as a yellowish solid. <sup>1</sup>H NMR (400 MHz, DMSO-*d*<sub>6</sub>) δ 11.75 (s, 1H), 10.11 (s, 1H), 9.89 (s, 1H), 8.38 (d, *J* = 2.2 Hz, 1H), 8.12 (d, *J* = 2.2 Hz, 1H), 7.66 – 7.56 (m, 2H), 7.52 (d, *J* = 2.5 Hz, 1H), 7.26 (d, *J* = 8.0 Hz, 1H), 6.42 (dd, *J* = 17.0, 10.1 Hz, 1H), 6.22 (dd, *J* = 17.0, 2.0 Hz, 1H), 5.72 (dd, *J* = 10.1, 2.0 Hz, 1H), 2.83 – 2.71 (m, 1H), 2.22 (s, 3H), 1.93 – 1.43 (m, 8H) ppm; <sup>13</sup>C NMR (100 MHz, DMSO-*d*<sub>6</sub>) δ 174.4, 163.0, 144.9, 136.9, 136.1, 134.1, 132.0, 131.0, 130.7, 129.5, 126.6, 125.4, 121.0, 118.1, 117.7, 113.7, 45.1, 30.1, 25.7, 20.0 ppm. TLC-MS (ESI) *m/z*: 411.3 [M + Na]<sup>+</sup>; 387.3 [M - 1]<sup>-</sup>. HRMS ESI-TOF [M + H]<sup>+</sup> *m/z* calcd. for C<sub>23</sub>H<sub>24</sub>N<sub>4</sub>O<sub>2</sub>: 389.1978 found: 389.1975. HPLC *t*<sub>ret</sub> = 7.48 min. (Method C)

*N*-(3-(5-acrylamido-2-fluorophenyl)-1H-pyrrolo[2,3-*b*]pyridin-5-yl)cyclopentane carboxamide (**76**):

The preparation was carried out following *General Procedure F* starting from 76 mg of **135** (0.15 mmol). Flash purification by eluting with DCM/MeOH (gradient: 2-4% of MeOH) afforded 35 mg (59%) of the title compound as a white solid. <sup>1</sup>H NMR (400 MHz, DMSO-*d*<sub>6</sub>) δ 11.94 (s, 1H), 10.26 (s, 1H), 9.94 (s, 1H), 8.44 (d, *J* = 2.1 Hz, 1H), 8.33 (s, 1H), 7.91 (dd, *J* = 6.8, 2.4 Hz, 1H), 7.70 – 7.65 (m, 2H), 7.29 (dd, *J* = 10.1, 9.2 Hz, 1H), 6.44 (dd, *J* = 17.0, 10.1 Hz, 1H), 6.27 (dd, *J* = 17.0, 1.9 Hz, 1H), 5.77 (dd, *J* = 10.1, 1.9 Hz, 1H), 2.82 – 2.78 (m, 1H), 1.88 – 1.55 (m, 8H) ppm; <sup>13</sup>C NMR (100 MHz, DMSO-*d*<sub>6</sub>) δ 212.3, 176.3, 174.4, 163.1, 156.2, 153.8, 145.2, 136.9, 135.6, 135.6, 131.8, 129.7, 127.0, 126.3, 126.2, 122.5, 122.2, 120.5, 118.6, 118.6, 118.5, 117.2, 116.2, 116.0, 115.9, 107.9, 45.1, 30.1, 25.7 ppm. TLC-MS (ESI) *m/z*: 415.2 [M + Na]<sup>+</sup>; 391.1 [M - H]<sup>-</sup>. HRMS ESI-TOF [M + H]<sup>+</sup> *m/z* calcd. for C<sub>22</sub>H<sub>21</sub>FN<sub>4</sub>O<sub>2</sub>: 393.1727 found: 393.1724. HPLC *t*<sub>ret</sub> = 7.79 min. (Method C)

3-(4,4,5,5-tetramethyl-1,3,2-dioxaborolan-2-yl)aniline (**78**):

The preparation was carried out following *General Procedure A* starting from 2 g of **77** (11.6 mmol) in 60 mL of dry dioxane. Flash purification by eluting with hexane/EtOAc (gradient: 10-15% of EtOAc) afforded 1.48 g (58%) of the title compound as a brown oil. <sup>1</sup>H NMR (400 MHz, CDCl<sub>3</sub>) δ 7.24 – 7.07 (m, 3H), 6.79 (ddd, *J* = 7.6, 2.4, 1.3 Hz, 1H), 3.58 (bs, 2H), 1.34 (s, 12H) ppm. <sup>13</sup>C NMR (100 MHz, CDCl<sub>3</sub>) δ 146.2, 129.2, 125.4,

121.6, 118.5, 84.1, 25.3 ppm. TLC-MS (ESI) m/z: 220.2 [M + H]<sup>+</sup>. HPLC t<sub>ret</sub> = 7.84 min. (Method D)

*N*-(3-(4,4,5,5-tetramethyl-1,3,2-dioxaborolan-2-yl)phenyl)acrylamide (**79**):

The reaction was carried out following *General Procedure B* starting from 1.48 g of **78** (6.74 mmol) in 28 mL of DCM. Flash purification by eluting with hexane/EtOAc (gradient: 20-30% of EtOAc) afforded 1.21 g (65%) of the title compound as a yellowish solid. <sup>1</sup>H NMR (400 MHz, CDCl<sub>3</sub>) δ 7.93 (d, *J* = 7.3 Hz, 1H), 7.76 (s, 1H), 7.65 (bs, 1H), 7.55 (d, *J* = 7.2 Hz, 1H), 7.34 (t, *J* = 7.7 Hz, 1H), 6.41 (d, *J* = 16.8 Hz, 1H), 6.25 (dd, *J* = 16.9, 10.2 Hz, 1H), 5.72 (dd, *J* = 10.2, 0.9 Hz, 1H), 1.32 (s, 12H) ppm. <sup>13</sup>C NMR (100 MHz, CDCl<sub>3</sub>) δ 163.8, 137.4, 131.4, 130.9, 128.7, 127.8, 126.2, 123.3, 84.1, 25.0 ppm. TLC-MS (ESI) m/z: 272.1 [M - H]<sup>-</sup>. HPLC t<sub>ret</sub> = 10.66 min. (Method D)

*3-bromo-5-nitro-1H-pyrrolo[2,3-b]pyridine* (**81**):

2.62 g of N-bromosuccinimide (14.7 mmol) were added portion-wise to an ice-cooled solution of 2 g of **80** (12.3 mmol) in 48 mL of DMF. After complete addition, the mixture was warmed to room temperature and stirred for 3 h. After starting compound consumption, the mixture was diluted with water, and a precipitate formed. The solid was isolated by filtration and dried at 50 °C in a convection oven to afford the titled compound as 2.54 g (83%) of a yellow solid. <sup>1</sup>H NMR (400 MHz, DMSO-*d*<sub>6</sub>) 12.92 (bs, 1H), 9.14 (d, *J* = 2.4 Hz, 1H), 8.60 (d, *J* = 2.3 Hz, 1H), 8.04 (d, *J* = 2.4 Hz, 1H) ppm. <sup>13</sup>C NMR (100 MHz, DMSO-*d*<sub>6</sub>) δ 149.6, 140.4, 139.5, 130.5, 123.4, 118.4, 90.1 ppm. TLC-MS (ESI) m/z: 240.2 [M - H]<sup>-</sup>. HPLC t<sub>ret</sub> = 10.70 min. (Method D)

*3-bromo-5-nitro-1-((2-(trimethylsilyl)ethoxy)methyl)-1H-pyrrolo[2,3-b]pyridine* (**82**):

302 mg of NaH (12.6 mmol) were added portion-wise to a solution of 3.55 g of **81** (12.6 mmol) in 29 mL of dry DMF in an inert atmosphere. After 1 h. of stirring 2.32 g of SEM-Cl (13.9 mmol) were added dropwise. The reaction was warmed to room temperature and stirred overnight. The reaction was diluted with 200 mL of EtOAc and transferred to a separatory funnel. The organic phase was washed four times with water (400 mL x 4) successively, it was dried over Na<sub>2</sub>SO<sub>4</sub> and evaporated. The titled compound was obtained as 4.60 g (99%) of brown solid and was used without further purification. <sup>1</sup>H NMR (400 MHz, CDCl<sub>3</sub>) δ 9.24 (d, *J* = 2.4 Hz, 1H), 8.72 (d, *J* = 2.4 Hz, 1H), 7.58 (s, 1H), 5.70 (s, 2H), 3.65 – 3.47 (m, 2H), 0.99 – 0.89 (m, 2H), -0.05 (s, 8H) ppm. <sup>13</sup>C NMR

(100 MHz, CDCl<sub>3</sub>)  $\delta$  149.0, 140.9, 140.2, 130.4, 124.5, 119.4, 92.3, 73.5, 67.2, 17.9, -1.3 ppm. TLC-MS (ESI) m/z: 371.1 [M + H]<sup>+</sup>. HPLC  $t_{\text{ret}}$  = 13.58 min. (Method D)

*3-bromo-1-((2-(trimethylsilyl)ethoxy)methyl)-1H-pyrrolo[2,3-b]pyridin-5-amine (83):*

4.01 g of powdered zinc (61.75 mmol) and 3.89 g of ammonium formate (61.75 mmol) were added to a solution of 4.60 g of **82** (12.35 mmol) in 90 mL of EtOH. The mixture was heated to 50 °C and stirred overnight. Then, the unreacted zinc was removed by filtration and the organic layer was evaporated. The residue obtained was purified by automated flash column chromatography on silica gel by eluting with hexane/EtOAc (gradient: 20-50% of EtOAc). The titled compound was afforded as 2.78 g (66%) of brown oil. <sup>1</sup>H NMR (400 MHz, CDCl<sub>3</sub>)  $\delta$  7.98 (d,  $J$  = 2.2 Hz, 1H), 7.28 (s, 1H), 7.22 (d,  $J$  = 2.4 Hz, 1H), 5.55 (s, 2H), 4.24 (bs, 2H), 3.57 – 3.43 (m, 2H), 0.94 – 0.81 (m, 2H), -0.08 (s, 12H) ppm. <sup>13</sup>C NMR (100 MHz, CDCl<sub>3</sub>)  $\delta$  142.9, 135.5, 135.4, 127.7, 120.4, 114.1, 89.0, 73.1, 66.5, 17.9, -1.3 ppm. TLC-MS (ESI) m/z: 341.2 [M + H]<sup>+</sup>. HPLC  $t_{\text{ret}}$  = 11.67 min. (Method D)

*N-(3-bromo-1-((2-(trimethylsilyl)ethoxy)methyl)-1H-pyrrolo[2,3-b]pyridin-5-yl)isobutyramide (86):*

The preparation was carried out following *General Procedure C* starting from 100 mg of **83** (0.29 mmol) in 3 mL of DCM. Flash purification by eluting with hexane/EtOAc (gradient: 20-30% of EtOAc) afforded 119 mg (99%) of the title compound as a brown oil. <sup>1</sup>H NMR (400 MHz, CDCl<sub>3</sub>)  $\delta$  8.24 (d,  $J$  = 2.2 Hz, 1H), 7.64 (bs, 1H), 7.34 (s, 1H), 5.58 (s, 2H), 3.57 – 3.43 (m, 2H), 2.64 – 2.50 (m, 1H), 1.27 (d,  $J$  = 6.9 Hz, 6H), 0.98 – 0.80 (m, 2H), -0.07 (s, 9H) ppm. <sup>13</sup>C NMR (100 MHz, CDCl<sub>3</sub>)  $\delta$  176.0, 144.4, 138.2, 129.3, 127.9, 120.2, 119.9, 90.1, 73.1, 66.6, 36.5, 19.8, 17.9, -1.3 ppm. TLC-MS (ESI) m/z: 434.2 [M + Na]<sup>+</sup>; 466.3 [M+Na+MeOH]<sup>+</sup>; 410.1 [M - H]<sup>-</sup>. HPLC  $t_{\text{ret}}$  = 12.68 min. (Method D)

*N-(3-bromo-1-((2-(trimethylsilyl)ethoxy)methyl)-1H-pyrrolo[2,3-b]pyridin-5-yl)propionamide (87):*

The preparation was carried out following *General Procedure C* starting from 100 mg of **83** (0.29 mmol) in 3 mL of DCM. Flash purification by eluting with hexane/EtOAc (gradient: 20-40% of EtOAc) afforded 104 mg (90%) of the title compound as a brown oil. <sup>1</sup>H NMR (400 MHz, CDCl<sub>3</sub>)  $\delta$  8.26 (d,  $J$  = 2.1 Hz, 1H), 8.18 (d,  $J$  = 2.2 Hz, 1H), 7.79

(bs, 1H), 7.33 (s, 1H), 5.57 (s, 2H), 3.56 – 3.44 (m, 2H), 2.43 (q,  $J = 7.5$  Hz, 2H), 1.25 (t,  $J = 7.5$  Hz, 3H), 1.00 – 0.78 (m, 2H), -0.08 (s, 9H) ppm.  $^{13}\text{C}$  NMR (100 MHz,  $\text{CDCl}_3$ )  $\delta$  172.9, 144.4, 138.4, 129.3, 127.8, 120.2, 119.8, 90.0, 73.1, 66.6, 30.5, 17.9, 9.8, -1.3 ppm. TLC-MS (ESI)  $m/z$ : 420.2  $[\text{M} + \text{Na}]^+$ ; 452.2  $[\text{M} + \text{Na} + \text{MeOH}]^+$ ; 396.1  $[\text{M} - \text{H}]^-$ . HPLC  $t_{\text{ret}} = 12.40$  min. (Method D)

*N*-(3-bromo-1-((2-(trimethylsilyl)ethoxy)methyl)-1H-pyrrolo[2,3-*b*]pyridin-5-yl)cyclopropanecarboxamide (**88**):

The preparation was carried out following *General Procedure C* starting from 100 mg of **83** (0.29 mmol) in 3 mL of DCM. Flash purification by eluting with hexane/EtOAc (gradient: 0-30% of EtOAc) afforded 120 mg (> 99%) of the title compound as a brown oil.  $^1\text{H}$  NMR (400 MHz,  $\text{CDCl}_3$ )  $\delta$  8.33 (s, 1H), 8.28 (s, 1H), 8.16 (bs, 1H), 7.34 (s, 1H), 5.60 (s, 2H), 3.62 – 3.45 (m, 2H), 1.68 – 1.53 (m, 1H), 1.14 – 1.06 (m, 2H), 0.92 – 0.76 (m, 4H), -0.07 (s, 9H) ppm.  $^{13}\text{C}$  NMR (100 MHz,  $\text{CDCl}_3$ )  $\delta$  172.8, 143.5, 137.4, 129.7, 128.1, 120.7, 120.3, 90.3, 73.4, 66.7, 17.9, 15.6, 9.0, 8.2, -1.3 ppm. TLC-MS (ESI)  $m/z$ : 432.2  $[\text{M} + \text{Na}]^+$ ; 464.3  $[\text{M} + \text{Na} + \text{MeOH}]^+$ . HPLC  $t_{\text{ret}} = 12.53$  min. (Method D)

*N*-(3-bromo-1-((2-(trimethylsilyl)ethoxy)methyl)-1H-pyrrolo[2,3-*b*]pyridin-5-yl)cyclobutanecarboxamide (**89**):

The preparation was carried out following *General Procedure D* starting from 100 mg of **83** (0.29 mmol) in 5 mL of DCM. Flash purification by eluting with hexane/EtOAc (gradient: 20-40% of EtOAc) afforded 108 mg (88%) of the title compound as a yellow oil.  $^1\text{H}$  NMR (400 MHz,  $\text{CDCl}_3$ )  $\delta$  8.28 (d,  $J = 2.0$  Hz, 1H), 8.24 (d,  $J = 2.0$  Hz, 1H), 7.40 (bs, 1H), 7.35 (s, 1H), 5.59 (s, 2H), 3.62 – 3.45 (m, 2H), 3.29 – 3.14 (m, 1H), 2.53 – 2.34 (m, 2H), 2.34 – 2.16 (m, 2H), 2.13 – 1.82 (m, 2H), 0.98 – 0.80 (m, 2H), -0.07 (s, 9H) ppm.  $^{13}\text{C}$  NMR (100 MHz,  $\text{CDCl}_3$ )  $\delta$  173.8, 144.4, 138.2, 129.3, 127.9, 120.0, 119.9, 90.1, 73.1, 66.6, 40.7, 25.5, 18.3, 17.9, -1.3 ppm. TLC-MS (ESI)  $m/z$ : 446.3  $[\text{M} + \text{Na}]^+$ ; 478.6  $[\text{M} + \text{Na} + \text{MeOH}]^+$ ; 422.3  $[\text{M} - \text{H}]^-$ . HPLC  $t_{\text{ret}} = 10.38$  min. (Method C)

*N*-(3-bromo-1-((2-(trimethylsilyl)ethoxy)methyl)-1H-pyrrolo[2,3-*b*]pyridin-5-yl)cyclohexanecarboxamide (**90**):

The preparation was carried out following *General Procedure C* starting from 100 mg of **83** (0.29 mmol) in 3 mL of DCM. Flash purification by eluting with hexane/EtOAc (gradient: 0-40% of EtOAc) afforded 84 mg (93%) of the title compound as a yellow oil.

<sup>1</sup>H NMR (400 MHz, CDCl<sub>3</sub>) δ 8.41 (s, 1H), 8.38 (s, 1H), 7.86 (bs, 1H), 7.37 (s, 1H), 5.63 (s, 2H), 3.62 – 3.43 (m, 2H), 2.43 – 2.27 (m, 1H), 2.07 – 1.19 (m, 10H), 0.99 – 0.80 (m, 2H), -0.06 (s, 9H) ppm. <sup>13</sup>C NMR (100 MHz, CDCl<sub>3</sub>) δ 175.3, 142.9, 136.7, 129.8, 128.3, 121.4, 120.7, 90.5, 73.6, 66.7, 46.3, 29.8, 25.8, 25.8, 17.9, -1.3 ppm. TLC-MS (ESI) m/z: 474.1 [M + Na]<sup>+</sup>; 450.2 [M - H]<sup>-</sup>. HPLC *t*<sub>ret</sub> = 13.29 min. (Method D)

*N*-(3-bromo-1-((2-(trimethylsilyl)ethoxy)methyl)-1H-pyrrolo[2,3-*b*]pyridin-5-yl)thiophene-3-carboxamide (**91**):

The preparation was carried out following *General Procedure D* starting from 100 mg of **83** (0.29 mmol) in 5 mL of DCM. Flash purification by eluting with hexane/EtOAc (gradient: 20-40% of EtOAc) afforded 87 mg (69%) of the title compound as a yellow solid. <sup>1</sup>H NMR (400 MHz, CDCl<sub>3</sub>) δ 8.36 (d, *J* = 2.2 Hz, 1H), 8.21 (d, *J* = 2.1 Hz, 1H), 8.08 (bs, 1H), 7.85 (s, 1H), 7.48 (t, *J* = 1.7 Hz, 1H), 7.37 (s, 1H), 6.77 (s, 1H), 5.60 (s, 2H), 3.60 – 3.45 (m, 2H), 1.01 – 0.81 (m, 2H), -0.06 (s, 9H) ppm. <sup>13</sup>C NMR (100 MHz, CDCl<sub>3</sub>) δ 161.4, 145.5, 144.7, 144.3, 138.8, 128.8, 128.1, 122.8, 120.8, 120.0, 108.5, 90.1, 73.2, 66.6, 17.9, -1.3 ppm. TLC-MS (ESI) m/z: 458.3 [M + Na]<sup>+</sup>; 503.6 [M + Na + MeOH]<sup>+</sup>; 434.2 [M - H]<sup>-</sup>. HPLC *t*<sub>ret</sub> = 9.92 min. (Method C)

*N*-(3-bromo-1-((2-(trimethylsilyl)ethoxy)methyl)-1H-pyrrolo[2,3-*b*]pyridin-5-yl)furan-3-carboxamide (**92**):

The preparation was carried out following *General Procedure D* starting from 100 mg of **83** (0.29 mmol) in 5 mL of DCM. Flash purification by eluting with hexane/EtOAc (gradient: 20-40% of EtOAc) afforded 67 mg (51%) of the title compound as a yellowish solid. <sup>1</sup>H NMR (400 MHz, CDCl<sub>3</sub>) δ 8.37 (d, *J* = 2.3 Hz, 1H), 8.27 (bs, 1H), 8.20 (d, *J* = 2.3 Hz, 1H), 8.04 (dd, *J* = 2.8, 1.1 Hz, 1H), 7.53 (dd, *J* = 5.1, 1.2 Hz, 1H), 7.36 – 7.30 (m, *J* = 5.1, 2.9 Hz, 2H), 5.58 (s, 2H), 3.70 – 3.39 (m, 2H), 0.93 – 0.83 (m, 2H), -0.07 (s, 9H) ppm. <sup>13</sup>C NMR (100 MHz, CDCl<sub>3</sub>) δ 161.9, 144.5, 138.9, 137.4, 129.2, 129.0, 127.9, 126.9, 126.4, 120.8, 119.8, 90.1, 73.1, 66.6, 17.9, -1.3 ppm. TLC-MS (ESI) m/z: 474.2 [M + Na]<sup>+</sup>; 450.1 [M - H]<sup>-</sup>. HPLC *t*<sub>ret</sub> = 10.23 min. (Method C)

*N*-(3-bromo-1-((2-(trimethylsilyl)ethoxy)methyl)-1H-pyrrolo[2,3-*b*]pyridin-5-yl)-4-methylthiophene-2-carboxamide (**93**):

The preparation was carried out following *General Procedure D* starting from 100 mg of **83** (0.29 mmol) in 5 mL of DCM. Flash purification by eluting with hexane/EtOAc

(gradient: 20-40% of EtOAc) afforded 114 mg (84%) of the title compound as a yellowish oil. <sup>1</sup>H NMR (400 MHz, CDCl<sub>3</sub>) δ 8.37 (d, *J* = 2.3 Hz, 1H), 8.23 (d, *J* = 2.3 Hz, 1H), 8.07 (bs, 1H), 7.50 (d, *J* = 1.1 Hz, 1H), 7.35 (s, 1H), 7.19 – 7.08 (m, 1H), 5.59 (s, 2H), 3.58 – 3.47 (m, 2H), 2.27 (s, 3H), 0.94 – 0.82 (m, 2H), -0.07 (s, 9H) ppm. <sup>13</sup>C NMR (100 MHz, CDCl<sub>3</sub>) δ 160.8, 144.6, 138.8, 138.7, 138.3, 131.1, 128.9, 128.0, 126.7, 120.7, 119.9, 90.1, 73.1, 66.6, 17.9, 15.8, -1.3 ppm. TLC-MS (ESI) *m/z*: 488.3 [M + Na]<sup>+</sup>; 520.3 [M + Na + MeOH]<sup>+</sup>; 464.2 [M - H]<sup>-</sup>. HPLC *t*<sub>ret</sub> = 10.57 min. (Method C)

*N*-(3-bromo-1-((2-(trimethylsilyl)ethoxy)methyl)-1*H*-pyrrolo[2,3-*b*]pyridin-5-yl)-5-chlorothiophene-2-carboxamide (**94**):

The preparation was carried out following *General Procedure C* starting from 69 mg of **83** (0.20 mmol) in 2 mL of DCM. Flash purification by eluting with hexane/EtOAc (gradient: 0-40% of EtOAc) afforded 84 mg (93%) of the e title compound as a yellow oil. <sup>1</sup>H NMR (400 MHz, CDCl<sub>3</sub>) δ 8.65 (bs, 1H), 8.36 (d, *J* = 2.2 Hz, 1H), 8.15 (d, *J* = 2.2 Hz, 1H), 7.52 (d, *J* = 4.0 Hz, 1H), 7.32 (s, 1H), 6.85 (d, *J* = 4.0 Hz, 1H), 5.56 (s, 2H), 3.56 – 3.43 (m, 2H), 0.93 – 0.84 (m, 2H), -0.08 (s, 9H) ppm. <sup>13</sup>C NMR (100 MHz, CDCl<sub>3</sub>) δ 160.1, 143.8, 138.2, 137.5, 136.6, 128.7, 128.3, 128.2, 127.4, 121.5, 120.1, 90.2, 73.4, 66.7, 17.9, -1.3 ppm. TLC-MS (ESI) *m/z*: 508.2 [M + Na]<sup>+</sup>; 540.9 [M + Na + MeOH]<sup>+</sup>; 484.2 [M - H]<sup>-</sup>. HPLC *t*<sub>ret</sub> = 13.43 min. (Method D)

*N*-(3-bromo-1-((2-(trimethylsilyl)ethoxy)methyl)-1*H*-pyrrolo[2,3-*b*]pyridin-5-yl)-4-chlorobenzamide (**95**):

The preparation was carried out following *General Procedure D* starting from 80 mg of **83** (0.23 mmol) in 4 mL of DCM. Flash purification by eluting with hexane/EtOAc (gradient: 5-30% of EtOAc) afforded 111 mg (> 99%) of the e title compound as a brownish oil. <sup>1</sup>H NMR (400 MHz, CDCl<sub>3</sub>) δ 8.43 (d, *J* = 1.9 Hz, 1H), 8.34 (bs, 1H), 8.30 (d, *J* = 1.9 Hz, 1H), 7.88 (s, 1H), 7.86 (s, 1H), 7.45 – 7.41 (m, 2H), 7.38 (s, 1H), 5.62 (s, 2H), 3.59 – 3.47 (m, 2H), 0.94 – 0.86 (m, 2H), -0.07 (s, 9H) ppm. <sup>13</sup>C NMR (100 MHz, CDCl<sub>3</sub>) δ 165.4, 144.1, 138.5, 138.2, 132.8, 129.2, 129.1, 128.8, 128.2, 121.3, 120.2, 90.3, 73.3, 66.7, 17.9, -1.3 ppm. TLC-MS (ESI) *m/z*: 502.0 [M + Na]<sup>+</sup>; 534.1 [M + Na + MeOH]<sup>+</sup>; 478.0 [M - H]<sup>-</sup>. HPLC *t*<sub>ret</sub> = 11.17 min. (Method C)

*N*-(3-bromo-1-((2-(trimethylsilyl)ethoxy)methyl)-1*H*-pyrrolo[2,3-*b*]pyridin-5-yl)-3-chlorobenzamide (**96**):

The preparation was carried out following *General Procedure C* starting from 100 mg of **83** (0.29 mmol) in 3 mL of DCM. Flash purification by eluting with hexane/EtOAc (gradient: 0-10% of EtOAc) afforded 119 mg (86%) of the e title compound as a yellow oil. <sup>1</sup>H NMR (400 MHz, CDCl<sub>3</sub>) δ 8.32 (d, *J* = 2.1 Hz, 1H), 8.23 (bs, 1H), 8.17 (d, *J* = 2.0 Hz, 1H), 7.79 (d, *J* = 1.6 Hz, 1H), 7.68 (d, *J* = 7.7 Hz, 1H), 7.39 (dd, *J* = 8.0, 1.1 Hz, 1H), 7.29 (d, *J* = 7.8 Hz, 1H), 7.14 (s, 1H), 5.50 (s, 2H), 3.66 – 3.25 (m, 2H), 0.92 – 0.64 (m, 2H), -0.18 (s, 9H) ppm. <sup>13</sup>C NMR (100 MHz, CDCl<sub>3</sub>) δ 165.1, 144.1, 136.2, 135.1, 132.2, 130.2, 129.0, 128.2, 127.7, 125.5, 121.3, 120.0, 90.3, 73.3, 66.7, 17.9, -1.3 ppm. TLC-MS (ESI) *m/z*: 502.2 [M + Na]<sup>+</sup>; 534.3 [M + Na + MeOH]<sup>+</sup>; 478.2 [M - H]<sup>-</sup>. HPLC *t*<sub>ret</sub> = 13.34 min. (Method D)

*N*-(3-bromo-1-((2-(trimethylsilyl)ethoxy)methyl)-1*H*-pyrrolo[2,3-*b*]pyridin-5-yl)-4-fluorobenzamide (**97**):

The preparation was carried out following *General Procedure D* starting from 100 mg of **83** (0.29 mmol) in 5 mL of DCM. Flash purification by eluting with hexane/EtOAc (gradient: 10-20% of EtOAc) afforded 127 mg (94%) of the e title compound as a yellow oil. <sup>1</sup>H NMR (400 MHz, CDCl<sub>3</sub>) δ 8.53 (s, 1H), 8.45 (s, 1H), 8.32 (bs, 1H), 8.00 (dd, *J* = 8.7, 5.2 Hz, 2H), 7.41 (s, 1H), 7.18 (t, *J* = 8.6 Hz, 2H), 5.67 (s, 2H), 3.61 – 3.45 (m, 2H), 0.99 – 0.81 (m, 2H), -0.05 (s, 9H) ppm. <sup>13</sup>C NMR (100 MHz, CDCl<sub>3</sub>) δ 166.5, 165.3, 164.0, 130.6, 130.5, 129.9, 129.8, 129.4, 128.5, 122.0, 120.7, 116.2, 116.0, 90.6, 73.6, 66.8, 17.9, -1.3 ppm. TLC-MS (ESI) *m/z*: 486.4 [M + Na]<sup>+</sup>; 518.2 [M + Na + MeOH]<sup>+</sup>; 462.4 [M - H]<sup>-</sup>. HPLC *t*<sub>ret</sub> = 12.94 min. (Method D)

*N*-(3-bromo-1-((2-(trimethylsilyl)ethoxy)methyl)-1*H*-pyrrolo[2,3-*b*]pyridin-5-yl)-3-fluorobenzamide (**98**):

The preparation was carried out following *General Procedure C* starting from 100 mg of **83** (0.29 mmol) in 3 mL of DCM. Flash purification by eluting with hexane/EtOAc (gradient: 10-30% of EtOAc) afforded 135 mg (> 99%) of the e title compound as a yellow oil. <sup>1</sup>H NMR (400 MHz, CDCl<sub>3</sub>) δ 8.53 – 8.35 (m, 2H), 8.27 (s, 1H), 7.69 (d, *J* = 7.7 Hz, 1H), 7.64 (d, *J* = 9.0 Hz, 1H), 7.42 (dt, *J* = 13.2, 6.7 Hz, 1H), 7.36 (s, 1H), 7.22 (t, *J* = 8.2 Hz, 1H), 5.60 (s, 2H), 3.58 – 3.45 (m, 2H), 0.93 – 0.85 (m, 2H), -0.07 (s, 9H) ppm. <sup>13</sup>C NMR (100 MHz, CDCl<sub>3</sub>) δ 165.1, 164.1, 161.7, 144.2, 144.1, 138.3, 136.7, 130.6, 130.5, 129.0, 128.2, 122.9, 121.2, 120.1, 119.2, 119.0, 114.9, 114.7, 90.4, 73.3,

66.66, 60.59, 17.87, -1.33.ppm. TLC-MS (ESI) m/z: 486.2 [M + Na]<sup>+</sup>; 518.2 [M + Na + MeOH]<sup>+</sup>; 462.2 [M - H]<sup>-</sup>.HPLC  $t_{\text{ret}}$  = 13.00 min. (Method D)

*N*-(3-bromo-1-((2-(trimethylsilyl)ethoxy)methyl)-1H-pyrrolo[2,3-*b*]pyridin-5-yl)-2-(4-fluorophenyl) acetamide (**99**):

The preparation was carried out following *General Procedure D* starting from 100 mg of **83** (0.29 mmol) in 5 mL of DCM. Flash purification by eluting with hexane/EtOAc (gradient: 10-30% of EtOAc) afforded 100 mg (72%) of the e title compound as a yellow oil. <sup>1</sup>H NMR (400 MHz, CDCl<sub>3</sub>) δ 8.15 (d, *J* = 1.9 Hz, 1H), 8.08 (d, *J* = 2.0 Hz, 1H), 7.62 (bs, 1H), 7.30 – 7.19 (m, 3H), 6.97 (t, *J* = 8.6 Hz, 2H), 5.49 (s, 2H), 3.64 (s, 2H), 3.53 – 3.30 (m, 2H), 0.89 – 0.67 (m, 2H), -0.17 (s, 9H) ppm. <sup>13</sup>C NMR (100 MHz, CDCl<sub>3</sub>) δ 169.7, 163.6, 161.1, 143.9, 137.6, 131.3, 131.2, 130.2, 129.0, 128.2, 120.9, 120.1, 116.2, 116.0, 90.2, 73.3, 66.7, 43.5, 17.9, -1.3 ppm. TLC-MS (ESI) m/z: 500.2 [M + Na]<sup>+</sup>; 532.2 [M + Na + MeOH]<sup>+</sup>; 476.3 [M - H]<sup>-</sup>.HPLC  $t_{\text{ret}}$  = 12.95 min. (Method D)

*N*-(3-bromo-1-((2-(trimethylsilyl)ethoxy)methyl)-1H-pyrrolo[2,3-*b*]pyridin-5-yl)-2-(4-chlorophenyl) acetamide (**100**):

The preparation was carried out following *General Procedure D* starting from 80 mg of **83** (0.23 mmol) in 4 mL of DCM. Flash purification by eluting with hexane/EtOAc (gradient: 10-40% of EtOAc) afforded 67 mg (59%) of the e title compound as a yellow oil. <sup>1</sup>H NMR (400 MHz, CDCl<sub>3</sub>) δ 8.30 (s, 1H), 8.21 (d, *J* = 1.8 Hz, 1H), 7.94 (bs, 1H), 7.44 – 7.31 (m, 5H), 5.65 (s, 2H), 3.77 (s, 2H), 3.60 – 3.53 (m, 2H), 0.99 – 0.92 (m, 2H), -0.00 (s, 9H) ppm. <sup>13</sup>C NMR (100 MHz, CDCl<sub>3</sub>) δ 169.5, 144.0, 137.8, 133.6, 132.9, 130.9, 130.3, 129.3, 129.0, 128.9, 128.1, 120.7, 120.0, 90.1, 73.3, 66.7, 43.6, 17.9, -1.3 ppm. TLC-MS (ESI) m/z: 516.3 [M + Na]<sup>+</sup>; 547.8 [M + Na + MeOH]<sup>+</sup>; 492.0 [M - H]<sup>-</sup>. HPLC  $t_{\text{ret}}$  = 11.10 min. (Method C)

*N*-(3-bromo-1-((2-(trimethylsilyl)ethoxy)methyl)-1H-pyrrolo[2,3-*b*]pyridin-5-yl)-2-(2,4-difluorophenyl) acetamide (**101**):

The preparation was carried out following *General Procedure D* starting from 100 mg of **83** (0.29 mmol) in 5 mL of DCM. Flash purification by eluting with hexane/EtOAc (gradient: 20-40% of EtOAc) afforded 117 mg (81%) of the title compound as a yellow oil. <sup>1</sup>H NMR (400 MHz, CDCl<sub>3</sub>) δ 8.23 (d, *J* = 2.3 Hz, 1H), 8.14 (d, *J* = 2.3 Hz, 1H), 7.63 (bs, 1H), 7.35 (s, 2H), 6.95 – 6.81 (m, 2H), 5.58 (s, 2H), 3.73 (s, 2H), 3.57 – 3.42 (m,



2H), 0.97 – 0.80 (m, 2H), -0.07 (s, 9H) ppm. <sup>13</sup>C NMR (100 MHz, CDCl<sub>3</sub>) δ 168.5, 163.9, 163.8, 162.4, 162.3, 161.5, 161.3, 159.9, 159.8, 144.6, 138.4, 132.6, 132.5, 132.5, 132.4, 128.8, 128.0, 120.4, 119.8, 117.8, 117.7, 117.6, 112.1, 112.1, 111.9, 111.9, 104.6, 104.3, 104.1, 90.1, 73.1, 66.6, 37.0, 37.0, 17.9, -1.3 ppm. TLC-MS (ESI) m/z: 518.3 [M + Na]<sup>+</sup>; 550.3 [M + Na + MeOH]<sup>+</sup>; 530.2 [M - H]<sup>-</sup>. HPLC t<sub>ret</sub> = 10.52 min. (Method D)

*N*-(3-bromo-1-((2-(trimethylsilyl)ethoxy)methyl)-1H-pyrrolo[2,3-*b*]pyridin-5-yl)-2-(3-chloro-5-fluorophenyl)acetamide (**102**):

104 mg of thionyl chloride (0.87 mmol) was added dropwise to an ice-cooled solution of 61 mg of 3-chloro-5-fluorobenzoic acid in DCM, in presence of a catalytic amount of DMF (1 drop). The mixture was warmed to 40 °C and stirred for 3 h. Then organic layer was evaporated and a solution of 3-chloro-5-fluorobenzoyl chloride in 2 mL of DCM was added dropwise to a solution of 100 mg of **83** (0.29 mmol) and 65 mg of Et<sub>3</sub>N (0.64 mmol) in 1 mL of DCM. The reaction was stirred at room temperature for 1 h. Then, solvent was evaporated and the residue was purified via automated flash column chromatography on silica gel by eluting with hexane/EtOAc (gradient: 10-20% of EtOAc) to afford 127 mg (88%) of the title compound as a yellow oil. <sup>1</sup>H NMR (400 MHz, CDCl<sub>3</sub>) δ 8.44 (bs, 1H), 8.41 (d, *J* = 1.9 Hz, 1H), 8.24 (d, *J* = 2.0 Hz, 1H), 7.70 (s, 1H), 7.55 (d, *J* = 8.6 Hz, 1H), 7.37 (s, 1H), 7.27 – 7.22 (m, 1H), 5.61 (s, 2H), 3.59 – 3.46 (m, 2H), 0.93 – 0.85 (m, 2H), -0.06 (s, 9H) ppm. <sup>13</sup>C NMR (100 MHz, CDCl<sub>3</sub>) δ 164.0, 163.9, 161.5, 144.4, 138.4, 137.6, 137.6, 135.9, 135.8, 128.6, 128.3, 123.5, 123.5, 121.2, 120.0, 119.9, 119.6, 113.5, 113.3, 90.3, 73.3, 66.7, 17.9, -1.3 ppm. TLC-MS (ESI) m/z: 520.0 [M + Na]<sup>+</sup>; 552.1 [M + Na + MeOH]<sup>+</sup>; 496.2 [M - H]<sup>-</sup>. HPLC t<sub>ret</sub> = 13.62 min. (Method D)

*N*-(3-bromo-1-((2-(trimethylsilyl)ethoxy)methyl)-1H-pyrrolo[2,3-*b*]pyridin-5-yl)-2-(5-chloro-2,4-difluorophenyl)acetamide (**103**):

The preparation was carried out following *General Procedure D* starting from 69 mg of **83** (0.20 mmol) in 2 mL of DCM. Flash purification by eluting with hexane/EtOAc (gradient: 0-40% of EtOAc) afforded 84 mg (93%) of the title compound as a yellow oil. <sup>1</sup>H NMR (400 MHz, CDCl<sub>3</sub>) δ 8.29 (s, 1H), 8.24 (s, 1H), 7.87 (bs, 1H), 7.45 (t, *J* = 7.8 Hz, 1H), 7.37 (s, 1H), 6.96 (t, *J* = 9.0 Hz, 1H), 5.61 (s, 2H), 3.72 (s, 2H), 3.61 – 3.40 (m, 2H), 0.98 – 0.83 (m, 2H), -0.07 (s, 9H) ppm. <sup>13</sup>C NMR (100 MHz, CDCl<sub>3</sub>) δ 167.9, 160.6, 159.0, 158.8, 158.2, 158.1, 156.5, 156.3, 143.9, 137.5, 132.7, 132.7, 132.7, 128.9, 128.3, 128.3, 121.0, 120.3, 119.0, 119.0, 118.9, 118.8, 117.1, 117.1, 116.9, 116.9, 105.6,

105.4, 105.1, 90.3, 73.4, 66.7, 36.6, 17.9, -1.3 ppm. TLC-MS (ESI) m/z: 552.1 [M + Na]<sup>+</sup>; 584.0 [M + Na + MeOH]<sup>+</sup>; 528.0 [M - H]<sup>-</sup>. HPLC t<sub>ret</sub> = 11.14 min. (Method C)

*N*-(3-(5-isobutyramido-1-((2-(trimethylsilyl)ethoxy)methyl)-1H-pyrrolo[2,3-b]pyridin-3-yl)phenyl)acrylamide (**104**):

The preparation was carried out following *General Procedure E* starting from 105 mg of **86** (0.20 mmol) and using 0.6 mL of K<sub>2</sub>CO<sub>3</sub> (0.5 M sol.). The reaction was carried out at 80 °C. Flash purification by eluting with hexane/EtOAc (gradient: 30-50% of EtOAc) afforded 61 mg (49%) of the e title compound as a yellowish solid. <sup>1</sup>H NMR (400 MHz, CDCl<sub>3</sub>) δ 8.50 (d, *J* = 2.1 Hz, 1H), 8.34 (d, *J* = 2.2 Hz, 1H), 8.10 (s, 1H), 7.81 (s, 1H), 7.73 (s, 1H), 7.54 (d, *J* = 6.7 Hz, 1H), 7.48 (s, 1H), 7.34 – 7.28 (m, 2H), 6.44 (dd, *J* = 16.9, 1.5 Hz, 1H), 6.33 (dd, *J* = 16.8, 10.0 Hz, 1H), 5.74 (dd, *J* = 10.0, 1.4 Hz, 1H), 5.62 (s, 2H), 3.61 – 3.49 (m, 2H), 2.59 (m, 1H), 0.93 – 0.88 (m, 2H), -0.07 (s, 9H) ppm. <sup>13</sup>C NMR (100 MHz, CDCl<sub>3</sub>) δ 176.2, 164.1, 146.1, 141.5, 138.5, 138.4, 137.6, 135.3, 131.5, 129.8, 129.5, 129.0, 128.1, 127.9, 126.4, 123.4, 123.1, 121.1, 120.1, 119.3, 118.8, 118.5, 118.2, 116.1, 73.3, 66.6, 36.6, 19.8, 18.0, -1.3 ppm. TLC-MS (ESI) m/z: 501.6 [M + Na]<sup>+</sup>; 477.5 [M - H]<sup>-</sup>; 513.5 [M + Cl]<sup>-</sup>. HPLC t<sub>ret</sub> = 12.34 min. (Method D)

*N*-(3-(5-propionamido-1-((2-(trimethylsilyl)ethoxy)methyl)-1H-pyrrolo[2,3-b]pyridin-3-yl)phenyl)acrylamide (**105**):

The preparation was carried out following *General Procedure E* starting from 104 mg of **87** (0.26 mmol) and using 0.5 mL of K<sub>2</sub>CO<sub>3</sub> (0.5 M sol.). The reaction was carried out at 80 °C. Flash purification by eluting with hexane/EtOAc (gradient: 30-40% of EtOAc) afforded 42 mg (35%) of the e title compound as a yellowish solid. <sup>1</sup>H NMR (400 MHz, CDCl<sub>3</sub>) δ 8.51 (d, *J* = 2.1 Hz, 1H), 8.35 (d, *J* = 2.1 Hz, 1H), 7.88 (s, 1H), 7.75 (s, 1H), 7.57 – 7.46 (m, 3H), 7.39 – 7.30 (m, 2H), 6.46 (dd, *J* = 16.8, 1.2 Hz, 1H), 6.31 (dd, *J* = 16.8, 10.1 Hz, 1H), 5.78 (dd, *J* = 10.1, 1.2 Hz, 1H), 5.66 (s, 2H), 3.65 – 3.46 (m, 2H), 2.45 (q, *J* = 7.5 Hz, 2H), 1.28 (t, *J* = 8.5 Hz, 3H), 0.97 – 0.89 (m, 2H), -0.06 (s, 9H) ppm. <sup>13</sup>C NMR (100 MHz, CDCl<sub>3</sub>) δ 172.7, 163.9, 146.1, 138.5, 137.6, 135.4, 131.4, 129.8, 129.0, 128.0, 126.4, 123.2, 121.0, 118.5, 118.1, 116.1, 73.3, 66.6, 30.6, 18.0, 9.8, -1.3 ppm. TLC-MS (ESI) m/z: 487.3[M + Na]<sup>+</sup>; 463.3 [M - H]<sup>-</sup>; 499.3 [M + Cl]<sup>+</sup>. HPLC t<sub>ret</sub> = 12.07 min. (Method D)

*N*-(3-(3-acrylamidophenyl)-1-((2-(trimethylsilyl)ethoxy)methyl)-1*H*-pyrrolo[2,3-*b*]pyridin-5-yl)cyclopropanecarboxamide (**106**):

The preparation was carried out following *General Procedure E* starting from 120 mg of **88** (0.29 mmol) and using 0.6 mL of K<sub>2</sub>CO<sub>3</sub> (0.5 M sol.). The reaction was carried out at room temperature. Flash purification by eluting with DCM/MeOH (gradient: 0.1-0.2% of MeOH) afforded 95 mg (69%) of the e title compound as a white solid. <sup>1</sup>H NMR (400 MHz, CDCl<sub>3</sub>) δ 8.90 (s, 1H), 8.63 (s, 1H), 8.50 (d, *J* = 14.1 Hz, 2H), 7.75 (s, 1H), 7.56 (d, *J* = 7.5 Hz, 1H), 7.40 (s, 1H), 7.24 (d, *J* = 7.9 Hz, 1H), 7.16 (d, *J* = 7.4 Hz, 1H), 6.46 – 6.41 (m, 2H), 5.74 (dd, *J* = 7.6, 3.9 Hz, 1H), 5.57 (s, 2H), 3.60 – 3.46 (m, 2H), 1.79 – 1.57 (m, 1H), 1.07 – 1.00 (m, 2H), 0.94 – 0.77 (m, 4H), -0.07 (s, 9H) ppm. <sup>13</sup>C NMR (100 MHz, CDCl<sub>3</sub>) δ 173.7, 164.5, 138.9, 133.2, 131.5, 130.3, 129.7, 127.9, 127.5, 124.9, 122.6, 119.1, 118.7, 117.1, 74.7, 67.1, 18.0, 15.5, 8.6, -1.3 ppm. TLC-MS (ESI) *m/z*: 499.5 [M + Na]<sup>+</sup>; 475.5 [M - H]<sup>-</sup>; 511.4 [M + Cl]<sup>-</sup>. HPLC *t*<sub>ret</sub> = 12.20 min. (Method D)

*N*-(3-(3-acrylamidophenyl)-1-((2-(trimethylsilyl)ethoxy)methyl)-1*H*-pyrrolo[2,3-*b*]pyridin-5-yl)cyclobutanecarboxamide (**107**):

The preparation was carried out following *General Procedure E* starting from 39 mg of **89** (0.09 mmol) and using 0.2 mL of K<sub>2</sub>CO<sub>3</sub> (0.5 M sol.). The reaction was carried out at 80 °C. Flash purification by eluting with hexane/EtOAc (gradient: 30-60% of EtOAc) afforded 30 mg (68%) of the e title compound as a yellowish solid. <sup>1</sup>H NMR (400 MHz, CDCl<sub>3</sub>) δ 8.57 (d, *J* = 2.2 Hz, 1H), 8.33 (d, *J* = 2.2 Hz, 1H), 7.82 (d, *J* = 26.0 Hz, 2H), 7.54 (s, 1H), 7.37 (d, *J* = 6.7 Hz, 2H), 6.46 (dd, *J* = 16.8, 1.4 Hz, 1H), 6.32 (dd, *J* = 16.8, 10.1 Hz, 1H), 5.78 (dd, *J* = 10.1, 1.4 Hz, 1H), 5.66 (s, 2H), 3.62 – 3.53 (m, 2H), 3.32 – 3.15 (m, 1H), 2.55 – 2.34 (m, 2H), 2.32 – 2.19 (m, 2H), 2.11 – 1.90 (m, 2H), 0.99 – 0.87 (m, 2H), -0.06 (s, 7H) ppm. <sup>13</sup>C NMR (100 MHz, CDCl<sub>3</sub>) δ 173.9, 163.9, 146.1, 138.5, 137.4, 135.34, 131.4, 129.8, 129.0, 127.9, 126.4, 123.1, 120.9, 118.5, 118.1, 116.1, 73.3, 66.6, 40.8, 25.5, 25.0, 18.3, 18.0, -1.3 ppm. TLC-MS (ESI) *m/z*: 513.2 [M + Na]<sup>+</sup>; 489.2 [M - H]<sup>-</sup>; 525.2 [M + Cl]<sup>-</sup>. HPLC *t*<sub>ret</sub> = 7.31 min. (Method C)

*N*-(3-(3-acrylamidophenyl)-1-((2-(trimethylsilyl)ethoxy)methyl)-1*H*-pyrrolo[2,3-*b*]pyridin-5-yl)cyclohexanecarboxamide (**108**):

The preparation was carried out following *General Procedure E* starting from 143 mg of **90** (0.22 mmol) and using 0.7 mL of K<sub>2</sub>CO<sub>3</sub> (0.5 M sol.). The reaction was carried out at

room temperature. Flash purification by eluting with hexane/EtOAc (gradient: 30-60% of EtOAc) afforded 70 mg (56%) of the e title compound as a white solid.  $^1\text{H}$  NMR (400 MHz,  $\text{CDCl}_3$ )  $\delta$  8.75 (s, 2H), 8.58 (s, 1H), 7.78 (s, 1H), 7.58 (d,  $J = 7.3$  Hz, 1H), 7.44 (s, 1H), 7.31 – 7.23 (m, 2H), 7.16 (d,  $J = 6.6$  Hz, 1H), 6.50 – 6.45 (m, 2H), 5.76 (dd,  $J = 7.3$ , 3.9 Hz, 1H), 5.64 (s, 2H), 3.61 – 3.52 (m, 2H), 2.39 (t,  $J = 11.4$  Hz, 1H), 2.02 – 1.92 (m,  $J = 11.7$  Hz, 2H), 1.88 – 1.77 (m,  $J = 12.1$  Hz, 2H), 1.77 – 1.64 (m,  $J = 10.6$  Hz, 2H), 1.65 – 1.45 (m,  $J = 23.1$ , 11.1 Hz, 4H), 0.93 – 0.87 (m, 2H), -0.06 (s, 9H) ppm.  $^{13}\text{C}$  NMR (100 MHz,  $\text{CDCl}_3$ )  $\delta$  176.1, 164.5, 138.9, 138.1, 131.6, 130.0, 129.7, 127.9, 127.4, 122.8, 119.1, 117.1, 74.9, 67.0, 46.1, 29.8, 25.8, 18.0, -1.3 ppm. TLC-MS (ESI)  $m/z$ : 541.4 [ $\text{M} + \text{Na}$ ] $^+$ ; 517.4 [ $\text{M} - \text{H}$ ] $^-$ ; 553.3 [ $\text{M} + \text{Cl}$ ] $^-$ . HPLC  $t_{\text{ret}} = 12.94$  min. (Method D)

*N*-(3-(3-acrylamidophenyl)-1-((2-(trimethylsilyl)ethoxy)methyl)-1H-pyrrolo[2,3-*b*]pyridin-5-yl)furan-3-carboxamide (**109**):

The preparation was carried out following *General Procedure E* starting from 57 mg of **91** (0.12 mmol) and using 0.25 mL of  $\text{K}_2\text{CO}_3$  (0.5 M sol.). The reaction was carried out at 80 °C. Flash purification by eluting with hexane/EtOAc (gradient: 30-60% of EtOAc) afforded 25 mg (38%) of the e title compound as a yellowish solid.  $^1\text{H}$  NMR (400 MHz,  $\text{DMSO}-d_6$ )  $\delta$  10.25 (s, 1H), 10.15 (s, 1H), 8.60 (s, 2H), 8.41 (d,  $J = 0.5$  Hz, 1H), 8.02 (s, 1H), 7.99 (s, 1H), 7.83 (t,  $J = 1.7$  Hz, 1H), 7.64 (d,  $J = 8.1$  Hz, 1H), 7.44 (t,  $J = 7.8$  Hz, 1H), 7.39 (dt,  $J = 7.7$ , 1.3 Hz, 1H), 7.04 (d,  $J = 1.1$  Hz, 1H), 6.48 (dd,  $J = 17.0$ , 10.1 Hz, 1H), 6.29 (dd,  $J = 17.0$ , 2.0 Hz, 1H), 5.79 (dd,  $J = 10.1$ , 2.0 Hz, 1H), 5.68 (s, 2H), 3.65 – 3.53 (m, 2H), 0.92 – 0.81 (m, 2H), -0.08 (s, 9H) ppm.  $^{13}\text{C}$  NMR (100 MHz,  $\text{DMSO}-d_6$ )  $\delta$  163.3, 160.7, 145.9, 145.2, 144.3, 139.7, 137.9, 134.7, 131.9, 129.7, 129.5, 127.5, 127.0, 122.8, 121.7, 120.3, 117.4, 114.5, 109.2, 72.6, 65.6, 17.2, -1.4 ppm. TLC-MS (ESI)  $m/z$ : 503.4 [ $\text{M} + 1$ ] $^+$ ; 525.3 [ $\text{M} + \text{Na}$ ] $^+$ ; 501.2 [ $\text{M} - \text{H}$ ] $^-$ ; 537.2 [ $\text{M} + \text{Cl}$ ] $^-$ . HPLC  $t_{\text{ret}} = 9.71$  min. (Method C)

*N*-(3-(3-acrylamidophenyl)-1-((2-(trimethylsilyl)ethoxy)methyl)-1H-pyrrolo[2,3-*b*]pyridin-5-yl)thiophene-3-carboxamide (**110**):

The preparation was carried out following *General Procedure E* starting from 67 mg of **92** (0.15 mmol) and using 0.3 mL of  $\text{K}_2\text{CO}_3$  (0.5 M sol.). The reaction was carried out at 80 °C. Flash purification by eluting with hexane/EtOAc (gradient: 30-60% of EtOAc) afforded 44 mg (57%) of the e title compound as a white solid.  $^1\text{H}$  NMR (400 MHz,  $\text{DMSO}-d_6$ )  $\delta$  10.27 (d,  $J = 3.5$  Hz, 2H), 8.62 (s, 2H), 8.38 (t,  $J = 2.1$  Hz, 1H), 8.00 (d,  $J =$

14.4 Hz, 2H), 7.68 (d,  $J = 2.1$  Hz, 2H), 7.62 (d,  $J = 8.0$  Hz, 1H), 7.53 – 7.34 (m, 2H), 6.47 (dd,  $J = 17.0, 10.1$  Hz, 1H), 6.28 (dd,  $J = 17.0, 1.9$  Hz, 1H), 5.78 (dd,  $J = 10.1, 1.9$  Hz, 1H), 5.68 (s, 2H), 3.63 – 3.57 (m, 2H), 0.89 – 0.80 (m, 2H), -0.08 (s, 9H) ppm.  $^{13}\text{C}$  NMR (100 MHz, DMSO- $d_6$ )  $\delta$  163.4, 161.3, 145.2, 139.7, 138.1, 137.6, 134.8, 131.9, 129.9, 129.6, 127.6, 127.2, 121.8, 120.5, 117.4, 114.6, 72.7, 65.7, 17.3, -1.3 ppm. TLC-MS (ESI)  $m/z$ : 541.4[M + Na] $^+$ ; 517.4 [M - H] $^-$ ; 553.3 [M + Cl] $^-$ . HPLC  $t_{\text{ret}} = 9.78$  min. (Method C)

*N*-(3-(3-acrylamidophenyl)-1-((2-(trimethylsilyl)ethoxy)methyl)-1H-pyrrolo[2,3-*b*]pyridin-5-yl)-4-methylthiophene-2-carboxamide (**111**):

The preparation was carried out following *General Procedure E* starting from 114 mg of **93** (0.25 mmol) and using 0.5 mL of K<sub>2</sub>CO<sub>3</sub> (0.5 M sol.). The reaction was carried out at 80 °C. Flash purification by eluting with hexane/EtOAc (gradient: 30-80% of EtOAc) afforded 109 mg (82%) of the e title compound as a white solid.  $^1\text{H}$  NMR (400 MHz, DMSO- $d_6$ )  $\delta$  10.35 (s, 1H), 10.24 (s, 1H), 8.60 (dd,  $J = 5.2, 2.2$  Hz, 2H), 7.99 (d,  $J = 12.1$  Hz, 2H), 7.86 (d,  $J = 1.1$  Hz, 1H), 7.62 (d,  $J = 8.0$  Hz, 1H), 7.48 – 7.44 (m, 1H), 7.42 (d,  $J = 7.9$  Hz, 1H), 7.37 (d,  $J = 7.7$  Hz, 1H), 6.47 (dd,  $J = 17.0, 10.1$  Hz, 1H), 6.27 (dd,  $J = 17.0, 2.0$  Hz, 1H), 5.77 (dd,  $J = 10.1, 2.0$  Hz, 1H), 5.67 (s, 2H), 3.64 – 3.49 (m, 2H), 2.28 (s, 3H), 0.93 – 0.78 (m, 2H), -0.09 (s, 9H) ppm.  $^{13}\text{C}$  NMR (100 MHz, DMSO- $d_6$ )  $\delta$   $^{13}\text{C}$  NMR (101 MHz, DMSO)  $\delta$  163.2, 160.2, 145.1, 139.6, 139.2, 138.0, 137.8, 134.7, 131.9, 131.0, 129.7, 129.4, 127.5, 127.2, 127.0, 121.7, 120.2, 117.3, 114.5, 72.6, 65.6, 17.2, 15.4-1.4 ppm. TLC-MS (ESI)  $m/z$ : 555.4 [M + Na] $^+$ ; 531.3 [M - H] $^-$ ; 567.3 [M + Cl] $^-$ . HPLC  $t_{\text{ret}} = 10.07$  min. (Method C)

*N*-(3-(3-acrylamidophenyl)-1-((2-(trimethylsilyl)ethoxy)methyl)-1H-pyrrolo[2,3-*b*]pyridin-5-yl)-5-chlorothiophene-2-carboxamide (**112**):

The preparation was carried out following *General Procedure E* starting from 119 mg of **94** (0.19 mmol) and using 0.5 mL of K<sub>2</sub>CO<sub>3</sub> (0.5 M sol.). The reaction was carried out at 80 °C. Flash purification by eluting with hexane/EtOAc (gradient: 10-70% of EtOAc) afforded 93 mg (60%) of the e title compound as a white solid.  $^1\text{H}$  NMR (400 MHz, DMSO- $d_6$ )  $\delta$  10.53 (s, 1H), 10.25 (s, 1H), 8.58 (dd,  $J = 8.8, 2.2$  Hz, 2H), 8.02 (s, 1H), 8.00 (s, 1H), 7.94 (d,  $J = 4.1$  Hz, 1H), 7.63 (d,  $J = 8.0$  Hz, 1H), 7.44 (t,  $J = 7.8$  Hz, 1H), 7.38 (d,  $J = 7.7$  Hz, 1H), 7.30 (d,  $J = 4.1$  Hz, 1H), 6.48 (dd,  $J = 17.0, 10.1$  Hz, 1H), 6.28 (dd,  $J = 17.0, 1.9$  Hz, 1H), 5.78 (dd,  $J = 10.1, 1.9$  Hz, 1H), 5.68 (s, 2H), 3.67 – 3.52 (m, 2H), 0.91 – 0.80 (m, 2H), -0.08 (s, 9H) ppm.  $^{13}\text{C}$  NMR (100 MHz, DMSO- $d_6$ )  $\delta$  163.3,

159.2, 145.3, 139.7, 138.9, 138.0, 134.7, 134.0, 131.9, 129.5, 129.2, 129.2, 128.4, 127.7, 127.1, 121.8, 120.6, 117.4, 114.6, 72.7, 65.6, 17.2, -1.3 ppm. TLC-MS (ESI) m/z: 575.6 [M + Na]<sup>+</sup>; 551.6 [M - H]<sup>-</sup>; 587.5 [M + Cl]<sup>-</sup>. HPLC t<sub>ret</sub> = 13.05 min. (Method D)

*N*-(3-(3-acrylamidophenyl)-1-((2-(trimethylsilyl)ethoxy)methyl)-1H-pyrrolo[2,3-*b*]pyridin-5-yl)-4-chlorobenzamide (**113**):

The preparation was carried out following *General Procedure E* starting from 111 mg of **95** (0.23 mmol) and using 0.4 mL of K<sub>2</sub>CO<sub>3</sub> (0.5 M sol.). The reaction was carried out at 80 °C. Flash purification by eluting with hexane/EtOAc (gradient: 10-80% of EtOAc) afforded 95 mg (75%) of the e title compound as a yellowish solid. <sup>1</sup>H NMR (400 MHz, DMSO-*d*<sub>6</sub>) δ 10.51 (s, 1H), 10.24 (s, 1H), 8.64 (s, 2H), 8.10 – 7.93 (m, 4H), 7.62 (d, *J* = 8.6 Hz, 3H), 7.49 – 7.34 (m, 2H), 6.46 (dd, *J* = 17.0, 10.1 Hz, 1H), 6.26 (dd, *J* = 16.9, 2.0 Hz, 1H), 5.76 (dd, *J* = 10.1, 2.0 Hz, 1H), 5.67 (s, 2H), 3.64 – 3.52 (m, 2H), 0.89 – 0.77 (m, 2H), -0.10 (s, 9H) ppm. <sup>13</sup>C NMR (100 MHz, DMSO-*d*<sub>6</sub>) δ 164.7, 163.3, 145.2, 139.6, 138.1, 136.6, 134.7, 133.3, 131.9, 129.9, 129.7, 129.5, 128.6, 127.6, 127.1, 121.8, 120.5, 117.4, 117.4, 114.6, 72.5, 65.7, 17.2, -1.3 ppm. TLC-MS (ESI) m/z: 569.5 [M + Na]<sup>+</sup>; 601.4 [M + Na + MeOH]<sup>+</sup>; [M - H]<sup>-</sup>. HPLC t<sub>ret</sub> = 12.93 min. (Method D)

*N*-(3-(3-acrylamidophenyl)-1-((2-(trimethylsilyl)ethoxy)methyl)-1H-pyrrolo[2,3-*b*]pyridin-5-yl)-3-chlorobenzamide (**114**):

The preparation was carried out following *General Procedure E* starting from 119 mg of **96** (0.25 mmol) and using 0.5 mL of K<sub>2</sub>CO<sub>3</sub> (0.5 M sol.). The reaction was carried out at room temperature. Flash purification by eluting with hexane/EtOAc (gradient: 10-70% of EtOAc) afforded 67 mg (49%) of the e title compound as a yellow solid. <sup>1</sup>H NMR (400 MHz, DMSO-*d*<sub>6</sub>) δ 10.56 (s, 1H), 10.25 (s, 1H), 8.67 (q, *J* = 2.2 Hz, 2H), 8.09 (t, *J* = 1.8 Hz, 1H), 8.03 (s, 1H), 8.00 (s, 1H), 7.98 (s, 1H), 7.76 – 7.66 (m, 1H), 7.61 (dd, *J* = 14.6, 6.9 Hz, 2H), 7.45 (t, *J* = 7.8 Hz, 1H), 7.39 (d, *J* = 7.8 Hz, 1H), 6.48 (dd, *J* = 17.0, 10.1 Hz, 1H), 6.29 (dd, *J* = 17.0, 2.0 Hz, 1H), 5.78 (dd, *J* = 10.1, 2.0 Hz, 1H), 5.69 (s, 2H), 3.69 – 3.51 (m, 40H), 0.93 – 0.76 (m, 42H), -0.07 (s, 154H) ppm. <sup>13</sup>C NMR (100 MHz, DMSO-*d*<sub>6</sub>) δ 164.2, 163.3, 145.29, 139.7, 138.1, 136.6, 134.8, 133.3, 131.9, 131.6, 130.6, 129.9, 129.6, 127.6, 127.4, 127.1, 126.5, 121.8, 120.5, 117.4, 117.3, 114.6, 72.8, 65.5, 17.2, -1.3 ppm. TLC-MS (ESI) m/z: 547.4 [M + 1]<sup>+</sup>; 569.5 [M + Na]<sup>+</sup>; 545.6 [M - H]<sup>-</sup>; 581.3 [M + Cl]<sup>-</sup>. HPLC t<sub>ret</sub> = 12.96 min. (Method D)

*N*-(3-(3-acrylamidophenyl)-1-((2-(trimethylsilyl)ethoxy)methyl)-1*H*-pyrrolo[2,3-*b*]pyridin-5-yl)-4-fluorobenzamide (**115**):

The preparation was carried out following *General Procedure E* starting from 127 mg of **97** (0.27 mmol) and using 0.5 mL of K<sub>2</sub>CO<sub>3</sub> (0.5 M sol.). The reaction was carried out at 80 °C. Flash purification by eluting with hexane/EtOAc (gradient: 10-70% of EtOAc) afforded 106 mg (63%) of the e title compound as a yellowish solid. <sup>1</sup>H NMR (400 MHz, DMSO-*d*<sub>6</sub>) δ 10.45 (s, 1H), 10.24 (s, 1H), 8.63 (s, 2H), 8.14 – 8.05 (m, 2H), 8.01 (s, 1H), 7.98 (s, 1H), 7.61 (d, *J* = 8.0 Hz, 1H), 7.47 – 7.34 (m, 4H), 6.46 (dd, *J* = 17.0, 10.1 Hz, 1H), 6.27 (dd, *J* = 16.9, 1.9 Hz, 1H), 5.76 (dd, *J* = 10.1, 2.0 Hz, 1H), 5.67 (s, 2H), 3.68 – 3.49 (m, 2H), 0.90 – 0.77 (m, 2H), -0.09 (s, 9H) ppm. <sup>13</sup>C NMR (100 MHz, DMSO-*d*<sub>6</sub>) δ 164.6, 163.4, 163.0, 145.2, 139.7, 138.1, 134.8, 131.9, 131.0, 130.5, 130.4, 130.0, 129.5, 127.6, 127.1, 121.8, 120.5, 117.4, 115.5, 115.3, 114.7, 72.6, 65.6, 17.2, -1.6 ppm. TLC-MS (ESI) *m/z*: 553.7 [M + Na]<sup>+</sup>; 585.5[M + Na + MeOH]<sup>+</sup>. HPLC *t*<sub>ret</sub> = 12.57 min. (Method D)

*N*-(3-(3-acrylamidophenyl)-1-((2-(trimethylsilyl)ethoxy)methyl)-1*H*-pyrrolo[2,3-*b*]pyridin-5-yl)-3-fluorobenzamide (**116**):

The preparation was carried out following *General Procedure E* starting from 135 mg of **98** (0.29 mmol) and using 0.5 mL of K<sub>2</sub>CO<sub>3</sub> (0.5 M sol.). The reaction was carried out at 80 °C. Flash purification by eluting with hexane/EtOAc (gradient: 30-70% of EtOAc) afforded 95 mg (58%) of the e title compound as a white solid. <sup>1</sup>H NMR (400 MHz, DMSO-*d*<sub>6</sub>) δ 10.53 (s, 1H), 10.27 (s, 1H), 8.66 (s, 2H), 8.03 (s, 1H), 8.00 (s, 1H), 7.88 (d, *J* = 7.9 Hz, 1H), 7.84 (d, *J* = 9.4 Hz, 1H), 7.73 – 7.57 (m, 2H), 7.57 – 7.33 (m, 3H), 6.47 (dd, *J* = 17.0, 10.1 Hz, 1H), 6.28 (dd, *J* = 17.0, 1.9 Hz, 1H), 5.78 (dd, *J* = 10.1, 1.9 Hz, 1H), 5.69 (s, 2H), 3.68 – 3.50 (m, 2H), 0.94 – 0.80 (m, 2H), -0.08 (s, 9H) ppm. <sup>13</sup>C NMR (100 MHz, DMSO-*d*<sub>6</sub>) δ 164.3, 163.2, 160.9, 145.4, 139.7, 138.1, 136.8, 134.6, 132.0, 130.7, 129.8, 129.6, 127.6, 127.0, 123.8, 121.7, 120.5, 118.8, 118.5, 117.4, 114.6, 114.4, 72.8, 65.6, 17.2, 17.2, -1.3, -1.3 ppm. TLC-MS (ESI) *m/z*: 553.1 [M + Na]<sup>+</sup>; 585.1 [M + Na + MeOH]<sup>+</sup>; 529.3 [M - H]<sup>-</sup>. HPLC *t*<sub>ret</sub> = 12.62 min. (Method D)

*N*-(3-(5-(2-(4-fluorophenyl)acetamido)-1-((2-(trimethylsilyl)ethoxy)methyl)-1*H*-pyrrolo[2,3-*b*]pyridin-3-yl)phenyl)acrylamide (**117**):

The preparation was carried out following *General Procedure E* starting from 100 mg of **99** (0.21 mmol) and using 0.35 mL of K<sub>2</sub>CO<sub>3</sub> (0.5 M sol.). The reaction was carried out

at room temperature. Flash purification by eluting with hexane/EtOAc (gradient: 10-70% of EtOAc) afforded 61 mg (54%) of the e title compound as a yellowish solid. <sup>1</sup>H NMR (400 MHz, DMSO-*d*<sub>6</sub>) δ 10.37 (s, 1H), 10.26 (s, 1H), 8.56 (d, *J* = 2.2 Hz, 1H), 8.49 (d, *J* = 2.2 Hz, 1H), 8.00 (s, 1H), 7.95 (s, 1H), 7.60 (d, *J* = 8.6 Hz, 1H), 7.48 – 7.37 (m, 3H), 7.33 (d, *J* = 7.8 Hz, 1H), 7.23 – 7.11 (m, 2H), 6.48 (dd, *J* = 16.9, 10.1 Hz, 1H), 6.29 (dd, *J* = 17.0, 2.0 Hz, 1H), 5.79 (dd, *J* = 10.1, 2.0 Hz, 1H), 5.65 (s, 2H), 3.70 (s, 2H), 3.64 – 3.49 (m, 2H), 0.91 – 0.76 (m, 2H), -0.09 (s, 9H) ppm. <sup>13</sup>C NMR (100 MHz, DMSO-*d*<sub>6</sub>) δ 169.3, 163.3, 162.6, 160.2, 144.9, 139.8, 136.6, 134.8, 132.1, 132.0, 131.9, 131.2, 131.1, 130.3, 129.5, 127.5, 127.0, 72.8, 65.7, 42.18, 17.2, -1.4 ppm. TLC-MS (ESI) *m/z*: 567.0 [M + Na]<sup>+</sup>; 599.0 [M + Na + MeOH]<sup>+</sup>. HPLC *t*<sub>ret</sub> = 12.59 min. (Method D)

*N*-(3-(5-(2-(4-chlorophenyl)acetamido)-1-((2-(trimethylsilyl)ethoxy)methyl)-1*H*-pyrrolo[2,3-*b*]pyridin-3-yl)phenyl)acrylamide (**118**):

The preparation was carried out following *General Procedure E* starting from 67 mg of **100** (0.14 mmol) and using 0.25 mL of K<sub>2</sub>CO<sub>3</sub> (0.5 M sol.). The reaction was carried out at room temperature. Flash purification by eluting with hexane/EtOAc (gradient: 10-80% of EtOAc) afforded 37 mg (47%) of the e title compound as a white solid. <sup>1</sup>H NMR (400 MHz, DMSO-*d*<sub>6</sub>) δ 10.38 (s, 1H), 10.24 (s, 1H), 8.53 (d, *J* = 2.2 Hz, 1H), 8.47 (d, *J* = 2.2 Hz, 1H), 7.98 (s, 1H), 7.93 (s, 1H), 7.58 (d, *J* = 8.1 Hz, 1H), 7.43 – 7.36 (m, 5H), 7.32 (d, *J* = 7.8 Hz, 1H), 6.46 (dd, *J* = 17.0, 10.1 Hz, 1H), 6.27 (dd, *J* = 17.0, 2.0 Hz, 1H), 5.77 (dd, *J* = 10.1, 2.0 Hz, 1H), 5.63 (s, 2H), 3.69 (s, 2H), 3.61 – 3.49 (m, 2H), 0.91 – 0.76 (m, 2H), -0.11 (s, 9H) ppm. <sup>13</sup>C NMR (100 MHz, DMSO-*d*<sub>6</sub>) δ 169.0, 163.4, 145.0, 139.7, 136.7, 134.9, 134.8, 131.9, 131.4, 131.2, 130.3, 129.5, 128.3, 127.6, 127.1, 121.8, 118.8, 117.4, 114.6, 72.7, 65.6, 42.2, 17.2, -1.3 ppm. TLC-MS (ESI) *m/z*: [M + Na + MeOH]<sup>+</sup>. HPLC *t*<sub>ret</sub> = 12.97 min. (Method D)

*N*-(3-(5-(2-(2,4-difluorophenyl)acetamido)-1-((2-(trimethylsilyl)ethoxy)methyl)-1*H*-pyrrolo[2,3-*b*]pyridin-3-yl)phenyl)acrylamide (**119**):

The preparation was carried out following *General Procedure E* starting from 117 mg of **101** (0.24 mmol) and using 0.46 mL of K<sub>2</sub>CO<sub>3</sub> (0.5 M sol.). The reaction was carried out at room temperature. Flash purification by eluting with hexane/EtOAc (gradient: 30-60% of EtOAc) afforded 66 mg (49%) of the e title compound as a white solid. <sup>1</sup>H NMR (400 MHz, DMSO-*d*<sub>6</sub>) δ 10.40 (s, 1H), 10.24 (s, 1H), 8.55 (d, *J* = 2.2 Hz, 1H), 8.50 (d, *J* = 2.2 Hz, 1H), 8.00 (s, 1H), 7.95 (s, 1H), 7.60 (d, *J* = 8.8 Hz, 1H), 7.52 – 7.44 (m, 1H), 7.42 (d,



$J = 7.9$  Hz, 1H), 7.34 (d,  $J = 7.8$  Hz, 1H), 7.29 – 7.18 (m, 1H), 7.12 – 7.03 (m, 1H), 6.48 (dd,  $J = 17.0, 10.1$  Hz, 1H), 6.28 (dd,  $J = 17.0, 2.0$  Hz, 1H), 5.79 (dd,  $J = 10.1, 2.0$  Hz, 1H), 5.66 (s, 2H), 3.78 (s, 2H), 3.65 – 3.52 (m, 2H), 0.89 – 0.81 (m, 2H), -0.09 (s, 9H) ppm.  $^{13}\text{C}$  NMR (100 MHz, DMSO- $d_6$ )  $\delta$  168.1, 163.3, 144.9, 139.6, 136.6, 134.7, 133.1, 131.9, 130.2, 129.4, 127.5, 127.0, 121.7, 118.6, 117.4, 114.5, 103.8, 103.6, 72.6, 65.6, 35.4, 17.2, -1.4 ppm. TLC-MS (ESI)  $m/z$ : 585.3  $[\text{M} + \text{Na}]^+$ ; 561.2  $[\text{M} - \text{H}]^-$ . HPLC  $t_{\text{ret}} = 10.22$  min. (Method C)

*N*-(3-(3-acrylamidophenyl)-1-((2-(trimethylsilyl)ethoxy)methyl)-1H-pyrrolo[2,3-*b*]pyridin-5-yl)-3-chloro-5-fluorobenzamide (**120**):

The preparation was carried out following *General Procedure E* starting from 127 mg of **102** (0.25 mmol) and using 0.45 mL of  $\text{K}_2\text{CO}_3$  (0.5 M sol.). The reaction was carried out at 80 °C. Flash purification by eluting with hexane/EtOAc (gradient: 10-70% of EtOAc) afforded 81 mg (57%) of the title compound as a white solid.  $^1\text{H}$  NMR (400 MHz, DMSO- $d_6$ )  $\delta$  10.60 (s, 1H), 10.25 (s, 1H), 8.64 (dd,  $J = 5.1, 2.1$  Hz, 2H), 8.02 (s, 1H), 7.99 (s, 1H), 7.95 (s, 1H), 7.82 (d,  $J = 8.7$  Hz, 1H), 7.73 (dd,  $J = 8.5, 1.9$  Hz, 1H), 7.61 (d,  $J = 8.0$  Hz, 1H), 7.44 (t,  $J = 7.8$  Hz, 1H), 7.38 (d,  $J = 7.7$  Hz, 1H), 6.46 (dd,  $J = 17.0, 10.1$  Hz, 1H), 6.27 (dd,  $J = 17.0, 1.9$  Hz, 1H), 5.77 (dd,  $J = 10.1, 1.9$  Hz, 1H), 5.68 (s, 2H), 3.66 – 3.53 (m, 2H), 0.93 – 0.77 (m, 2H), -0.09 (s, 9H) ppm.  $^{13}\text{C}$  NMR (100 MHz, DMSO- $d_6$ )  $\delta$  163.3, 163.0, 160.8, 145.3, 139.7, 138.1, 138.0, 134.7, 134.4, 134.3, 131.9, 129.6, 129.5, 127.7, 127.1, 124.0, 124.0, 121.8, 120.8, 120.5, 119.3, 119.1, 117.5, 117.4, 117.4, 114.7, 114.0, 113.8, 72.6, 65.5, 17.1, -1.1 ppm. TLC-MS (ESI)  $m/z$ : 586.9  $[\text{M} + \text{Na}]^+$ ; 563.0  $[\text{M} - \text{H}]^-$ ; 598.9  $[\text{M} + \text{Cl}]^-$ . HPLC  $t_{\text{ret}} = 13.15$  min. (Method D)

*N*-(3-(5-(2-(5-chloro-2,4-difluorophenyl)acetamido)-1-((2-(trimethylsilyl)ethoxy)methyl)-1H-pyrrolo[2,3-*b*]pyridin-3-yl) phenyl)acrylamide (**121**):

The preparation was carried out following *General Procedure E* starting from 102 mg of **103** (0.19 mmol) and using 0.35 mL of  $\text{K}_2\text{CO}_3$  (0.5 M sol.). The reaction was carried out at 80 °C. Flash purification by eluting with hexane/EtOAc (gradient: 10-80% of EtOAc) afforded 45 mg (47%) of the title compound as a white solid.  $^1\text{H}$  NMR (400 MHz, DMSO- $d_6$ )  $\delta$  10.42 (s, 1H), 10.24 (s, 1H), 8.53 (d,  $J = 2.2$  Hz, 1H), 8.47 (d,  $J = 2.2$  Hz, 1H), 7.99 (s, 1H), 7.94 (s, 1H), 7.69 (t,  $J = 8.0$  Hz, 1H), 7.57 (d,  $J = 8.1$  Hz, 1H), 7.51 (t,  $J = 9.6$  Hz, 1H), 7.41 (t,  $J = 7.9$  Hz, 1H), 7.32 (d,  $J = 7.7$  Hz, 1H), 6.46 (dd,  $J = 17.0, 10.1$  Hz, 1H), 6.27 (dd,  $J = 17.0, 2.0$  Hz, 1H), 5.77 (dd,  $J = 10.1, 2.0$  Hz, 1H), 5.64 (s, 2H),

3.79 (s, 2H), 3.65 – 3.50 (m, 2H), 0.91 – 0.74 (m, 2H), -0.11 (s, 9H) ppm. <sup>13</sup>C NMR (100 MHz, DMSO-*d*<sub>6</sub>) δ 167.6, 163.3, 144.9, 139.7, 136.6, 134.7, 133.0, 132.9, 131.9, 130.2, 129.5, 127.6, 127.1, 121.8, 118.7, 117.5, 114.4, 105.6, 105.3, 105.1, 72.6, 65.7, 35.5, 17.2, -1.2 ppm. TLC-MS (ESI) m/z: 651.4 [M + Na + MeOH]<sup>+</sup>. HPLC t<sub>ret</sub> = 12.98 min. (Method D)

*(E)*-*N*-(3-(4,4,5,5-tetramethyl-1,3,2-dioxaborolan-2-yl)phenyl)but-2-enamide (**122**):

87 mg of HATU (0.23 mmol) were added to an ice-cooled solution of 22 mg of (*E*)-2-butenoic acid (0.26 mmol), and 44 mg of DIPEA (0.35 mmol) in 5.6 mL of THF. After 15 min 50 mg of **78** (0.23 mmol) were added, the reaction the reaction was warmed to room temperature and stirred overnight. The solvent was evaporated and the crude obtained was purified by automated flash column chromatography on silica gel by eluting with hexane/EtOAc (gradient: 10-20% of EtOAc) to afford 39 mg (60%) of the titled product as yellow oil. <sup>1</sup>H NMR (400 MHz, CDCl<sub>3</sub>) δ 7.94 (d, *J* = 5.4 Hz, 1H), 7.71 (bs, 1H), 7.53 (d, *J* = 7.3 Hz, 1H), 7.33 (t, *J* = 7.7 Hz, 2H), 6.96 (dd, *J* = 15.1, 6.9 Hz, 1H), 5.92 (dd, *J* = 15.1, 1.7 Hz, 1H), 1.88 (dd, *J* = 6.9, 1.6 Hz, 3H), 1.33 (s, 12H) ppm. <sup>13</sup>C NMR (100 MHz, CDCl<sub>3</sub>) δ 164.2, 141.6, 137.7, 130.7, 128.7, 126.0, 125.6, 123.2, 84.0, 25.0, 18.0 ppm. TLC-MS (ESI) m/z: 288.2 [M + H]<sup>+</sup>. HPLC t<sub>ret</sub> = 10.95 min. (Method D)

*N*-(3-(4,4,5,5-tetramethyl-1,3,2-dioxaborolan-2-yl)phenyl)but-2-ynamide (**123**):

A solution of 21 mg 2-butynoic acid (0.25 mmol) in 3 mL of DCM was ice-cooled and 52 mg of DCC (0.25 mmol), 50 mg of **78** (0.23 mmol) and a catalytic amount of DMAP were added. The mixture was stirred at room temperature overnight. The solvent was evaporated and the crude obtained was purified by flash column chromatography on silica gel by eluting with hexane/EtOAc (gradient: 10-20% of EtOAc) to afford 31 mg (47) of the titled product as yellowish oil. <sup>1</sup>H NMR (400 MHz, CDCl<sub>3</sub>) δ 7.88 (dd, *J* = 8.1, 1.1 Hz, 1H), 7.63 (d, *J* = 1.4 Hz, 1H), 7.55 (d, *J* = 7.3 Hz, 1H), 7.47 (bs, 1H), 7.34 (t, *J* = 7.7 Hz, 1H), 1.99 (s, 3H), 1.33 (s, 12H) ppm. <sup>13</sup>C NMR (100 MHz, CDCl<sub>3</sub>) δ 151.1, 137.0, 131.2, 128.8, 125.8, 123.3, 84.5, 84.1, 77.2, 76.8, 75.5, 75.2. TLC-MS (ESI) m/z: 308.2 [M + Na]<sup>+</sup>; 340.3 [M + Na + MeOH]<sup>+</sup>; [M - H]<sup>-</sup> 283.9. HPLC t<sub>ret</sub> = 10.74 min. (Method D)

3-bromo-4-fluoroaniline (**126**):

A solution of 100 mg (0.45 mmol) of **125** in 8 mL of EtOH was heated to 75 °C. Then a solution of 382 mg SnCl<sub>2</sub> (2 mmol) in 2.5 mL of HCl (37%) was added dropwise to the mixture. After 30 min. reaction control by TLC showed complete consumption of **125**. The solvent and the HCl solution were evaporated giving 85 mg (> 99%) of the titled compound as a yellowish solid that was used without further purification. <sup>1</sup>H NMR (400 MHz, CDCl<sub>3</sub>) δ 6.93 – 6.81 (m, 2H), 6.59 – 6.50 (m, 1H), 3.58 (bs, 2H) ppm. <sup>13</sup>C NMR (100 MHz, CDCl<sub>3</sub>) δ 153.9, 151.6, 143.5, 119.3, 116.9, 116.7, 115.2, 115.2, 109.3, 109.1 ppm. TLC-MS (ESI) m/z: 187,7 [M + Na]<sup>+</sup>; 211,4 [M - H]<sup>-</sup>. HPLC t<sub>ret</sub> = 8.06 min. (Method D)

*4-methyl-3-(4,4,5,5-tetramethyl-1,3,2-dioxaborolan-2-yl)aniline (127):*

The preparation was carried out following *General Procedure A* starting from 100 mg of **124** (0.54 mmol) in 2 mL of dry dioxane. Flash purification (hexane/EtOAc (10–20%)) afforded 55 mg (44%) of the e title compound as a brown oil. <sup>1</sup>H NMR (400 MHz, CDCl<sub>3</sub>) δ 7.13 (d, J = 2.7 Hz, 1H), 6.97 (d, J = 8.1 Hz, 1H), 6.69 (dd, J = 8.1, 2.7 Hz, 1H), 3.51 (bs, 2H), 2.43 (s, 3H), 1.34 (s, 12H) ppm. <sup>13</sup>C NMR (100 MHz, CDCl<sub>3</sub>) δ 143.3, 134.9, 130.8, 122.6, 118.0, 83.5, 24.99, 21.3 ppm. TLC-MS (ESI) m/z: 234.2 [M + H]<sup>+</sup>. HPLC t<sub>ret</sub> = 7.66 min.

*4-fluoro-3-(4,4,5,5-tetramethyl-1,3,2-dioxaborolan-2-yl)aniline (128):*

The preparation was carried out following *General Procedure A* starting from 500 mg of **126** (2.65 mmol) in 10 mL of dry dioxane. Flash purification by eluting with hexane/EtOAc (gradient: 10-25% of EtOAc) afforded 270 mg (43%) of the e title compound as a brown oil. <sup>1</sup>H NMR (400 MHz, CDCl<sub>3</sub>) δ 7.15 (m, 1H), 6.88 (m, 2H), 4.48 (s, 2H), 1.35 (s, 12H) ppm. <sup>13</sup>C NMR (100 MHz, CDCl<sub>3</sub>) δ 163.3, 160.8, 139.1, 124.0, 123.9, 121.4, 121.3, 116.3, 116.0, 84.1, 24.9 ppm. TLC-MS (ESI) m/z: 260.7 [M + Na]<sup>+</sup>. HPLC t<sub>ret</sub> = 7.78 min. (Method D)

*N-(4-methyl-3-(4,4,5,5-tetramethyl-1,3,2-dioxaborolan-2-yl)phenyl)acrylamide (129):*

The reaction was carried out following *General Procedure B* starting from 60 mg of **127** (0.26 mmol) in 1.5 mL of DCM. Flash purification by eluting with hexane/EtOAc + 20% MeOH (gradient: 6-9%) afforded 68 mg (91%) of the e title compound as a yellowish solid. <sup>1</sup>H NMR (400 MHz, CDCl<sub>3</sub>) δ 7.87 (d, J = 6.7 Hz, 1H), 7.62 (d, J = 1.9 Hz, 1H), 7.36 (bs, 1H), 7.15 (d, J = 8.3 Hz, 1H), 6.40 (d, J = 16.2 Hz, 1H), 6.21 (dd, J = 16.9, 10.2

Hz, 1H), 5.72 (dd,  $J = 10.2, 1.2$  Hz, 1H), 2.49 (s, 3H), 1.33 (s, 12H) ppm.  $^{13}\text{C}$  NMR (100 MHz,  $\text{CDCl}_3$ )  $\delta$  163.5, 141.3, 134.8, 131.5, 130.7, 127.5, 127.1, 123.0, 83.7, 25.0, 21.7 ppm. TLC-MS (ESI)  $m/z$ : 288.2  $[\text{M} + \text{H}]^+$ ; 310.2  $[\text{M} + \text{Na}]^+$ . HPLC  $t_{\text{ret}} = 11.49$  min. (Method D)

*N*-(4-fluoro-3-(4,4,5,5-tetramethyl-1,3,2-dioxaborolan-2-yl)phenyl)acrylamide (**130**):

The reaction was carried out following *General Procedure B* starting from 270 mg of **128** (1.14 mmol) in 7 mL of DCM. Flash purification by eluting with hexane/EtOAc (gradient: 20-30% of EtOAc) afforded 199 mg (60%) of the e title compound as a yellowish solid.  $^1\text{H}$  NMR (400 MHz,  $\text{CDCl}_3$ )  $\delta$  7.97 – 7.79 (m, 1H), 7.74 – 7.63 (m, 1H), 7.49 (bs, 1H), 7.01 (t,  $J = 8.8$  Hz, 1H), 6.41 (d,  $J = 16.7$  Hz, 1H), 6.22 (dd,  $J = 16.9, 10.2$  Hz, 1H), 5.75 (dd,  $J = 10.2, 1.1$  Hz, 1H), 1.34 (s, 12H) ppm.  $^{13}\text{C}$  NMR (100 MHz,  $\text{CDCl}_3$ )  $\delta$  165.2, 163.6, 162.7, 133.5, 131.1, 128.2, 128.1, 128.0, 125.7, 125.6, 116.1, 115.9, 84.2, 25.0 ppm. TLC-MS (ESI)  $m/z$ : 314.0  $[\text{M} + \text{Na}]^+$ ; 289.8  $[\text{M} - \text{H}]^-$ . HPLC  $t_{\text{ret}} = 10.29$  min. (Method D)

*N*-(3-bromo-1-((2-(trimethylsilyl)ethoxy)methyl)-1H-pyrrolo[2,3-b]pyridin-5-yl)cyclopentanecarboxamide (**131**):

The reaction was carried out following *General Procedure D* using 500 mg of **82** (1.46 mmol) in 9 mL of DCM. Flash purification by eluting with hexane/EtOAc (gradient: 20-40% of EtOAc) afforded 568 mg (88%) of the e title compound as a yellow oil.  $^1\text{H}$  NMR (400 MHz,  $\text{CDCl}_3$ )  $\delta$  8.32 (d,  $J = 7.3$  Hz, 2H), 7.58 (bs, 1H), 7.36 (s, 1H), 5.61 (s, 2H), 3.52 (t, 2H), 2.86 – 2.70 (m, 1H), 2.05 – 1.57 (m, 8H), 0.89 (t, 3H), -0.06 (s, 9H) ppm.  $^{13}\text{C}$  NMR (100 MHz,  $\text{CDCl}_3$ )  $\delta$  175.5, 136.7, 129.9, 128.2, 121.1, 120.6, 90.5, 73.6, 66.7, 46.7, 30.8, 26.2, 17.9, -1.3 ppm. TLC-MS (ESI)  $m/z$ : 460.3  $[\text{M} + \text{Na}]^+$ ; 436.1  $[\text{M} - \text{H}]^-$ . HPLC  $t_{\text{ret}} = 13.07$  min. (Method D)

*(E)*-*N*-(3-(3-(but-2-enamido)phenyl)-1-((2-(trimethylsilyl)ethoxy)methyl)-1H-pyrrolo[2,3-b]pyridin-5-yl)cyclopentanecarboxamide (**132**):

The preparation was carried out following *General Procedure E* starting from 118 mg of **131** (0.26 mmol) and using 0.6 mL of  $\text{K}_2\text{CO}_3$  (0.5 M sol.). The reaction was carried out at room temperature. Flash purification by eluting with hexane/EtOAc (gradient: 30-40% of EtOAc) afforded 79 mg (56%) of the e title compound as a yellow solid.  $^1\text{H}$  NMR

(400 MHz, CDCl<sub>3</sub>)  $\delta$  8.26 (d,  $J$  = 2.2 Hz, 1H), 8.21 (d,  $J$  = 2.2 Hz, 1H), 8.05 (s, 1H), 7.91 (s, 1H), 7.63 (s, 1H), 7.31 (d,  $J$  = 6.4 Hz, 1H), 7.13 – 7.05 (m,  $J$  = 9.5, 5.3 Hz, 3H), 6.80 (dd,  $J$  = 15.1, 6.9 Hz, 1H), 5.86 (dd,  $J$  = 15.1, 1.6 Hz, 1H), 5.42 (s, 2H), 3.45 – 3.34 (m, 2H), 2.58 (m, 1H), 1.85 – 1.64 (m, 4H), 1.67 (dd,  $J$  = 6.9, 1.5 Hz, 3H), 1.64 – 1.51 (m, 2H), 1.51 – 1.34 (m, 2H), 0.79 – 0.70 (m, 2H), -0.23 (s, 9H) ppm. <sup>13</sup>C NMR (100 MHz, CDCl<sub>3</sub>)  $\delta$  175.7, 164.7, 145.9, 141.5, 138.8, 137.7, 135.09, 129.5, 129.3, 126.1, 125.7, 122.7, 120.9, 118.5, 118.4, 118.2, 116.0, 73.2, 66.5, 46.5, 30.7, 26.2, 17.9, -1.3 ppm. TLC-MS (ESI) m/z: 519.6 [M + H]<sup>+</sup>; 541.5[M + Na]<sup>+</sup>; 517.6 [M - H]<sup>-</sup>; 553.5 [M + Cl]<sup>-</sup>. HPLC  $t_{\text{ret}}$  = 10.37 min. (Method C)

*N*-(3-(3-(but-2-ynamido)phenyl)-1-((2-(trimethylsilyl)ethoxy)methyl)-1H-pyrrolo[2,3-*b*]pyridin-5-yl)cyclopentanecarboxamide (**133**):

The preparation was carried out following *General Procedure E* starting from 102 mg of **131** (0.23) and using 0.5 mL of K<sub>2</sub>CO<sub>3</sub> (0.5 M sol.). The reaction was carried out at room temperature. Flash purification by eluting with hexane/EtOAc (gradient: 30-40% of EtOAc) afforded 32 mg (27%) of the e title compound as a yellow solid. <sup>1</sup>H NMR (400 MHz, CDCl<sub>3</sub>)  $\delta$  8.55 (s, 1H), 8.35 (s, 1H), 7.85 (s, 1H), 7.77 (s, 1H), 7.53 (s, 2H), 7.47 (s, 1H), 7.37 (d,  $J$  = 3.9 Hz, 2H), 5.66 (s, 2H), 3.61 – 3.52 (m, 2H), 2.81 – 2.68 (m, 1H), 1.96 (dd,  $J$  = 18.1, 11.1 Hz, 7H), 1.78 (d,  $J$  = 16.9 Hz, 2H), 1.69 – 1.50 (m, 2H), 0.93 (d,  $J$  = 8.3 Hz, 2H), -0.06 (s, 9H) ppm. <sup>13</sup>C NMR (100 MHz, CDCl<sub>3</sub>)  $\delta$  175.3, 151.4, 146.0, 138.1, 137.5, 135.5, 129.8, 129.3, 126.4, 123.4, 120.7, 118.4, 118.3, 118.0, 116.0, 84.7, 75.6, 73.3, 66.6, 46.8, 30.76, 26.21, 14.25, 3.9, -1.3 ppm. TLC-MS (ESI) m/z: 517.5 [M + H]<sup>+</sup>; <sup>539.5</sup>[M + Na]<sup>+</sup>; 515.4 [M - H]<sup>-</sup>; 551.5[M + Cl]<sup>-</sup>. HPLC  $t_{\text{ret}}$  = 10.11min. (Method C)

*N*-(3-(5-acrylamido-2-methylphenyl)-1-((2-(trimethylsilyl)ethoxy)methyl)-1H-pyrrolo[2,3-*b*]pyridin-5-yl)cyclopentanecarboxamide (**134**):

The preparation was carried out following *General Procedure E* starting from 51 mg of **131** (0.12 mmol) and using 0.25 mL of K<sub>2</sub>CO<sub>3</sub> (0.5 M sol.). The reaction was carried out at room temperature. Flash purification by eluting with DCM/MeOH (gradient: 0.5-1.5% of MeOH) afforded 79 mg (56%) of the e title compound as a yellow solid. <sup>1</sup>H NMR (400 MHz, CDCl<sub>3</sub>)  $\delta$  8.31 (d,  $J$  = 1.6 Hz, 1H), 8.13 (s, 1H), 7.66 (s, 1H), 7.56 (d,  $J$  = 7.9 Hz, 1H), 7.46 (d,  $J$  = 7.2 Hz, 2H), 7.32 (s, 1H), 7.23 (s, 1H), 6.40 (d,  $J$  = 16.0 Hz, 1H), 6.26 (dd,  $J$  = 16.7, 10.2 Hz, 1H), 5.72 (dd,  $J$  = 10.1, 1.2 Hz, 1H), 5.68 (s, 2H), 3.64 – 3.52 (m, 2H), 2.79 – 2.63 (m, 1H), 2.27 (s, 3H), 2.04 – 1.82 (m, 4H), 1.82 – 1.66 (m, 2H), 1.66 –

1.54 (m, 2H), 0.97 – 0.88 (m, 2H), -0.06 (s, 9H) ppm. <sup>13</sup>C NMR (100 MHz, CDCl<sub>3</sub>) δ 175.3, 163.8, 145.5, 137.5, 135.8, 133.8, 132.9, 131.3, 128.9, 127.5, 122.1, 121.2, 119.9, 119.2, 115.4, 73.3, 66.5, 46.7, 30.7, 26.2, 20.4, 18.0, -1.3 ppm. TLC-MS (ESI) m/z: 541.5 [M + Na]<sup>+</sup>; 517.4[M - H]<sup>-</sup>; 553.4[M + Cl]<sup>-</sup>. HPLC t<sub>ret</sub> = 12.77 min. (Method D)

*N*-(3-(5-acrylamido-2-fluorophenyl)-1-((2-(trimethylsilyl)ethoxy)methyl)-1H-pyrrolo[2,3-*b*]pyridin-5-yl)cyclopentanecarboxamide (**135**):

The preparation was carried out following *General Procedure E* starting from 100 mg of **131** (0.23 mmol) and using 0.5 mL of K<sub>2</sub>CO<sub>3</sub> (0.5 M sol.). The reaction was carried out at room temperature. Flash purification by eluting with hexane/EtOAc (gradient: 20-50% of EtOAc) afforded 58 mg (48%) of the e title compound as a yellow solid. <sup>1</sup>H NMR (400 MHz, CDCl<sub>3</sub>) δ 8.47 (s, 1H), 8.35 (d, *J* = 1.8 Hz, 2H), 7.79 (s, 2H), 7.65 (d, *J* = 1.6 Hz, 1H), 7.58 (d, *J* = 7.8 Hz, 1H), 7.06 (t, *J* = 9.6 Hz, 1H), 6.42 (d, *J* = 16.1 Hz, 1H), 6.31 (dd, *J* = 16.8, 10.0 Hz, 1H), 5.72 (d, *J* = 10.8 Hz, 1H), 5.65 (s, 2H), 3.63 – 3.52 (m, 2H), 2.85 – 2.69 (m, 1H), 2.03 – 1.84 (m, 4H), 1.84 – 1.69 (m, 2H), 1.69 – 1.55 (m, 2H), 0.97 – 0.88 (m, *J* = 11.1, 5.3 Hz, 2H), -0.06 (s, 9H) ppm. <sup>13</sup>C NMR (100 MHz, CDCl<sub>3</sub>) δ 175.7, 164.0, 157.5, 155.1, 145.5, 137.5, 134.5, 131.3, 129.2, 129.1, 127.7, 122.4, 121.1, 120.9, 119.5, 118.7, 116.6, 116.3, 109.1, 73.4, 66.6, 46.7, 30.8, 26.2, 17.9, -1.3 ppm. TLC-MS (ESI) m/z: 545.4 [M + Na]<sup>+</sup>; 521.4 [M - H]<sup>-</sup>; 557.4[M + Cl]<sup>-</sup>. HPLC t<sub>ret</sub> = 10.47 min. (Method C)

# Bibliography

- (1) Shabab, T.; Khanabdali, R.; Moghadamtousi, S. Z.; Kadir, H. A.; Mohan, G. Neuroinflammation pathways: a general review. *Int J Neurosci* **2017**, *127* (7), 624-633. DOI: 10.1080/00207454.2016.1212854.
- (2) DiSabato, D. J.; Quan, N.; Godbout, J. P. Neuroinflammation: the devil is in the details. *J Neurochem* **2016**, *139 Suppl 2*, 136-153. DOI: 10.1111/jnc.13607.
- (3) Jäkel, S.; Dimou, L. Glial Cells and Their Function in the Adult Brain: A Journey through the History of Their Ablation. *Front Cell Neurosci* **2017**, *11*, 24. DOI: 10.3389/fncel.2017.00024.
- (4) Hanslik, K. L.; Marino, K. M.; Ulland, T. K. Modulation of Glial Function in Health, Aging, and Neurodegenerative Disease. *Front Cell Neurosci* **2021**, *15*, 718324. DOI: 10.3389/fncel.2021.718324.
- (5) Ransohoff, R. M. How neuroinflammation contributes to neurodegeneration. *Science* **2016**, *353* (6301), 777-783. DOI: 10.1126/science.aag2590.
- (6) Liu, T.; Zhang, L.; Joo, D.; Sun, S.-C. NF- $\kappa$ B signaling in inflammation. *Signal Transduct Target* **2017**, *2* (1), 1-9.
- (7) Sochocka, M.; Diniz, B. S.; Leszek, J. Inflammatory response in the CNS: friend or foe? *Mol Neurobiol* **2017**, *54* (10), 8071-8089. DOI: 10.1007/s12035-016-0297-1.
- (8) Salvi, V.; Sozio, F.; Sozzani, S.; Del Prete, A. Role of Atypical Chemokine Receptors in Microglial Activation and Polarization. *Front Aging Neurosci* **2017**, *9*, 148. DOI: 10.3389/fnagi.2017.00148.
- (9) Martinez, F. O.; Gordon, S. The M1 and M2 paradigm of macrophage activation: time for reassessment. *F1000Prime Rep* **2014**, *6*, 13. DOI: 10.12703/P6-13.
- (10) Tang, Y.; Le, W. Differential Roles of M1 and M2 Microglia in Neurodegenerative Diseases. *Mol Neurobiol* **2016**, *53* (2), 1181-1194. DOI: 10.1007/s12035-014-9070-5.
- (11) Hickman, S.; Izzy, S.; Sen, P.; Morsett, L.; El Khoury, J. Microglia in neurodegeneration. *Nat Neurosci* **2018**, *21* (10), 1359-1369. DOI: 10.1038/s41593-018-0242-x.
- (12) Subhramanyam, C. S.; Wang, C.; Hu, Q.; Dheen, S. T. Microglia-mediated neuroinflammation in neurodegenerative diseases. *Semin Cell Dev Biol* **2019**, *94*, 112-120. DOI: 10.1016/j.semcdb.2019.05.004.
- (13) Salas, I. H.; Burgado, J.; Allen, N. J. Glia: victims or villains of the aging brain? *Neurobiol Dis* **2020**, *143*, 105008. DOI: 10.1016/j.nbd.2020.105008.
- (14) Ho, M. S. Microglia in Parkinson's disease. *Neuroglia in Neurodegenerative Diseases* **2019**, 335-353.
- (15) Mehra, S.; Sahay, S.; Maji, S. K.  $\alpha$ -Synuclein misfolding and aggregation: Implications in Parkinson's disease pathogenesis. *Biochim Biophys Acta Proteins Proteom* **2019**, *1867* (10), 890-908. DOI: 10.1016/j.bbapap.2019.03.001.
- (16) Ouchi, Y.; Yagi, S.; Yokokura, M.; Sakamoto, M. Neuroinflammation in the living brain of Parkinson's disease. *Parkinsonism Relat Disord* **2009**, *15 Suppl 3*, S200-204. DOI: 10.1016/S1353-8020(09)70814-4.
- (17) Higaki, H.; Choudhury, M. E.; Kawamoto, C.; Miyamoto, K.; Islam, A.; Ishii, Y.; Miyanishi, K.; Takeda, H.; Seo, N.; Sugimoto, K.; et al. The hypnotic bromovalerylurea ameliorates 6-hydroxydopamine-induced dopaminergic neuron loss while suppressing expression of interferon regulatory factors by microglia. *Neurochem Int* **2016**, *99*, 158-168. DOI: 10.1016/j.neuint.2016.06.013.
- (18) Rojanathammanee, L.; Murphy, E. J.; Combs, C. K. Expression of mutant alpha-synuclein modulates microglial phenotype in vitro. *J Neuroinflammation* **2011**, *8*, 44. DOI: 10.1186/1742-2094-8-44.

- (19) Roodveldt, C.; Labrador-Garrido, A.; Gonzalez-Rey, E.; Fernandez-Montesinos, R.; Caro, M.; Lachaud, C. C.; Waudby, C. A.; Delgado, M.; Dobson, C. M.; Pozo, D. Glial innate immunity generated by non-aggregated alpha-synuclein in mouse: differences between wild-type and Parkinson's disease-linked mutants. *PLoS One* **2010**, *5* (10), e13481. DOI: 10.1371/journal.pone.0013481.
- (20) Park, J. Y.; Paik, S. R.; Jou, I.; Park, S. M. Microglial phagocytosis is enhanced by monomeric alpha-synuclein, not aggregated alpha-synuclein: implications for Parkinson's disease. *Glia* **2008**, *56* (11), 1215-1223. DOI: 10.1002/glia.20691.
- (21) Kiernan, M. C.; Vucic, S.; Cheah, B. C.; Turner, M. R.; Eisen, A.; Hardiman, O.; Burrell, J. R.; Zoing, M. C. Amyotrophic lateral sclerosis. *Lancet* **2011**, *377* (9769), 942-955. DOI: 10.1016/S0140-6736(10)61156-7.
- (22) Juliani, J.; Vassileff, N.; Spiers, J. G. Inflammatory-Mediated Neuron-Glia Communication Modulates ALS Pathophysiology. *J Neurosci* **2021**, *41* (6), 1142-1144. DOI: 10.1523/JNEUROSCI.1970-20.2020.
- (23) Correia, A. S.; Patel, P.; Dutta, K.; Julien, J. P. Inflammation Induces TDP-43 Mislocalization and Aggregation. *PLoS One* **2015**, *10* (10), e0140248. DOI: 10.1371/journal.pone.0140248.
- (24) Hensley, K.; Fedynyshyn, J.; Ferrell, S.; Floyd, R. A.; Gordon, B.; Grammas, P.; Hamdheydari, L.; Mhatre, M.; Mou, S.; Pye, Q. N. Message and protein-level elevation of tumor necrosis factor  $\alpha$  (TNF $\alpha$ ) and TNF $\alpha$ -modulating cytokines in spinal cords of the G93A-SOD1 mouse model for amyotrophic lateral sclerosis. *Neurobiol of dis* **2003**, *14* (1), 74-80. DOI: 10.1016/s0969-9961(03)00087-1.
- (25) Geloso, M.; Corvino, V.; Marchese, E.; Serrano, A.; Michetti, F.; D'Ambrosi, N. The Dual Role of Microglia in ALS: Mechanisms and Therapeutic Approaches. *Front Aging Neurosci* **2017**, *9*, Review. DOI: 10.3389/fnagi.2017.00242.
- (26) Lee, J. D.; Lo, M. W.; Fung, J. N. T.; Woodruff, T. M. Neuroinflammation in Huntington's Disease. *Neurodegener Dis Biomarkers*, Springer, **2022**; 215-233. DOI: 10.1007/978-1-0716-1712-0\_9.
- (27) Yang, H.-M.; Yang, S.; Huang, S.-S.; Tang, B.-S.; Guo, J.-F. Microglial activation in the pathogenesis of Huntington's disease. *Front aging neurosci* **2017**, *9*, 193. DOI: 10.3389/fnagi.2017.00193.
- (28) Crotti, A.; Glass, C. K. The choreography of neuroinflammation in Huntington's disease. *Trends Immunol* **2015**, *36* (6), 364-373. DOI: 10.1016/j.it.2015.04.007.
- (29) Palpagama, T. H.; Waldvogel, H. J.; Faull, R. L. M.; Kwakowsky, A. The Role of Microglia and Astrocytes in Huntington's Disease. *Front Mol Neurosci* **2019**, *12*, 258. DOI: 10.3389/fnmol.2019.00258.
- (30) Tai, Y. F.; Pavese, N.; Gerhard, A.; Tabrizi, S. J.; Barker, R. A.; Brooks, D. J.; Piccini, P. Imaging microglial activation in Huntington's disease. *Brain Res Bull* **2007**, *72* (2-3), 148-151. DOI: 10.1016/j.brainresbull.2006.10.029.
- (31) Tai, Y. F.; Pavese, N.; Gerhard, A.; Tabrizi, S. J.; Barker, R. A.; Brooks, D. J.; Piccini, P. Microglial activation in presymptomatic Huntington's disease gene carriers. *Brain* **2007**, *130* (Pt 7), 1759-1766. DOI: 10.1093/brain/awm044.
- (32) Sampath, D.; Sathyanesan, M.; Newton, S. S. Cognitive dysfunction in major depression and Alzheimer's disease is associated with hippocampal-prefrontal cortex dysconnectivity. *Neuropsychiatr Dis Treat* **2017**, *13*, 1509-1519. DOI: 10.2147/ndt.s136122.
- (33) Hampel, H.; Hardy, J.; Blennow, K.; Chen, C.; Perry, G.; Kim, S. H.; Villemagne, V. L.; Aisen, P.; Vendruscolo, M.; Iwatsubo, T. The Amyloid- $\beta$  Pathway in Alzheimer's Disease. *Mol Psychiatry* **2021**, 1-23. DOI: 10.1038/s41380-021-01249-0.



- (34) Sarlus, H.; Heneka, M. T. Microglia in Alzheimer's disease. *J Clin Invest* **2017**, *127* (9), 3240-3249. DOI: 10.1172/JCI90606.
- (35) Chen, Y.; Colonna, M. Two-faced behavior of microglia in Alzheimer's disease. *Nat neurosci* **2021**, *25* (1), 3-4. DOI: 10.1038/s41593-021-00963-w.
- (36) Martin, E.; Boucher, C.; Fontaine, B.; Delarasse, C. Distinct inflammatory phenotypes of microglia and monocyte-derived macrophages in Alzheimer's disease models: Effects of aging and amyloid pathology. *Aging cell* **2017**, *16* (1), 27-38. DOI: 10.1111/ace1.12522.
- (37) Imbimbo, B. P. The potential role of non-steroidal anti-inflammatory drugs in treating Alzheimer's disease. *Expert Opin Investig Drugs* **2004**, *13* (11), 1469-1481. DOI: 10.1517/13543784.13.11.1469.
- (38) Wang, Y. J.; Montegudo, A.; Downey, M. A.; Ashton-Rickardt, P. G.; Elmaleh, D. R. Cromolyn inhibits the secretion of inflammatory cytokines by human microglia (HMC3). *Sci Rep* **2021**, *11* (1), 8054. DOI: 10.1038/s41598-021-85702-8.
- (39) Zhang, C.; Griciuc, A.; Hudry, E.; Wan, Y.; Quinti, L.; Ward, J.; Forte, A. M.; Shen, X.; Ran, C.; Elmaleh, D. R. Cromolyn reduces levels of the Alzheimer's disease-associated amyloid  $\beta$ -protein by promoting microglial phagocytosis. *Sci Rep* **2018**, *8* (1), 1-9. DOI: 10.1038/s41598-018-19641-2.
- (40) Brazier, D.; Perry, R.; Keane, J.; Barrett, K.; Elmaleh, D. R. Pharmacokinetics of Cromolyn and Ibuprofen in Healthy Elderly Volunteers. *Clin Drug Investig* **2017**, *37* (11), 1025-1034. DOI: 10.1007/s40261-017-0549-5.
- (41) ClinicalTrials.gov. <https://clinicaltrials.gov/ct2/show/NCT04570644?term=cromolyn&cond=Alzheimer+Disease&draw=2&rank=1>. (accessed 2021 14 November).
- (42) ClinicalTrials.gov. <https://clinicaltrials.gov/ct2/show/NCT02547818?term=cromolyn&cond=Alzheimer+Disease&draw=2&rank=1>. (accessed 2021 14 November)
- (43) Albertini, C.; Naldi, M.; Petralla, S.; Strocchi, S.; Grifoni, D.; Monti, B.; Bartolini, M.; Bolognesi, M. L. From Combinations to Single-Molecule Polypharmacology-Cromolyn-Ibuprofen Conjugates for Alzheimer's Disease. *Molecules* **2021**, *26* (4), 1112. DOI: 10.3390/molecules26041112.
- (44) Li, Y.; Zhou, Y.; Jiang, J.; Wang, X.; Fu, Y.; Gong, T.; Sun, X.; Zhang, Z. Mechanism of brain targeting by dexibuprofen prodrugs modified with ethanolamine-related structures. *J Cereb Blood Flow Metab* **2015**, *35* (12), 1985-1994. DOI: 10.1038/jcbfm.2015.160.
- (45) Shoup, T. M.; Griciuc, A.; Normandin, M. D.; Quinti, L.; Walsh, L. V.; Dhaynaut, M.; Moon, S. H.; Guehl, N. J.; Brugarolas, P.; Elmaleh, D. R.; et al. Evaluation of Fluorinated Cromolyn Derivatives as Potential Therapeutics for Alzheimer's Disease. *J Alzheimers Dis* **2021**, *80* (2), 775-786. DOI: 10.3233/jad-201419.
- (46) Wager, T. T.; Hou, X.; Verhoest, P. R.; Villalobos, A. Central Nervous System Multiparameter Optimization Desirability: Application in Drug Discovery. *ACS Chem Neurosci* **2016**, *7* (6), 767-775. DOI: 10.1021/acchemneuro.6b00029.
- (47) Haddad, J. J. VX-745. Vertex Pharmaceuticals. *Curr Opin Investig Drugs* **2001**, *2* (8), 1070-1076.
- (48) Alam, J. J. Selective Brain-Targeted Antagonism of p38 MAPK $\alpha$  Reduces Hippocampal IL-1 $\beta$  Levels and Improves Morris Water Maze Performance in Aged Rats. *J Alzheimers Dis* **2015**, *48* (1), 219-227. DOI: 10.3233/jad-150277.
- (49) Prins, N. D.; Harrison, J. E.; Chu, H. M.; Blackburn, K.; Alam, J. J.; Scheltens, P.; Investigators, R.-S. S. A phase 2 double-blind placebo-controlled 24-week treatment clinical study of the p38 alpha kinase

- inhibitor neflamapimod in mild Alzheimer's disease. *Alzheimers Res Ther* **2021**, *13* (1), 106. DOI: 10.1186/s13195-021-00843-2.
- (50) Asih, P. R.; Prikas, E.; Stefanoska, K.; Tan, A. R. P.; Ahel, H. I.; Ittner, A. Functions of p38 MAP Kinases in the Central Nervous System. *Front Mol Neurosci* **2020**, *13*, 570586. DOI: 10.3389/fnmol.2020.570586.
- (51) Youdim, M. B.; Weinstock, M. Molecular basis of neuroprotective activities of rasagiline and the anti-Alzheimer drug TV3326 [(N-propargyl-(3R)aminoindan-5-YL)-ethyl methyl carbamate]. *Cell Mol Neurobiol* **2001**, *21* (6), 555-573. DOI: 10.1023/a:1015131516649.
- (52) Song, I. U.; Im, J. J.; Jeong, H.; Na, S. H.; Chung, Y. A. Possible neuroprotective effects of rasagiline in Alzheimer's disease: a SPECT study. *Acta Radiol* **2020**, *62* (6), 784-790. DOI: 10.1177/0284185120940264.
- (53) Matthews, D. C.; Ritter, A.; Thomas, R. G.; Andrews, R. D.; Lukic, A. S.; Revta, C.; Kinney, J. W.; Tousi, B.; Leverenz, J. B.; Fillit, H.; et al. Rasagiline effects on glucose metabolism, cognition, and tau in Alzheimer's dementia. *Alzheimers Dement (N Y)* **2021**, *7* (1), e12106. DOI: 10.1002/trc2.12106.
- (54) Maruyama, W.; Akao, Y.; Carrillo, M. C.; Kitani, K.; Youdium, M. B.; Naoi, M. Neuroprotection by propargylamines in Parkinson's disease: suppression of apoptosis and induction of prosurvival genes. *Neurotoxicol Teratol* **2002**, *24* (5), 675-682. DOI: 10.1016/s0892-0362(02)00221-0.
- (55) Duffy, J. P.; Harrington, E. M.; Salituro, F. G.; Cochran, J. E.; Green, J.; Gao, H.; Bemis, G. W.; Evindar, G.; Galullo, V. P.; Ford, P. J.; et al. The Discovery of VX-745: A Novel and Selective p38 $\alpha$  Kinase Inhibitor. *ACS Med Chem Lett* **2011**, *2* (10), 758-763. DOI: 10.1021/ml2001455.
- (56) Francesco, S.; Guy, B.; Ghotas, E. Inhibitors of p38. WO0170695A1 **2001**.
- (57) Qiu, L.; Wang, F.; Liu, S.; Chen, X. L. Current understanding of tyrosine kinase BMX in inflammation and its inhibitors. *Burns Trauma* **2014**, *2* (3), 121-124. DOI: 10.4103/2321-3868.135483.
- (58) Wu, J. C.; Chen, K. Y.; Yu, Y. W.; Huang, S. W.; Shih, H. M.; Chiu, W. T.; Chiang, Y. H.; Shiao, C. Y. Location and level of Etk expression in neurons are associated with varied severity of traumatic brain injury. *PLoS One* **2012**, *7* (6), e39226. DOI: 10.1371/journal.pone.0039226.
- (59) Yu, Y. W.; Hsieh, T. H.; Chen, K. Y.; Wu, J. C.; Hoffer, B. J.; Greig, N. H.; Li, Y.; Lai, J. H.; Chang, C. F.; Lin, J. W.; et al. Glucose-Dependent Insulinotropic Polypeptide Ameliorates Mild Traumatic Brain Injury-Induced Cognitive and Sensorimotor Deficits and Neuroinflammation in Rats. *J Neurotrauma* **2016**, *33* (22), 2044-2054. DOI: 10.1089/neu.2015.4229.
- (60) Ray, S.; Murkin, A. S. New Electrophiles and Strategies for Mechanism-Based and Targeted Covalent Inhibitor Design. *Biochemistry* **2019**, *58* (52), 5234-5244. DOI: 10.1021/acs.biochem.9b00293.
- (61) Forster, M.; Liang, X. J.; Schröder, M.; Gerstenecker, S.; Chaikuad, A.; Knapp, S.; Laufer, S.; Gehring, M. Discovery of a Novel Class of Covalent Dual Inhibitors Targeting the Protein Kinases BMX and BTK. *Int J Mol Sci* **2020**, *21* (23). DOI: 10.3390/ijms21239269.
- (62) World-Alzheimer-Report-2021. <https://www.alzint.org/u/World-Alzheimer-Report-2021.pdf>. (accessed 2021 15 November).
- (63) Wortmann, M. Dementia: a global health priority - highlights from an ADI and World Health Organization report. *Alzheimers Res Ther* **2012**, *4* (5), 40. DOI: 10.1186/alzrt143.
- (64) <https://www.alz.co.uk/research/world-report-2019>. *World Alzheimer Report 2019: Attitudes to dementia*. 2019. (accessed 2021 15 November).

- (65) 2021 Alzheimer's disease facts and figures. *Alzheimers Dement* **2021**, *17* (3), 327-406. DOI: 10.1002/alz.12328.
- (66) De Strooper, B.; Karran, E. The Cellular Phase of Alzheimer's Disease. *Cell* **2016**, *164* (4), 603-615. DOI: 10.1016/j.cell.2015.12.056.
- (67) Venegas, C.; Kumar, S.; Franklin, B. S.; Dierkes, T.; Brinkschulte, R.; Tejera, D.; Vieira-Saecker, A.; Schwartz, S.; Santarelli, F.; Kummer, M. P.; et al. Microglia-derived ASC specks cross-seed amyloid- $\beta$  in Alzheimer's disease. *Nature* **2017**, *552* (7685), 355-361. DOI: 10.1038/nature25158.
- (68) Sweeney, M. D.; Sagare, A. P.; Zlokovic, B. V. Blood-brain barrier breakdown in Alzheimer disease and other neurodegenerative disorders. *Nat Rev Neurol* **2018**, *14* (3), 133-150. DOI: 10.1038/nrneurol.2017.188.
- (69) Terry, A. V.; Buccafusco, J. J. The cholinergic hypothesis of age and Alzheimer's disease-related cognitive deficits: recent challenges and their implications for novel drug development. *J Pharmacol Exp Ther* **2003**, *306* (3), 821-827. DOI: 10.1124/jpet.102.041616.
- (70) Scheltens, P.; De Strooper, B.; Kivipelto, M.; Holstege, H.; Ch  telat, G.; Teunissen, C. E.; Cummings, J.; van der Flier, W. M. Alzheimer's disease. *Lancet* **2021**, *397* (10284), 1577-1590. DOI: 10.1016/S0140-6736(20)32205-4.
- (71) Holmes, C.; Cunningham, C.; Zotova, E.; Woolford, J.; Dean, C.; Kerr, S.; Culliford, D.; Perry, V. H. Systemic inflammation and disease progression in Alzheimer disease. *Neurology* **2009**, *73* (10), 768-774. DOI: 10.1212/WNL.0b013e3181b6bb95.
- (72) Chen, W. W.; Zhang, X.; Huang, W. J. Role of neuroinflammation in neurodegenerative diseases (Review). *Mol Med Rep* **2016**, *13* (4), 3391-3396. DOI: 10.3892/mmr.2016.4948.
- (73) Gray, S. C.; Kinghorn, K. J.; Woodling, N. S. Shifting equilibriums in Alzheimer's disease: The complex roles of microglia in neuroinflammation, neuronal survival and neurogenesis. *Neural Regen Res* **2020**, *15* (7), 1208. DOI: 10.4103/1673-5374.272571.
- (74) Schwab, C.; McGeer, P. L. Inflammatory aspects of Alzheimer disease and other neurodegenerative disorders. *J Alzheimers Dis* **2008**, *13* (4), 359-369. DOI: 10.3233/jad-2008-13402.
- (75) Heneka, M. T.; Carson, M. J.; El Khoury, J.; Landreth, G. E.; Brosseron, F.; Feinstein, D. L.; Jacobs, A. H.; Wyss-Coray, T.; Vitorica, J.; Ransohoff, R. M. Neuroinflammation in Alzheimer's disease. *Lancet Neurol* **2015**, *14* (4), 388-405. DOI: 10.1016/S1474-4422(15)70016-5.
- (76) Brendel, M.; Kleinberger, G.; Probst, F.; Jaworska, A.; Overhoff, F.; Blume, T.; Albert, N. L.; Carlsen, J.; Lindner, S.; Gildehaus, F. J. Increase of TREM2 during aging of an Alzheimer's disease mouse model is paralleled by microglial activation and amyloidosis. *Front Aging Neurosci* **2017**, *9*, 8. DOI: 10.3389/fnagi.2017.00008.
- (77) (CADRO), C. A. s. a. R. D. R. O. <https://iadrp.nia.nih.gov/about/cadro>. (accessed 2021 17 November).
- (78) Fu, W. Y.; Wang, X.; Ip, N. Y. Targeting Neuroinflammation as a Therapeutic Strategy for Alzheimer's Disease: Mechanisms, Drug Candidates, and New Opportunities. *ACS Chem Neurosci* **2019**, *10* (2), 872-879. DOI: 10.1021/acchemneuro.8b00402.
- (79) Zhang, C.; Wang, Y.; Wang, D.; Zhang, J.; Zhang, F. NSAID Exposure and Risk of Alzheimer's Disease: An Updated Meta-Analysis From Cohort Studies. *Front Aging Neurosci* **2018**, *10*, 83. DOI: 10.3389/fnagi.2018.00083.

- (80) ClinicalTrials.gov. <https://clinicaltrials.gov/ct2/show/NCT02702817?term=naproxen&cond=Alzheimer+Disease&draw=2&rank=1>. (accessed 2022 24 January).
- (81) ClinicalTrials.gov. <https://clinicaltrials.gov/ct2/show/NCT00004845?term=naproxen&cond=Alzheimer+Disease&draw=2&rank=2>. (accessed 2022 24 January).
- (82) ClinicalTrials.gov. <https://clinicaltrials.gov/ct2/show/NCT00007189?term=naproxen&cond=Alzheimer+Disease&draw=2&rank=3>. (accessed 2022 24 January).
- (83) ClinicalTrials.gov. <https://clinicaltrials.gov/ct2/show/NCT00322036?term=NCT00322036&draw=2&rank=1>. (accessed 2022 24 January).
- ClinicalTrials.gov. <https://clinicaltrials.gov/ct2/results?cond=&term=NCT00105547&cntry=&state=&city=&dist=>. (accessed 2022 24 January).
- (84) ClinicalTrials.gov. <https://clinicaltrials.gov/ct2/show/NCT00239746?term=ibuprofen&cond=Alzheimer+Disease&draw=2&rank=2>. (accessed 2021 24 November).
- (85) ClinicalTrials.gov. <https://clinicaltrials.gov/ct2/results?cond=&term=NCT01436188&cntry=&state=&city=&dist=>. (accessed 2022 24 January).
- (86) ClinicalTrials.gov. <https://clinicaltrials.gov/ct2/show/NCT00432081?term=NCT00432081&draw=2&rank=1>. (accessed 2022 24 January).
- (87) ClinicalTrials.gov. <https://clinicaltrials.gov/ct2/show/NCT01117948?term=lornoxicam&cond=Alzheimer+Disease&draw=2&rank=1>. (accessed 2022 24 January).
- (88) ClinicalTrials.gov. <https://clinicaltrials.gov/ct2/show/NCT00000178?term=prednisone&cond=Alzheimer+Disease&draw=2&rank=1>. (accessed 2022 24 January).
- (89) Aisen, P. S.; Davis, K. L.; Berg, J. D.; Schafer, K.; Campbell, K.; Thomas, R. G.; Weiner, M. F.; Farlow, M. R.; Sano, M.; Grundman, M.; et al. A randomized controlled trial of prednisone in Alzheimer's disease. Alzheimer's Disease Cooperative Study. *Neurology* **2000**, *54* (3), 588-593. DOI: 10.1212/wnl.54.3.588.
- (90) ClinicalTrials.gov. <https://clinicaltrials.gov/ct2/show/NCT01409915?term=NCT01409915&draw=2&rank=1>. (accessed 2022 24 January).
- ClinicalTrials.gov. <https://clinicaltrials.gov/ct2/show/NCT04902703?term=NCT04902703&draw=2&rank=1>. (accessed 2022 24 January).
- (91) Potter, H.; Woodcock, J. H.; Boyd, T. D.; Coughlan, C. M.; O'Shaughnessy, J. R.; Borges, M. T.; Thaker, A. A.; Raj, B. A.; Adamszuk, K.; Scott, D.; et al. Safety and efficacy of sargramostim (GM-CSF) in the treatment of Alzheimer's disease. *Alzheimers Dement (N Y)* **2021**, *7* (1), e12158. DOI: 10.1002/trc2.12158.
- (92) ClinicalTrials.gov. <https://clinicaltrials.gov/ct2/results?cond=&term=NCT00203320&cntry=&state=&city=&dist=>. (accessed 2022 24 January).
- ClinicalTrials.gov. <https://clinicaltrials.gov/ct2/show/NCT00203359?term=NCT00203359&draw=2&rank=1>. (accessed 2022 24 January).
- ClinicalTrials.gov. <https://clinicaltrials.gov/ct2/show/NCT01716637?term=NCT01716637&draw=2&rank=1>. (accessed 2022 24 January).
- ClinicalTrials.gov. <https://clinicaltrials.gov/ct2/show/NCT01068353?term=NCT01068353&draw=2&rank=1>. (accessed 2022 24 January).

- (93) Butchart, J.; Brook, L.; Hopkins, V.; Teeling, J.; Püntener, U.; Culliford, D.; Sharples, R.; Sharif, S.; McFarlane, B.; Raybould, R.; et al. Etanercept in Alzheimer disease: A randomized, placebo-controlled, double-blind, phase 2 trial. *Neurology* **2015**, *84* (21), 2161-2168. DOI: 10.1212/WNL.0000000000001617.
- (94) ClinicalTrials.gov. <https://clinicaltrials.gov/ct2/show/NCT02471833?term=NCT02471833&draw=2&rank=1>. (accessed 2022 24 January).
- ClinicalTrials.gov. <https://clinicaltrials.gov/ct2/show/NCT02085265?term=NCT02085265&draw=2&rank=1>. (accessed 2022 24 January).
- (95) Benson, S. C.; Pershadsingh, H. A.; Ho, C. I.; Chittiboyina, A.; Desai, P.; Pravenec, M.; Qi, N.; Wang, J.; Avery, M. A.; Kurtz, T. W. Identification of telmisartan as a unique angiotensin II receptor antagonist with selective PPARgamma-modulating activity. *Hypertension* **2004**, *43* (5), 993-1002. DOI: 10.1161/01.HYP.0000123072.34629.57.
- (96) ClinicalTrials.gov. <https://clinicaltrials.gov/ct2/show/NCT00982202?term=NCT00982202&draw=2&rank=1>. (accessed 2022 24 January).
- ClinicalTrials.gov. <https://clinicaltrials.gov/ct2/show/NCT01931566?term=NCT01931566&draw=2&rank=1>. (accessed 2022 24 January).
- ClinicalTrials.gov. <https://clinicaltrials.gov/ct2/show/NCT02284906?term=NCT01931566&draw=2&rank=2>. (accessed 2022 24 January).
- (97) Burns, D. K.; Alexander, R. C.; Welsh-Bohmer, K. A.; Culp, M.; Chiang, C.; O'Neil, J.; Evans, R. M.; Harrigan, P.; Plassman, B. L.; Burke, J. R.; et al. Safety and efficacy of pioglitazone for the delay of cognitive impairment in people at risk of Alzheimer's disease (TOMMORROW): a prognostic biomarker study and a phase 3, randomised, double-blind, placebo-controlled trial. *Lancet Neurol* **2021**, *20* (7), 537-547. DOI: 10.1016/S1474-4422(21)00043-0.
- (98) Dong, Y. F.; Kataoka, K.; Tokutomi, Y.; Nako, H.; Nakamura, T.; Toyama, K.; Sueta, D.; Koibuchi, N.; Yamamoto, E.; Ogawa, H.; et al. Perindopril, a centrally active angiotensin-converting enzyme inhibitor, prevents cognitive impairment in mouse models of Alzheimer's disease. *FASEB J* **2011**, *25* (9), 2911-2920. DOI: 10.1096/fj.11-182873.
- (99) Leng, F.; Edison, P. Neuroinflammation and microglial activation in Alzheimer disease: where do we go from here? *Nat Rev Neurol* **2021**, *17* (3), 157-172. DOI: 10.1038/s41582-020-00435-y.
- (100) ClinicalTrials.gov is a database, <https://clinicaltrials.gov/>.
- (101) Crismon, M. L. Tacrine: first drug approved for Alzheimer's disease. *Ann Pharmacother* **1994**, *28* (6), 744-751. DOI: 10.1177/106002809402800612.
- (102) Qizilbash, N.; Birks, J.; Lopez Arrieta, J.; Lewington, S.; Szeto, S. WITHDRAWN: Tacrine for Alzheimer's disease. *Cochrane Database Syst Rev* **2007**, (3), CD000202. DOI: 10.1002/14651858.
- (103) Marucci, G.; Buccioni, M.; Ben, D. D.; Lambertucci, C.; Volpini, R.; Amenta, F. Efficacy of acetylcholinesterase inhibitors in Alzheimer's disease. *Neuropharmacology* **2021**, *190*, 108352. DOI: 10.1016/j.neuropharm.2020.108352.
- (104) Reisberg, B.; Doody, R.; Stöffler, A.; Schmitt, F.; Ferris, S.; Möbius, H. J.; Group, M. S. Memantine in moderate-to-severe Alzheimer's disease. *N Engl J Med* **2003**, *348* (14), 1333-1341. DOI: 10.1056/NEJMoa013128.
- (105) Syed, Y. Y. Sodium Oligomannate: First Approval. *Drugs* **2020**, *80* (4), 441-444. DOI: 10.1007/s40265-020-01268-1.

- (106) Xiao, S.; Chan, P.; Wang, T.; Hong, Z.; Wang, S.; Kuang, W.; He, J.; Pan, X.; Zhou, Y.; Ji, Y.; et al. A 36-week multicenter, randomized, double-blind, placebo-controlled, parallel-group, phase 3 clinical trial of sodium oligomannate for mild-to-moderate Alzheimer's dementia. *Alzheimers Res Ther* **2021**, *13* (1), 62. DOI: 10.1186/s13195-021-00795-7.
- (107) Schneider, L. A resurrection of aducanumab for Alzheimer's disease. *Lancet Neurol* **2020**, *19* (2), 111-112. DOI: 10.1016/S1474-4422(19)30480-6.
- (108) Agency, E. M. <https://www.ema.europa.eu/en/medicines/human/summaries-opinion/aduhelm>. (accessed 2022 17 January).
- (109) Cummings, J.; Feldman, H. H.; Scheltens, P. The "rights" of precision drug development for Alzheimer's disease. *Alzheimers Res Ther* **2019**, *11* (1), 76. DOI: 10.1186/s13195-019-0529-5.
- (110) Anderson, R. M.; Hadjichrysanthou, C.; Evans, S.; Wong, M. M. Why do so many clinical trials of therapies for Alzheimer's disease fail? *Lancet* **2017**, *390* (10110), 2327-2329. DOI: 10.1016/S0140-6736(17)32399-1.
- (111) Strebhardt, K.; Ullrich, A. Paul Ehrlich's magic bullet concept: 100 years of progress. *Nat Rev Cancer* **2008**, *8* (6), 473-480. DOI: 10.1038/nrc2394.
- (112) Hopkins, A. L. Network pharmacology: the next paradigm in drug discovery. *Nat Chem Biol* **2008**, *4* (11), 682-690. DOI: 10.1038/nchembio.118.
- (113) Prati, F.; Cavalli, A.; Bolognesi, M. L. Navigating the Chemical Space of Multitarget-Directed Ligands: From Hybrids to Fragments in Alzheimer's Disease. *Molecules* **2016**, *21* (4), 466. DOI: 10.3390/molecules21040466.
- (114) Morphy, R.; Rankovic, Z. Designed multiple ligands. An emerging drug discovery paradigm. *J Med Chem* **2005**, *48* (21), 6523-6543. DOI: 10.1021/jm058225d.
- (115) Albertini, C.; Salerno, A.; de Sena Murteira Pinheiro, P.; Bolognesi, M. L. From combinations to multitarget-directed ligands: A continuum in Alzheimer's disease polypharmacology. *Med Res Rev* **2020**. DOI: 10.1002/med.21699.
- (116) Anighoro, A.; Bajorath, J.; Rastelli, G. Polypharmacology: challenges and opportunities in drug discovery. *J Med Chem* **2014**, *57* (19), 7874-7887. DOI: 10.1021/jm5006463.
- (117) Proschak, E.; Stark, H.; Merk, D. Polypharmacology by Design: A Medicinal Chemist's Perspective on Multitargeting Compounds. *J Med Chem* **2019**, *62* (2), 420-444. DOI: 10.1021/acs.jmedchem.8b00760.
- (118) Bolognesi, M. L.; Cavalli, A. Multitarget Drug Discovery and Polypharmacology. *ChemMedChem* **2016**, *11* (12), 1190-1192. DOI: 10.1002/cmdc.201600161.
- (119) Deardorff, W. J.; Grossberg, G. T. A fixed-dose combination of memantine extended-release and donepezil in the treatment of moderate-to-severe Alzheimer's disease. *Drug Des Devel Ther* **2016**, *10*, 3267-3279. DOI: 10.2147/DDDT.S86463.
- (120) Bolognesi, M. L. Polypharmacology in a single drug: multitarget drugs. *Curr Med Chem* **2013**, *20* (13), 1639-1645. DOI: 10.2174/0929867311320130004.
- (121) Parsons, C. G. CNS repurposing - Potential new uses for old drugs: Examples of screens for Alzheimer's disease, Parkinson's disease and spasticity. *Neuropharmacology* **2019**, *147*, 4-10. DOI: 10.1016/j.neuropharm.2018.08.027.

- (122) Bangalore, S.; Kamalakkannan, G.; Parkar, S.; Messerli, F. H. Fixed-dose combinations improve medication compliance: a meta-analysis. *Am J Med* **2007**, *120* (8), 713-719. DOI: 10.1016/j.amjmed.2006.08.033.
- (123) Cavalli, A.; Bolognesi, M. L.; Minarini, A.; Rosini, M.; Tumiatti, V.; Recanatini, M.; Melchiorre, C. Multi-target-directed ligands to combat neurodegenerative diseases. *J Med Chem* **2008**, *51* (3), 347-372. DOI: 10.1021/jm7009364.
- (124) Das, N.; Dhanawat, M.; Dash, B.; Nagarwal, R. C.; Shrivastava, S. K. Codrug: an efficient approach for drug optimization. *Eur J Pharm Sci* **2010**, *41* (5), 571-588. DOI: 10.1016/j.ejps.2010.09.014.
- (125) Vu, C. B.; Bemis, J. E.; Benson, E.; Bista, P.; Carney, D.; Fahrner, R.; Lee, D.; Liu, F.; Lonkar, P.; Milne, J. C.; et al. Synthesis and Characterization of Fatty Acid Conjugates of Niacin and Salicylic Acid. *J Med Chem* **2016**, *59* (3), 1217-1231. DOI: 10.1021/acs.jmedchem.5b01961.
- (126) Rossi, M.; Petralla, S.; Protti, M.; Baiula, M.; Kobrlova, T.; Soukup, O.; Spampinato, S. M.; Mercolini, L.; Monti, B.; Bolognesi, M. L.  $\alpha$ -Linolenic Acid-Valproic Acid Conjugates: Toward Single-Molecule Polypharmacology for Multiple Sclerosis. *ACS Med Chem Lett* **2020**, *11* (12), 2406-2413. DOI: 10.1021/acsmchemlett.0c00375.
- (127) Ivasiv, V.; Albertini, C.; Gonçalves, A. E.; Rossi, M.; Bolognesi, M. L. Molecular Hybridization as a Tool for Designing Multitarget Drug Candidates for Complex Diseases. *Curr Top Med Chem* **2019**, *19*, 1694-1711. DOI: 10.2174/1568026619666190619115735.
- (128) Pajouhesh, H.; Lenz, G. R. Medicinal chemical properties of successful central nervous system drugs. *NeuroRx* **2005**, *2* (4), 541-553. DOI: 10.1602/neurorx.2.4.541.
- (129) Wager, T. T.; Hou, X.; Verhoest, P. R.; Villalobos, A. Moving beyond rules: the development of a central nervous system multiparameter optimization (CNS MPO) approach to enable alignment of druglike properties. *ACS Chem Neurosci* **2010**, *1* (6), 435-449. DOI: 10.1021/cn100008c.
- (130) Decker, M. *Design of hybrid molecules for drug development*; Elsevier, 2017.
- (131) Chen, X.; Cassady, K. E.; Adams, J. N.; Harrison, T. M.; Baker, S. L.; Jagust, W. J. Regional Tau Effects on Prospective Cognitive Change in Cognitively Normal Older Adults. *J Neurosci* **2021**, *41* (2), 366-375. DOI: 10.1523/JNEUROSCI.2111-20.2020.
- (132) Mawuenyega, K. G.; Sigurdson, W.; Ovod, V.; Munsell, L.; Kasten, T.; Morris, J. C.; Yarasheski, K. E.; Bateman, R. J. Decreased clearance of CNS beta-amyloid in Alzheimer's disease. *Science* **2010**, *330* (6012), 1774. DOI: 10.1126/science.1197623.
- (133) Thal, D. R.; Capetillo-Zarate, E.; Del Tredici, K.; Braak, H. The development of amyloid beta protein deposits in the aged brain. *Sci aging knowledge environ* **2006**, *2006* (6), re1. DOI: 10.1126/sageke.2006.6.re1.
- (134) Walsh, D. M.; Klyubin, I.; Fadeeva, J. V.; Cullen, W. K.; Anwyl, R.; Wolfe, M. S.; Rowan, M. J.; Selkoe, D. J. Naturally secreted oligomers of amyloid beta protein potently inhibit hippocampal long-term potentiation in vivo. *Nature* **2002**, *416* (6880), 535-539. DOI: 10.1038/416535a.
- (135) Gouwens, L. K.; Makoni, N. J.; Rogers, V. A.; Nichols, M. R. Amyloid- $\beta$ 42 protofibrils are internalized by microglia more extensively than monomers. *Brain Res* **2016**, *1648* (Pt A), 485-495. DOI: 10.1016/j.brainres.2016.08.016.
- (136) Gouwens, L. K.; Ismail, M. S.; Rogers, V. A.; Zeller, N. T.; Garrad, E. C.; Amtashar, F. S.; Makoni, N. J.; Osborn, D. C.; Nichols, M. R. A $\beta$ 42 Protofibrils Interact with and Are Trafficked through Microglial-

- Derived Microvesicles. *ACS Chem Neurosci* **2018**, *9* (6), 1416-1425. DOI: 10.1021/acchemneuro.8b00029.
- (137) Uddin, M. S.; Kabir, M. T.; Mamun, A. A.; Barreto, G. E.; Rashid, M.; Perveen, A.; Ashraf, G. M. Pharmacological approaches to mitigate neuroinflammation in Alzheimer's disease. *Int Immunopharmacol* **2020**, *84*, 106479. DOI: 10.1016/j.intimp.2020.106479.
- (138) Zhong, L.; Xu, Y.; Zhuo, R.; Wang, T.; Wang, K.; Huang, R.; Wang, D.; Gao, Y.; Zhu, Y.; Sheng, X. Soluble TREM2 ameliorates pathological phenotypes by modulating microglial functions in an Alzheimer's disease model. *Nature communications* **2019**, *10* (1), 1-16. DOI: 10.1038/s41467-019-09118-9.
- (139) LaFerla, F. M.; Green, K. N.; Oddo, S. Intracellular amyloid- $\beta$  in Alzheimer's disease. *Nat Rev Neurosci* **2007**, *8* (7), 499-509. DOI: 10.1038/nrn2168.
- (140) Foundation, A. s. D. D. <https://www.alzdiscovery.org/research-and-grants/priorities>. (accessed 2021 23 November).
- (141) Minutello, K.; Gupta, V. Cromolyn Sodium. In *StatPearls*, StatPearls Publishing Copyright © **2021**, StatPearls Publishing LLC., 2021.
- (142) Walker, S. R.; Evans, M. E.; Richards, A. J.; Paterson, J. W. The fate of (14C)disodium cromoglycate in man. *J Pharm Pharmacol* **1972**, *24* (7), 525-531. DOI: 10.1111/j.2042-7158.1972.tb09051.x.
- (143) Kurin, M.; Elangovan, A.; Alikhan, M. M.; Al Dulaijan, B.; Silver, E.; Kaelber, D. C.; Cooper, G. Irritable bowel syndrome is strongly associated with the primary and idiopathic mast cell disorders. *Neurogastroenterol Motil* **2021**, e14265. DOI: 10.1111/nmo.14265.
- (144) Liu, Y. L.; Hu, F. R.; Wang, I. J.; Chen, W. L.; Hou, Y. C. A double-masked study to compare the efficacy and safety of topical cromolyn for the treatment of allergic conjunctivitis. *J Formos Med Assoc* **2011**, *110* (11), 690-694. DOI: 10.1016/j.jfma.2011.09.004.
- (145) Méndez-Enríquez, E.; Hallgren, J. Mast Cells and Their Progenitors in Allergic Asthma. *Front Immunol* **2019**, *10*, 821. DOI: 10.3389/fimmu.2019.00821.
- (146) Ravula, A. R.; Teegala, S. B.; Kalakotla, S.; Pasangulapati, J. P.; Perumal, V.; Boyina, H. K. Fisetin, potential flavonoid with multifarious targets for treating neurological disorders: An updated review. *Eur J Pharmacol* **2021**, *910*, 174492. DOI: 10.1016/j.ejphar.2021.174492.
- (147) Ahmad, A.; Ali, T.; Park, H. Y.; Badshah, H.; Rehman, S. U.; Kim, M. O. Neuroprotective Effect of Fisetin Against Amyloid-Beta-Induced Cognitive/Synaptic Dysfunction, Neuroinflammation, and Neurodegeneration in Adult Mice. *Mol Neurobiol* **2017**, *54* (3), 2269-2285. DOI: 10.1007/s12035-016-9795-4.
- (148) Oka, T.; Kalesnikoff, J.; Starkl, P.; Tsai, M.; Galli, S. J. Evidence questioning cromolyn's effectiveness and selectivity as a 'mast cell stabilizer' in mice. *Lab Invest* **2012**, *92* (10), 1472-1482. DOI: 10.1038/labinvest.2012.116.
- (149) Hori, Y.; Takeda, S.; Cho, H.; Wegmann, S.; Shoup, T. M.; Takahashi, K.; Irimia, D.; Elmaleh, D. R.; Hyman, B. T.; Hudry, E. A Food and Drug Administration-approved asthma therapeutic agent impacts amyloid  $\beta$  in the brain in a transgenic model of Alzheimer disease. *J Biol Chem* **2015**, *290* (4), 1966-1978. DOI: 10.1074/jbc.M114.586602.



- (150) Wang, Y. J.; Downey, M. A.; Choi, S.; Shoup, T. M.; Elmaleh, D. R. Cromolyn platform suppresses fibrosis and inflammation, promotes microglial phagocytosis and neurite outgrowth. *Sci Rep* **2021**, *11* (1), 22161. DOI: 10.1038/s41598-021-00465-6.
- (151) Hao, H.; Wang, G.; Sun, J. Enantioselective pharmacokinetics of ibuprofen and involved mechanisms. *Drug Metab Rev* **2005**, *37* (1), 215-234. DOI: 10.1081/dmr-200047999.
- (152) Benito-León, J.; Contador, I.; Vega, S.; Villarejo-Galende, A.; Bermejo-Pareja, F. Non-steroidal anti-inflammatory drugs use in older adults decreases risk of Alzheimer's disease mortality. *Plos one* **2019**, *14* (9), e0222505. DOI: 10.1371/journal.pone.0222505.
- (153) Heneka, M. T.; Sastre, M.; Dumitrescu-Ozimek, L.; Hanke, A.; Dewachter, I.; Kuiperi, C.; O'Banion, K.; Klockgether, T.; Van Leuven, F.; Landreth, G. E. Acute treatment with the PPAR $\gamma$  agonist pioglitazone and ibuprofen reduces glial inflammation and A $\beta$ 1-42 levels in APPV717I transgenic mice. *Brain* **2005**, *128* (6), 1442-1453. DOI: 10.1093/brain/awh452.
- (154) Ettcheto, M.; Sánchez-Lopez, E.; Cano, A.; Carrasco, M.; Herrera, K.; Manzine, P. R.; Espinosa-Jimenez, T.; Busquets, O.; Verdaguer, E.; Olloquequi, J. Dexibuprofen ameliorates peripheral and central risk factors associated with Alzheimer's disease in metabolically stressed APP<sup>swe</sup>/PS1<sup>dE9</sup> mice. **2021**, *11* (1), 1-17. DOI: 10.1186/s13578-021-00646-w
- (155) Zhou, Y.; Su, Y.; Li, B.; Liu, F.; Ryder, J. W.; Wu, X.; Gonzalez-DeWhitt, P. A.; Gelfanova, V.; Hale, J. E.; May, P. C. Nonsteroidal anti-inflammatory drugs can lower amyloidogenic A $\beta$ 42 by inhibiting Rho. *Science* **2003**, *302* (5648), 1215-1217. DOI: 10.1126/science.1090154.
- (156) Puhl, A. C.; Milton, F. A.; Cvorovic, A.; Sieglaff, D. H.; Campos, J. C.; Bernardes, A.; Filgueira, C. S.; Lindemann, J. L.; Deng, T.; Neves, F. A.; et al. Mechanisms of peroxisome proliferator activated receptor  $\gamma$  regulation by non-steroidal anti-inflammatory drugs. *Nucl Recept Signal* **2015**, *13*, e004. DOI: 10.1621/nrs.13004.
- (157) Pasqualetti, P.; Bonomini, C.; Dal Forno, G.; Paulon, L.; Sinforiani, E.; Marra, C.; Zanetti, O.; Rossini, P. M. A randomized controlled study on effects of ibuprofen on cognitive progression of Alzheimer's disease. *Aging clin exp res* **2009**, *21* (2), 102-110. DOI: 10.1007/BF03325217.
- (158) ClinicalTrials.gov. <https://clinicaltrials.gov/ct2/show/NCT00046358?term=ibuprofen&cond=Dementia&draw=2&rank=1>. (accessed 2022 18 January).
- (159) ClinicalTrials.gov. <https://clinicaltrials.gov/ct2/show/NCT02547818?term=cromolyn&cond=Alzheimer+Disease&draw=2&rank=2>. (accessed 2021 14 November).
- (160) Koeberle, A.; Werz, O. Multi-target approach for natural products in inflammation. *Drug Discov Today* **2014**, *19* (12), 1871-1882. DOI: 10.1016/j.drudis.2014.08.006.
- (161) Van Broeck, B.; Timmers, M.; Ramael, S.; Bogert, J.; Shaw, L. M.; Mercken, M.; Slemmon, J.; Van Nueten, L.; Engelborghs, S.; Streffer, J. R. Impact of frequent cerebrospinal fluid sampling on A $\beta$  levels: systematic approach to elucidate influencing factors. *Alzheimer's Res Ther* **2016**, *8* (1), 1-9. DOI: 10.1186/s13195-016-0184-z.
- (162) Lim, G. P.; Yang, F.; Chu, T.; Chen, P.; Beech, W.; Teter, B.; Tran, T.; Ubeda, O.; Ashe, K. H.; Frautschy, S. A.; et al. Ibuprofen suppresses plaque pathology and inflammation in a mouse model for Alzheimer's disease. *J Neurosci* **2000**, *20* (15), 5709-5714. DOI: 10.1523/JNEUROSCI.20-15-05709.2000.

- (163) Mittal D.; Ali A.; Md S.; Baboota S.; Sahni J. K.; Ali J. Insights into direct nose to brain delivery: current status and future perspective. *Drug Deliv* **2014**, *21*(2), 75-86. DOI: 10.3109/10717544.2013.838713.
- (164) Ozkan, S.; Adapinar, D. O.; Elmaci, N. T.; Arslantas, D. Apraxia for differentiating Alzheimer's disease from subcortical vascular dementia and mild cognitive impairment. *Neuropsychiatr Dis Treat* **2013**, *9*, 947. DOI: 10.2147/NDT.S47879.
- (165) Rakesh, R.; Anoop, K. R. Formulation and optimization of nano-sized ethosomes for enhanced transdermal delivery of cromolyn sodium. *J Pharm Bioallied Sci* **2012**, *4* (4), 333-340. DOI: 10.4103/0975-7406.103274.
- (166) Ho, K. Y.; Gwee, K. A.; Cheng, Y. K.; Yoon, K. H.; Hee, H. T.; Omar, A. R. Nonsteroidal anti-inflammatory drugs in chronic pain: implications of new data for clinical practice. *J Pain Res* **2018**, *11*, 1937-1948. DOI: 10.2147/JPR.S168188.
- (167) Mori, T.; Nishimura, K.; Tamaki, S.; Nakamura, S.; Tsuda, H.; Takeya, N. Pro-drugs for the oral delivery of disodium cromoglycate. *Chem Pharm Bull (Tokyo)* **1988**, *36* (1), 338-344. DOI: 10.1248/cpb.36.338.
- (168) Placzek, A. T.; Ferrara, S. J.; Hartley, M. D.; Sanford-Crane, H. S.; Meinig, J. M.; Scanlan, T. S. Sobetirome prodrug esters with enhanced blood-brain barrier permeability. *Bioorg Med Chem* **2016**, *24* (22), 5842-5854. DOI: 10.1016/j.bmc.2016.09.038.
- (169) Guo, L.; Jia, S.; Diercks, C. S.; Yang, X.; Alshimiri, S. A.; Yaghi, O. M. Amidation, Esterification, and Thioesterification of a Carboxyl-Functionalized Covalent Organic Framework. *Angew Chem Int Ed Engl* **2020**, *59* (5), 2023-2027. DOI: 10.1002/anie.201912579.
- (170) Favia, A. D.; Habrant, D.; Scarpelli, R.; Migliore, M.; Albani, C.; Bertozzi, S. M.; Dionisi, M.; Tarozzo, G.; Piomelli, D.; Cavalli, A.; et al. Identification and characterization of carprofen as a multitarget fatty acid amide hydrolase/cyclooxygenase inhibitor. *J Med Chem* **2012**, *55* (20), 8807-8826. DOI: 10.1021/jm3011146.
- (171) Williams, A. S.; Taylor, G. Synthesis, characterization and release of cromoglycate from dextran conjugates. *Int J Pharm* **1992**, *83* (1-3), 233-239. DOI: 10.1016/0378-5173(82)90027-8.
- (172) Riggs-sauthier, J., Deng, B. Oligomer-Bis-Chromonyl Compound Conjugates. US20110112183, **2011**.
- (173) Gayo, L. M.; Suto, M. J. Ion-exchange resins for solution phase parallel synthesis of chemical libraries. *Tetrahedron lett* **1997**, *38* (4), 513-516. DOI: 10.1016/S0040-4039(96)02362-3
- (174) Zhang, H.; Ding, J.; Zhao, Z. Microwave assisted esterification of acidified oil from waste cooking oil by CERP/PES catalytic membrane for biodiesel production. *Bioresour Technol* **2012**, *123*, 72-77. DOI: 10.1016/j.biortech.2012.06.082.
- (175) Cummings, J. L.; Morstorf, T.; Zhong, K. Alzheimer's disease drug-development pipeline: few candidates, frequent failures. *Alzheimers Res Ther* **2014**, *6* (4), 37. DOI: 10.1186/alzrt269. DOI: 10.1186/alzrt269.
- (176) Sozio, P.; D'Aurizio, E.; Iannitelli, A.; Cataldi, A.; Zara, S.; Cantalamessa, F.; Nasuti, C.; Di Stefano, A. Ibuprofen and lipoic acid diamides as potential codrugs with neuroprotective activity. *Arch Pharm (Weinheim)* **2010**, *343* (3), 133-142. DOI: 10.1002/ardp.200900152.

- (177) Lagorce, D.; Bouslama, L.; Becot, J.; Miteva, M. A.; Villoutreix, B. O. FAF-Drugs4: free ADME-tox filtering computations for chemical biology and early stages drug discovery. *Bioinformatics* **2017**, *33* (22), 3658-3660. DOI: 10.1093/bioinformatics/btx491.
- (178) DeGoey, D. A.; Chen, H.-J.; Cox, P. B.; Wendt, M. D. Beyond the Rule of 5: Lessons Learned from AbbVie's Drugs and Compound Collection: Miniperspective. *J Med Chem* **2017**, *61* (7), 2636-2651. DOI: 10.1021/acs.jmedchem.7b00717.
- (179) Levine Iii, H. Thioflavine T interaction with synthetic Alzheimer's disease  $\beta$ -amyloid peptides: Detection of amyloid aggregation in solution. *Protein Sci* **1993**, *2* (3), 404-410. DOI: 10.1002/pro.5560020312.
- (180) Giorgetti, S.; Greco, C.; Tortora, P.; Aprile, F. A. Targeting amyloid aggregation: an overview of strategies and mechanisms. *Int J Mol Sci* **2018**, *19* (9), 2677. DOI: 10.3390/ijms19092677.
- (181) Bolus, H.; Crocker, K.; Boekhoff-Falk, G.; Chtarbanova, S. Modeling Neurodegenerative Disorders in. *Int J Mol Sci* **2020**, *21* (9). DOI: 10.3390/ijms21093055.
- (182) Costa, R.; Speretta, E.; Crowther, D. C.; Cardoso, I. Testing the therapeutic potential of doxycycline in a *Drosophila melanogaster* model of Alzheimer disease. *J Biol Chem* **2011**, *286* (48), 41647-41655. DOI: 10.1074/jbc.M111.274548.
- (183) Pecht, I.; Hemmerich, S. Cromolyn binding protein in highly purified form, and methods for the isolation thereof. US4996296A, **1991**.
- (184) Li, J. J. Fischer–Speier esterification. In *Name Reactions*, Springer, **2014**; pp 252-252.
- (185) Di Stefano, A.; Sozio, P.; Cocco, A.; Iannitelli, A.; Santucci, E.; Costa, M.; Pecci, L.; Nasuti, C.; Cantalamessa, F.; Pinnen, F. L-dopa- and dopamine-(R)-alpha-lipoic acid conjugates as multifunctional codrugs with antioxidant properties. *J Med Chem* **2006**, *49* (4), 1486-1493. DOI: 10.1021/jm051145p.
- (186) Manning, G.; Whyte, D. B.; Martinez, R.; Hunter, T.; Sudarsanam, S. The protein kinase complement of the human genome. *Science* **2002**, *298* (5600), 1912-1934. DOI: 10.1126/science.1075762.
- (187) Martin, J.; Anamika, K.; Srinivasan, N. Classification of protein kinases on the basis of both kinase and non-kinase regions. *PLoS One* **2010**, *5* (9), e12460. DOI: 10.1371/journal.pone.0012460.
- (188) Hanks, S. K.; Hunter, T. Protein kinases 6. The eukaryotic protein kinase superfamily: kinase (catalytic) domain structure and classification. *FASEB J* **1995**, *9* (8), 576-596. Niedner, R. H.; Buzko, O. V.; Haste, N. M.; Taylor, A.; Gribskov, M.; Taylor, S. S. Protein kinase resource: an integrated environment for phosphorylation research. *Proteins* **2006**, *63* (1), 78-86. DOI: 10.1002/prot.20825.
- (189) Hunter, T. [1] Protein kinase classification. *Methods enzymol* **1991**, *200*, 3-37.
- (190) Lai, S.; Safaei, J.; Pelech, S. Evolutionary Ancestry of Eukaryotic Protein Kinases and Choline Kinases. *J Biol Chem* **2016**, *291* (10), 5199-5205. DOI: 10.1074/jbc.M115.691428.
- (191) Modi, V.; Dunbrack, R. L. Defining a new nomenclature for the structures of active and inactive kinases. *Proc Natl Acad Sci U S A* **2019**, *116* (14), 6818-6827. DOI: 10.1073/pnas.1814279116.
- (192) Liao, J. J. Molecular recognition of protein kinase binding pockets for design of potent and selective kinase inhibitors. *J Med Chem* **2007**, *50* (3), 409-424. DOI: 10.1021/jm0608107.
- (193) D'Mello, S. R. When Good Kinases Go Rogue: GSK3, p38 MAPK and CDKs as Therapeutic Targets for Alzheimer's and Huntington's Disease. *Int J Mol Sci* **2021**, *22* (11). DOI: 10.3390/ijms22115911

- (194) Ravikumar, B.; Timonen, S.; Alam, Z.; Parri, E.; Wennerberg, K.; Aittokallio, T. Chemogenomic Analysis of the Druggable Kinome and Its Application to Repositioning and Lead Identification Studies. *Cell Chem Biol* **2019**, *26* (11), 1608-1622.e1606. DOI: 10.1016/j.chembiol.2019.08.007.
- (195) Tell, V.; Hilgeroth, A. Recent developments of protein kinase inhibitors as potential AD therapeutics. *Front Cell Neurosci* **2013**, *7*, 189. DOI: 10.3389/fncel.2013.00189.
- (196) Morrison, D. K. MAP kinase pathways. *Cold Spring Harb Perspect Biol* **2012**, *4* (11). DOI: 10.1101/cshperspect.a011254.
- (197) Kim, E. K.; Choi, E. J. Pathological roles of MAPK signaling pathways in human diseases. *Biochim Biophys Acta* **2010**, *1802* (4), 396-405. DOI: 10.1016/j.bbadis.2009.12.009.
- (198) Cargnello, M.; Roux, P. P. Activation and function of the MAPKs and their substrates, the MAPK-activated protein kinases. *Microbiol Mol Biol Rev* **2011**, *75* (1), 50-83. DOI: 10.1128/MMBR.00031-10.
- (199) Astolfi, A.; Iraci, N.; Sabatini, S.; Barreca, M. L.; Cecchetti, V. p38 $\alpha$  MAPK and Type I Inhibitors: Binding Site Analysis and Use of Target Ensembles in Virtual Screening. *Molecules* **2015**, *20* (9), 15842-15861. DOI: 10.3390/molecules200915842.
- (200) Machado, T. R.; Machado, T. R.; Pascutti, P. G. The p38 MAPK Inhibitors and Their Role in Inflammatory Diseases. *ChemistrySelect* **2021**, *6* (23), 5729-5742. DOI: 10.1002/slct.202100406.
- (201) Ahmed, T.; Zulfikar, A.; Arguelles, S.; Rasekhian, M.; Nabavi, S. F.; Silva, A. S.; Nabavi, S. M. Map kinase signaling as therapeutic target for neurodegeneration. *Pharmacol Res* **2020**, *160*, 105090. DOI: 10.1016/j.phrs.2020.105090.
- (202) Kheiri, G.; Dolatshahi, M.; Rahmani, F.; Rezaei, N. Role of p38/MAPKs in Alzheimer's disease: implications for amyloid beta toxicity targeted therapy. *Rev Neurosci* **2018**, *30* (1), 9-30. DOI: 10.1515/revneuro-2018-0008.
- (203) Lee, J. K.; Kim, N. J. Recent Advances in the Inhibition of p38 MAPK as a Potential Strategy for the Treatment of Alzheimer's Disease. *Molecules* **2017**, *22* (8). DOI: 10.3390/molecules22081287.
- (204) Roy, S. M.; Grum-Tokars, V. L.; Schavocky, J. P.; Saeed, F.; Staniszewski, A.; Teich, A. F.; Arancio, O.; Bachstetter, A. D.; Webster, S. J.; Van Eldik, L. J.; et al. Targeting human central nervous system protein kinases: An isoform selective p38 $\alpha$ MAPK inhibitor that attenuates disease progression in Alzheimer's disease mouse models. *ACS Chem Neurosci* **2015**, *6* (4), 666-680. DOI: 10.1021/acscemneuro.5b00002.
- (205) Roy, S. M.; Minasov, G.; Arancio, O.; Chico, L. W.; Van Eldik, L. J.; Anderson, W. F.; Pelletier, J. C.; Watterson, D. M. A Selective and Brain Penetrant p38 $\alpha$ MAPK Inhibitor Candidate for Neurologic and Neuropsychiatric Disorders That Attenuates Neuroinflammation and Cognitive Dysfunction. *J Med Chem* **2019**, *62* (11), 5298-5311. DOI: 10.1021/acs.jmedchem.9b00058. Tormählen, N. M.; Martorelli, M.; Kuhn, A.; Maier, F.; Guezguez, J.; Burnet, M.; Albrecht, W.; Laufer, S. A.; Koch, P. Design and Synthesis of Highly Selective Brain Penetrant p38 $\alpha$  Mitogen-Activated Protein Kinase Inhibitors. *J Med Chem* **2021**. DOI: 10.1021/acs.jmedchem.0c01773.
- (206) Hidaka, H.; Inagaki, M.; Kawamoto, S.; Sasaki, Y. Isoquinolinesulfonamides, novel and potent inhibitors of cyclic nucleotide dependent protein kinase and protein kinase C. *Biochemistry* **1984**, *23* (21), 5036-5041. DOI: 10.1021/bi00316a032.
- (207) Cohen, P.; Cross, D.; Jänne, P. A. Kinase drug discovery 20 years after imatinib: progress and future directions. *Nat Rev Drug Discov* **2021**, *20* (7), 551-569. DOI: 10.1038/s41573-021-00195-4.

- (208) ClinicalTrials.gov [https://clinicaltrials.gov/ct2/results?term=kinase+inhibitor&Search=Apply&recrs=a&recrs=f&recrs=d&age\\_v=&gndr=&type=&rslt=](https://clinicaltrials.gov/ct2/results?term=kinase+inhibitor&Search=Apply&recrs=a&recrs=f&recrs=d&age_v=&gndr=&type=&rslt=), C. g. (accessed 12 October 2021).
- (209) Zarrin, A. A.; Bao, K.; Lupardus, P.; Vucic, D. Kinase inhibition in autoimmunity and inflammation. *Nat Rev Drug Discov* **2021**, *20* (1), 39-63. DOI: 10.1038/s41573-020-0082-8.
- (210) Gehringer, M. Covalent inhibitors: back on track? *Future Med Chem* **2020**, *12* (15), 1363-1368. DOI: 10.4155/fmc-2020-0118.
- (211) Barf, T.; Kaptein, A. Irreversible protein kinase inhibitors: balancing the benefits and risks. *J Med Chem* **2012**, *55* (14), 6243-6262. DOI: 10.1021/jm3003203.
- (212) Krippendorff, B. F.; Neuhaus, R.; Lienau, P.; Reichel, A.; Huisinga, W. Mechanism-based inhibition: deriving K(I) and k(inact) directly from time-dependent IC(50) values. *J Biomol Screen* **2009**, *14* (8), 913-923. DOI: 10.1177/1087057109336751.
- (213) Roskoski, R. Classification of small molecule protein kinase inhibitors based upon the structures of their drug-enzyme complexes. *Pharmacol Res* **2016**, *103*, 26-48. DOI: 10.1016/j.phrs.2015.10.021.
- (214) Abdeldayem, A.; Raouf, Y. S.; Constantinescu, S. N.; Moriggl, R.; Gunning, P. T. Advances in covalent kinase inhibitors. *Chem Soc Rev* **2020**, *49* (9), 2617-2687. DOI: 10.1039/c9cs00720b.
- (215) Martinez, R.; Defnet, A.; Shapiro, P. Avoiding or Co-Opting ATP Inhibition: Overview of Type III, IV, V, and VI Kinase Inhibitors. *Next Generation Kinase Inhibitors* **2020**, 29-59. DOI: 10.1007/978-3-030-48283-1\_3.
- (216) Chaikuad, A.; Koch, P.; Laufer, S. A.; Knapp, S. The Cysteine of Protein Kinases as a Target in Drug Development. *Angew Chem Int Ed Engl* **2018**, *57* (16), 4372-4385. DOI: 10.1002/anie.201707875.
- (217) De Vita, E. 10 years into the resurgence of covalent drugs. *Future Med Chem* **2021**, *13* (2), 193-210. DOI: 10.4155/fmc-2020-0236.
- (218) Gehringer, M.; Laufer, S. A. Emerging and Re-Emerging Warheads for Targeted Covalent Inhibitors: Applications in Medicinal Chemistry and Chemical Biology. *J Med Chem* **2019**, *62* (12), 5673-5724. DOI: 10.1021/acs.jmedchem.8b01153.
- (219) Rajasekhar, K.; Govindaraju, T. Current progress, challenges and future prospects of diagnostic and therapeutic interventions in Alzheimer's disease. *RSC advances* **2018**, *8* (42), 23780-23804. DOI: 10.1039/C8RA03620A.
- (220) Altinbaş, K. Treatment of Comorbid Psychiatric Disorders with Bipolar Disorder. *Noro Psikiyatr Ars* **2021**, *58* (Suppl 1), S41-S46. DOI: 10.29399/npa.27615.
- (221) Cao, J.; Hou, J.; Ping, J.; Cai, D. Advances in developing novel therapeutic strategies for Alzheimer's disease. *Mol Neurodegener* **2018**, *13* (1), 1-20. DOI: 10.1186/s13024-018-0299-8
- (222) Pleen, J.; Townley, R. Alzheimer's disease clinical trial update 2019-2021. *J Neurol* **2021**. DOI: 10.1007/s00415-021-10790-5.
- (223) Feki, A.; Hibaoui, Y. DYRK1A Protein, A Promising Therapeutic Target to Improve Cognitive Deficits in Down Syndrome. *Brain Sci* **2018**, *8* (10). DOI: 10.3390/brainsci8100187.
- (224) Nygaard, H. B.; Wagner, A. F.; Bowen, G. S.; Good, S. P.; MacAvoy, M. G.; Strittmatter, K. A.; Kaufman, A. C.; Rosenberg, B. J.; Sekine-Konno, T.; Varma, P.; et al. A phase Ib multiple ascending dose study of the safety, tolerability, and central nervous system availability of AZD0530 (saracatinib) in Alzheimer's disease. *Alzheimers Res Ther* **2015**, *7* (1), 35. DOI: 10.1186/s13195-015-0119-0.

- (225) Cummings, J.; Lee, G.; Zhong, K.; Fonseca, J.; Taghva, K. Alzheimer's disease drug development pipeline: 2021. *Alzheimers Dement (N Y)* **2021**, *7* (1), e12179. DOI: 10.1002/trc2.12179.
- (226) Turner, R. S.; Hebron, M. L.; Lawler, A.; Mundel, E. E.; Yusuf, N.; Starr, J. N.; Anjum, M.; Pagan, F.; Torres-Yaghi, Y.; Shi, W.; et al. Nilotinib Effects on Safety, Tolerability, and Biomarkers in Alzheimer's Disease. *Ann Neurol* **2020**, *88* (1), 183-194. DOI: 10.1002/ana.25775.
- (227) ClinicalTrials.gov. <https://clinicaltrials.gov/ct2/show/NCT05143528?term=nilotinib&cond=Alzheimer+Disease&draw=2&rank=2>. (accessed 2022 23 January).
- (228) Xu, M.; Pirtskhalava, T.; Farr, J. N.; Weigand, B. M.; Palmer, A. K.; Weivoda, M. M.; Inman, C. L.; Ogradnik, M. B.; Hachfeld, C. M.; Fraser, D. G.; et al. Senolytics improve physical function and increase lifespan in old age. *Nat Med* **2018**, *24* (8), 1246-1256. DOI: 10.1038/s41591-018-0092-9.
- (229) ClinicalTrials.gov. <https://clinicaltrials.gov/ct2/show/NCT04063124?term=dasatinib&cond=Alzheimer+Disease&draw=2&rank=1>. (accessed 2022 23 January).
- (230) ClinicalTrials.gov. <https://clinicaltrials.gov/ct2/show/NCT04785300?term=dasatinib&cond=Alzheimer+Disease&draw=2&rank=2>. (accessed 2022 23 January).
- (231) ClinicalTrials.gov. <https://clinicaltrials.gov/ct2/show/NCT04685590?term=dasatinib&cond=Alzheimer+Disease&draw=2&rank=3>. (accessed 2022 23 January).
- (232) Anand David, A. V.; Arulmoli, R.; Parasuraman, S. Overviews of Biological Importance of Quercetin: A Bioactive Flavonoid. *Pharmacogn Rev* **2016**, *10* (20), 84-89. DOI: 10.4103/0973-7847.194044.
- (233) Kirkland, J. L.; Tchkonina, T. Senolytic drugs: from discovery to translation. *J Intern Med* **2020**, *288* (5), 518-536. DOI: 10.1111/joim.13141.
- (234) ClinicalTrials.gov. <https://clinicaltrials.gov/ct2/show/NCT04669028?term=NCT04669028&draw=2&rank=1>. (accessed 2022 23 January).
- (235) Reading, C. L.; Ahlem, C. N.; Murphy, M. F. NM101 Phase III study of NE3107 in Alzheimer's disease: rationale, design and therapeutic modulation of neuroinflammation and insulin resistance. *Neurodegener Dis Manag* **2021**, *11* (4), 289-298. DOI: 10.2217/nmt-2021-0022.
- (236) Haller, V.; Nahidino, P.; Forster, M.; Laufer, S. A. An updated patent review of p38 MAP kinase inhibitors (2014-2019). *Expert Opin Ther Pat* **2020**, *30* (6), 453-466, Review. DOI: 10.1080/13543776.2020.1749263 Scopus.
- (237) Miller, S.; Blanco, M. J. Small molecule therapeutics for neuroinflammation-mediated neurodegenerative disorders. *RSC Med Chem* **2021**, *12* (6), 871-886. DOI: 10.1039/d1md00036e.
- (238) Regan, J.; Capolino, A.; Cirillo, P. F.; Gilmore, T.; Graham, A. G.; Hickey, E.; Kroe, R. R.; Madwed, J.; Moriak, M.; Nelson, R. Structure– Activity Relationships of the p38 $\alpha$  MAP Kinase Inhibitor 1-(5-tert-Butyl-2-p-tolyl-2 H-pyrazol-3-yl)-3-[4-(2-morpholin-4-yl-ethoxy) naph-thalen-1-yl] urea (BIRB 796). *J Med Chem* **2003**, *46* (22), 4676-4686. DOI: 10.1021/jm030121k.
- (239) Cash, J. M.; Wilder, R. L. Treatment-resistant rheumatic disease. *Rheum Dis Clin N Am* **1995**, *21* (1), 1-18. DOI: 10.1016/S0889-857X(21)00367-7.
- (240) Ahn, Y. M.; Clare, M.; Ensinger, C. L.; Hood, M. M.; Lord, J. W.; Lu, W. P.; Miller, D. F.; Patt, W. C.; Smith, B. D.; Vogeti, L.; et al. Switch control pocket inhibitors of p38-MAP kinase. Durable type II inhibitors that do not require binding into the canonical ATP hinge region. *Bioorg Med Chem Lett* **2010**, *20* (19), 5793-5798. DOI: 10.1016/j.bmcl.2010.07.134

- (241) Cottin, V.; Maher, T. Long-term clinical and real-world experience with pirfenidone in the treatment of idiopathic pulmonary fibrosis. *Eur Respir Rev* **2015**, *24* (135), 58-64. DOI: 10.1183/09059180.00011514.
- (242) Patel, N. R.; Cunoosamy, D. M.; Fagerås, M.; Taib, Z.; Asimus, S.; Hegelund-Myrbäck, T.; Lundin, S.; Pardali, K.; Kurian, N.; Ersdal, E.; et al. The development of AZD7624 for prevention of exacerbations in COPD: a randomized controlled trial. *Int J Chron Obstruct Pulmon Dis* **2018**, *13*, 1009-1019. DOI: 10.2147/COPD.S150576.
- (243) ClinicalTrials.gov. <https://clinicaltrials.gov/ct2/show/NCT02753764?term=NCT02753764&draw=2&rank=1>. (accessed 2022 15 January)
- (244) ClinicalTrials.gov. <https://clinicaltrials.gov/ct2/show/NCT02145468?term=NCT02145468&draw=2&rank=1>. (accessed 2022 15 January)
- (245) O'Donoghue, M. L.; Glaser, R.; Cavender, M. A.; Aylward, P. E.; Bonaca, M. P.; Budaj, A.; Davies, R. Y.; Dellborg, M.; Fox, K. A.; Gutierrez, J. A.; et al. Effect of Losmapimod on Cardiovascular Outcomes in Patients Hospitalized With Acute Myocardial Infarction: A Randomized Clinical Trial. *JAMA* **2016**, *315* (15), 1591-1599. DOI: 10.1001/jama.2016.3609.
- (246) ClinicalTrials.gov. <https://clinicaltrials.gov/ct2/show/NCT04511819?term=NCT04511819&draw=2&rank=1>. (accessed 2022 15 January)
- (247) ClinicalTrials.gov. <https://clinicaltrials.gov/ct2/show/NCT04264442?term=NCT04264442&draw=2&rank=1>. (accessed 2022 15 January)
- (248) Muchir, A.; Wu, W.; Choi, J. C.; Iwata, S.; Morrow, J.; Homma, S.; Worman, H. J. Abnormal p38 $\alpha$  mitogen-activated protein kinase signaling in dilated cardiomyopathy caused by lamin A/C gene mutation. *Human molecular genetics* **2012**, *21* (19), 4325-4333. DOI: 10.1093/hmg/dds265.
- (249) ClinicalTrials.gov. <https://clinicaltrials.gov/ct2/show/NCT03439514?term=NCT03439514&draw=2&rank=1>. (accessed 2022 15 January)
- (250) ClinicalTrials.gov. <https://clinicaltrials.gov/ct2/show/NCT02351856?term=NCT02351856&draw=2&rank=1>. (accessed 2022 15 January)
- (251) ClinicalTrials.gov. <https://clinicaltrials.gov/ct2/show/NCT03980938?term=NCT03980938&draw=2&rank=1>. (accessed 2022 15 January)
- (252) ClinicalTrials.gov. <https://clinicaltrials.gov/ct2/show/NCT04001517?term=NCT04001517&draw=2&rank=1>. (accessed 2022 15 January)
- (253) ClinicalTrials.gov. <https://clinicaltrials.gov/ct2/show/NCT03435861?term=VX-745&cond=Alzheimer+Disease&draw=2&rank=2>. (accessed 2021 17 December).
- (254) Scheltens, P.; Prins, N.; Lammertsma, A.; Yaqub, M.; Gouw, A.; Wink, A. M.; Chu, H. M.; van Berckel, B. N. M.; Alam, J. An exploratory clinical study of p38 $\alpha$  kinase inhibition in Alzheimer's disease. *Ann Clin Transl Neurol* **2018**, *5* (4), 464-473. DOI: 10.1002/acn3.549.
- (255) ClinicalTrials.gov. <https://clinicaltrials.gov/ct2/show/NCT02423200?term=vx-745&draw=2&rank=1>. (accessed 2021 10 December).
- (256) Alam, J.; Blackburn, K.; Patrick, D. Neflamapimod: Clinical Phase 2b-Ready Oral Small Molecule Inhibitor of p38 $\alpha$  to Reverse Synaptic Dysfunction in Early Alzheimer's Disease. *J Prev Alzheimers Dis* **2017**, *4* (4), 273-278. DOI: 10.14283/jpad.2017.41.

- (257) ClinicalTrials.gov. <https://clinicaltrials.gov/ct2/show/NCT02423122?term=vx-745&draw=2&rank=2>. (accessed 2021 10 December).
- (258) Behl, T.; Kaur, D.; Sehgal, A.; Singh, S.; Sharma, N.; Zengin, G.; Andronie-Cioara, F. L.; Toma, M. M.; Bungau, S.; Bumbu, A. G. Role of Monoamine Oxidase Activity in Alzheimer's Disease: An Insight into the Therapeutic Potential of Inhibitors. *Molecules* **2021**, *26* (12), 3724. DOI: 10.3390/molecules26123724.
- (259) Cai, Z. Monoamine oxidase inhibitors: promising therapeutic agents for Alzheimer's disease (Review). *Mol Med Rep* **2014**, *9* (5), 1533-1541. DOI: 10.3892/mmr.2014.2040.
- (260) Schedin-Weiss, S.; Inoue, M.; Hromadkova, L.; Teranishi, Y.; Yamamoto, N. G.; Wiehager, B.; Bogdanovic, N.; Winblad, B.; Sandebring-Matton, A.; Frykman, S.; et al. Monoamine oxidase B is elevated in Alzheimer disease neurons, is associated with  $\gamma$ -secretase and regulates neuronal amyloid  $\beta$ -peptide levels. *Alzheimers Res Ther* **2017**, *9* (1), 57. DOI: 10.1186/s13195-017-0279-1.
- (261) Hensley, K.; Maitt, M. L.; Yu, Z.; Sang, H.; Markesbery, W. R.; Floyd, R. A. Electrochemical analysis of protein nitrotyrosine and dityrosine in the Alzheimer brain indicates region-specific accumulation. *J Neurosci* **1998**, *18* (20), 8126-8132. DOI: 10.1523/JNEUROSCI.18-20-08126.1998.
- (262) Binda, C.; Hubálek, F.; Li, M.; Herzig, Y.; Sterling, J.; Edmondson, D. E.; Mattevi, A. Crystal structures of monoamine oxidase B in complex with four inhibitors of the N-propargylaminoindan class. *J Med Chem* **2004**, *47* (7), 1767-1774. DOI: 10.1021/jm031087c.
- (263) do Carmo Carreiras, M.; Ismaili, L.; Marco-Contelles, J. Propargylamine-derived multi-target directed ligands for Alzheimer's disease therapy. *Bioorg Med Chem Lett* **2020**, *30* (3), 126880. DOI: 10.1016/j.bmcl.2019.126880.
- (264) Bar-Am, O.; Amit, T.; Weinreb, O.; Youdim, M. B.; Mandel, S. Propargylamine containing compounds as modulators of proteolytic cleavage of amyloid-beta protein precursor: involvement of MAPK and PKC activation. *J Alzheimers Dis* **2010**, *21* (2), 361-371. DOI: 10.3233/JAD-2010-100150.
- (265) ClinicalTrials.gov. <https://clinicaltrials.gov/ct2/show/NCT01429623?term=NCT01429623&draw=2&rank=1>. (accessed 2022 24 January).
- (266) ClinicalTrials.gov. <https://clinicaltrials.gov/ct2/show/NCT01354691?term=NCT01354691&draw=2&rank=1>. (accessed 2022 24 January).
- (267) Schneider, L. S.; Geffen, Y.; Rabinowitz, J.; Thomas, R. G.; Schmidt, R.; Ropele, S.; Weinstock, M.; Group, L. S. Low-dose ladostigil for mild cognitive impairment: A phase 2 placebo-controlled clinical trial. *Neurology* **2019**, *93* (15), e1474-e1484. DOI: 10.1212/WNL.0000000000008239.
- (268) ClinicalTrials.gov. <https://clinicaltrials.gov/ct2/results?cond=&term=NCT02359552&cntry=&state=&city=&dist=>. (accessed 2021 17 December).
- (269) Zhou, P.; Zhang, Y.; Xu, H.; Chen, F.; Chen, X.; Li, X.; Pi, X.; Wang, L.; Zhan, L.; Nan, F.; et al. P-retigabine: an N-propargylyed retigabine with improved brain distribution and enhanced antiepileptic activity. *Mol Pharmacol* **2015**, *87* (1), 31-38. DOI: 10.1124/mol.114.095190.
- (270) Li, W.; Yang, X.; Song, Q.; Cao, Z.; Shi, Y.; Deng, Y.; Zhang, L. Pyridoxine-resveratrol hybrids as novel inhibitors of MAO-B with antioxidant and neuroprotective activities for the treatment of Parkinson's disease. *Bioorg Chem* **2020**, *97*, 103707. DOI: 10.1016/j.bioorg.2020.103707.



- (271) Binda, C.; Aldeco, M.; Geldenhuys, W. J.; Tortorici, M.; Mattevi, A.; Edmondson, D. E. Molecular Insights into Human Monoamine Oxidase B Inhibition by the Glitazone Anti-Diabetes Drugs. *ACS Med Chem Lett* **2011**, *3* (1), 39-42. DOI: 10.1021/ml200196p.
- (272) Fries, P. H.; Imbert, D. Parallel NMR based on solution magnetic-susceptibility differences. Application to isotopic effects on self-diffusion. *J Chem Eng Data* **2010**, *55* (5), 2048-2054. DOI: 10.1021/je901031b.
- (273) Kochi, J. K. The mechanism of the Sandmeyer and Meerwein reactions. *J Am Chem Soc* **1957**, *79* (11), 2942-2948. DOI: 10.1021/ja01568a066.
- (274) Treu, M.; Jordis, U.; Lee, V. J. An Improved Synthesis of 5-(2,6-Dichlorophenyl)-2-(phenylthio)-6H-pyrimido[1,6-b]pyridazin-6-one (a VX-745 analog). *Molecules* **2001**, *6* (12), 959-963. Bagley, M. C.; Davis, T.; Dix, M. C.; Rokicki, M. J.; Kipling, D. Rapid synthesis of VX-745: p38 MAP kinase inhibition in Werner syndrome cells. *Bioorg Med Chem Lett* **2007**, *17* (18), 5107-5110. DOI: 10.1016/j.bmcl.2007.07.016.
- (275) Abu-Shanab, F. A.; Sherif, S. M.; Mousa, S. A. S. Dimethylformamide dimethyl acetal as a building block in heterocyclic synthesis. *J Heterocycl Chem* **2009**, *46* (5), 801-827. DOI: 10.1002/jhet.69.
- (276) McNamara, D. J.; Berman, E. M.; Fry, D. W.; Werbel, L. M. Potent inhibition of thymidylate synthase by two series of nonclassical quinazolines. *J Med Chem* **1990**, *33* (7), 2045-2051. DOI: 10.1021/jm00169a040.
- (277) Zhou, Y.; Feng, J.; Feng, L.; Xie, D.; Peng, H.; Cai, M.; He, H. Synthesis and Activity of 1, 2, 3-Triazole Aminopyrimidines against Cyanobacteria as PDHc-E1 Competitive Inhibitors. *J Agric Food Chem* **2019**, *67* (45), 12538-12546. DOI: 10.1021/acs.jafc.9b02878.
- (278) Cheng, H.; Lam, T. L.; Liu, Y.; Tang, Z.; Che, C. M. Photoinduced Hydroarylation and Cyclization of Alkenes with Luminescent Platinum(II) Complexes. *Angew Chem Int Ed Engl* **2021**, *60* (3), 1383-1389. DOI: 10.1002/anie.202011841.
- (279) Uliassi, E.; Peña-Altamira, L. E.; Morales, A. V.; Massenzio, F.; Petralla, S.; Rossi, M.; Roberti, M.; Martinez Gonzalez, L.; Martinez, A.; Monti, B.; et al. A Focused Library of Psychotropic Analogues with Neuroprotective and Neuroregenerative Potential. *ACS Chem Neurosci* **2018**. DOI: 10.1021/acchemneuro.8b00242.
- (280) Suwanjang, W.; Abramov, A. Y.; Govitrapong, P.; Chetsawang, B. Melatonin attenuates dexamethasone toxicity-induced oxidative stress, calpain and caspase activation in human neuroblastoma SH-SY5Y cells. *J Steroid Biochem Mol Biol* **2013**, *138*, 116-122. DOI: 10.1016/j.jsbmb.2013.04.008.
- (281) Johnson, S.; Tazik, S.; Lu, D.; Johnson, C.; Youdim, M. B.; Wang, J.; Rajkowska, G.; Ou, X. M. The New Inhibitor of Monoamine Oxidase, M30, has a Neuroprotective Effect Against Dexamethasone-Induced Brain Cell Apoptosis. *Front Neurosci* **2010**, *4*, 180. DOI: 10.3389/fnins.2010.00180.
- (282) Park, W. H. Effects of antioxidants and MAPK inhibitors on cell death and reactive oxygen species levels in H. *Oncol Lett* **2013**, *5* (5), 1633-1638. DOI: 10.3892/ol.2013.1216.
- (283) Mano, H. Tec family of protein-tyrosine kinases: an overview of their structure and function. *Cytokine Growth Factor Rev* **1999**, *10* (3-4), 267-280. DOI: 10.1016/s1359-6101(99)00019-2.
- (284) Yang, W. C.; Collette, Y.; Nunès, J. A.; Olive, D. Tec kinases: a family with multiple roles in immunity. *Immunity* **2000**, *12* (4), 373-382. DOI: 10.1016/s1074-7613(00)80189-2.

- (285) Smith, C. I.; Islam, T. C.; Mattsson, P. T.; Mohamed, A. J.; Nore, B. F.; Vihinen, M. The Tec family of cytoplasmic tyrosine kinases: mammalian Btk, Bmx, Itk, Tec, Txk and homologs in other species. *Bioessays* **2001**, *23* (5), 436-446. DOI: 10.1002/bies.1062.
- (286) Ortutay, C.; Nore, B. F.; Vihinen, M.; Smith, C. I. Phylogeny of Tec family kinases identification of a premetazoan origin of Btk, Bmx, Itk, Tec, Txk, and the Btk regulator SH3BP5. *Adv Genet* **2008**, *64*, 51-80. DOI: 10.1016/S0065-2660(08)00803-1.
- (287) Cenni, B.; Gutmann, S.; Gottar-Guillier, M. BMX and its role in inflammation, cardiovascular disease, and cancer. *Int Rev Immunol* **2012**, *31* (2), 166-173. DOI: 10.3109/08830185.2012.663838.
- (288) Robinson, D. R.; Wu, Y. M.; Lin, S. F. The protein tyrosine kinase family of the human genome. *Oncogene* **2000**, *19* (49), 5548-5557. DOI: 10.1038/sj.onc.1203957.
- (289) Muckelbauer, J.; Sack, J. S.; Ahmed, N.; Burke, J.; Chang, C. Y.; Gao, M.; Tino, J.; Xie, D.; Tebben, A. J. X-ray crystal structure of bone marrow kinase in the x chromosome: a Tec family kinase. *Chem Biol Drug Des* **2011**, *78* (5), 739-748. DOI: 10.1111/j.1747-0285.2011.01230.x.
- (290) Gocek, E.; Moulas, A. N.; Studzinski, G. P. Non-receptor protein tyrosine kinases signaling pathways in normal and cancer cells. *Crit Rev Clin Lab Sci* **2014**, *51* (3), 125-137. DOI: 10.3109/10408363.2013.874403.
- (291) Tripathi, D. K.; Poluri, K. M. Molecular insights into kinase mediated signaling pathways of chemokines and their cognate G protein coupled receptors. *Front Biosci (Landmark Ed)* **2020**, *25*, 1361-1385. DOI: 10.2741/4860.
- (292) Chen, S.; Jiang, X.; Gewinner, C. A.; Asara, J. M.; Simon, N. I.; Cai, C.; Cantley, L. C.; Balk, S. P. Tyrosine kinase BMX phosphorylates phosphotyrosine-primed motif mediating the activation of multiple receptor tyrosine kinases. *Sci Signal* **2013**, *6* (277), ra40. DOI: 10.1126/scisignal.2003936.
- (293) Nore, B. F.; Mattsson, P. T.; Antonsson, P.; Bäckesjö, C. M.; Westlund, A.; Lennartsson, J.; Hansson, H.; Löw, P.; Rönstrand, L.; Smith, C. I. Identification of phosphorylation sites within the SH3 domains of Tec family tyrosine kinases. *Biochim Biophys Acta* **2003**, *1645* (2), 123-132. DOI: 10.1016/s1570-9639(02)00524-1.
- (294) Seixas, J. D.; Sousa, B. B.; Marques, M. C.; Guerreiro, A.; Traquete, R.; Rodrigues, T.; Albuquerque, I. S.; Sousa, M. F. Q.; Lemos, A. R.; Sousa, P. M. F.; et al. Structural and biophysical insights into the mode of covalent binding of rationally designed potent BMX inhibitors. *RSC Chem Biol* **2020**, *1* (4), 251-262. DOI: 10.1039/d0cb00033g.
- (295) Kempuraj, D.; Ahmed, M. E.; Selvakumar, G. P.; Thangavel, R.; Raikwar, S. P.; Zaheer, S. A.; Iyer, S. S.; Govindarajan, R.; Nattanmai Chandrasekaran, P.; Burton, C.; et al. Acute Traumatic Brain Injury-Induced Neuroinflammatory Response and Neurovascular Disorders in the Brain. *Neurotox Res* **2021**, *39* (2), 359-368. DOI: 10.1007/s12640-020-00288-9.
- (296) Chen, K. Y.; Wu, C. C.; Chang, C. F.; Chen, Y. H.; Chiu, W. T.; Lou, Y. H.; Shih, H. M.; Chiang, Y. H. Suppression of Etk/Bmx protects against ischemic brain injury. *Cell Transplant* **2012**, *21* (1), 345-354. DOI: 10.3727/096368911X582741.
- (297) Sardi, F.; Manta, B.; Portillo-Ledesma, S.; Knoops, B.; Comini, M. A.; Ferrer-Sueta, G. Determination of acidity and nucleophilicity in thiols by reaction with monobromobimane and fluorescence detection. *Anal Biochem* **2013**, *435* (1), 74-82. DOI: 10.1016/j.ab.2012.12.017.

- (298) Cee, V. J.; Volak, L. P.; Chen, Y.; Bartberger, M. D.; Tegley, C.; Arvedson, T.; McCarter, J.; Tasker, A. S.; Fotsch, C. Systematic Study of the Glutathione (GSH) Reactivity of N-Arylacrylamides: 1. Effects of Aryl Substitution. *J Med Chem* **2015**, *58* (23), 9171-9178. DOI: 10.1021/acs.jmedchem.5b01018.
- (299) Reddi, R. N.; Resnick, E.; Rogel, A.; Rao, B. V.; Gabizon, R.; Goldenberg, K.; Gurwicz, N.; Zaidman, D.; Plotnikov, A.; Barr, H.; et al. Tunable Methacrylamides for Covalent Ligand Directed Release Chemistry. *J Am Chem Soc* **2021**, *143* (13), 4979-4992. DOI: 10.1021/jacs.0c10644.
- (300) Awoonor-Williams, E.; Rowley, C. N. How reactive are druggable cysteines in protein kinases? *J Chem Inf Model* **2018**, *58* (9), 1935-1946. DOI: 10.1021/acs.jcim.8b00454.
- (301) Blewett, M. M.; Xie, J.; Zaro, B. W.; Backus, K. M.; Altman, A.; Teijaro, J. R.; Cravatt, B. F. Chemical proteomic map of dimethyl fumarate-sensitive cysteines in primary human T cells. *Sci Signal* **2016**, *9* (445), rs10. DOI: 10.1126/scisignal.aaf7694.
- (302) Zaro, B. W.; Whitby, L. R.; Lum, K. M.; Cravatt, B. F. Metabolically Labile Fumarate Esters Impart Kinetic Selectivity to Irreversible Inhibitors. *J Am Chem Soc* **2016**, *138* (49), 15841-15844. DOI: 10.1021/jacs.6b10589.
- (303) Forristal, I. The chemistry of  $\alpha$ ,  $\beta$ -unsaturated sulfoxides and sulfones: an update. *J Sulphur Chem* **2005**, *26* (2), 163-185. DOI: 10.1080/17415990500100115.
- (304) Fell, J. B.; Fischer, J. P.; Baer, B. R.; Blake, J. F.; Bouhana, K.; Briere, D. M.; Brown, K. D.; Burgess, L. E.; Burns, A. C.; Burkard, M. R.; et al. Identification of the Clinical Development Candidate. *J Med Chem* **2020**, *63* (13), 6679-6693. DOI: 10.1021/acs.jmedchem.9b02052.
- (305) Oballa, R. M.; Truchon, J. F.; Bayly, C. I.; Chauret, N.; Day, S.; Crane, S.; Berthelette, C. A generally applicable method for assessing the electrophilicity and reactivity of diverse nitrile-containing compounds. *Bioorg Med Chem Lett* **2007**, *17* (4), 998-1002. DOI: 10.1016/j.bmcl.2006.11.044.
- (306) Pfaff, D.; Nemecek, G.; Podlech, J. A Lewis acid-promoted Pinner reaction. *Beilstein J Org Chem* **2013**, *9*, 1572-1577. DOI: 10.3762/bjoc.9.179.
- (307) McAulay, K.; Hoyt, E. A.; Thomas, M.; Schimpl, M.; Bodnarchuk, M. S.; Lewis, H. J.; Barratt, D.; Bhavsar, D.; Robinson, D. M.; Deery, M. J.; et al. Alkynyl Benzoxazines and Dihydroquinazolines as Cysteine Targeting Covalent Warheads and Their Application in Identification of Selective Irreversible Kinase Inhibitors. *J Am Chem Soc* **2020**, *142* (23), 10358-10372. DOI: 10.1021/jacs.9b13391.
- (308) Mons, E.; Jansen, I. D. C.; Loboda, J.; van Doodewaerd, B. R.; Hermans, J.; Verdoes, M.; van Boeckel, C. A. A.; van Veelen, P. A.; Turk, B.; Turk, D.; et al. The Alkyne Moiety as a Latent Electrophile in Irreversible Covalent Small Molecule Inhibitors of Cathepsin K. *J Am Chem Soc* **2019**, *141* (8), 3507-3514. DOI: 10.1021/jacs.8b11027.
- (309) Shindo, N.; Fuchida, H.; Sato, M.; Watari, K.; Shibata, T.; Kuwata, K.; Miura, C.; Okamoto, K.; Hatsuyama, Y.; Tokunaga, K.; et al. Selective and reversible modification of kinase cysteines with chlorofluoroacetamides. *Nat Chem Biol* **2019**, *15* (3), 250-258. DOI: 10.1038/s41589-018-0204-3.
- (310) Burger, J. A.; Tedeschi, A.; Barr, P. M.; Robak, T.; Owen, C.; Ghia, P.; Bairey, O.; Hillmen, P.; Bartlett, N. L.; Li, J.; et al. Ibrutinib as Initial Therapy for Patients with Chronic Lymphocytic Leukemia. *N Engl J Med* **2015**, *373* (25), 2425-2437. DOI: 10.1056/NEJMoa1509388.
- (311) Byrd, J. C.; Harrington, B.; O'Brien, S.; Jones, J. A.; Schuh, A.; Devereux, S.; Chaves, J.; Wierda, W. G.; Awan, F. T.; Brown, J. R.; et al. Acalabrutinib (ACP-196) in Relapsed Chronic Lymphocytic Leukemia. *N Engl J Med* **2016**, *374* (4), 323-332. DOI: 10.1056/NEJMoa1509981.

- (312) Guo, Y.; Liu, Y.; Hu, N.; Yu, D.; Zhou, C.; Shi, G.; Zhang, B.; Wei, M.; Liu, J.; Luo, L. Discovery of zanubrutinib (BGB-3111), a novel, potent, and selective covalent inhibitor of Bruton's tyrosine kinase. *J Med Chem* **2019**, *62* (17), 7923-7940. DOI: 10.1021/acs.jmedchem.9b00687.
- (313) Jaglowski, S. M.; Blazar, B. R. How ibrutinib, a B-cell malignancy drug, became an FDA-approved second-line therapy for steroid-resistant chronic GVHD. *Blood Adv* **2018**, *2* (15), 2012-2019. DOI: 10.1182/bloodadvances.2018013060.
- (314) Liu, Q.; Sabnis, Y.; Zhao, Z.; Zhang, T.; Buhrlage, S. J.; Jones, L. H.; Gray, N. S. Developing irreversible inhibitors of the protein kinase cysteinome. *Chem Biol* **2013**, *20* (2), 146-159. DOI: 10.1016/j.chembiol.2012.12.006.
- (315) Serafim, R. A. M.; Elkins, J. M.; Zuercher, W. J.; Laufer, S. A.; Gehringer, M. Chemical Probes for Understudied Kinases: Challenges and Opportunities. *J Med Chem* **2021**. DOI: 10.1021/acs.jmedchem.1c00980.
- (316) Dungo, R. T.; Keating, G. M. Afatinib: first global approval. *Drugs* **2013**, *73* (13), 1503-1515. DOI: 10.1007/s40265-013-0111-6.
- (317) Shirley, M. Dacomitinib: First Global Approval. *Drugs* **2018**, *78* (18), 1947-1953. DOI: 10.1007/s40265-018-1028-x.
- (318) Greig, S. L. Osimertinib: First Global Approval. *Drugs* **2016**, *76* (2), 263-273. DOI: 10.1007/s40265-015-0533-4.
- (319) Singh, H.; Walker, A. J.; Amiri-Kordestani, L.; Cheng, J.; Tang, S.; Balcazar, P.; Barnett-Ringgold, K.; Palmby, T. R.; Cao, X.; Zheng, N.; et al. U.S. Food and Drug Administration Approval: Neratinib for the Extended Adjuvant Treatment of Early-Stage HER2-Positive Breast Cancer. *Clin Cancer Res* **2018**, *24* (15), 3486-3491. DOI: 10.1158/1078-0432.CCR-17-3628.
- (320) Markham, A. Mobocertinib: First Approval. *Drugs* **2021**, *81* (17), 2069-2074. DOI: 10.1007/s40265-021-01632-9.
- (321) Zapf, C. W.; Gerstenberger, B. S.; Xing, L.; Limburg, D. C.; Anderson, D. R.; Caspers, N.; Han, S.; Aulabaugh, A.; Kurumbail, R.; Shakya, S.; et al. Covalent inhibitors of interleukin-2 inducible T cell kinase (itk) with nanomolar potency in a whole-blood assay. *J Med Chem* **2012**, *55* (22), 10047-10063. DOI: 10.1021/jm301190s.
- (322) Harling, J. D.; Deakin, A. M.; Campos, S.; Grimley, R.; Chaudry, L.; Nye, C.; Polyakova, O.; Bessant, C. M.; Barton, N.; Somers, D.; et al. Discovery of novel irreversible inhibitors of interleukin (IL)-2-inducible tyrosine kinase (Itk) by targeting cysteine 442 in the ATP pocket. *J Biol Chem* **2013**, *288* (39), 28195-28206. DOI: 10.1074/jbc.M113.474114.
- (323) Liu, F.; Zhang, X.; Weisberg, E.; Chen, S.; Hur, W.; Wu, H.; Zhao, Z.; Wang, W.; Mao, M.; Cai, C.; et al. Discovery of a selective irreversible BMX inhibitor for prostate cancer. *ACS Chem Biol* **2013**, *8* (7), 1423-1428. DOI: 10.1021/cb4000629.
- (324) Liang, X.; Lv, F.; Wang, B.; Yu, K.; Wu, H.; Qi, Z.; Jiang, Z.; Chen, C.; Wang, A.; Miao, W.; et al. Discovery of 2-((3-Acrylamido-4-methylphenyl)amino)-N-(2-methyl-5-(3,4,5-trimethoxybenzamido)phenyl)-4-(methylamino)pyrimidine-5-carboxamide (CHMFL-BMX-078) as a Highly Potent and Selective Type II Irreversible Bone Marrow Kinase in the X Chromosome (BMX) Kinase Inhibitor. *J Med Chem* **2017**, *60* (5), 1793-1816. DOI: 10.1021/acs.jmedchem.6b01413.

- (325) Arrowsmith, C. H.; Audia, J. E.; Austin, C.; Baell, J.; Bennett, J.; Blagg, J.; Bountra, C.; Brennan, P. E.; Brown, P. J.; Bunnage, M. E.; et al. The promise and peril of chemical probes. *Nat Chem Biol* **2015**, *11* (8), 536-541. DOI: 10.1038/nchembio.1867. DOI: 10.1038/nchembio.1867.
- (326) Garbaccio, R. M.; Parmee, E. R. The Impact of Chemical Probes in Drug Discovery: A Pharmaceutical Industry Perspective. *Cell Chem Biol* **2016**, *23* (1), 10-17. DOI: 10.1016/j.chembiol.2015.11.011.
- (327) Brown, P. J.; Müller, S. Open access chemical probes for epigenetic targets. *Future Med Chem* **2015**, *7* (14), 1901-1917. DOI: 10.4155/fmc.15.127.
- (328) Ishiyama, T.; Murata, M.; Miyaura, N. Palladium (0)-catalyzed cross-coupling reaction of alkoxydiboron with haloarenes: a direct procedure for arylboronic esters. *J Org Chem* **1995**, *60* (23), 7508-7510. DOI: 10.1021/jo00128a024.
- (329) Wagschal, S.; Perego, L. A.; Simon, A.; Franco-Espejo, A.; Tocqueville, C.; Albanese-Walker, J.; Jutand, A.; Grimaud, L. Formation of XPhos-Ligated Palladium (0) Complexes and Reactivity in Oxidative Additions. *Chem Eur J* **2019**, *25* (28), 6980-6987. DOI: 10.1002/chem.201900451.
- (330) Lennox, A. J. J.; Lloyd-Jones, G. C. Selection of boron reagents for Suzuki–Miyaura coupling. *Chem Soc Rev* **2014**, *43* (1), 412-443. DOI: 10.1039/C3CS60197H.
- (331) Shaughnessy, K. H. Development of Palladium Precatalysts that Efficiently Generate LPd (0) Active Species. *Isr J Chem* **2020**, *60* (3-4), 180-194. DOI: 10.1002/ijch.201900067.
- (332) Lima, C. F.; Rodrigues, A. S. M. C.; Silva, V. L. M.; Silva, A. M. S.; Santos, L. M. Role of the Base and Control of Selectivity in the Suzuki–Miyaura Cross-Coupling Reaction. *ChemCatChem* **2014**, *6* (5), 1291-1302. DOI: 10.1002/cctc.201301080.
- (333) Vedadi, M.; Niesen, F. H.; Allali-Hassani, A.; Fedorov, O. Y.; Finerty, P. J.; Wasney, G. A.; Yeung, R.; Arrowsmith, C.; Ball, L. J.; Berglund, H.; et al. Chemical screening methods to identify ligands that promote protein stability, protein crystallization, and structure determination. *Proc Natl Acad Sci U S A* **2006**, *103* (43), 15835-15840. DOI: 10.1073/pnas.0605224103.
- (334) Mallah, K.; Couch, C.; Borucki, D. M.; Toutonji, A.; Alshareef, M.; Tomlinson, S. Anti-inflammatory and Neuroprotective Agents in Clinical Trials for CNS Disease and Injury: Where Do We Go From Here? *Front Immunol* **2020**, *11*, 2021. DOI: 10.3389/fimmu.2020.02021.
- (335) Wu, L.; Lal, J.; Simon, K. A.; Burton, E. A.; Luk, Y. Y. Nonamphiphilic assembly in water: polymorphic nature, thread structure, and thermodynamic incompatibility. *J Am Chem Soc* **2009**, *131* (21), 7430-7443. DOI: 10.1021/ja9015149.
- (336) Vargas, J. L. Synthesis and Biological Evaluation of a Furanosteroid Library of PI3-kinase Inhibitors and Studies Toward the Total Synthesis of 9-Normethylpleurotin. **2009**. PhD Thesis. University of Pittsburgh. Elmaleh, D. P.
- (337) Tanzi, R. E.; Shoup, T. M.; Gricluc, A. Macrophages/microglia in neuro-inflammation associated with neurodegenerative diseases. WO2018045217 **2018**.